Reconstruction methods for ill-posed inverse problems

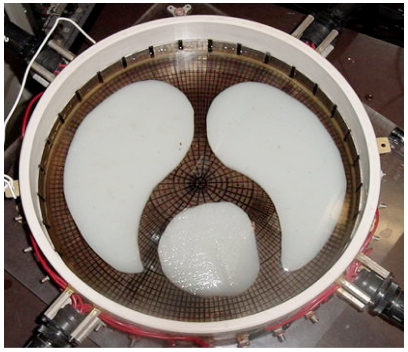

Samuli Siltanen

Department of Mathematics and Statistics
University of Helsinki, Finland
samuli.siltanen@helsinki.fi
www.siltanen-research.net

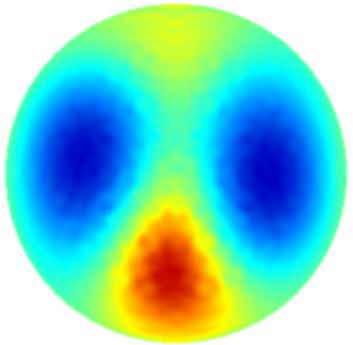

Summer Pre-School on Inverse Problems

April 16, 2015, CIRM, France

Finnish Centre of Excellence in Inverse Problems Research

OULUN YLIOPISTO UNIVERSITY of OULU

ACADEMY OF FINLAND

UNIVERSITY OF EASTERN FINLAND

UNIVERSITY OF JYVÄSKYLÄ

LAPPEENRANTA UNIVERSITY OF TECHNOLOGY

TAMPERE UNIVERSITY OF TECHNOLOGY

UNIVERSITY OF HELSINKI

http://wiki.helsinki.fi/display/inverse/Home

This my industrial-academic background

1999: PhD, Helsinki University of Technology, Finland

2000: R&D scientist at Instrumentarium Imaging

群馬

2002: Postdoc at Gunma University, Japan

2004: R&D scientist at GE Healthcare

2005: R&D scientist at Palodex Group

2006: Professor, Tampere University of Technology, Finland

2009: Professor, University of Helsinki, Finland

Direct problem: *given object, determine data*
Inverse problem: *given noisy data, recover object*

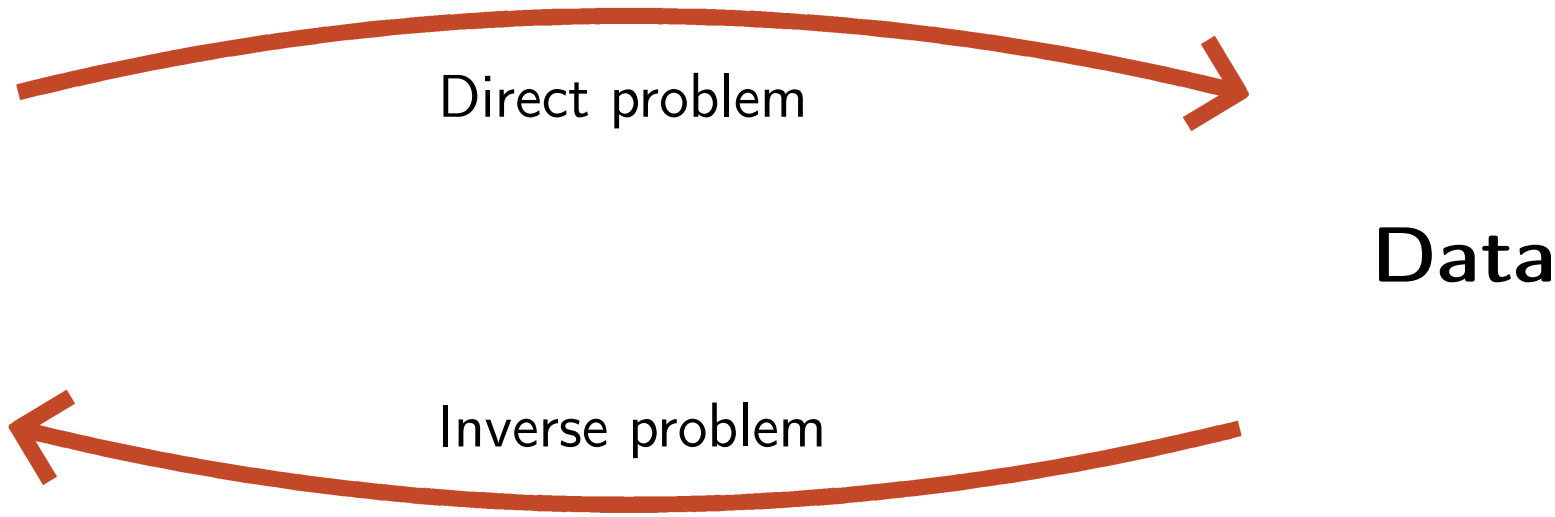

Direct problem: *given object, determine data*

Inverse problem: *given noisy data, recover object*

Object (positive photograph)

Data (negative photograph)

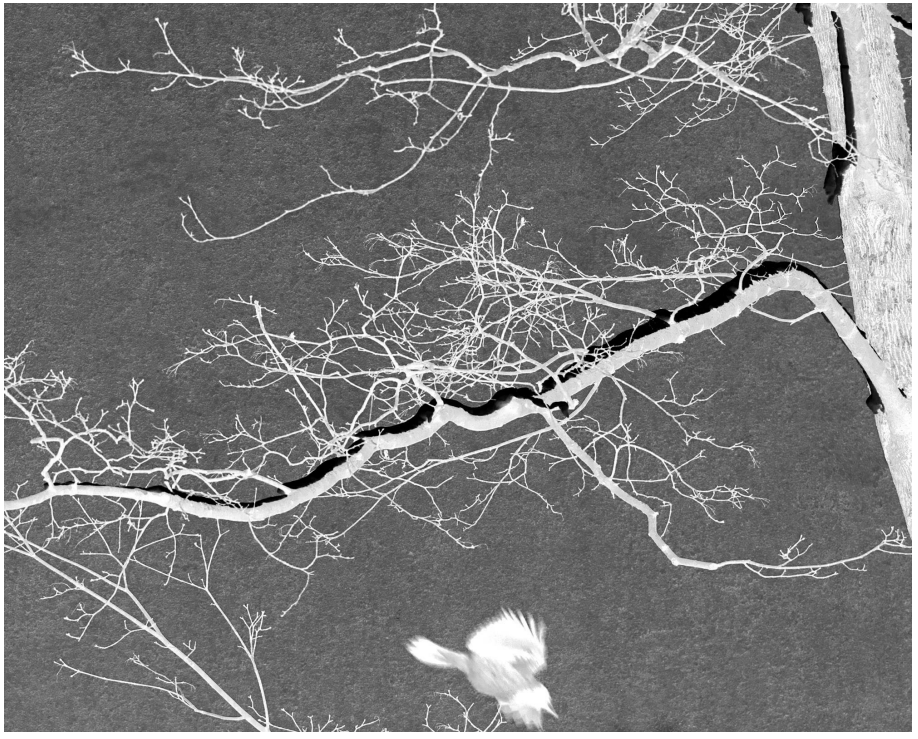

Forward map: subtraction from a constant

Direct problem: ***given object, determine data***
Inverse problem: ***given noisy data, recover object***

Object (sharp photograph)

Data (blurred photograph)

Forward map: convolution operator with smooth kernel

Direct problem: *given object, determine data*
Inverse problem: *given noisy data, recover object*

Object (X-ray attenuation)

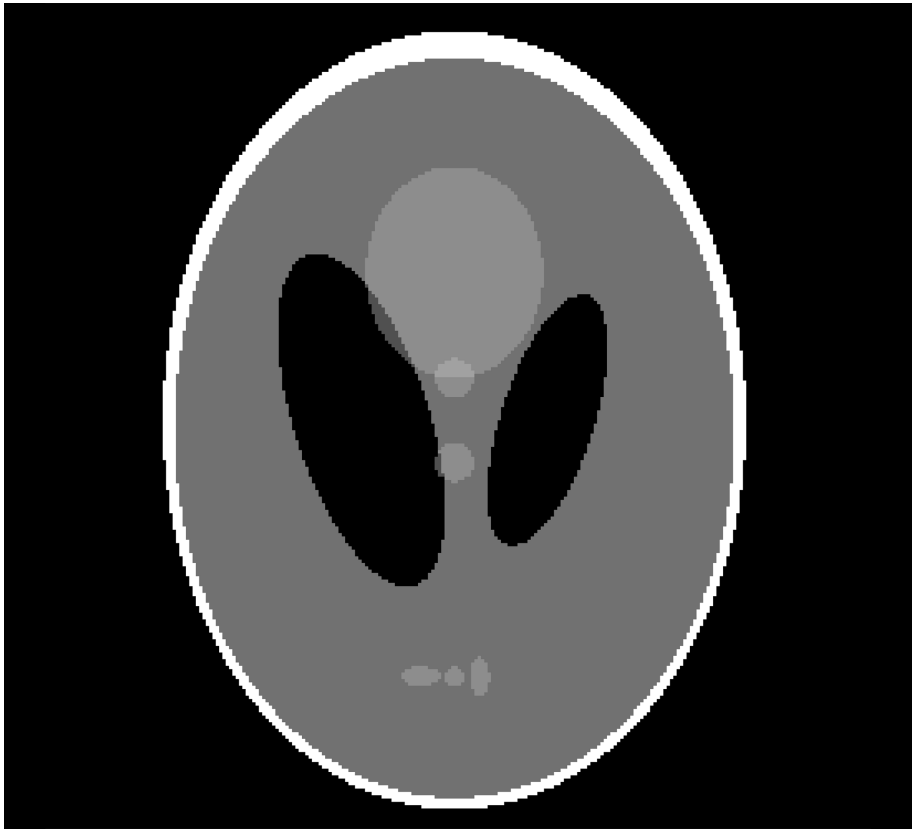

Data (sinogram)

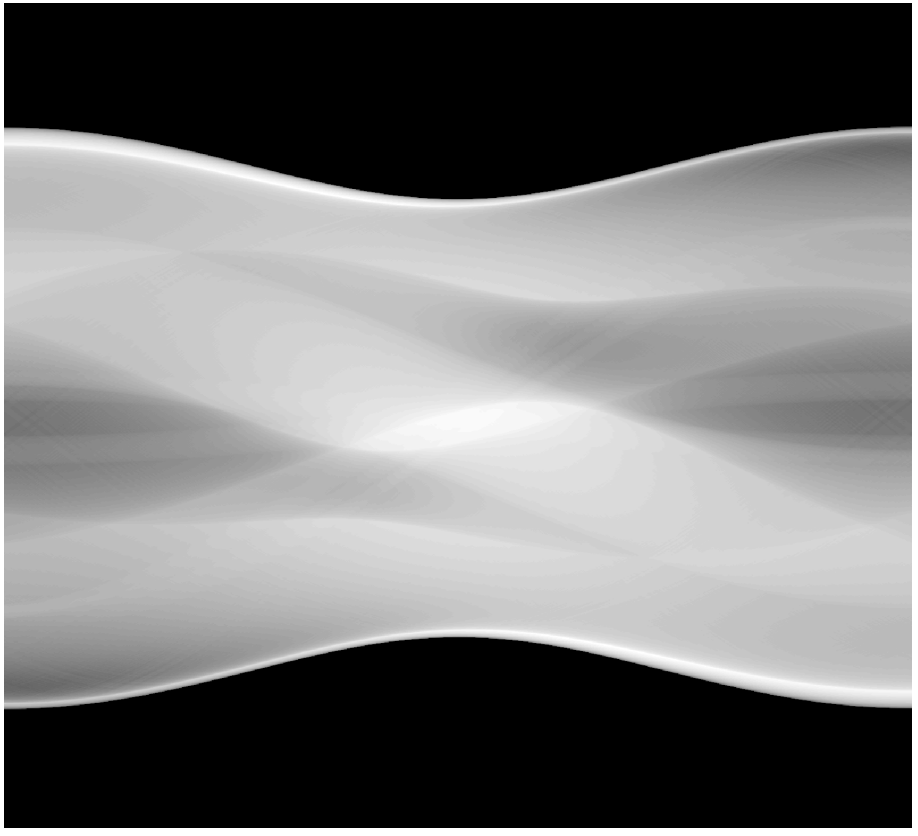

Forward map: discrete Radon transform

Direct problem: ***given object, determine data***
Inverse problem: ***given noisy data, recover object***

Object (conductivity)

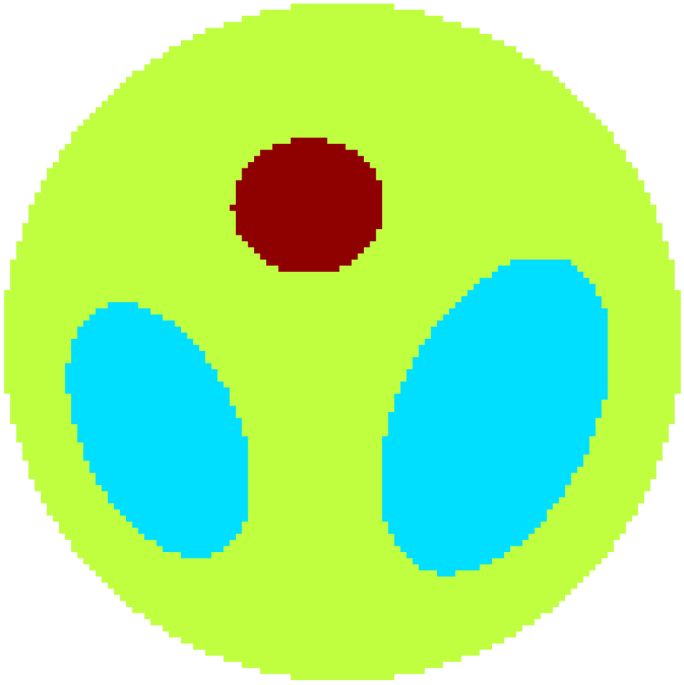

Data (voltage-to-current map)

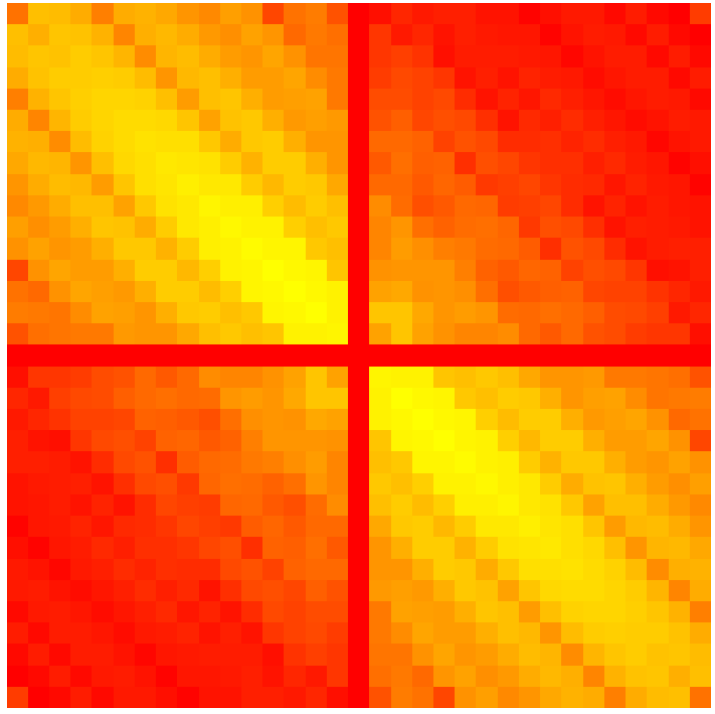

Forward map: electrical boundary measurements

Direct problem: ***given object, determine data***
Inverse problem: ***given noisy data, recover object***

Object (sound-hard obstacles)

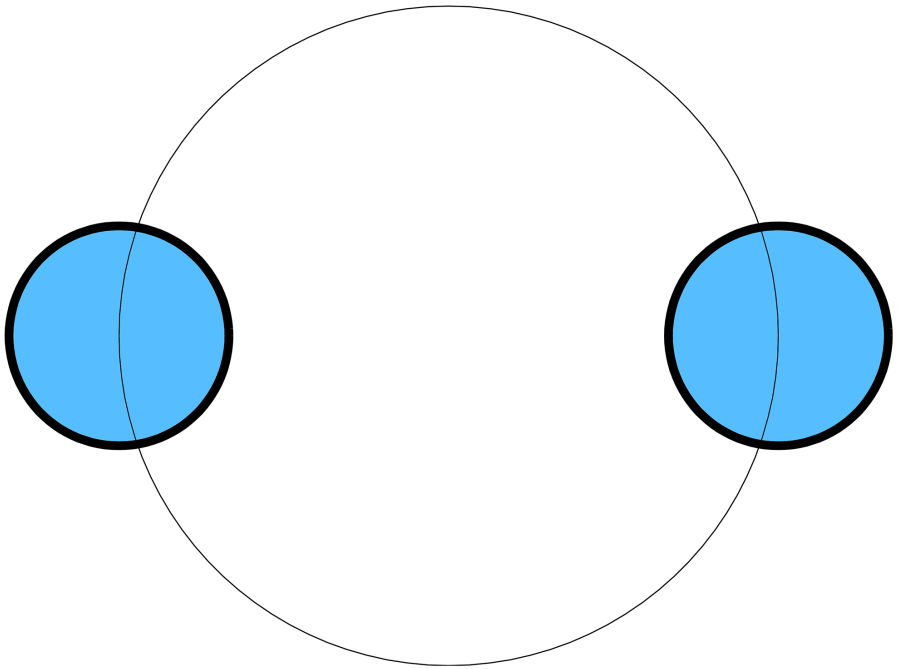

Data (far-field pattern)

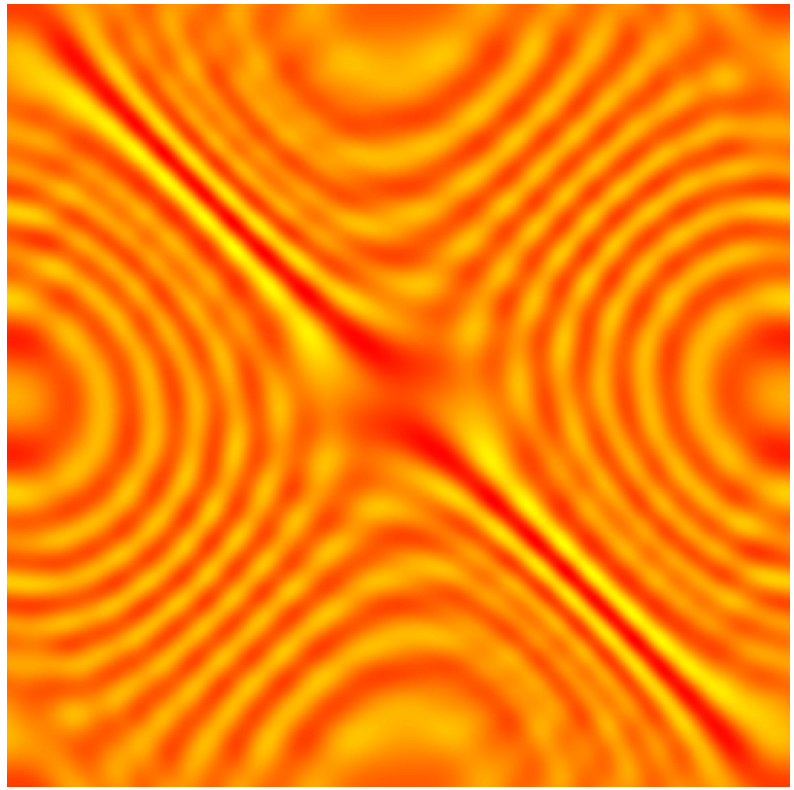

Forward map: far-away values of the scattered acoustic wave

Inverse problem = interpretation of an indirect measurement modelled by a forward map F

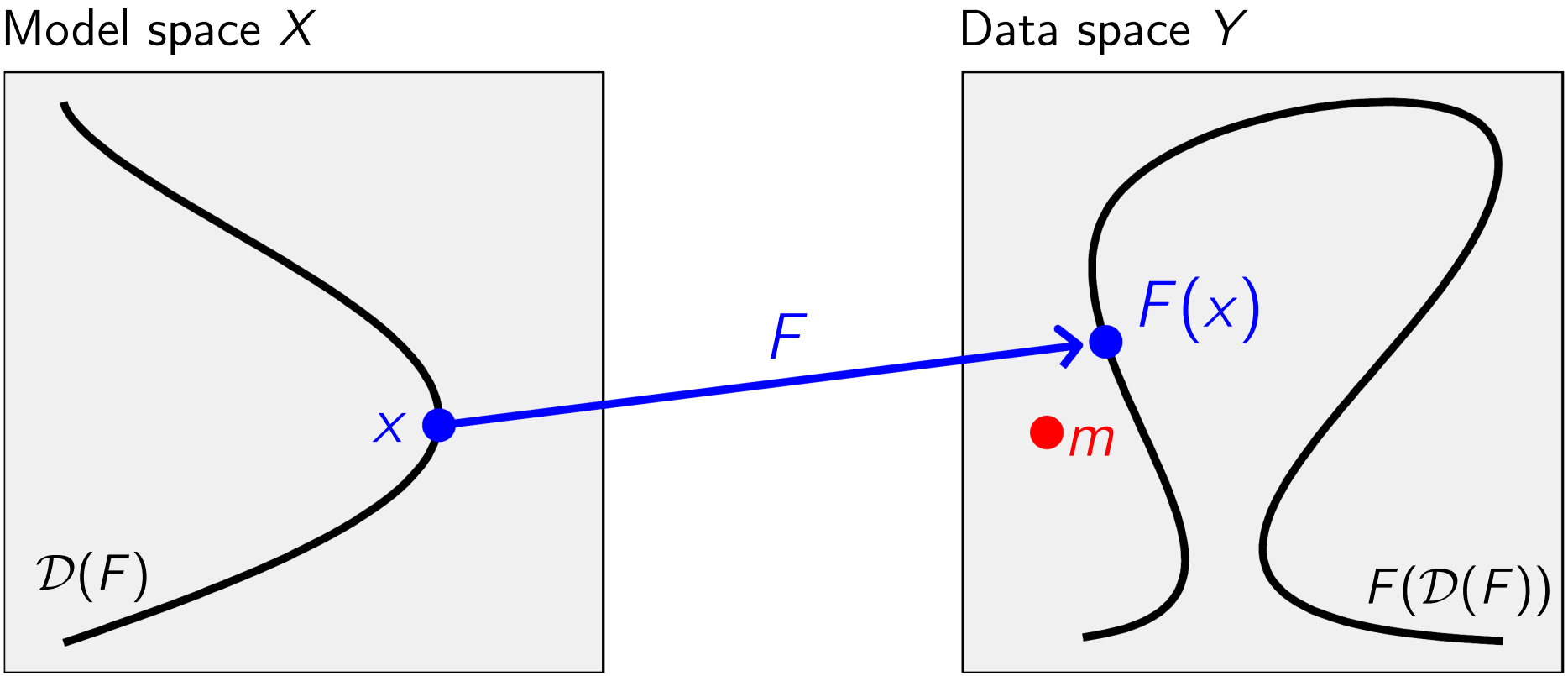

Consider the measurement model $m = F(x) + \varepsilon$. We want to know x, but all we can do is measure m that depends indirectly on x. Moreover, the measurement is corrupted with noise ε.

Ill-posed inverse problems are defined as opposites of well-posed direct problems

Hadamard (1903): a problem is well-posed if the following conditions hold.

1. A solution exists,
2. The solution is unique,
3. The solution depends continuously on the input.

Well-posed direct problem:
Input x, find infinite-precision data $F(x)$.

Ill-posed inverse problem:
Input noisy data $m = F(x) + \varepsilon$, recover x.

The solution of an inverse problem is a *set of instructions* for recovering x stably from m

Those instructions need to be

(i) backed up by rigorous mathematical theory, and

(ii) implementable as an effective computational algorithm.

The solution of an ill-posed inverse problems requires complementing insufficient measurement data by *a priori* information. This is done by designing and implementing a *regularization strategy* Γ_α.

Regularization means constructing a continuous map $\Gamma_\alpha : Y \to X$ that inverts F approximately

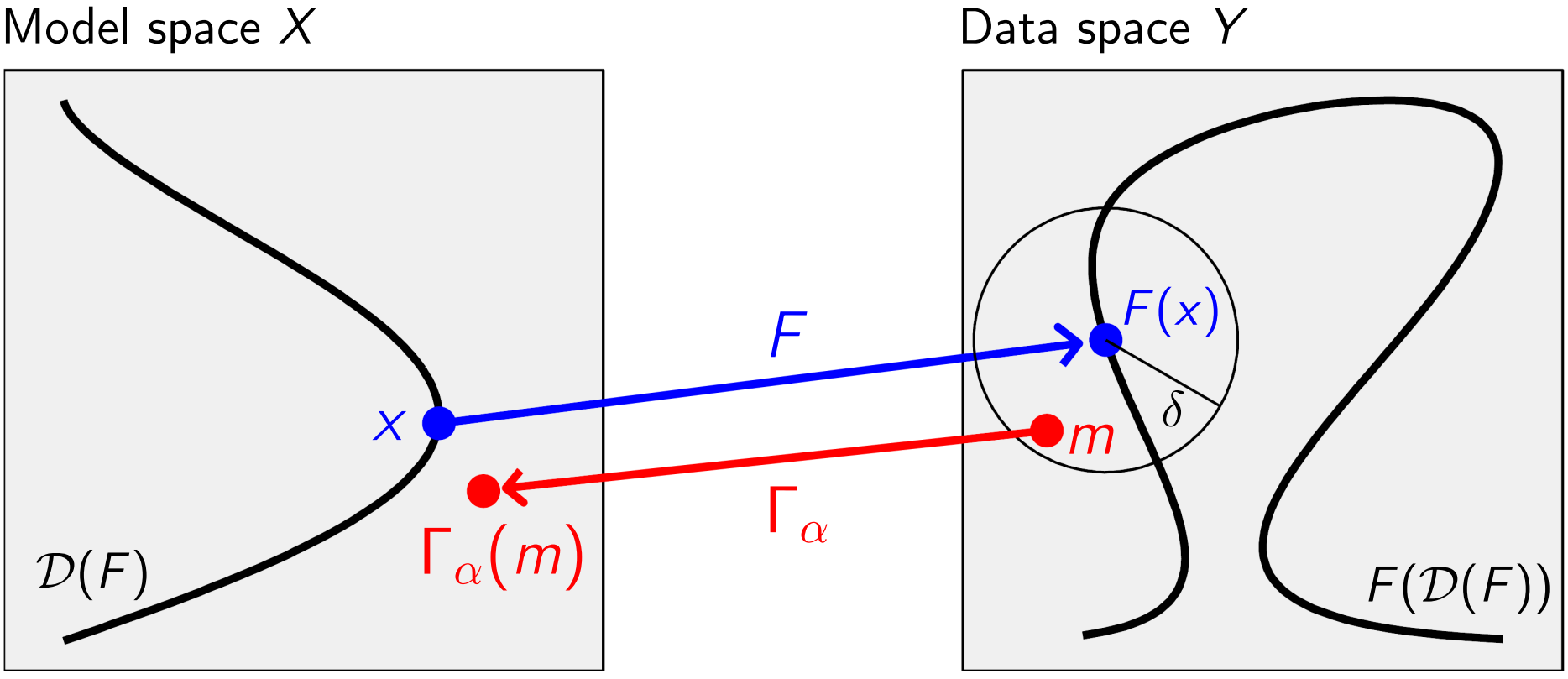

The reconstruction error $\|\Gamma_{\alpha(\delta)}(m) - x\|_X$ needs to vanish asymptotically as the zero-noise level $\delta \to 0$.

Outline

Wilhelm Conrad Röntgen invented X-rays and was awarded the first Nobel Prize in Physics in 1901

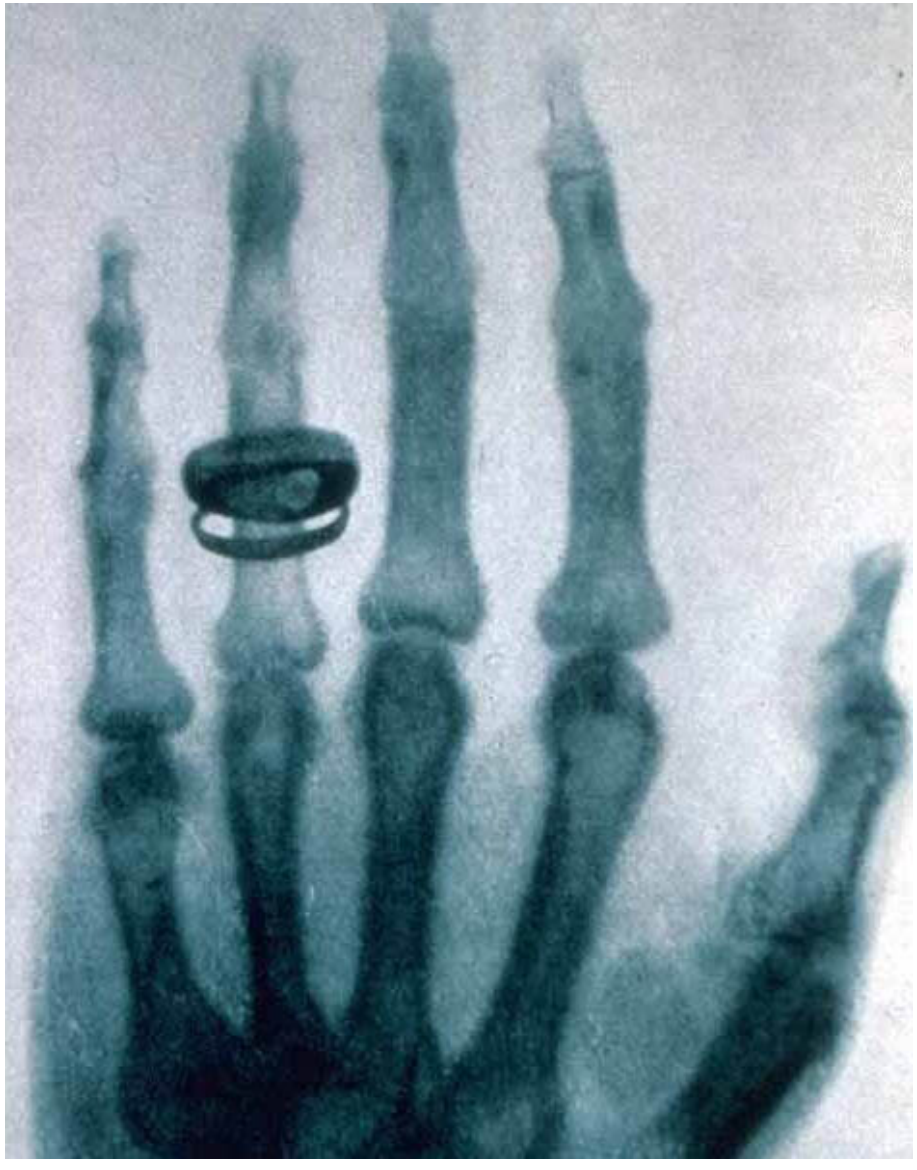

Godfrey Hounsfield and Allan McLeod Cormack were the first to develop X-ray tomography

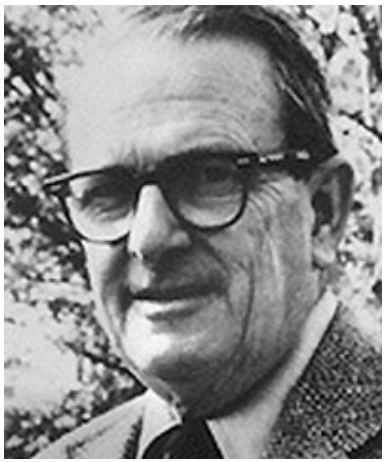

Hounsfield (top) and Cormack received Nobel prizes in 1979.

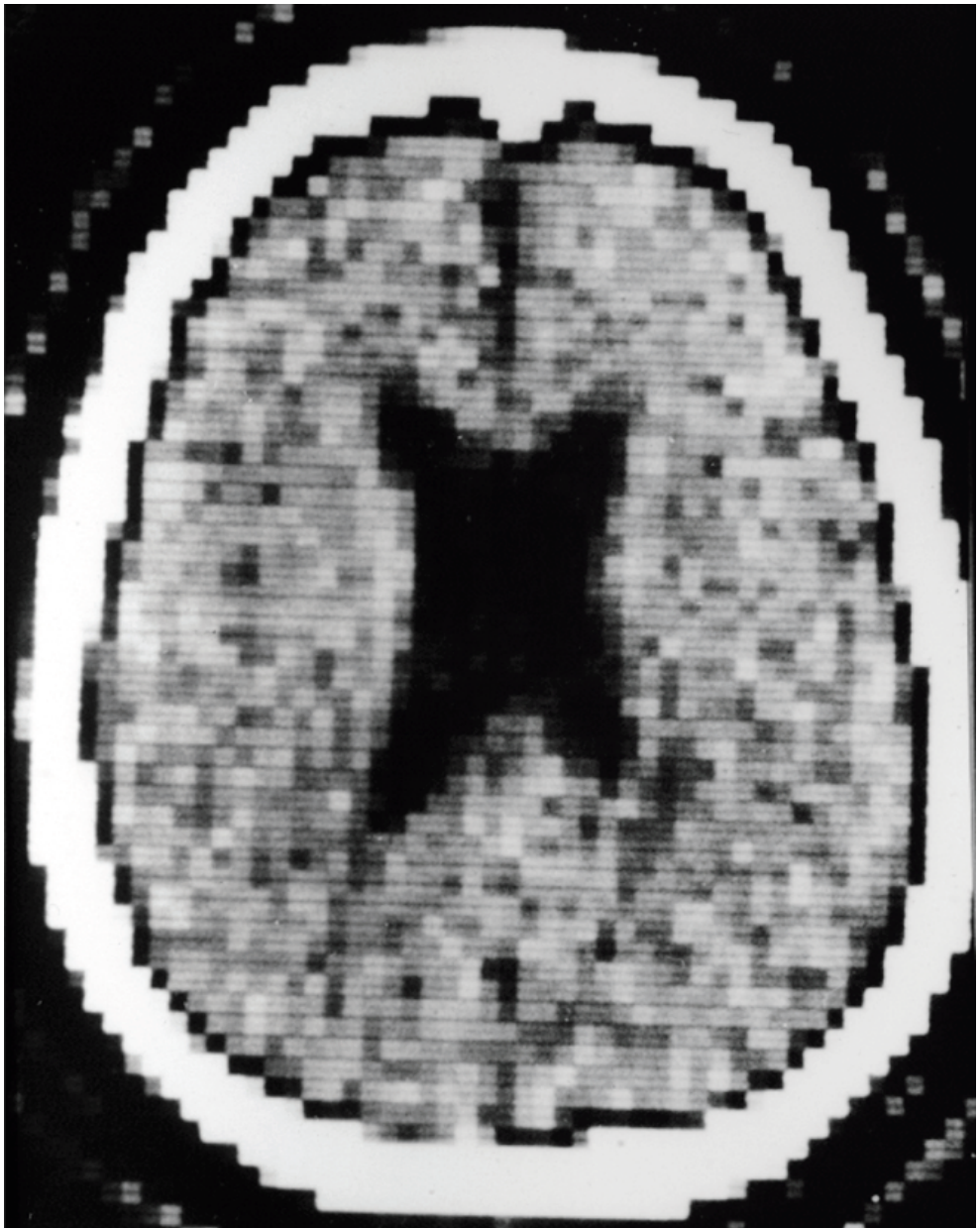

Reconstruction of a function from its line integrals was first invented by Johann Radon in 1917

Johann Radon (1887-1956)

$$f(P) = -\frac{1}{\pi}\int_0^\infty \frac{d\overline{F_p}(q)}{q}$$

Traditional X-ray tomography requires many projection images using small angular steps

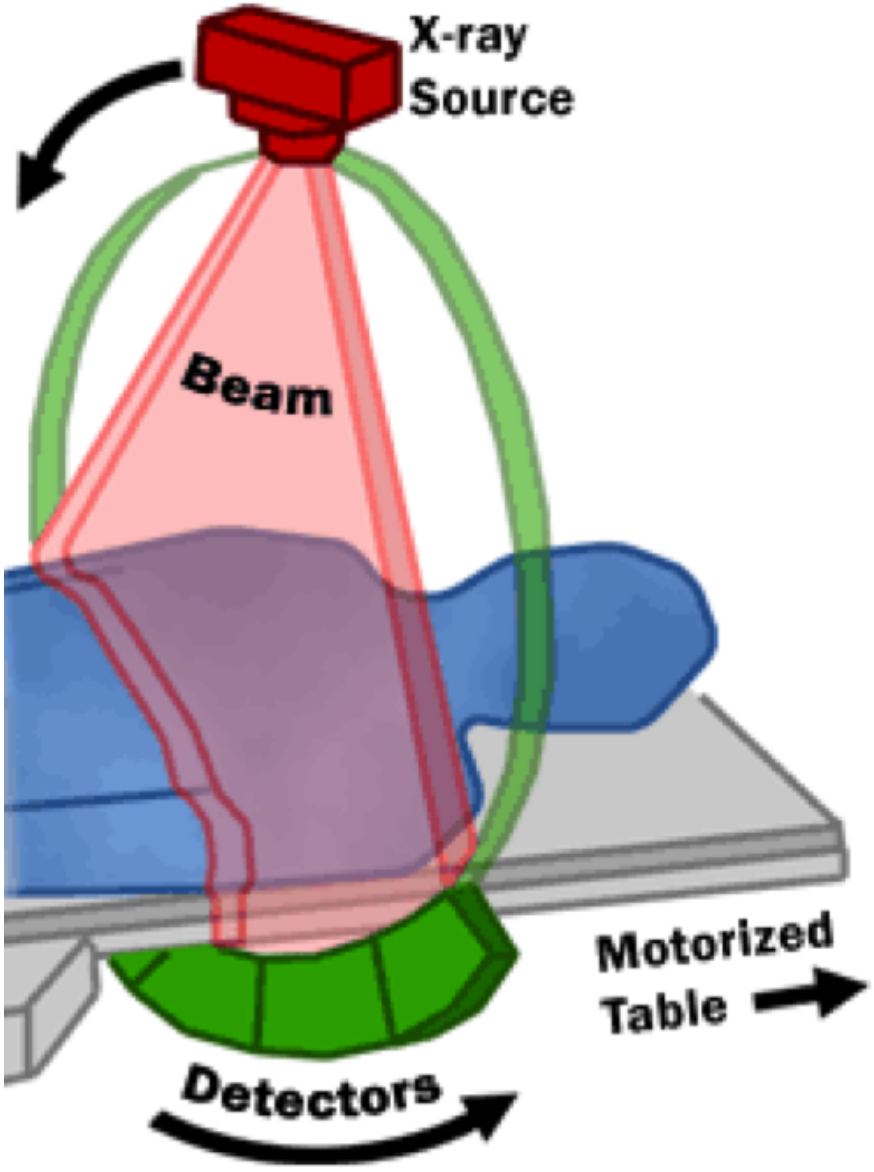

$$\frac{1}{4\pi^2}\int_{S^1}\int_{\mathbb{R}}\frac{\frac{d}{ds}(Rf)(\theta,s)}{x\cdot\theta-s}\,ds\,d\theta$$

Contrast-enhanced CT of abdomen, showing liver metastases

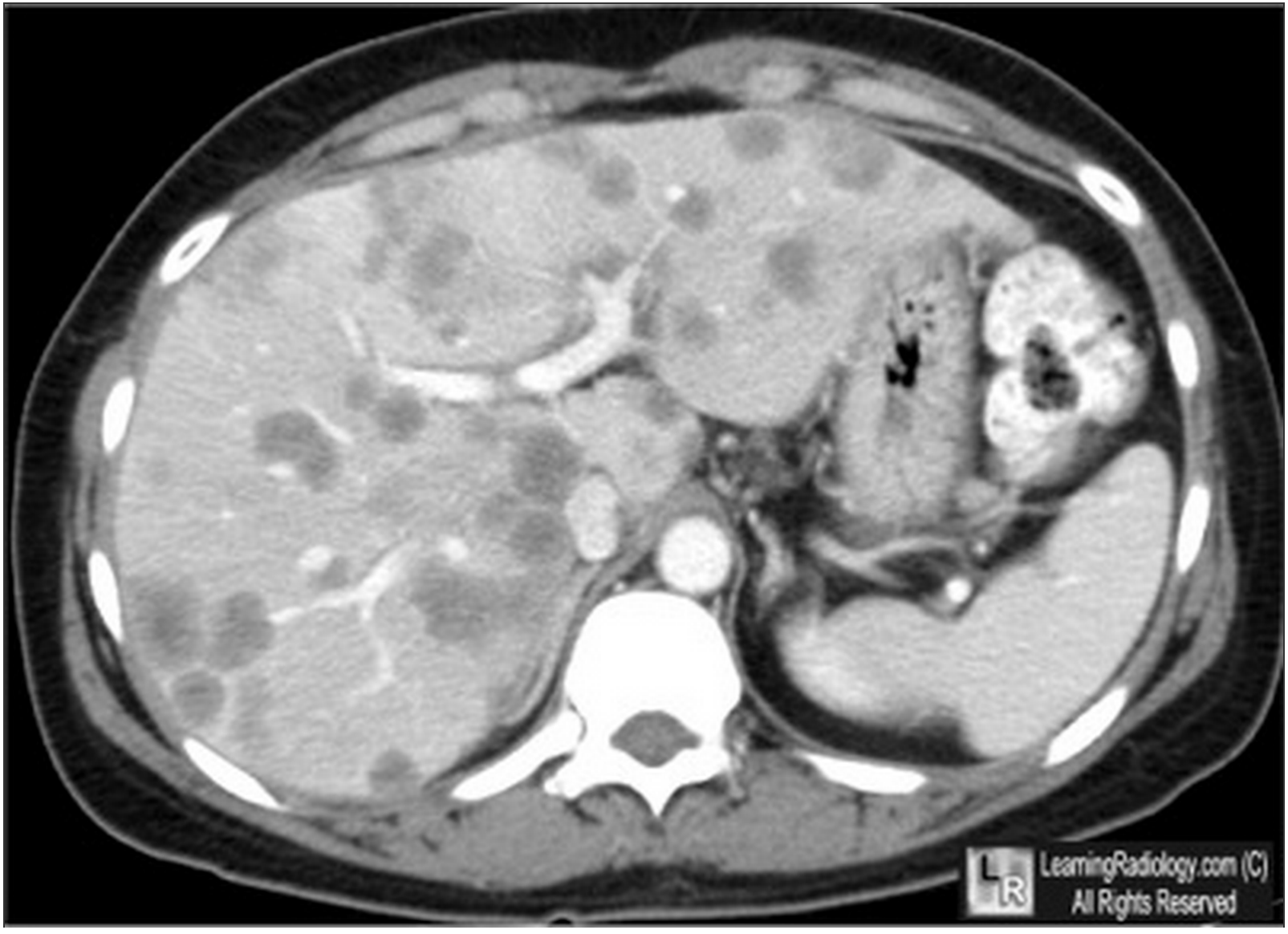

Head CT can be used for detecting and monitoring brain hemorrhage

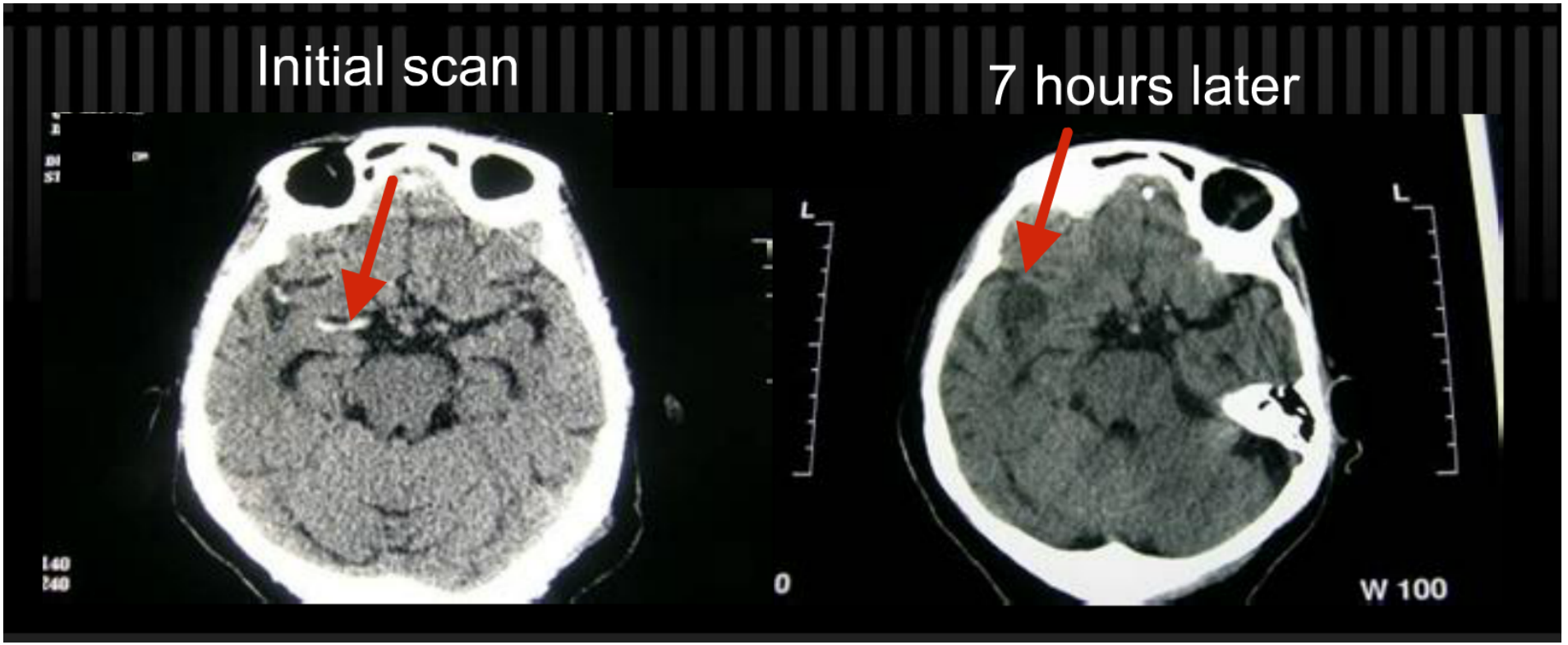

Source: LearningRadiology.com

Unusual variant of the Nutcracker Fracture of the calcaneus and tarsal navicular

Axial slice of the right foot

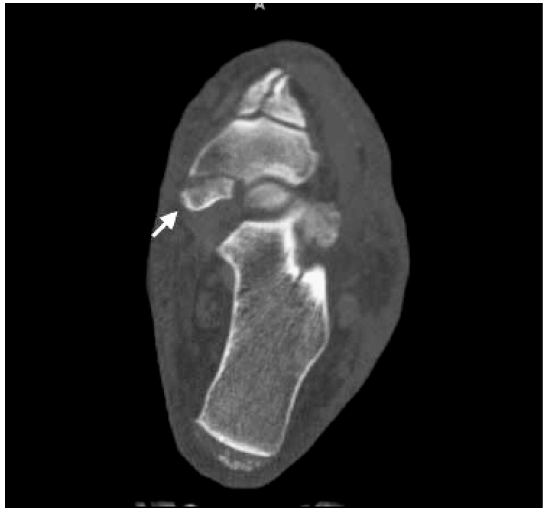

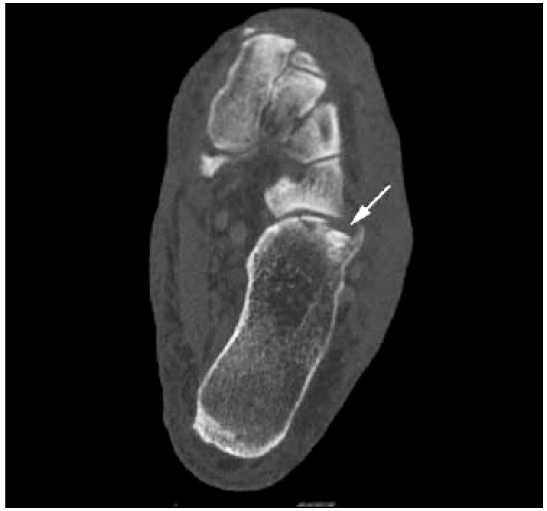

Another axial slice

Sagittal slice

3D render

[Gajendran, Yoo & Hunter, Radiology Case Reports **3** (2008)]

Outline

X-ray intensity attenuates inside matter, here shown with the Shepp-Logan phantom

(Loading video)

X-ray intensity attenuates inside matter, here shown with a homogeneous block

(Loading video)

X-ray intensity attenuates inside matter, here shown with two homogeneous blocks

(Loading video)

A digital X-ray detector counts how many photons arrive at each pixel

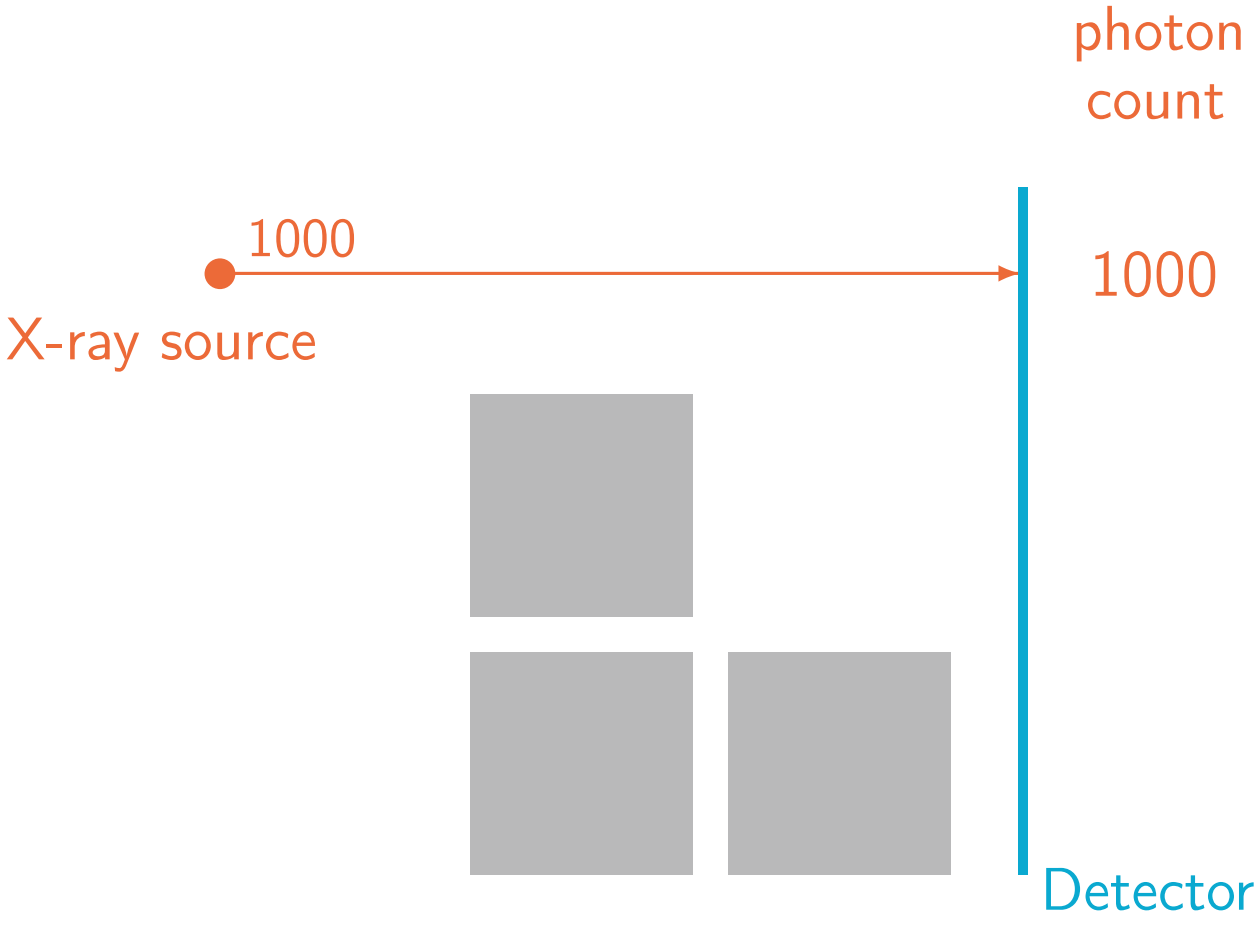

Adding material between the source and detector reveals the exponential X-ray attenuation law

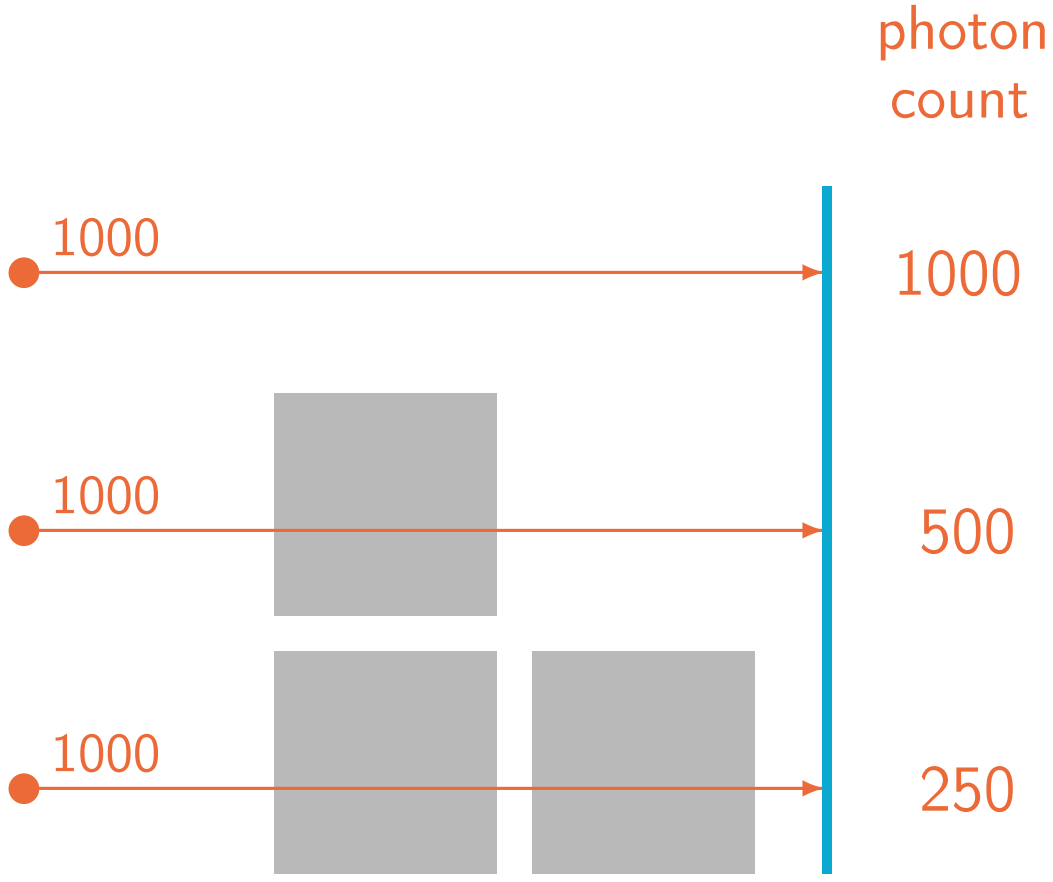

We take logarithm of the photon counts to compensate for the exponential attenuation law

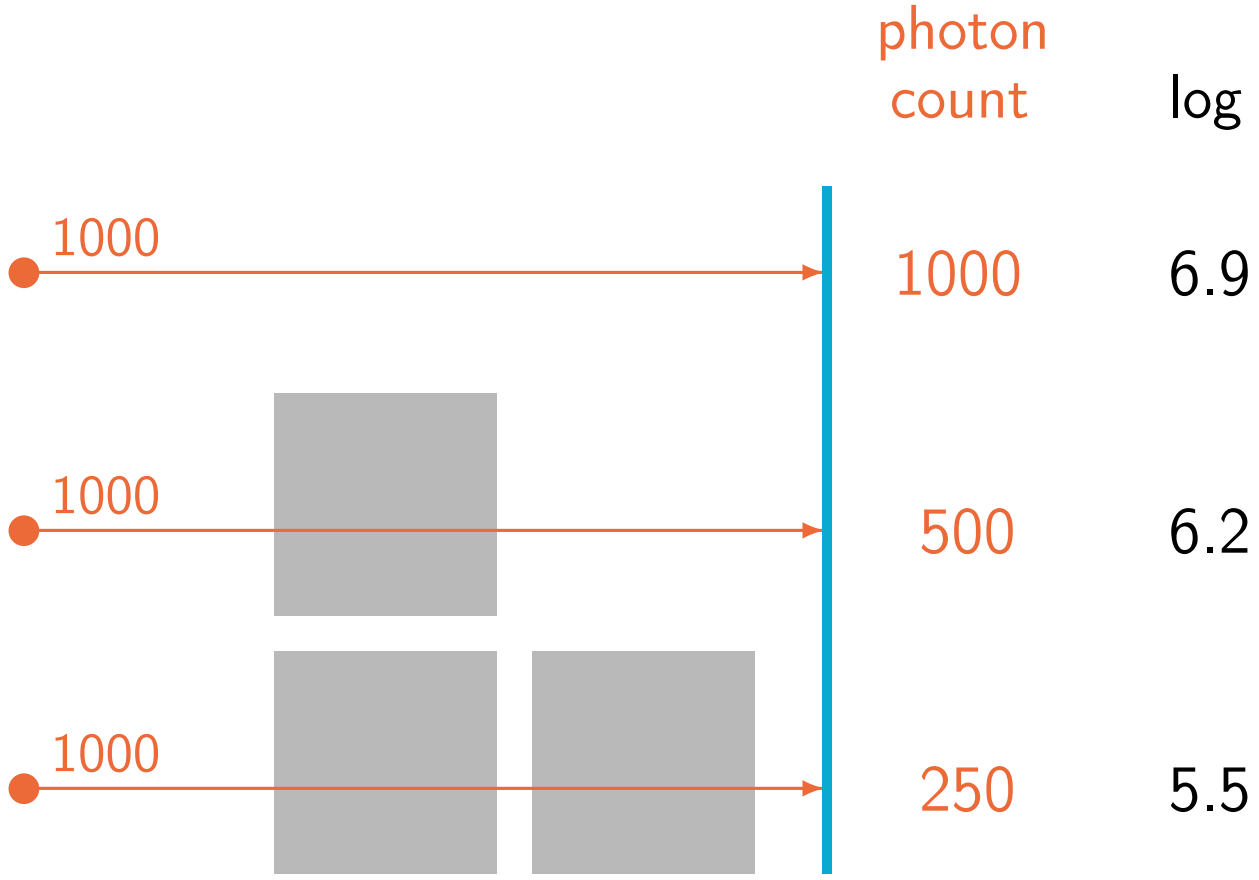

Final calibration step is to subtract the logarithms from the empty space value (here 6.9)

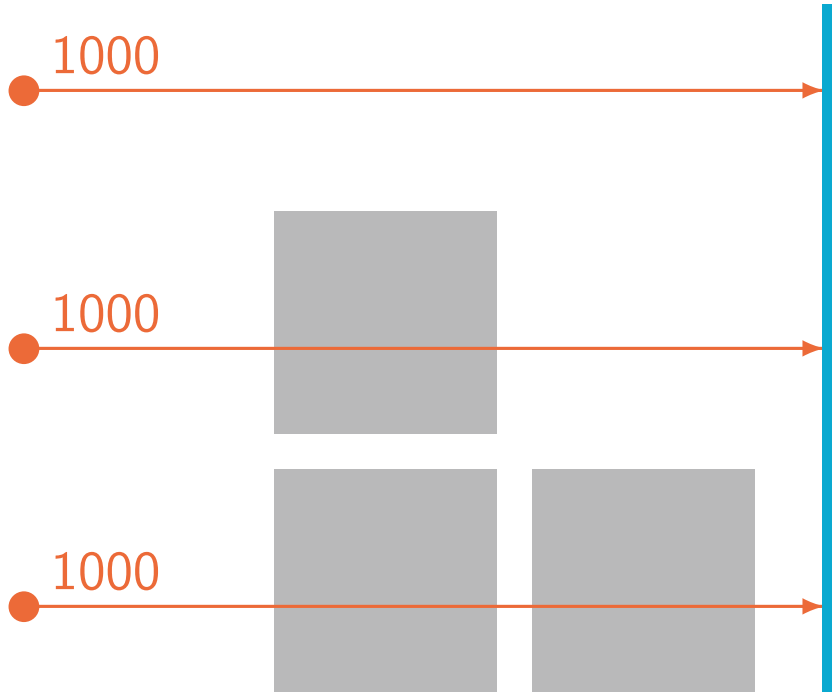

photon count	log	line integral
1000	6.9	0.0
500	6.2	0.7
250	5.5	1.4

After calibration we are observing how much attenuating matter the X-ray encounters

(Loading video)

After calibration we are observing how much attenuating matter the X-ray encounters

(Loading video)

This sweeping movement is the data collection mode of first-generation CT scanners

(Loading video)

Rotating around the object allows us to form the so-called *sinogram*

(Loading video)

This is an illustration of the standard reconstruction by filtered back-projection

(Loading video)

This is my new X-ray laboratory at University of Helsinki

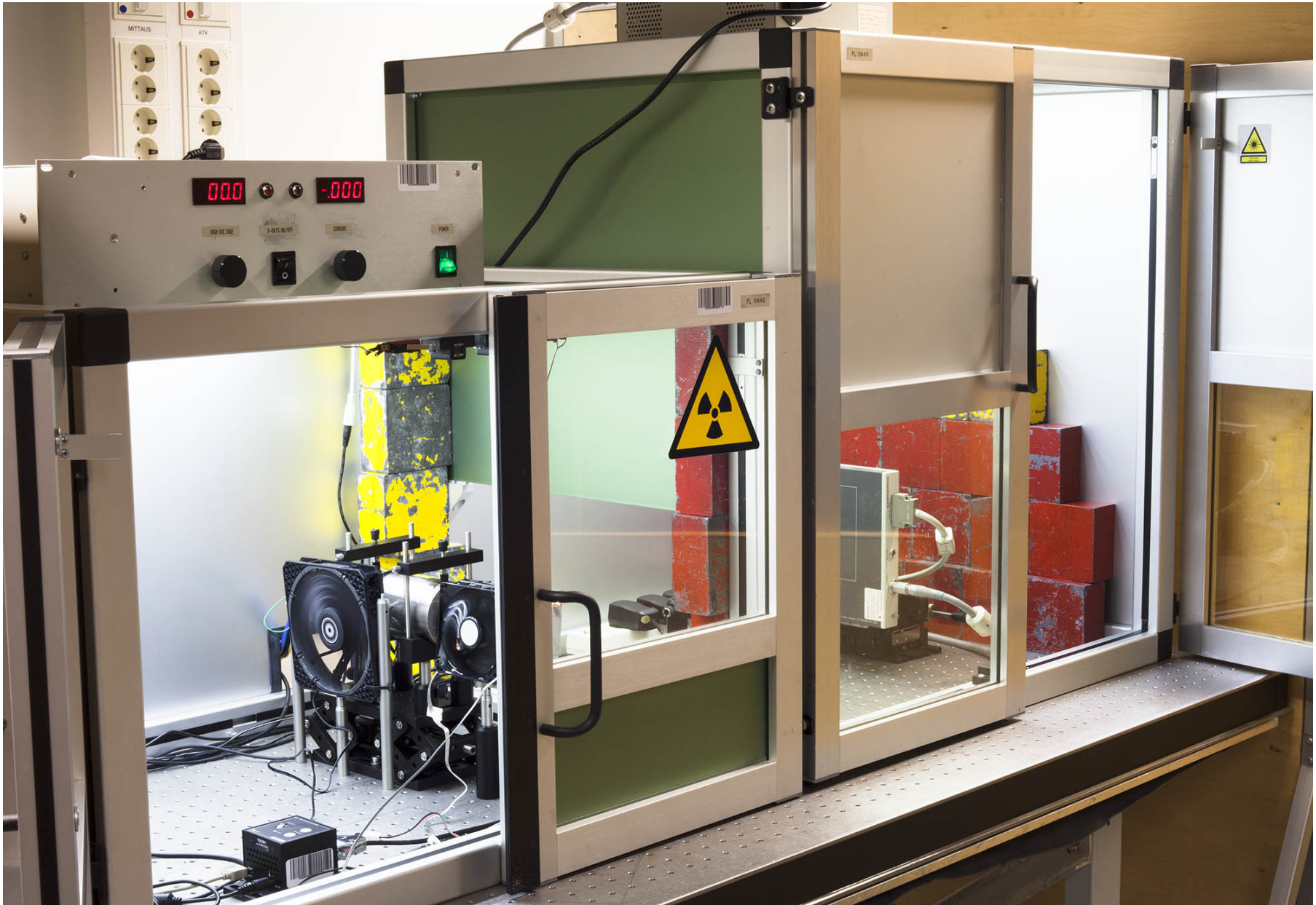

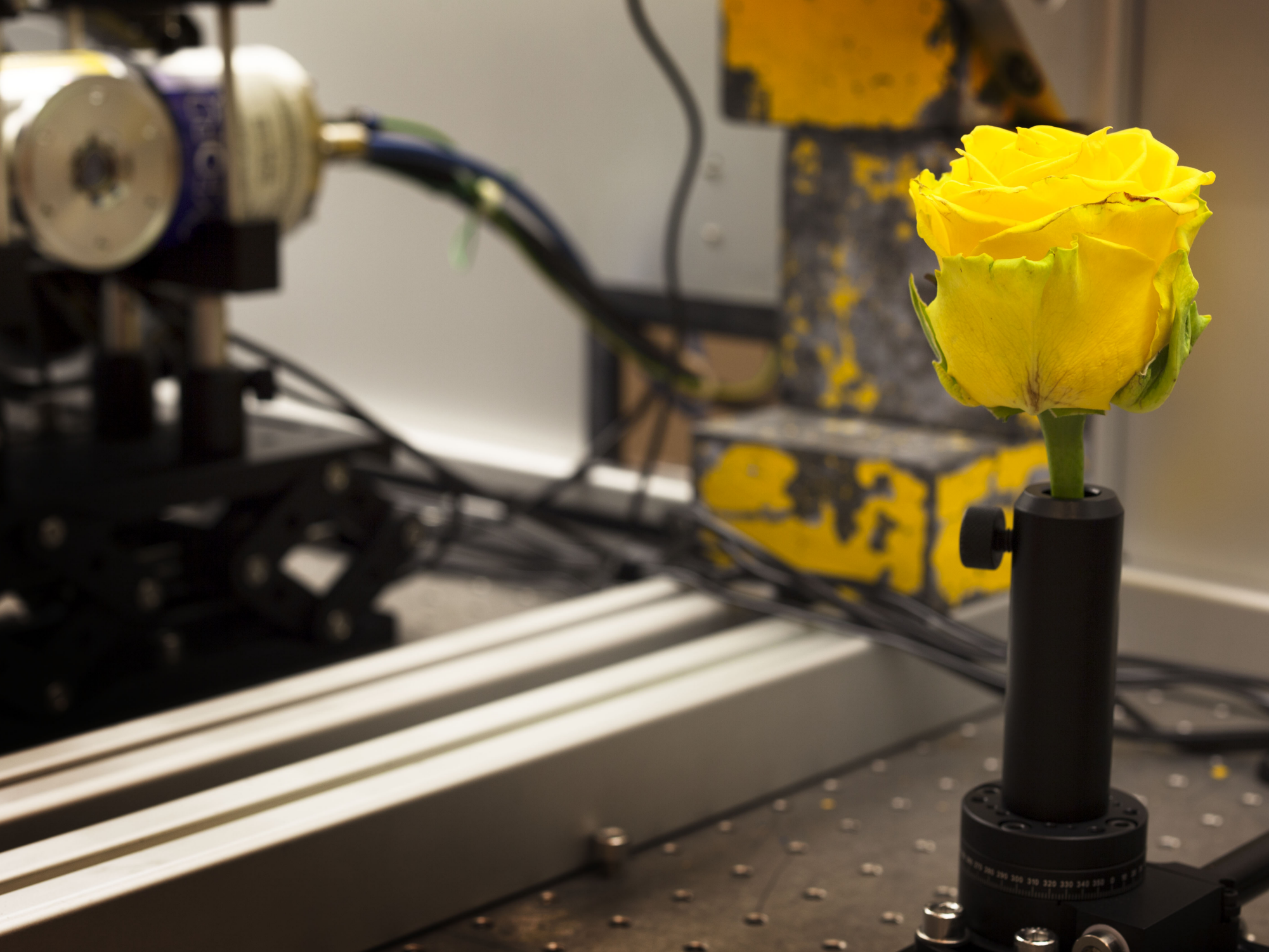

Outline

Let us study a simple two-dimensional example of tomographic imaging

4	4	5
1	3	4
1	0	2

Tomography is based on measuring densities of matter using X-ray attenuation data

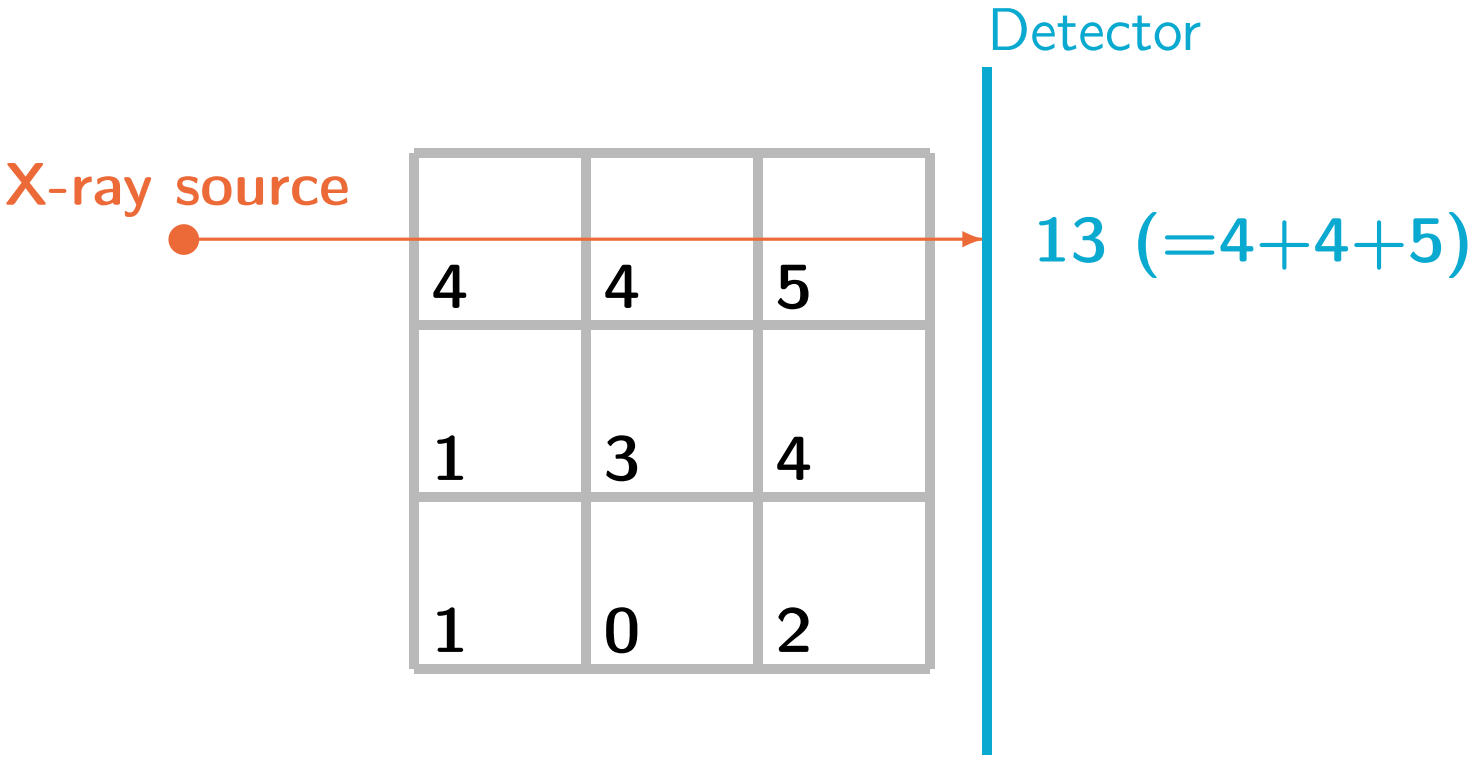

A projection image is produced by parallel X-rays and several detector pixels (here three pixels)

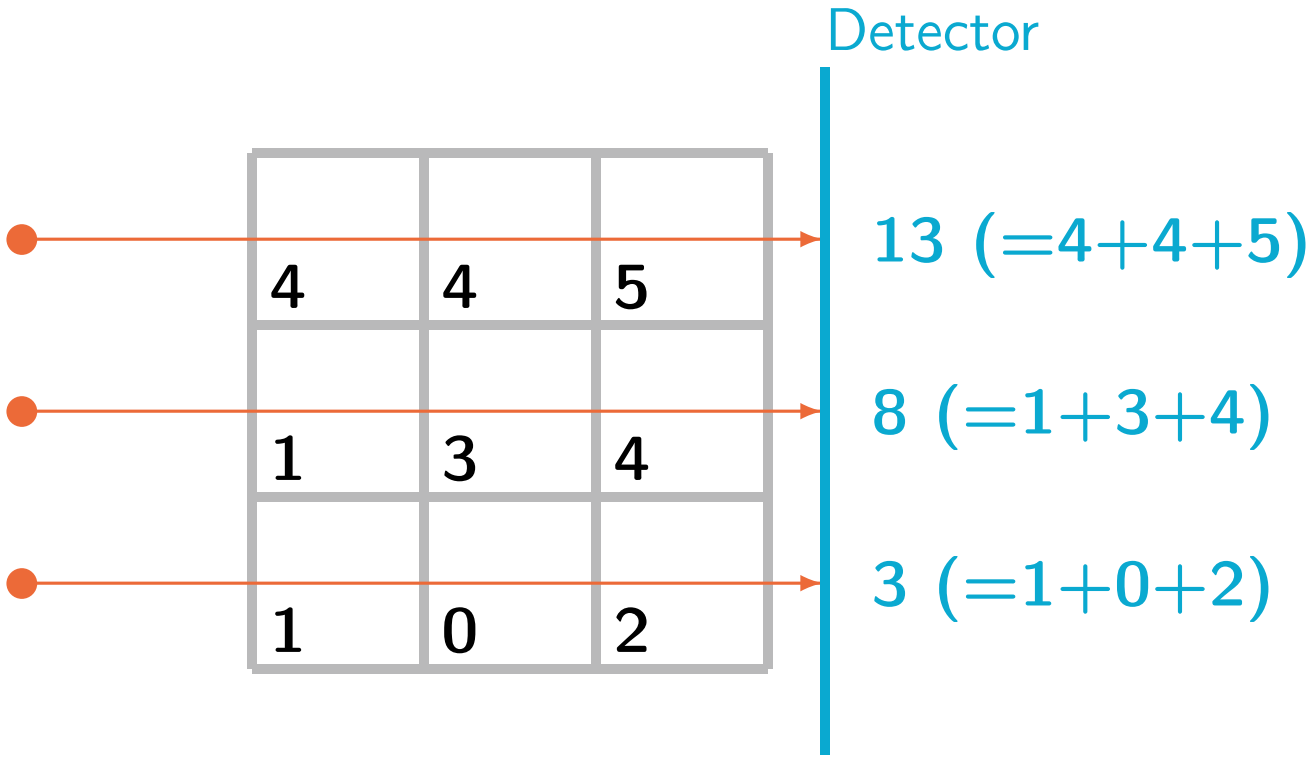

For tomographic imaging it is essential to record projection images from different directions

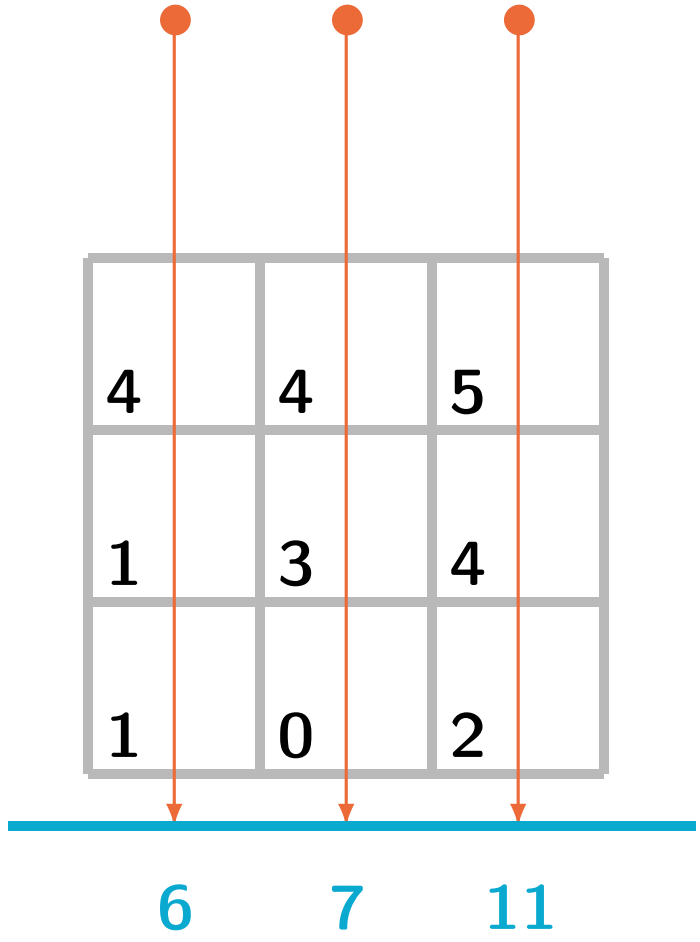

The length of X-rays traveling inside each pixel is important, thus here the square roots

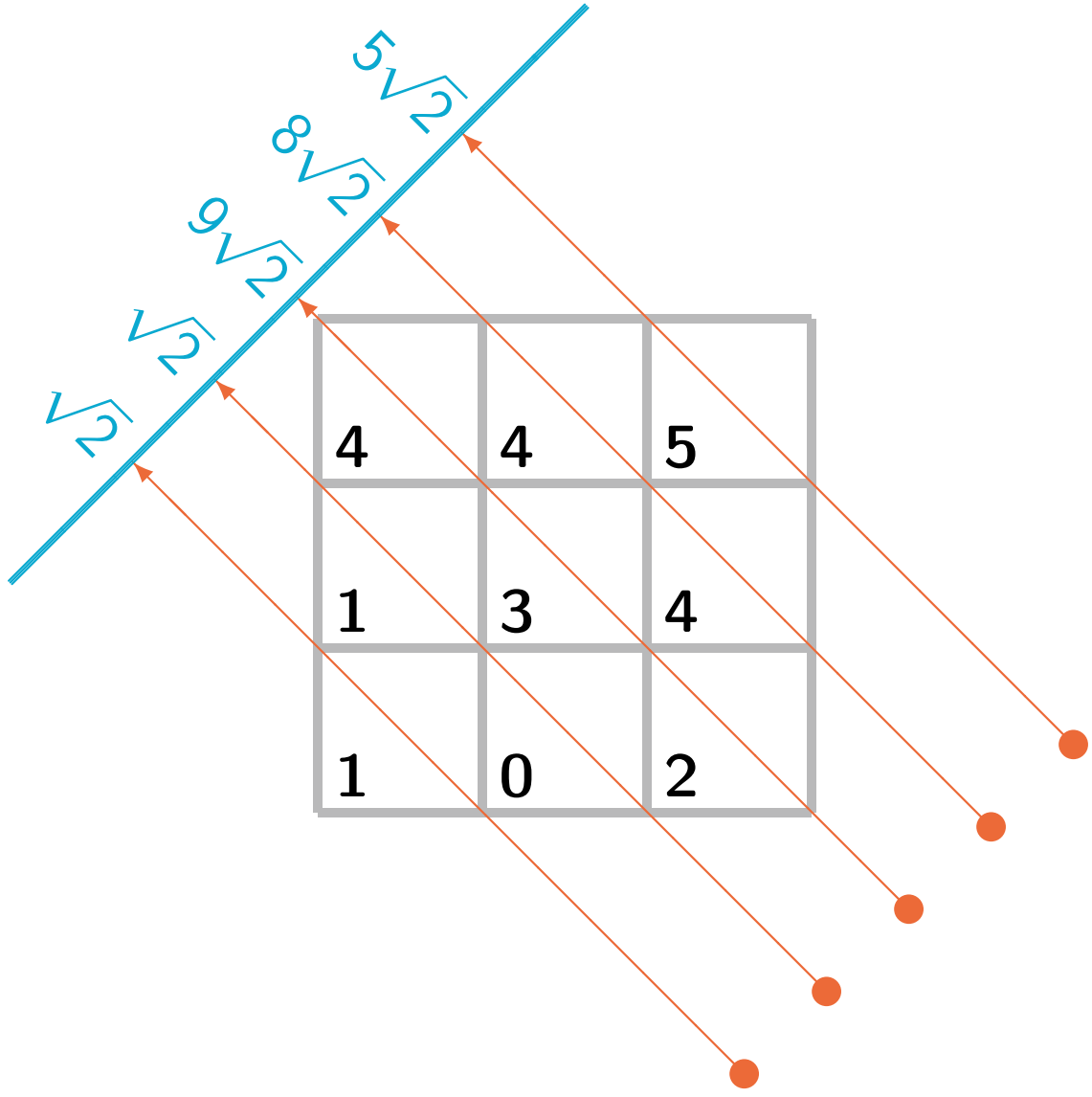

The direct problem of tomography is to find the projection images from known tissue

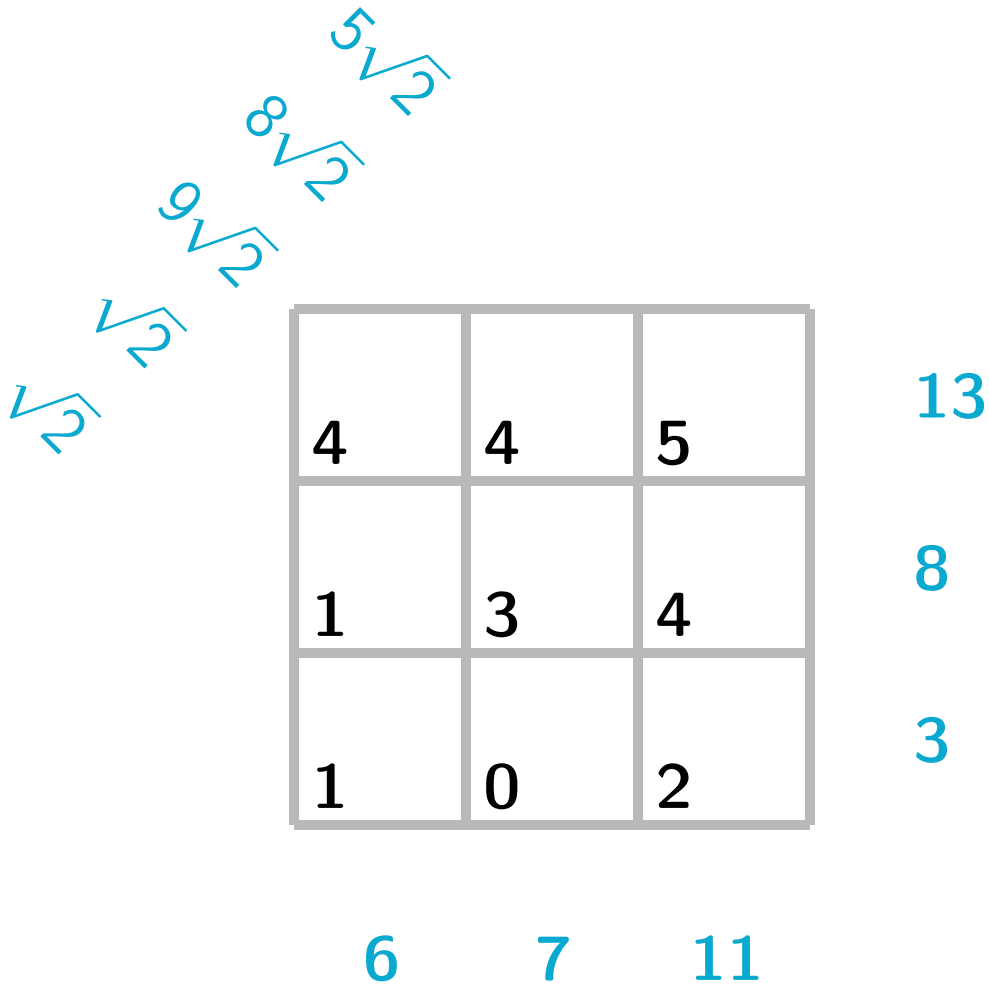

The inverse problem of tomography is to reconstruct the interior from X-ray data

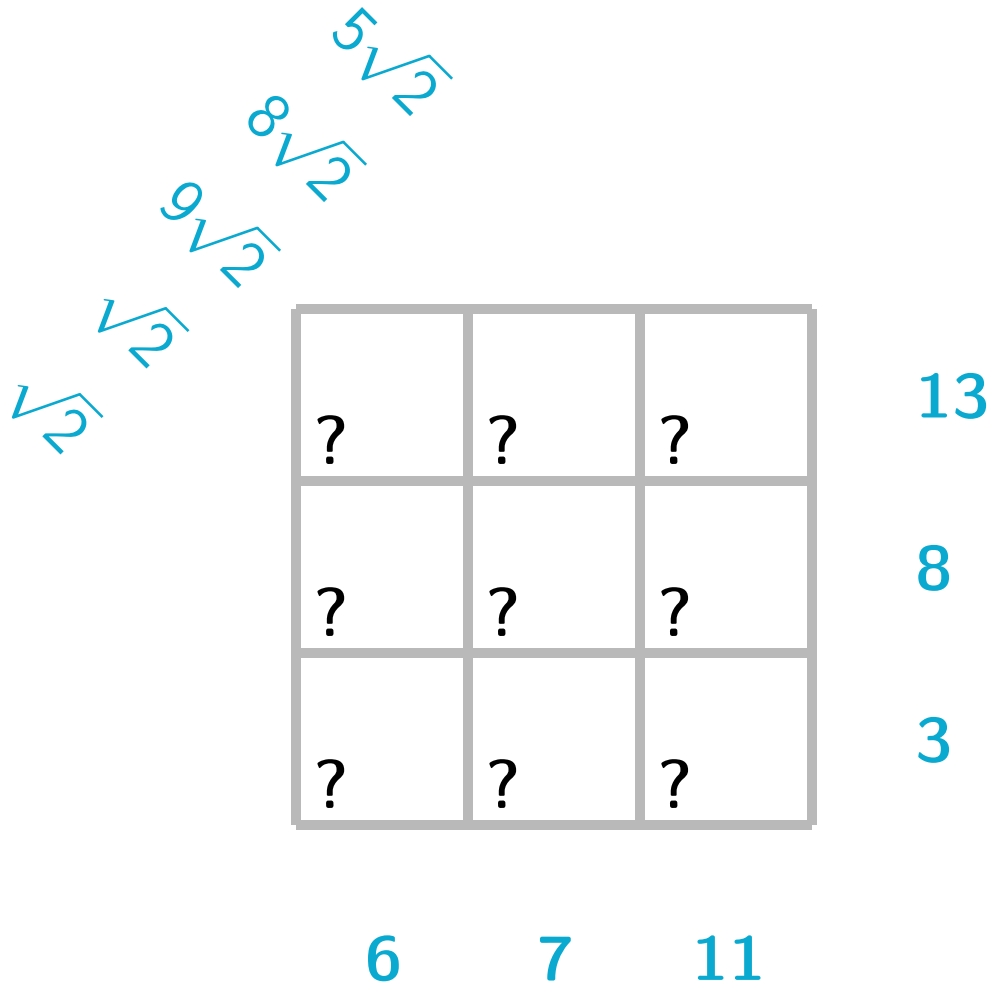

The limited-angle problem is harder than the full-angle problem

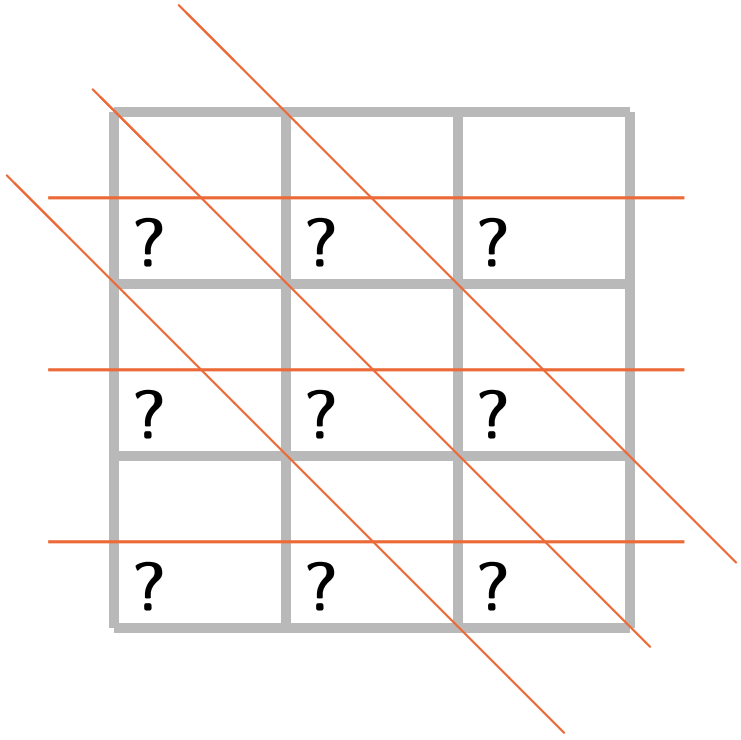

9 unknowns,
6 equations

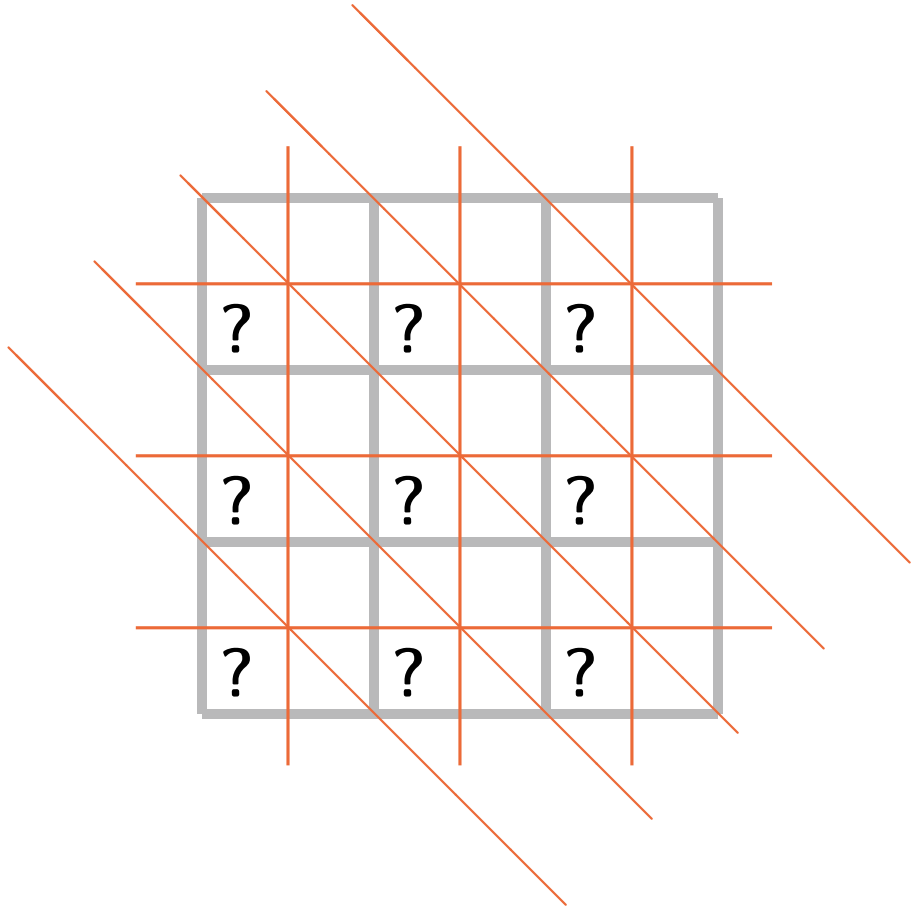

9 unknowns,
11 equations

In limited-angle imaging, different objects may produce the same data

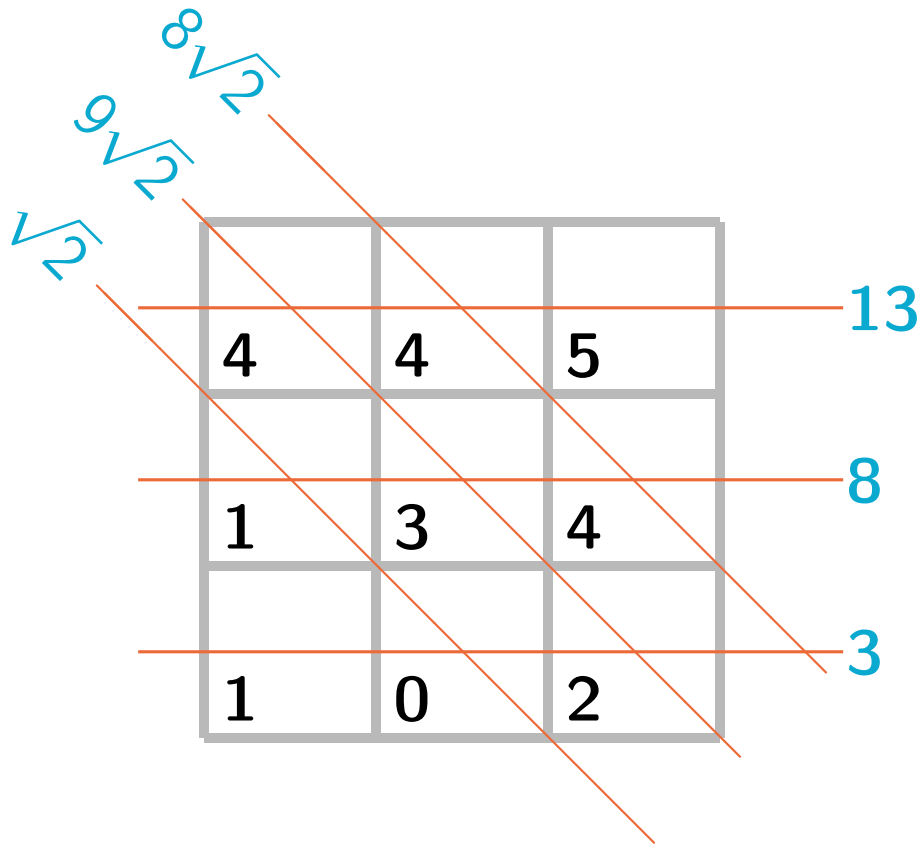

Reconstruction requires additional *a priori* information

5	6	2
1	5	2
4	0	-1

9	1	3
1	0	7
3	0	0

We write the reconstruction problem in matrix form

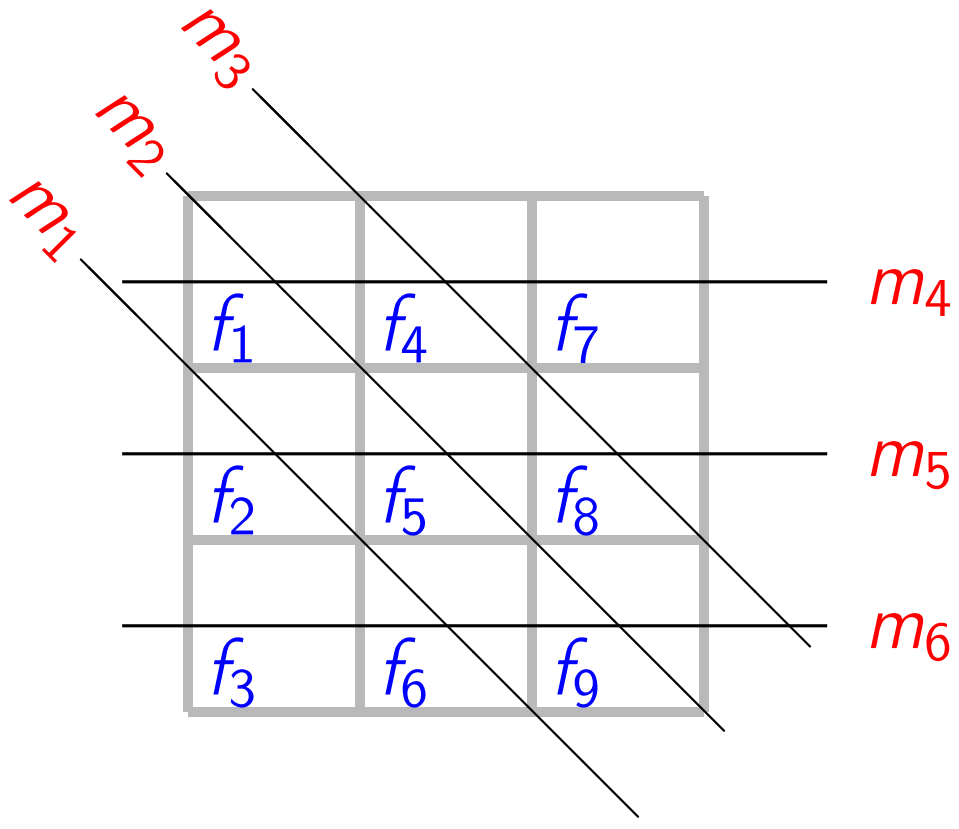

$$f = \begin{bmatrix} f_1 \\ f_2 \\ f_3 \\ f_4 \\ f_5 \\ f_6 \\ f_7 \\ f_8 \\ f_9 \end{bmatrix}, \quad m = \begin{bmatrix} m_1 \\ m_2 \\ m_3 \\ m_4 \\ m_5 \\ m_6 \end{bmatrix},$$

Measurement model: $m = Af + \varepsilon$

This is the matrix equation related to the above measurement

$$\begin{bmatrix} m_1 \\ m_2 \\ m_3 \\ m_4 \\ m_5 \\ m_6 \end{bmatrix} = \begin{bmatrix} 0 & \sqrt{2} & 0 & 0 & 0 & \sqrt{2} & 0 & 0 & 0 \\ \sqrt{2} & 0 & 0 & 0 & \sqrt{2} & 0 & 0 & 0 & \sqrt{2} \\ 0 & 0 & 0 & \sqrt{2} & 0 & 0 & 0 & \sqrt{2} & 0 \\ 1 & 0 & 0 & 1 & 0 & 0 & 1 & 0 & 0 \\ 0 & 1 & 0 & 0 & 1 & 0 & 0 & 1 & 0 \\ 0 & 0 & 1 & 0 & 0 & 1 & 0 & 0 & 1 \end{bmatrix} \begin{bmatrix} f_1 \\ f_2 \\ f_3 \\ f_4 \\ f_5 \\ f_6 \\ f_7 \\ f_8 \\ f_9 \end{bmatrix} + \begin{bmatrix} \varepsilon_1 \\ \varepsilon_2 \\ \varepsilon_3 \\ \varepsilon_4 \\ \varepsilon_5 \\ \varepsilon_6 \end{bmatrix}$$

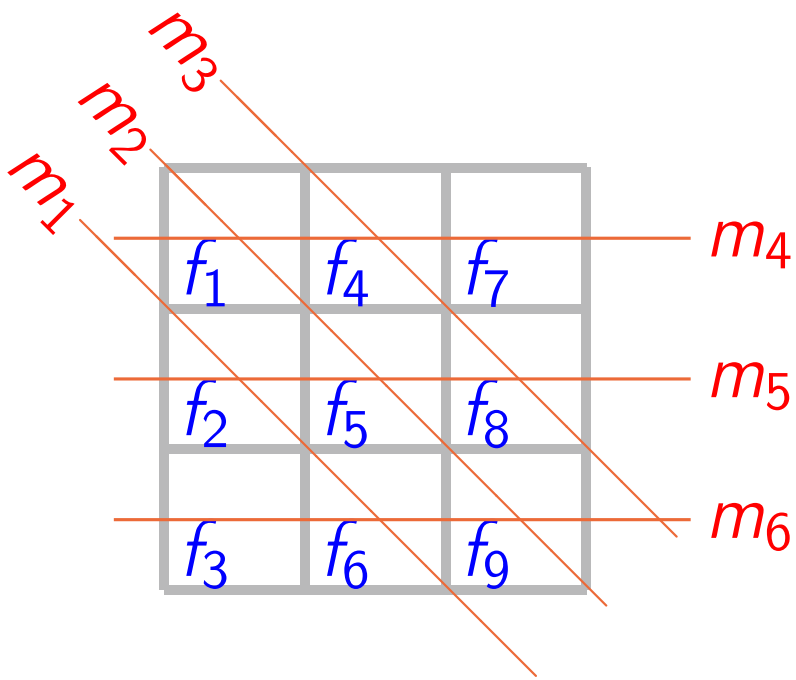

This is the matrix equation related to the above measurement

$$\begin{bmatrix} m_1 \\ m_2 \\ m_3 \\ m_4 \\ m_5 \\ m_6 \end{bmatrix} = \begin{bmatrix} 0 & \sqrt{2} & 0 & 0 & 0 & \sqrt{2} & 0 & 0 & 0 \\ \sqrt{2} & 0 & 0 & 0 & \sqrt{2} & 0 & 0 & 0 & \sqrt{2} \\ 0 & 0 & 0 & \sqrt{2} & 0 & 0 & 0 & \sqrt{2} & 0 \\ 1 & 0 & 0 & 1 & 0 & 0 & 1 & 0 & 0 \\ 0 & 1 & 0 & 0 & 1 & 0 & 0 & 1 & 0 \\ 0 & 0 & 1 & 0 & 0 & 1 & 0 & 0 & 1 \end{bmatrix} \begin{bmatrix} f_1 \\ f_2 \\ f_3 \\ f_4 \\ f_5 \\ f_6 \\ f_7 \\ f_8 \\ f_9 \end{bmatrix} + \begin{bmatrix} \varepsilon_1 \\ \varepsilon_2 \\ \varepsilon_3 \\ \varepsilon_4 \\ \varepsilon_5 \\ \varepsilon_6 \end{bmatrix}$$

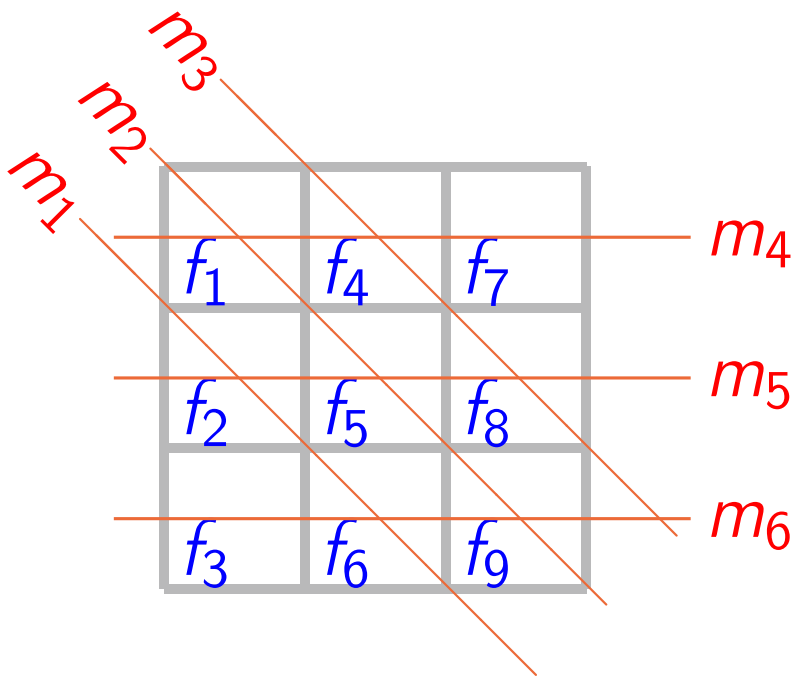

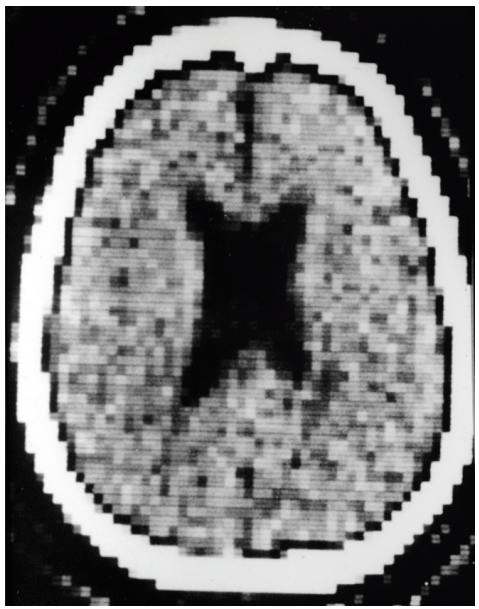

Construction of the sinogram

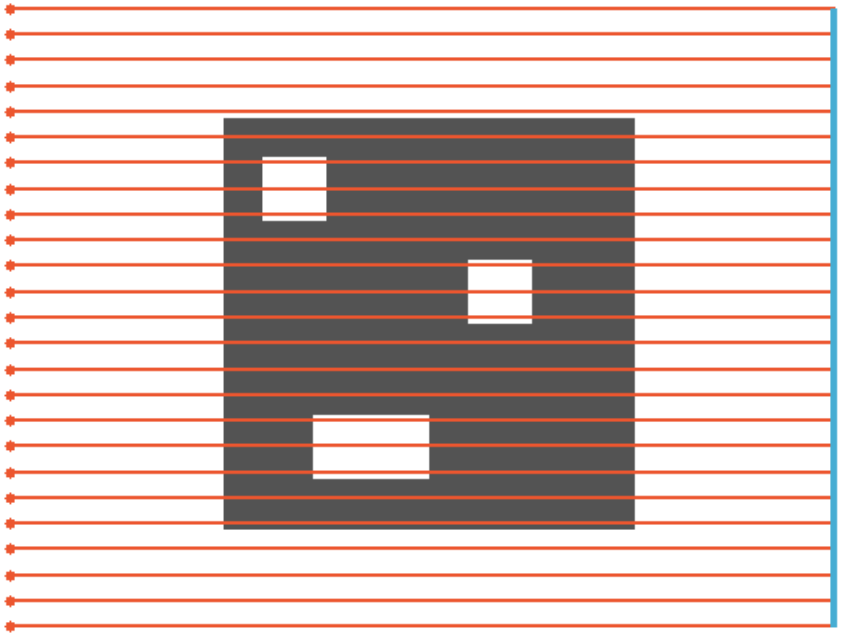

Construction of the sinogram

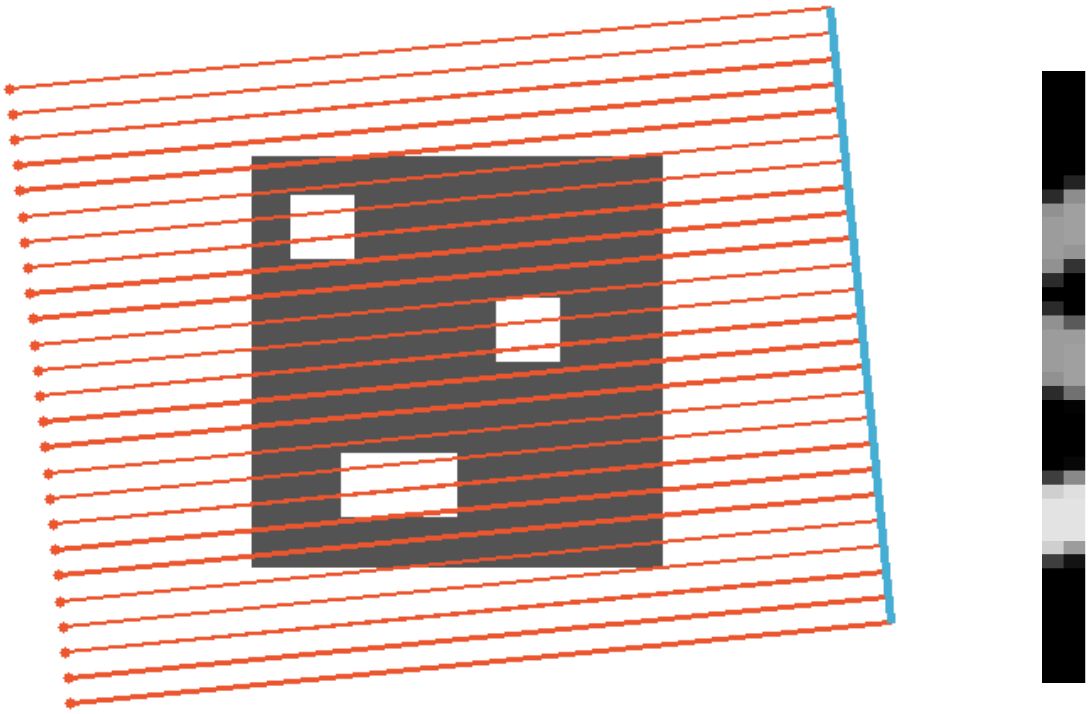

Construction of the sinogram

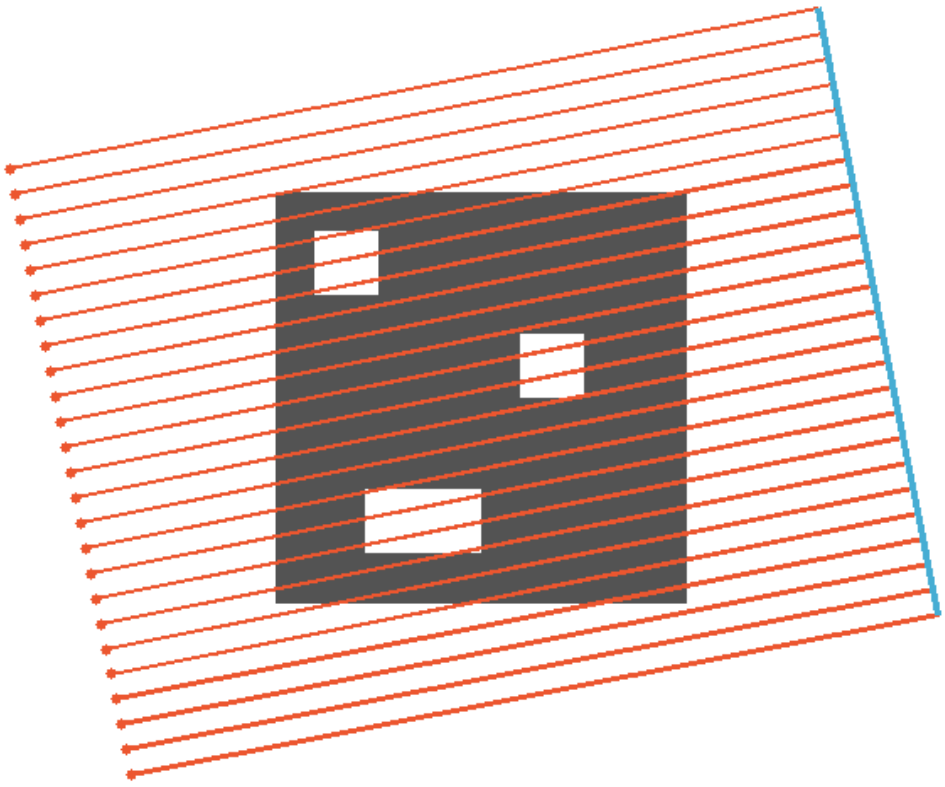

Construction of the sinogram

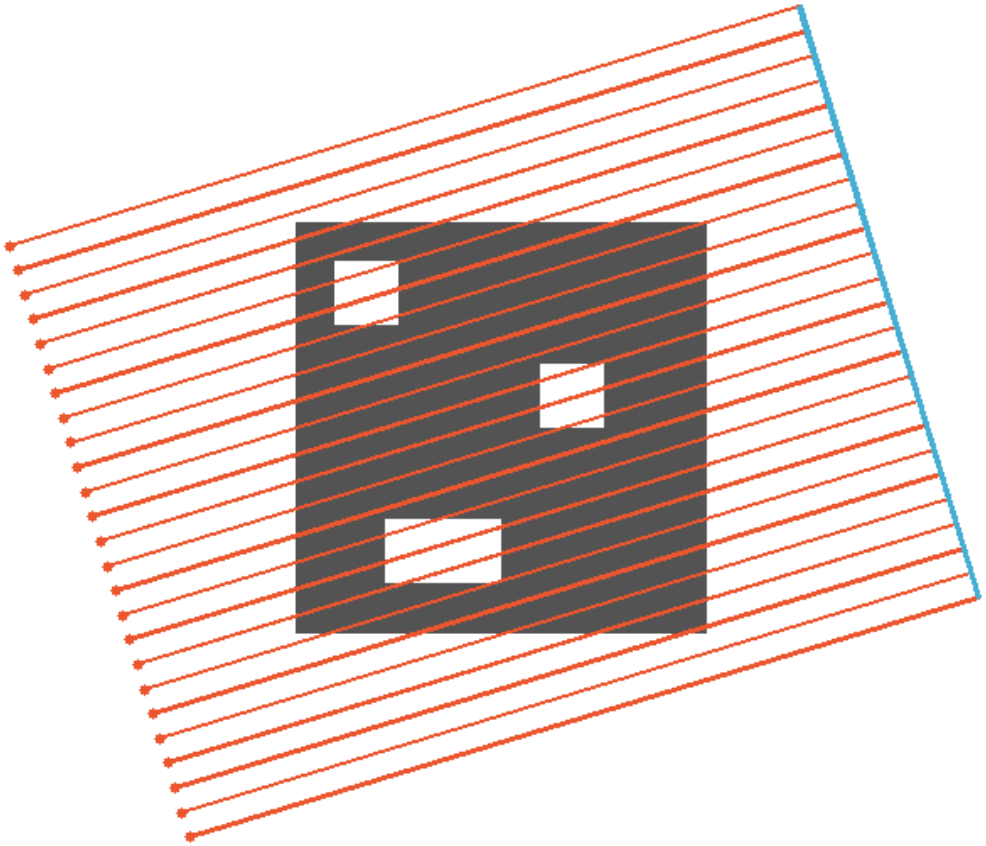

Construction of the sinogram

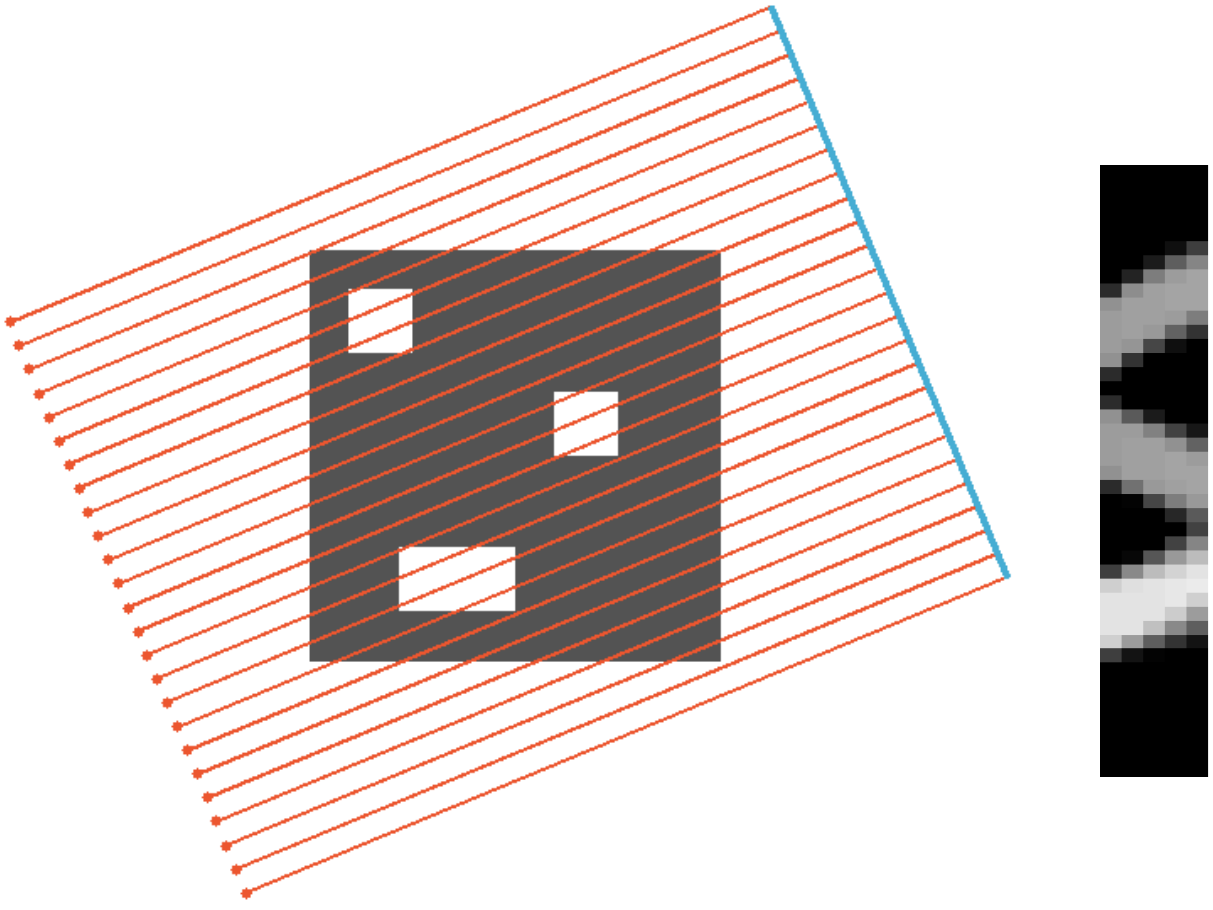

Construction of the sinogram

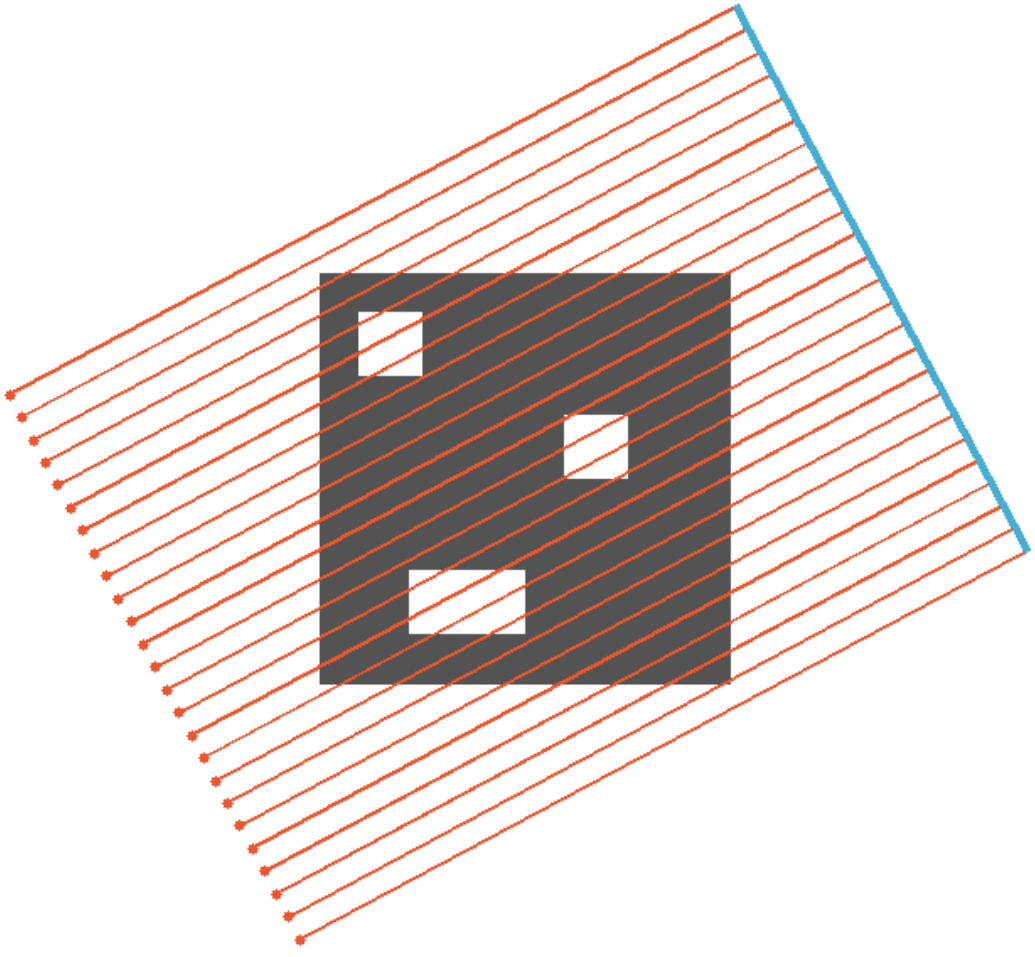

Construction of the sinogram

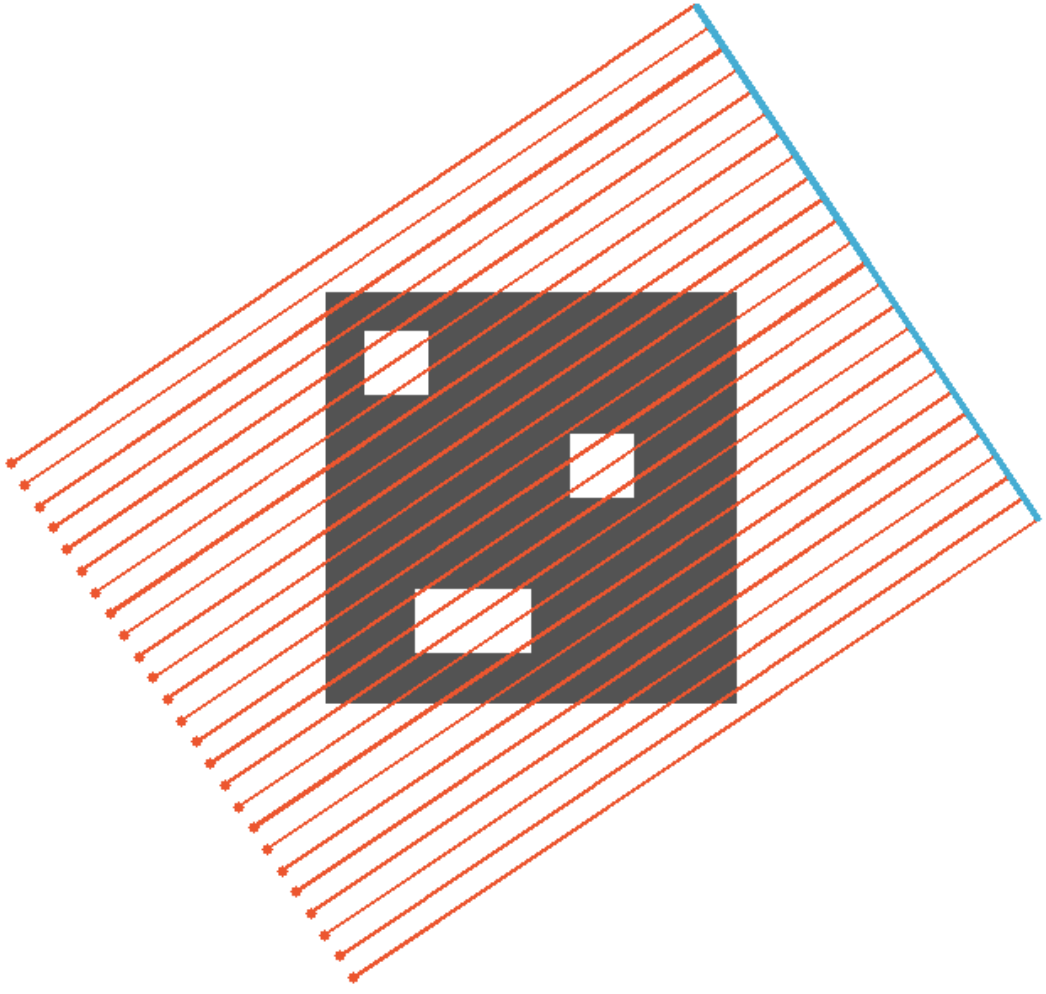

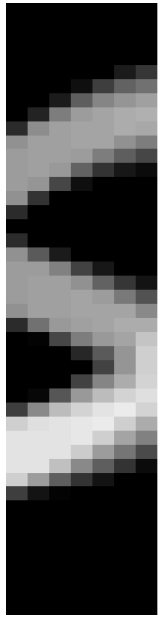

Construction of the sinogram

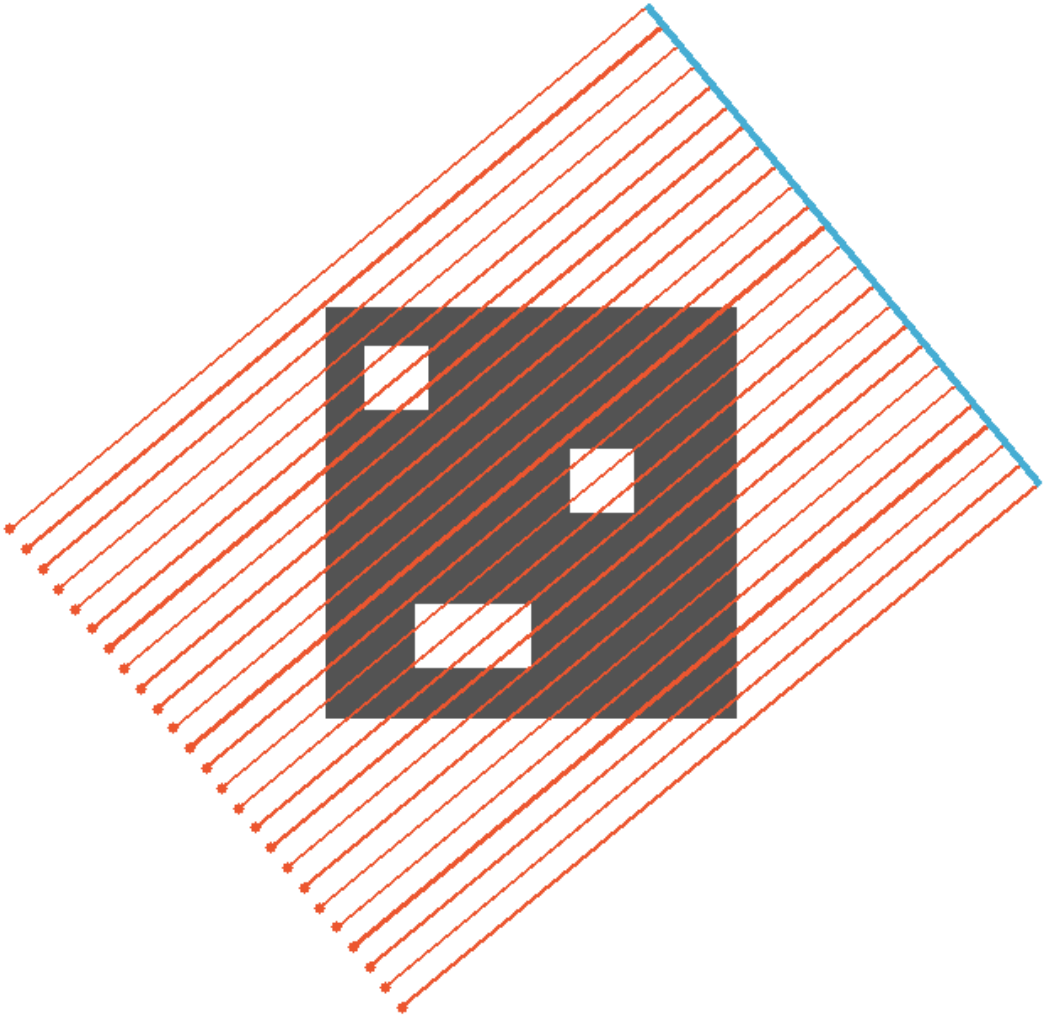

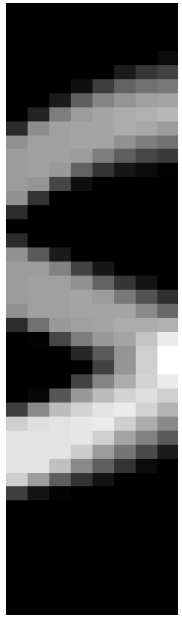

Construction of the sinogram

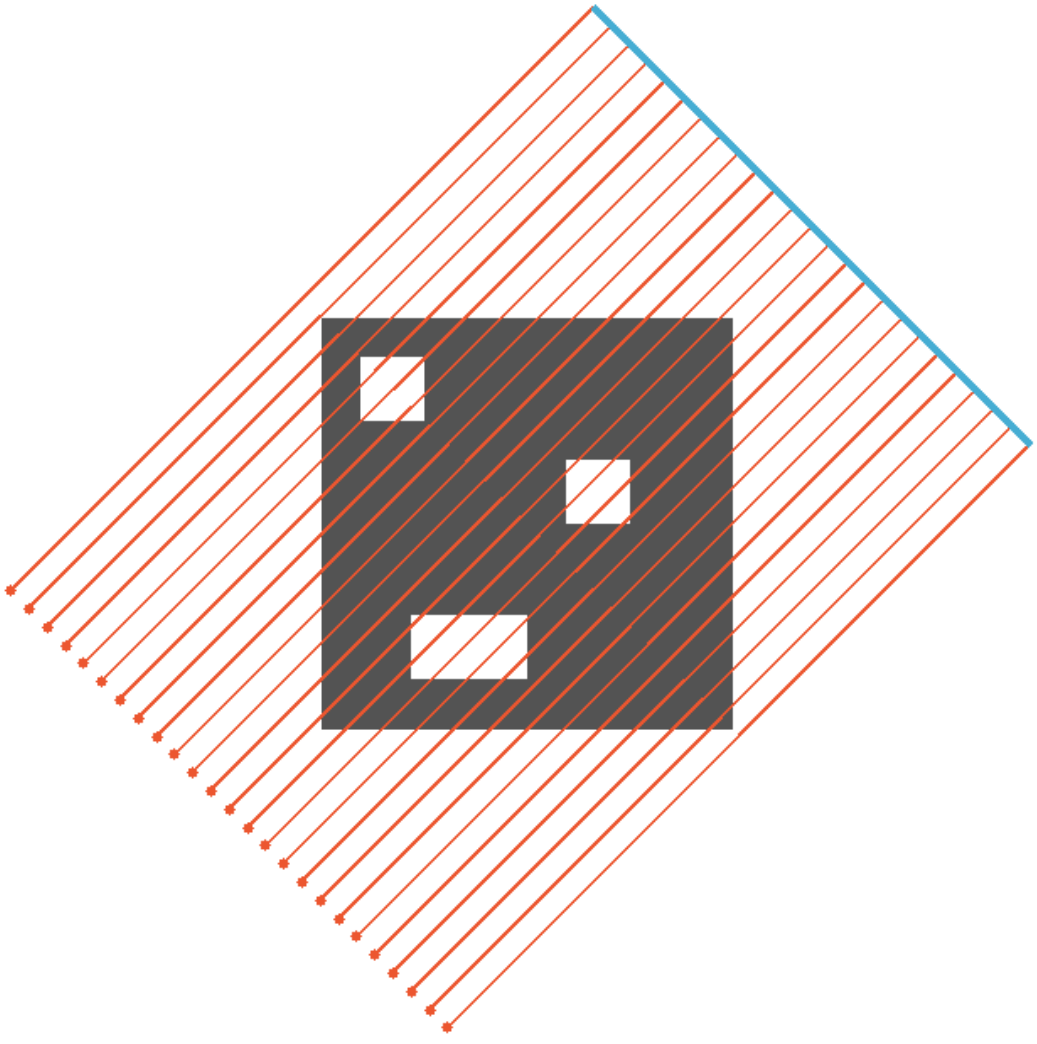

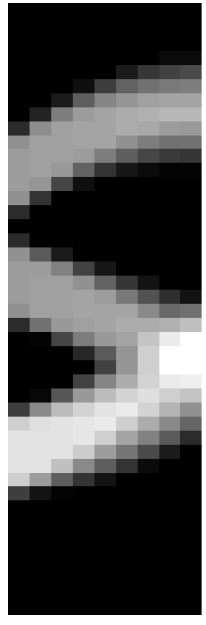

Construction of the sinogram

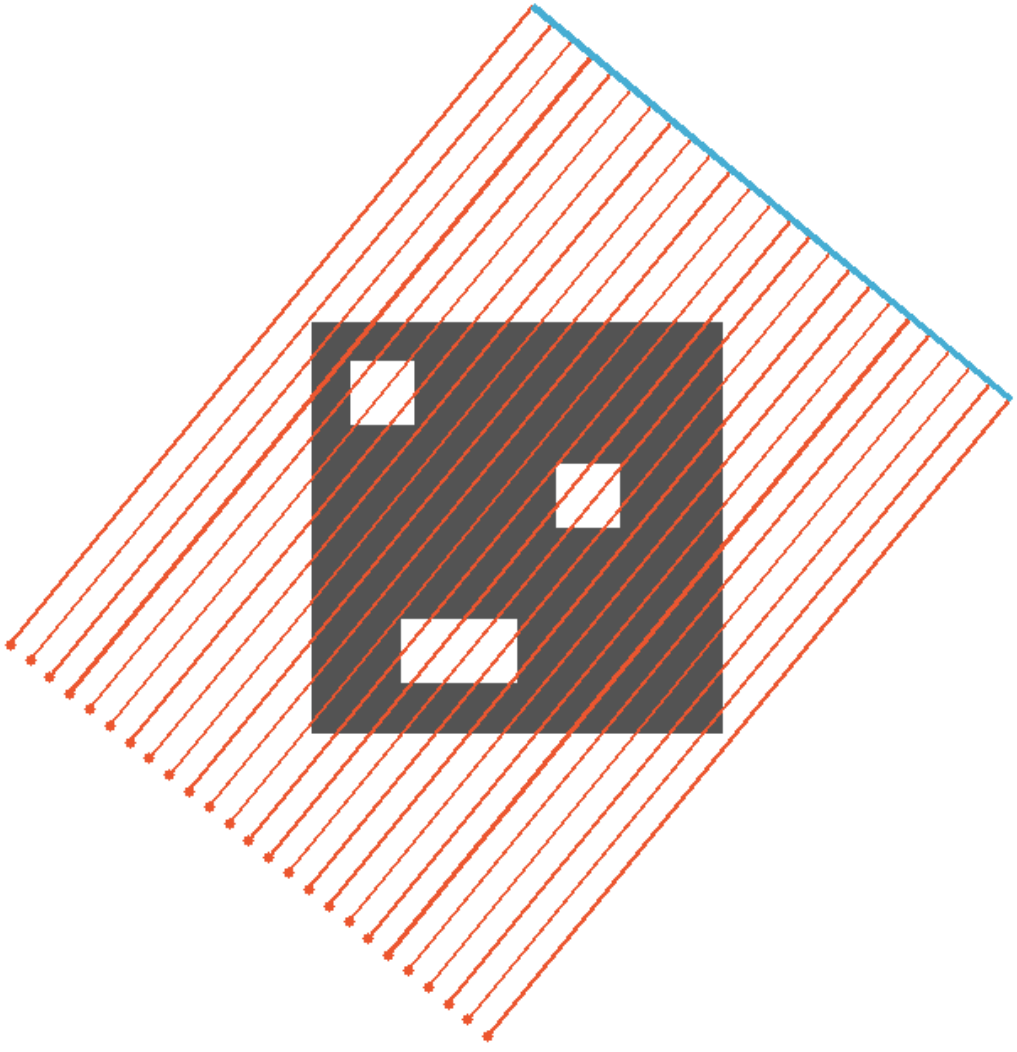

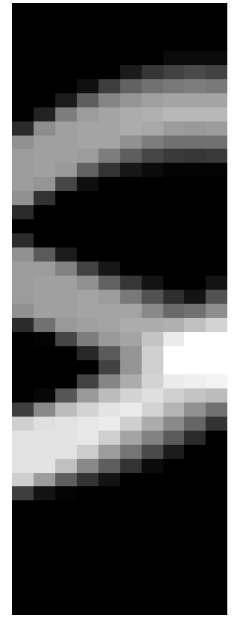

Construction of the sinogram

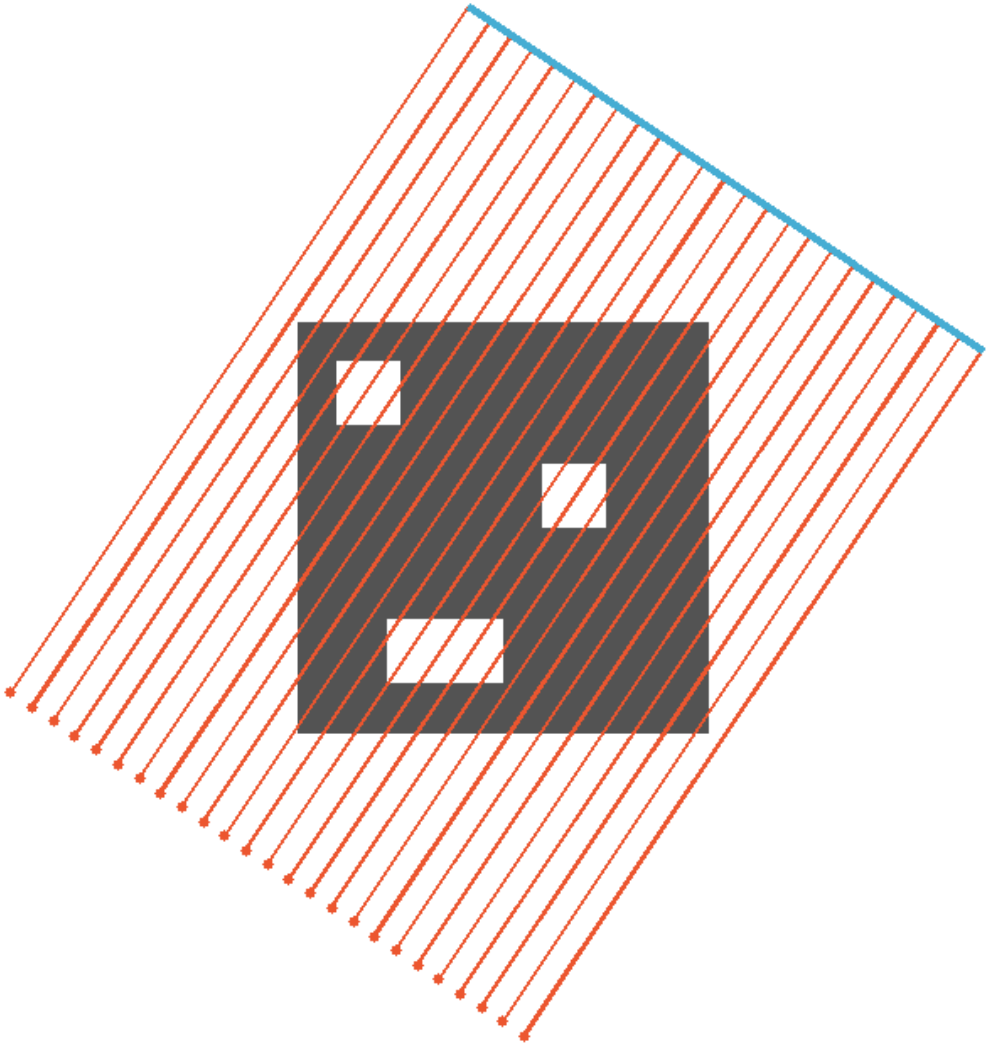

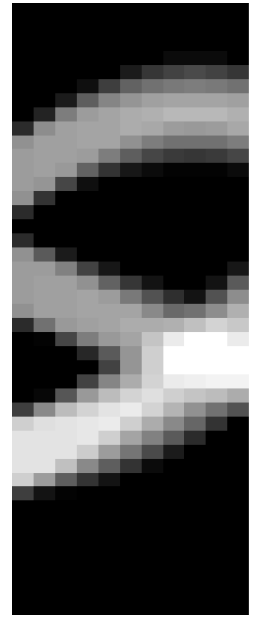

Construction of the sinogram

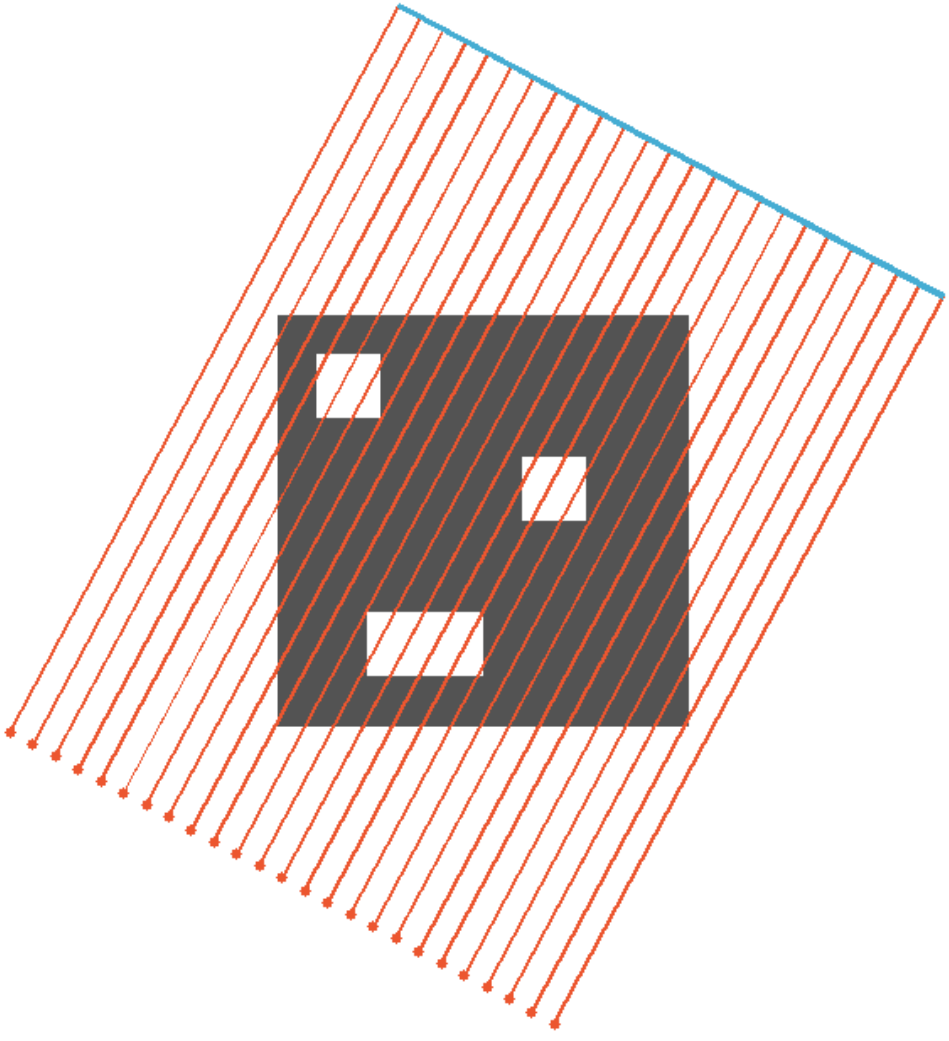

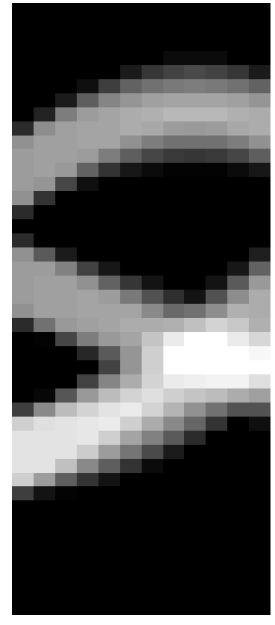

Construction of the sinogram

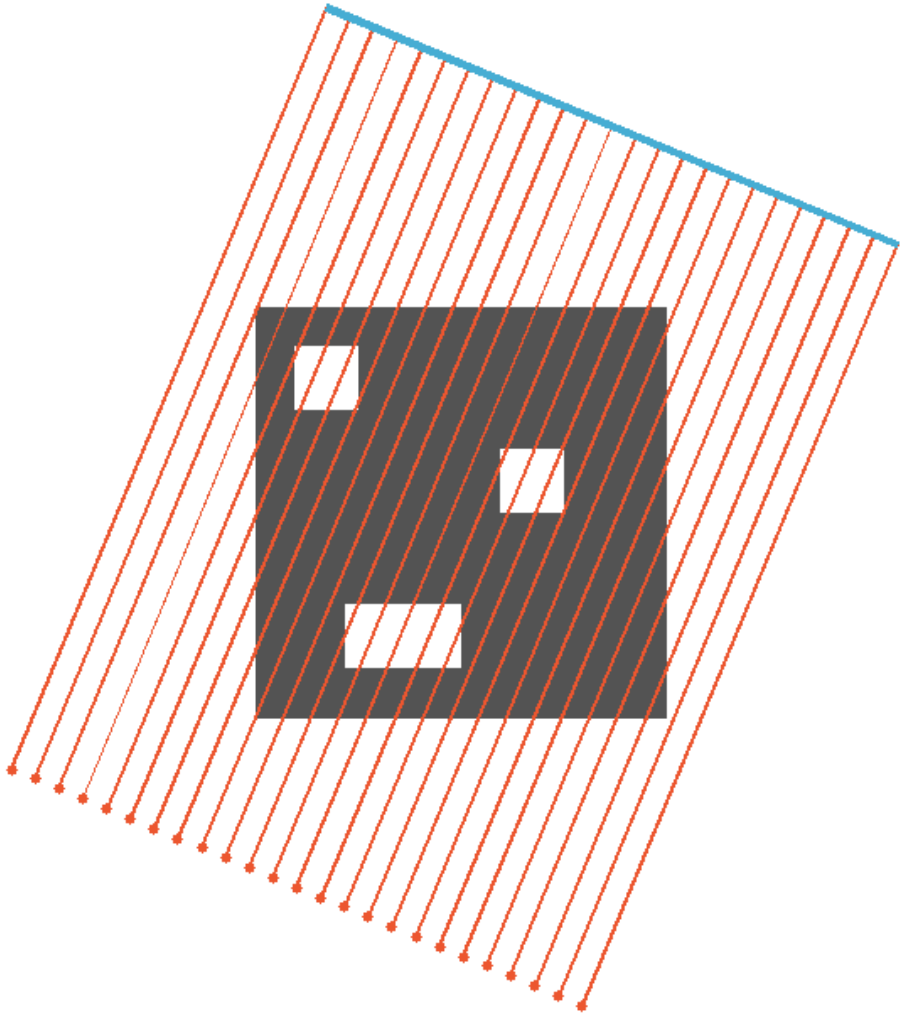

Construction of the sinogram

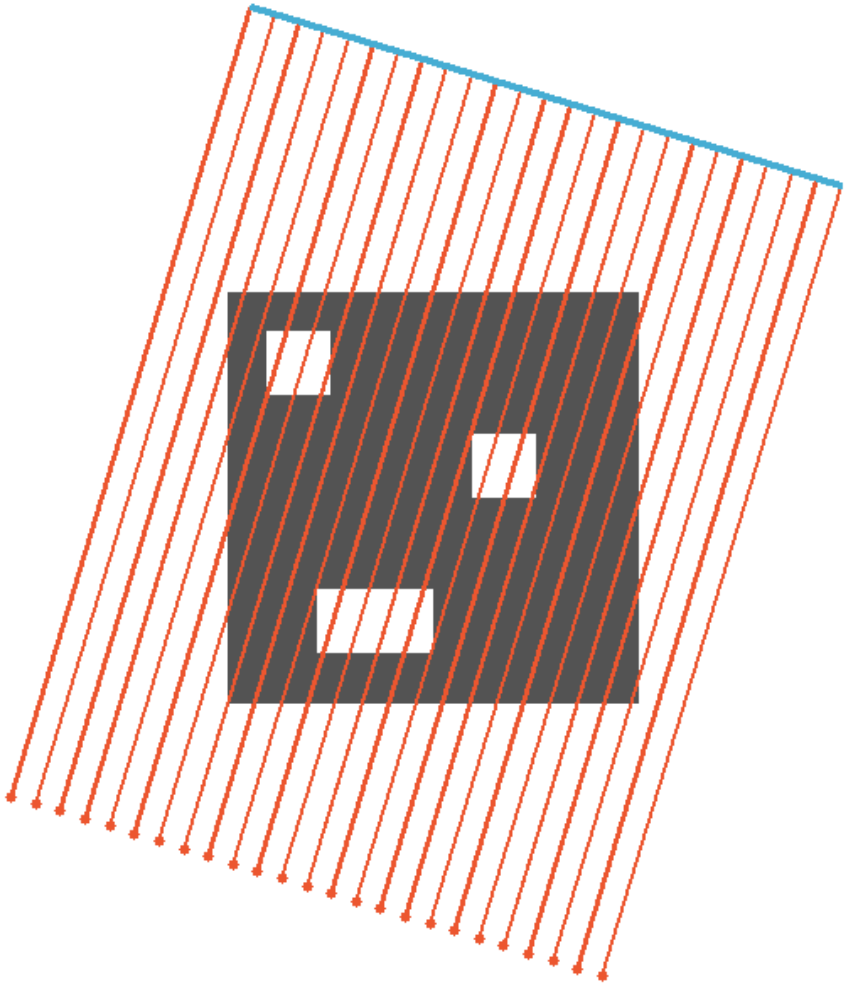

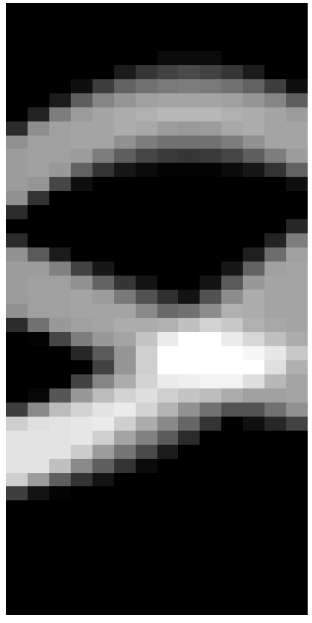

Construction of the sinogram

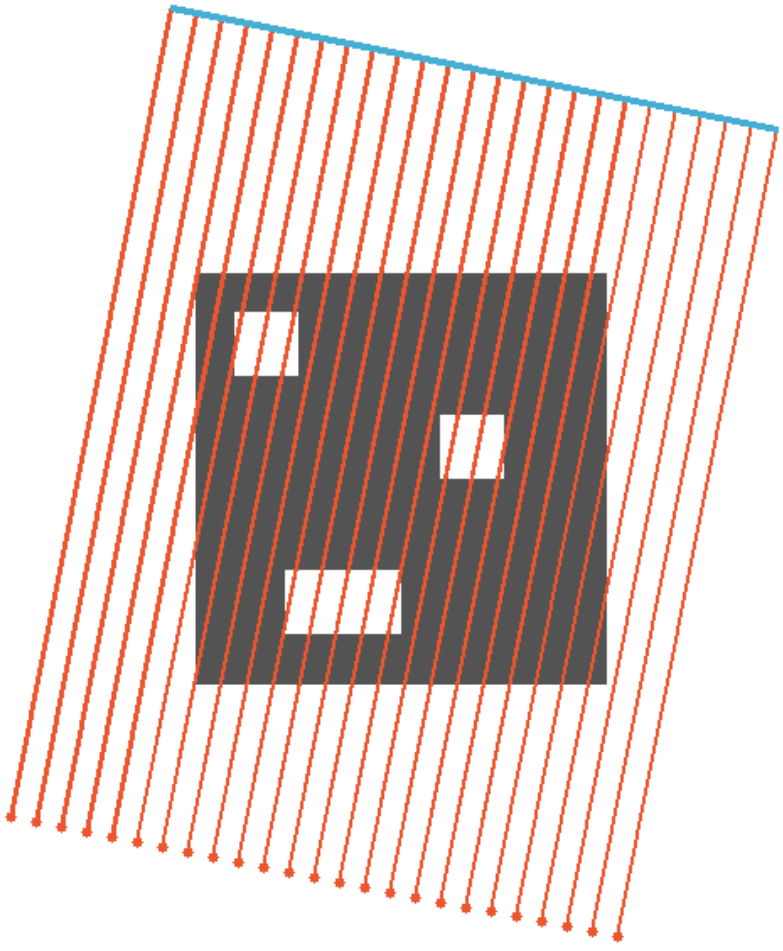

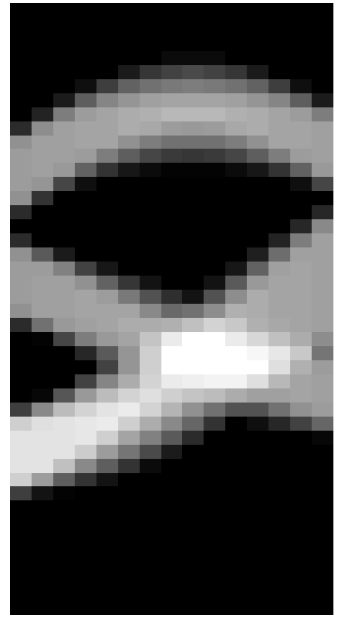

Construction of the sinogram

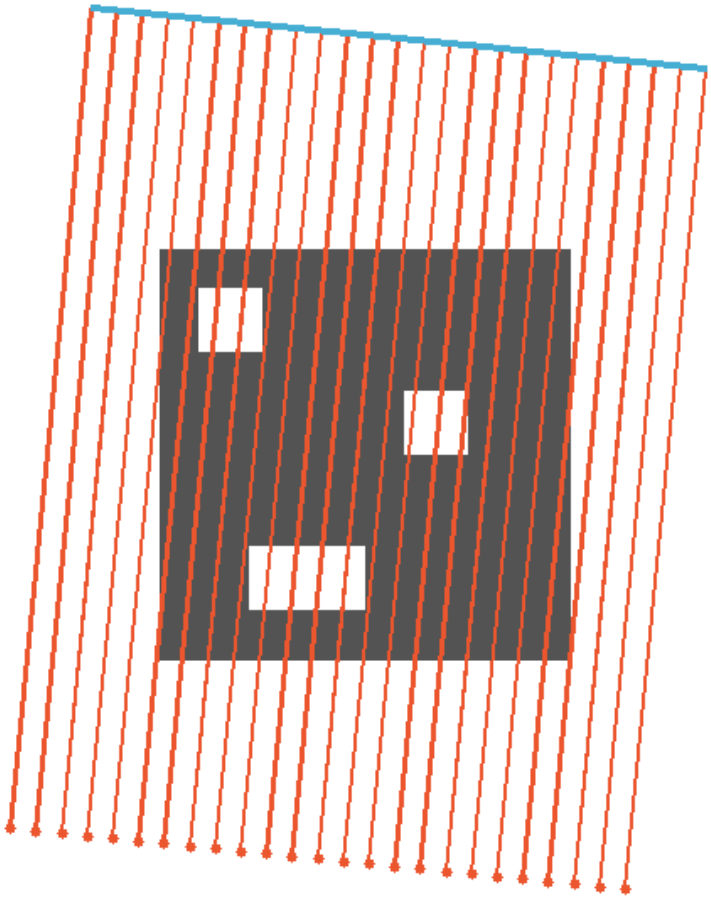

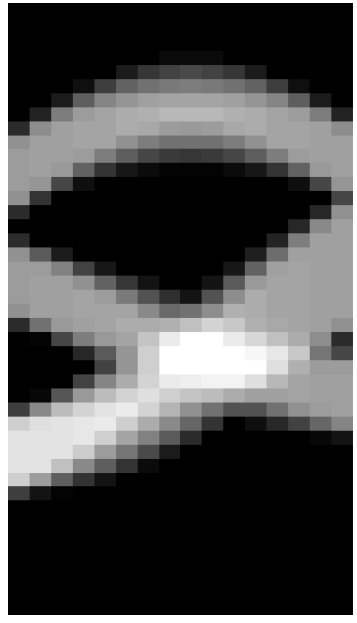

Construction of the sinogram

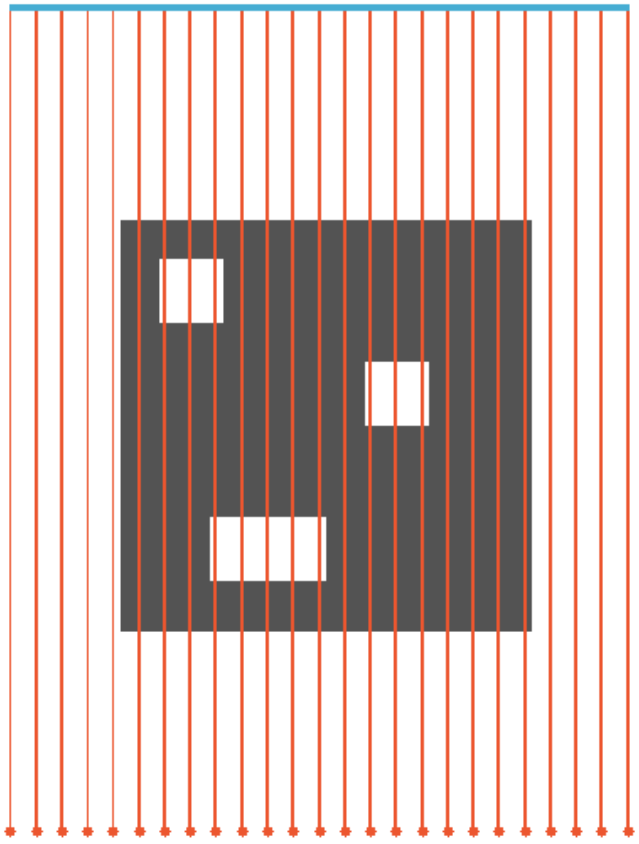

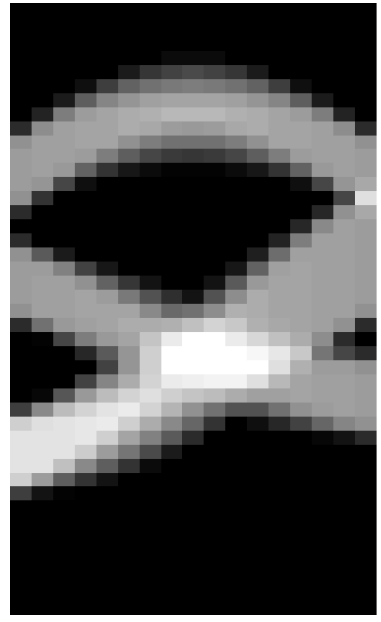

Construction of the sinogram

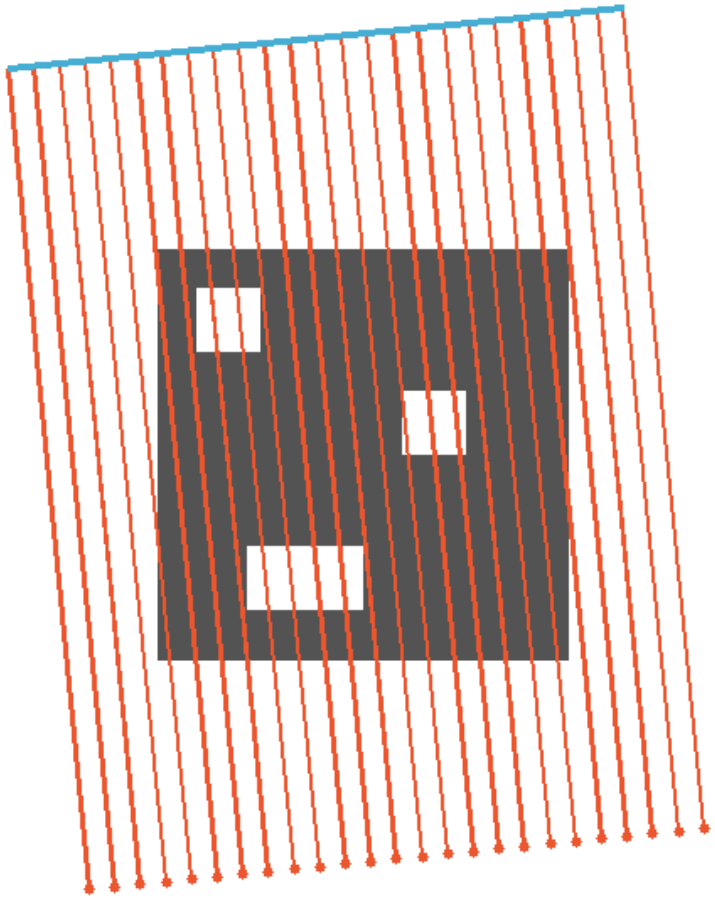

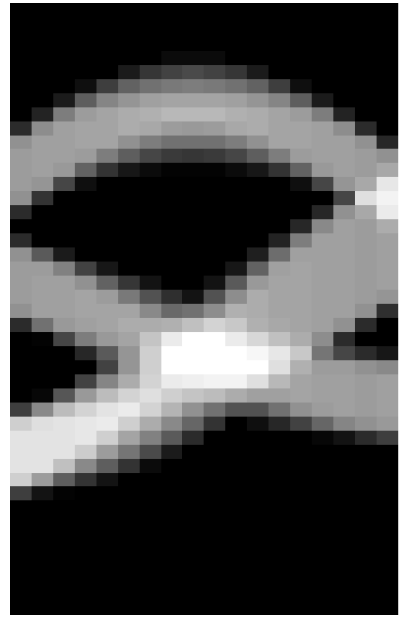

Construction of the sinogram

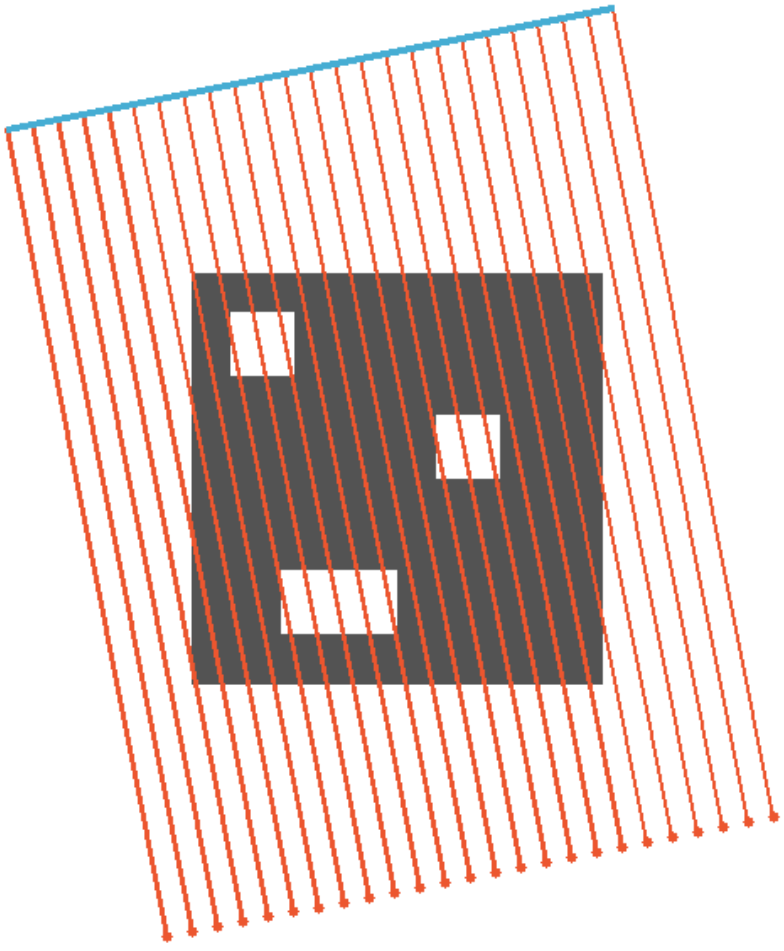

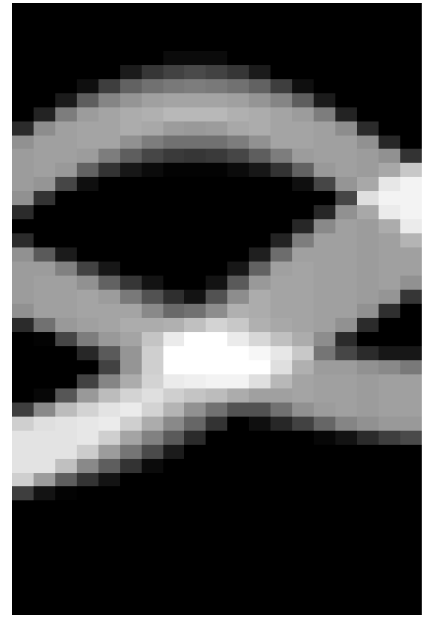

Construction of the sinogram

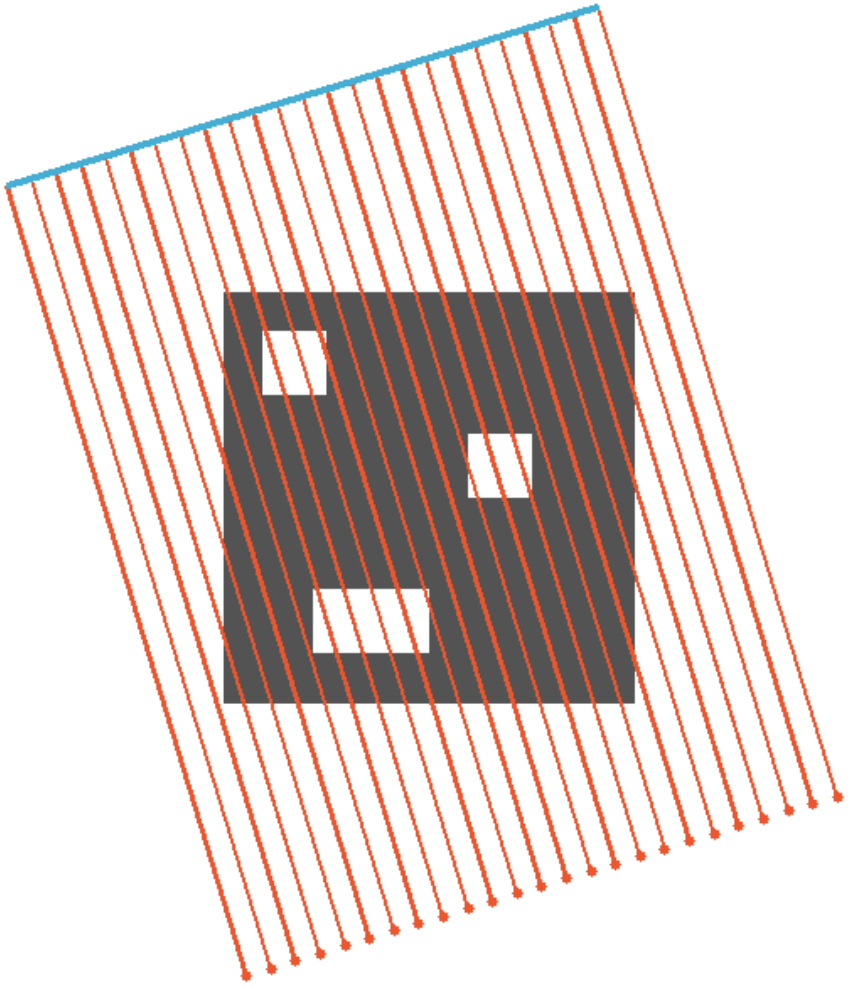

Construction of the sinogram

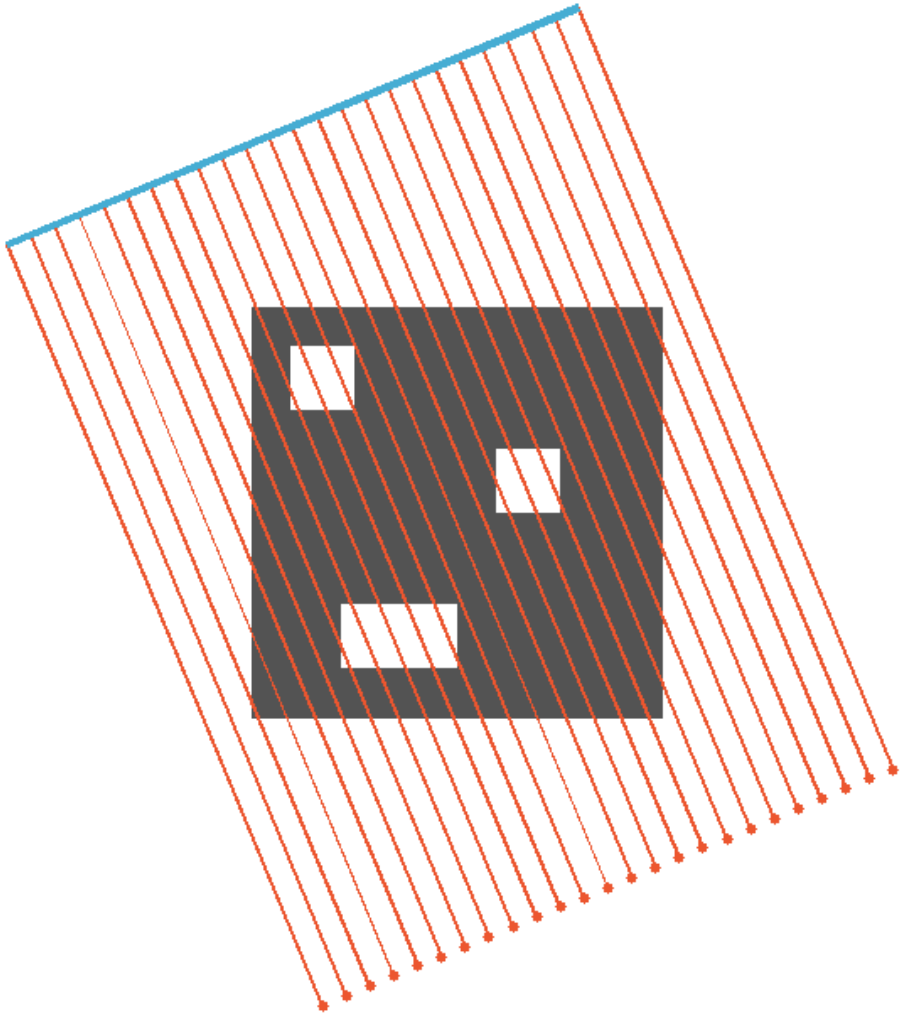

Construction of the sinogram

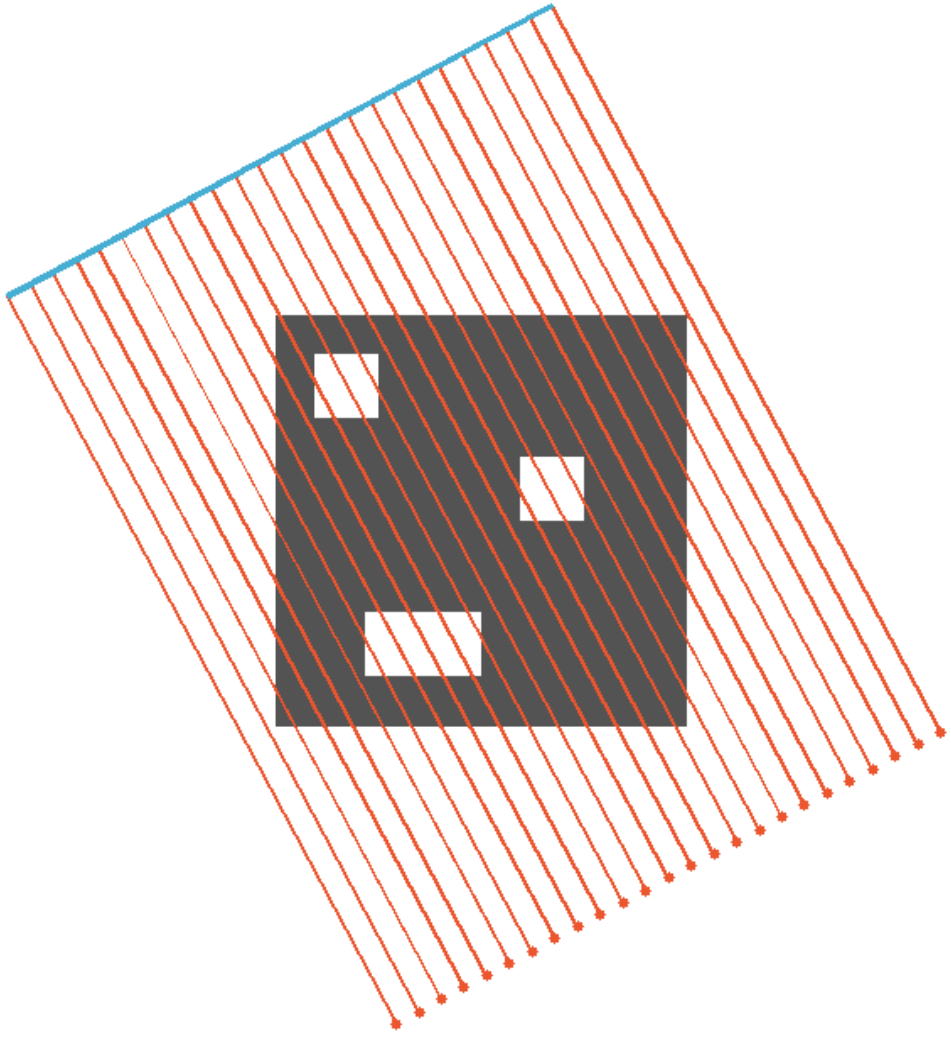

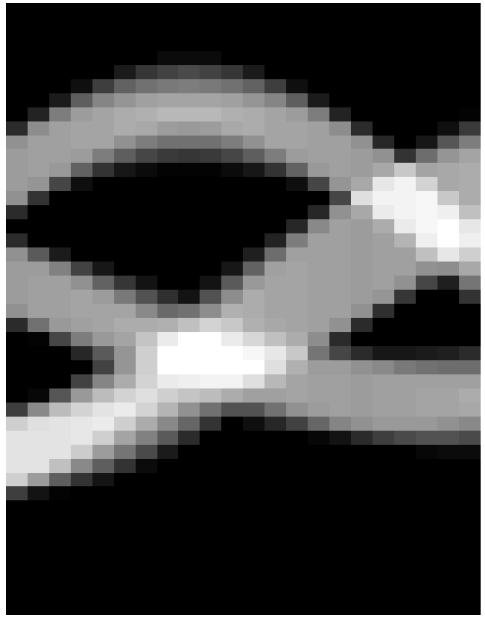

Construction of the sinogram

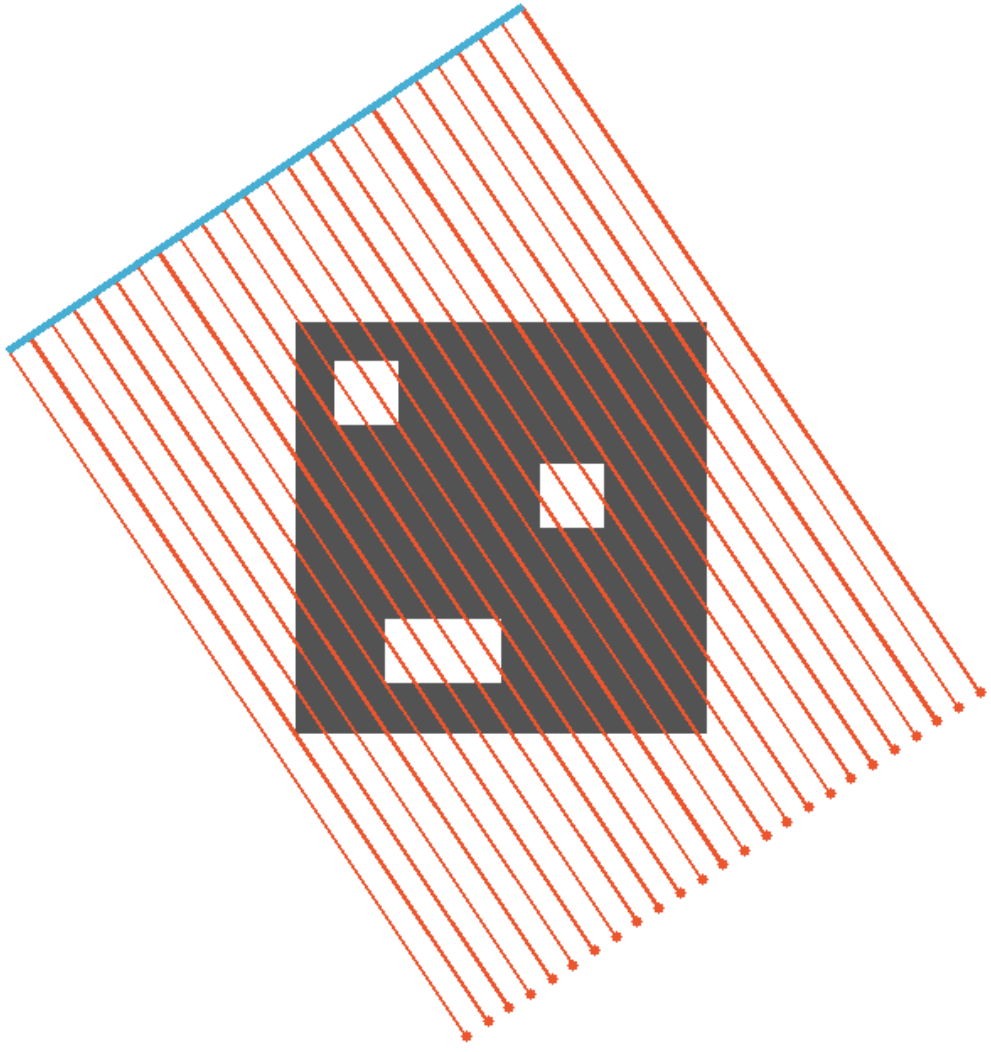

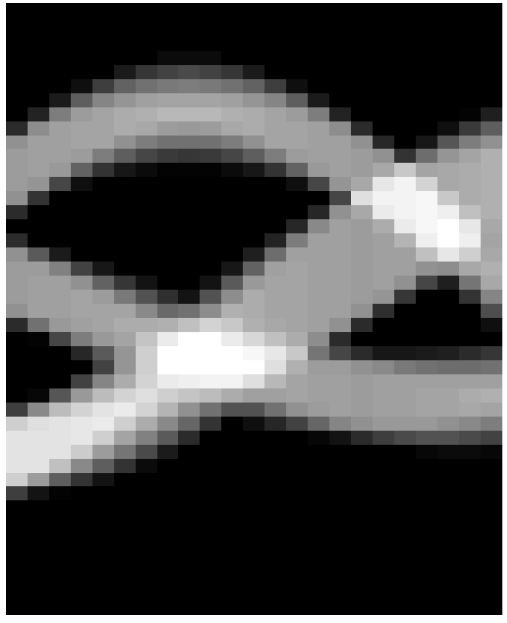

Construction of the sinogram

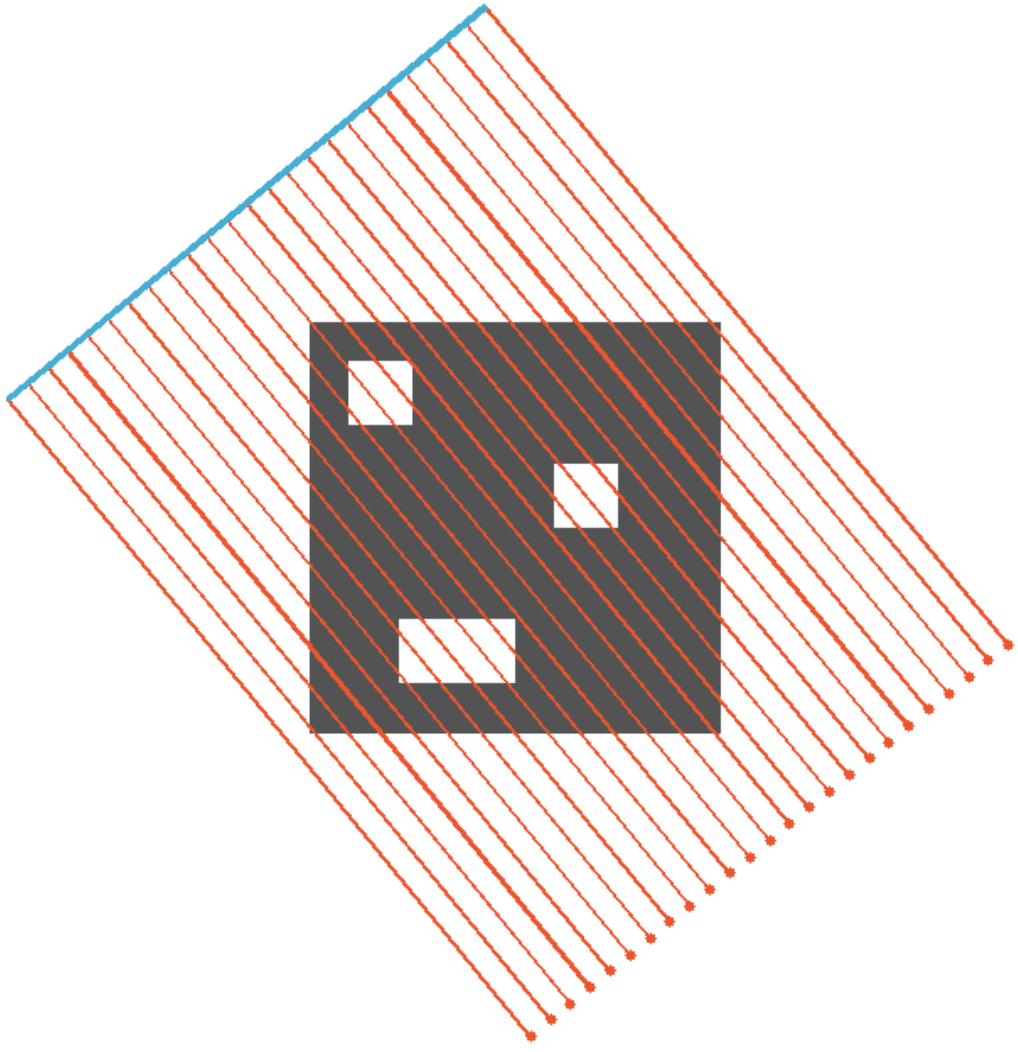

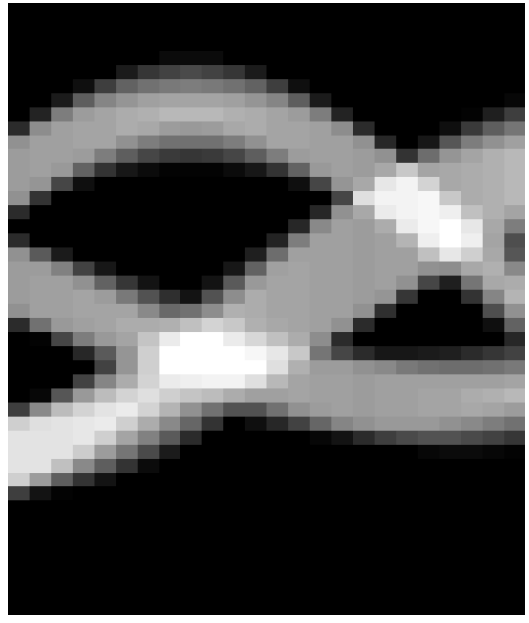

Construction of the sinogram

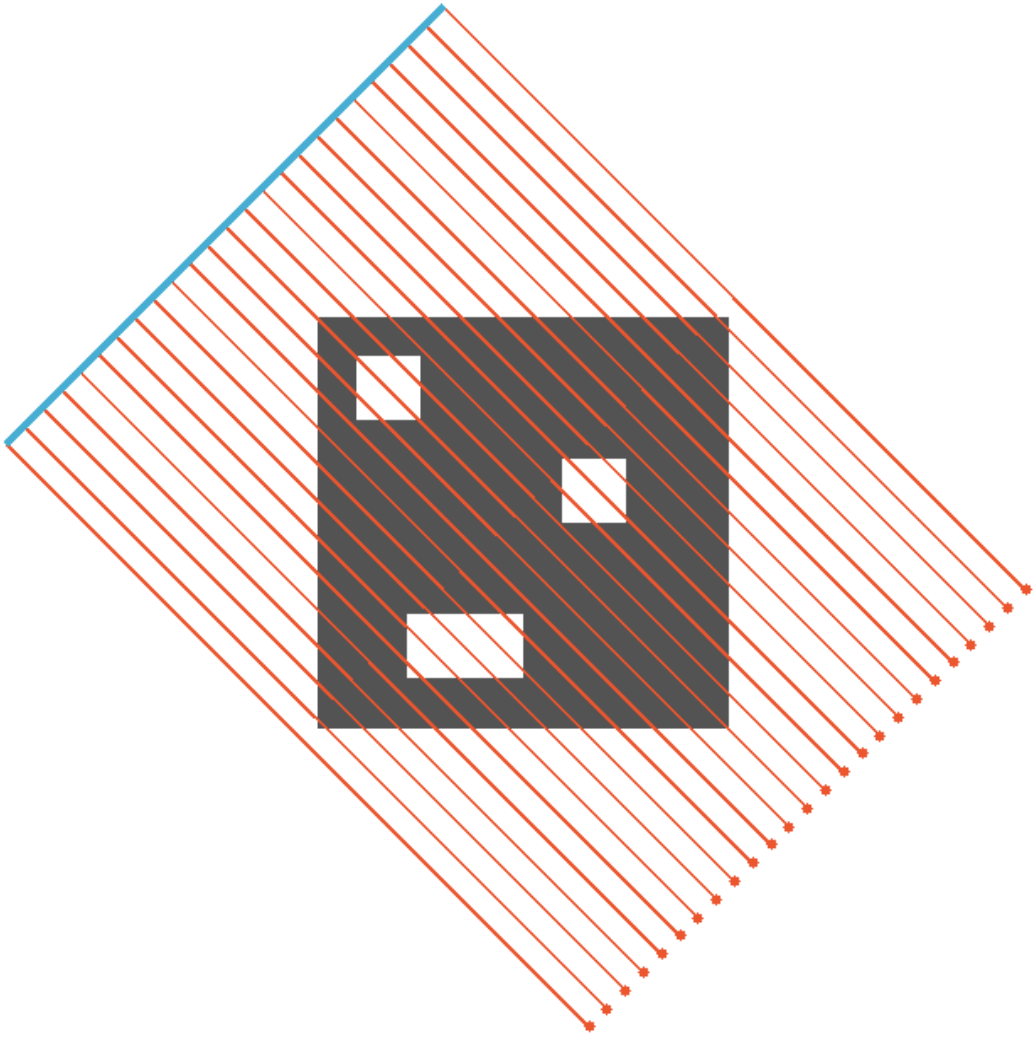

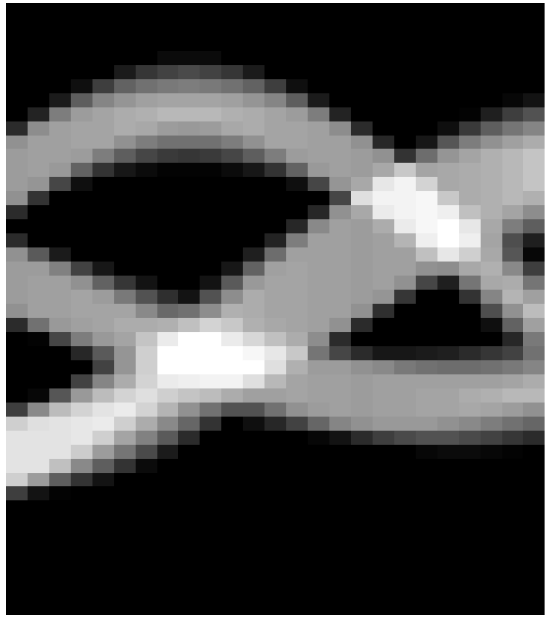

Construction of the sinogram

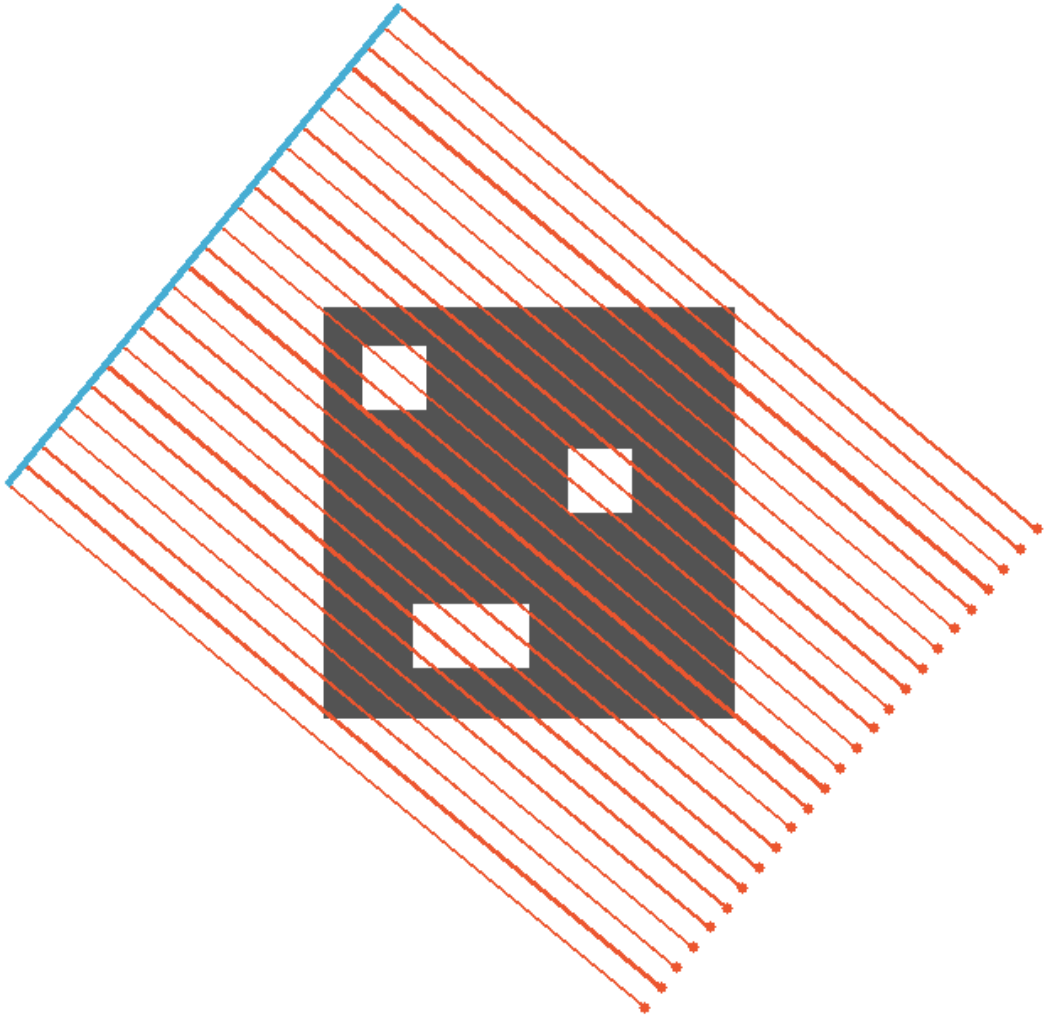

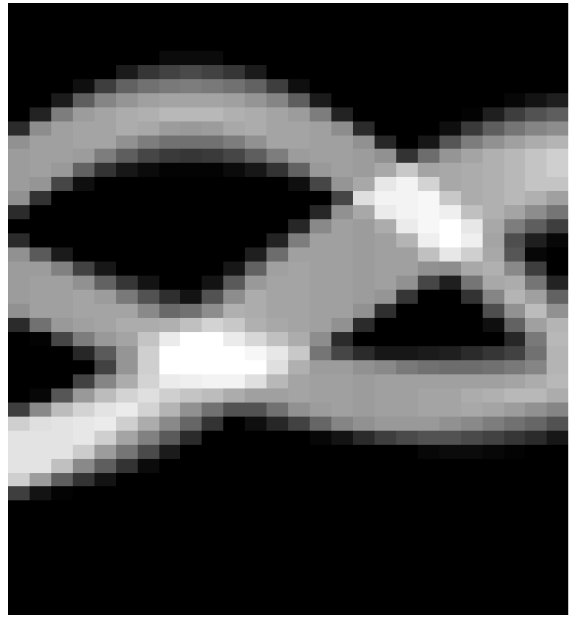

Construction of the sinogram

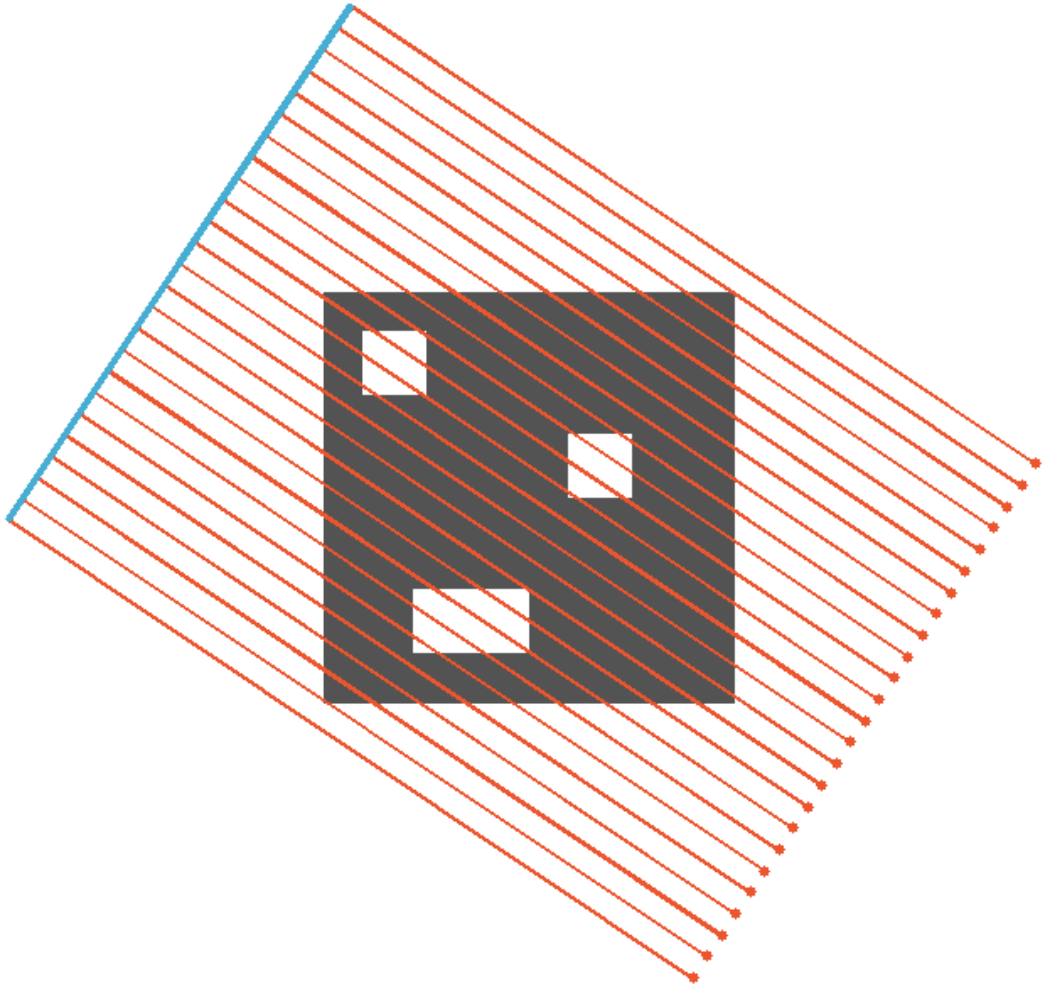

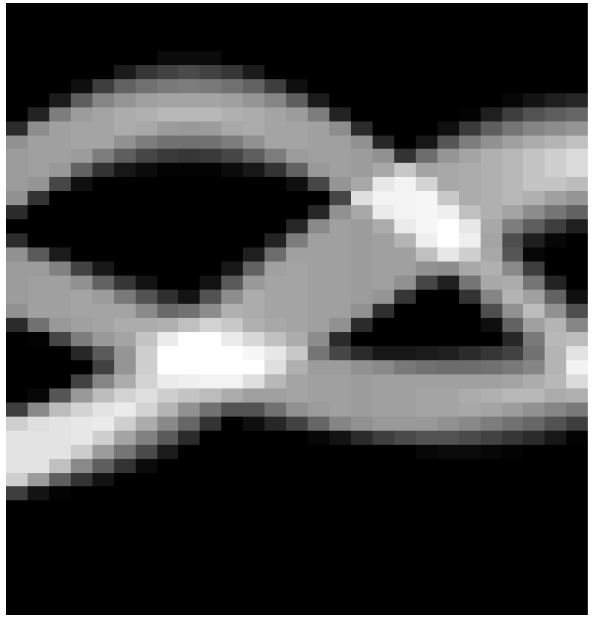

Construction of the sinogram

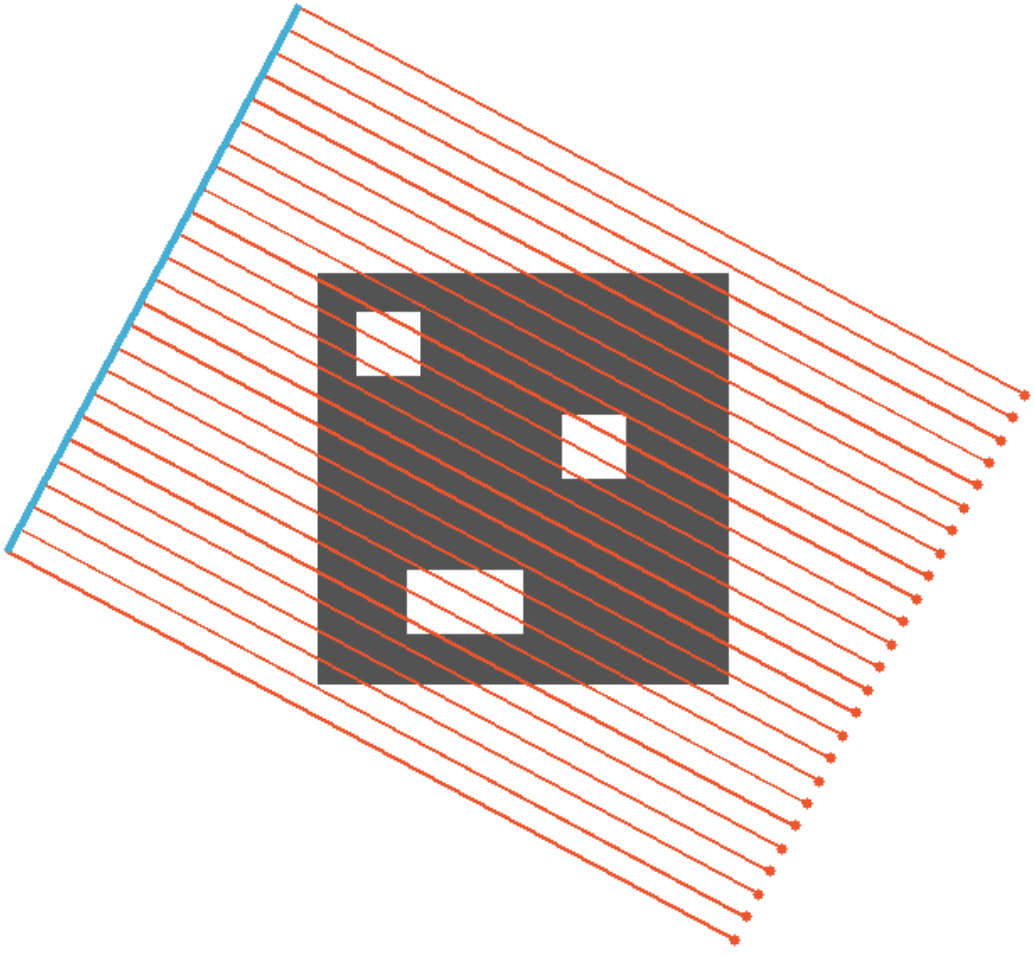

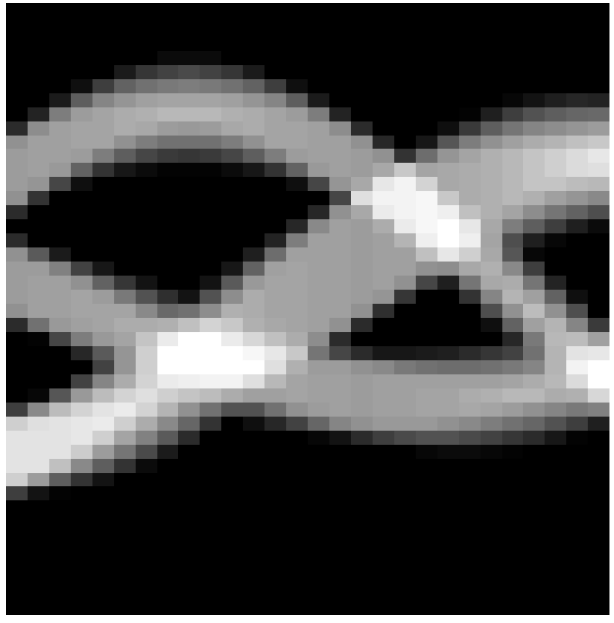

Construction of the sinogram

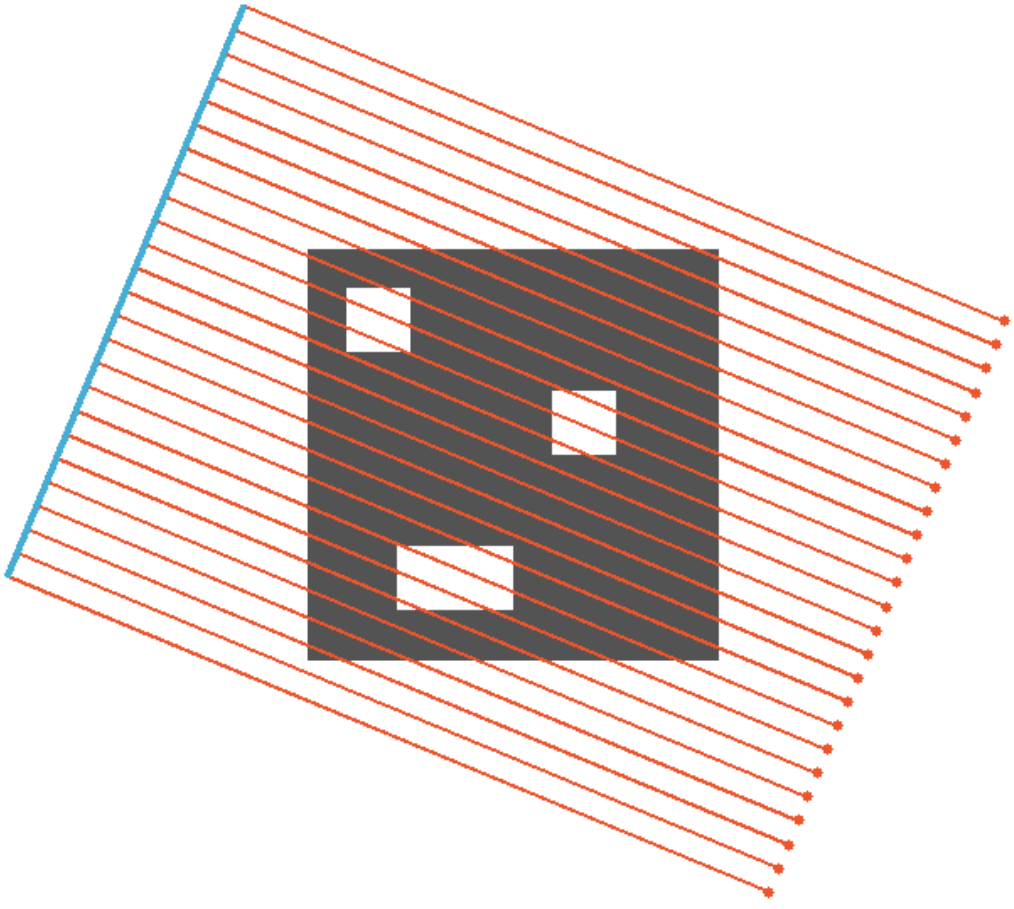

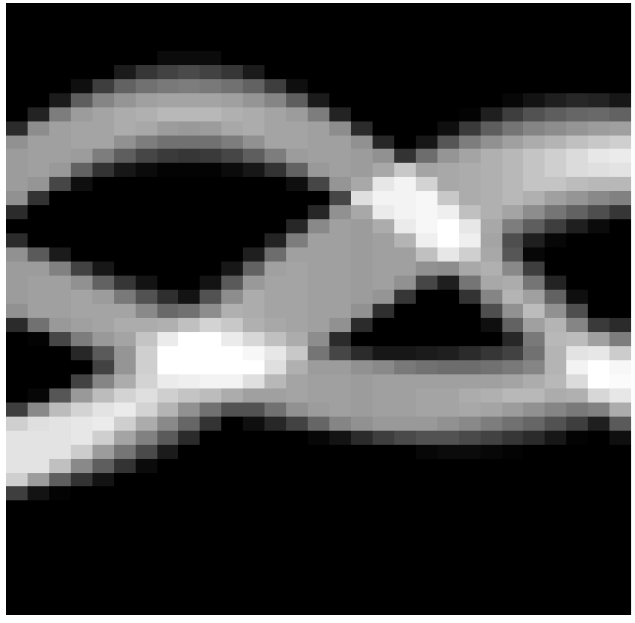

Construction of the sinogram

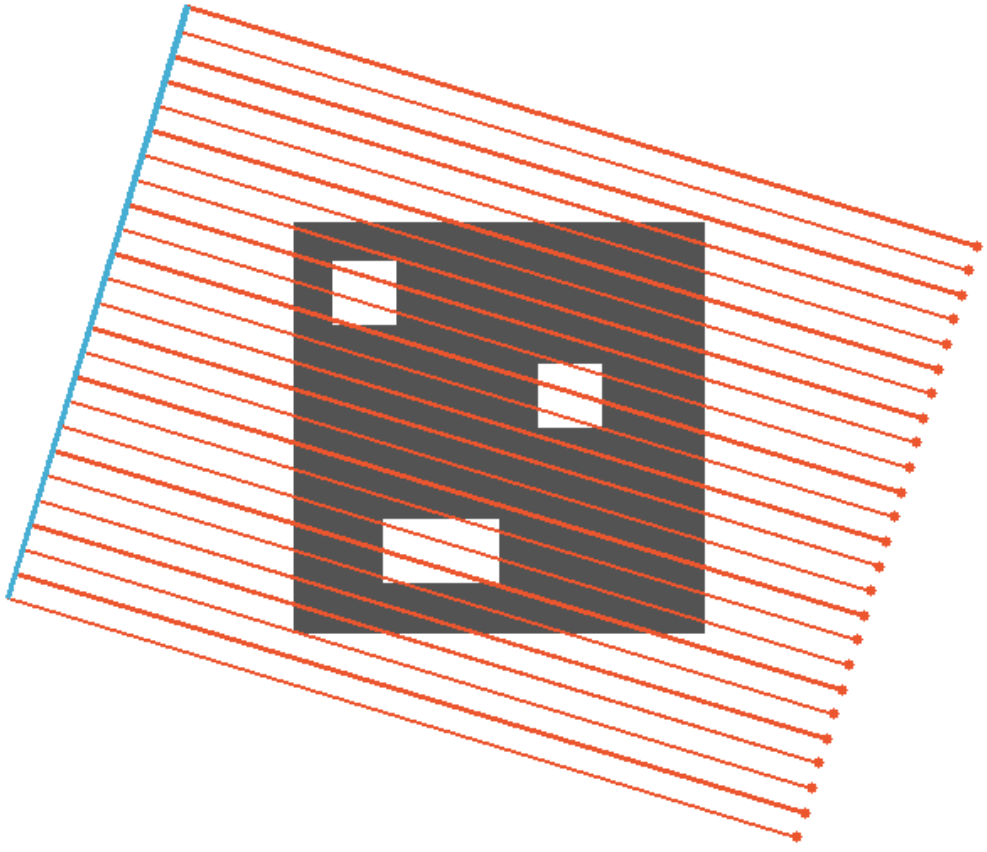

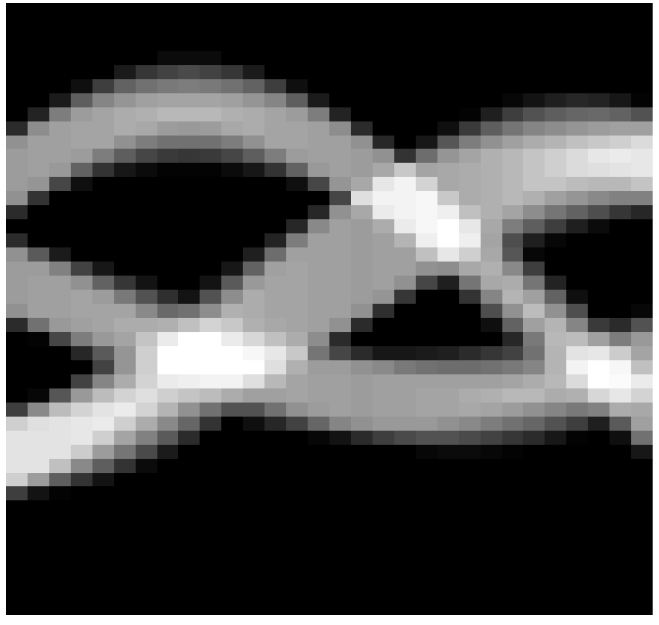

Construction of the sinogram

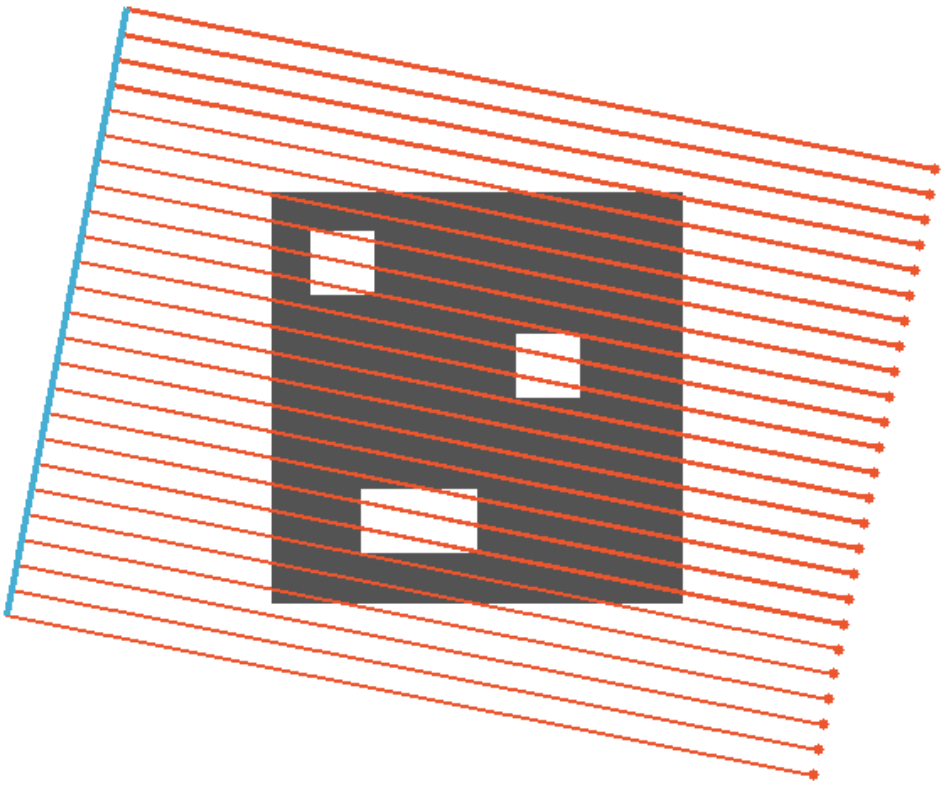

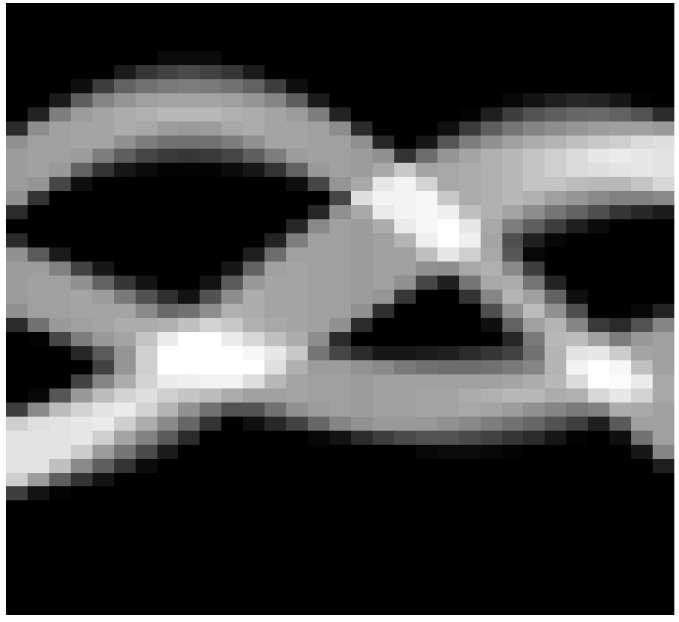

Construction of the sinogram

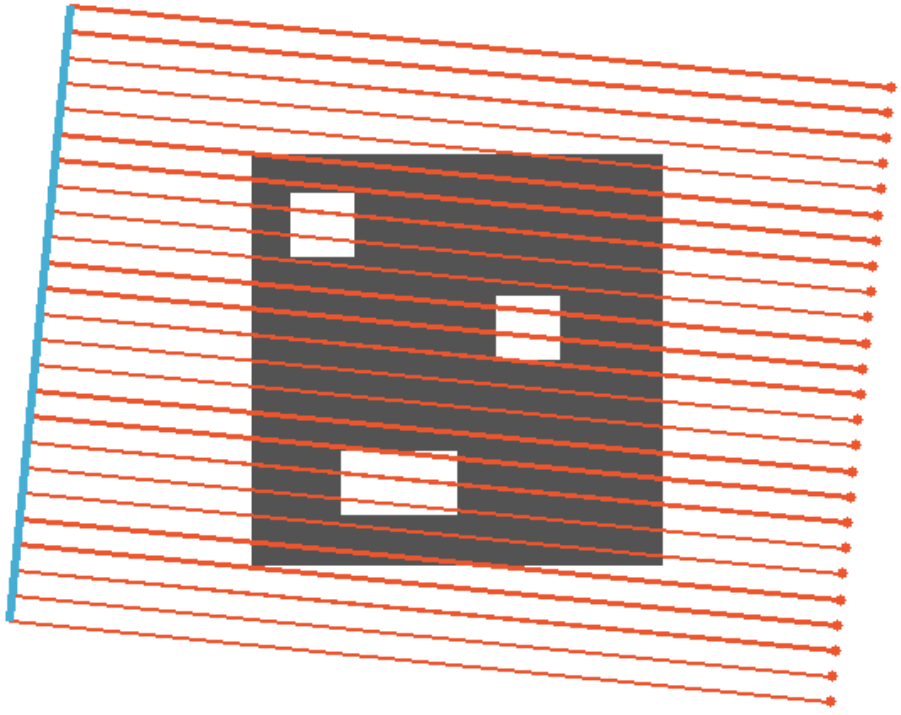

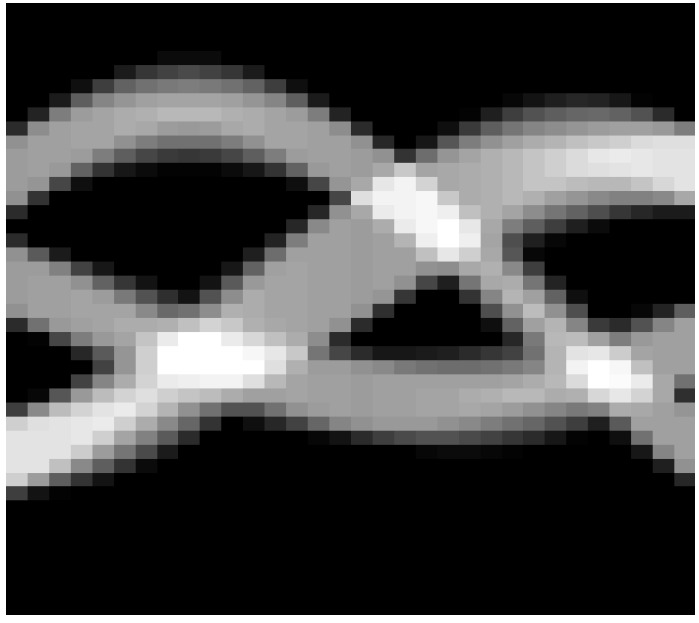

Construction of the sinogram

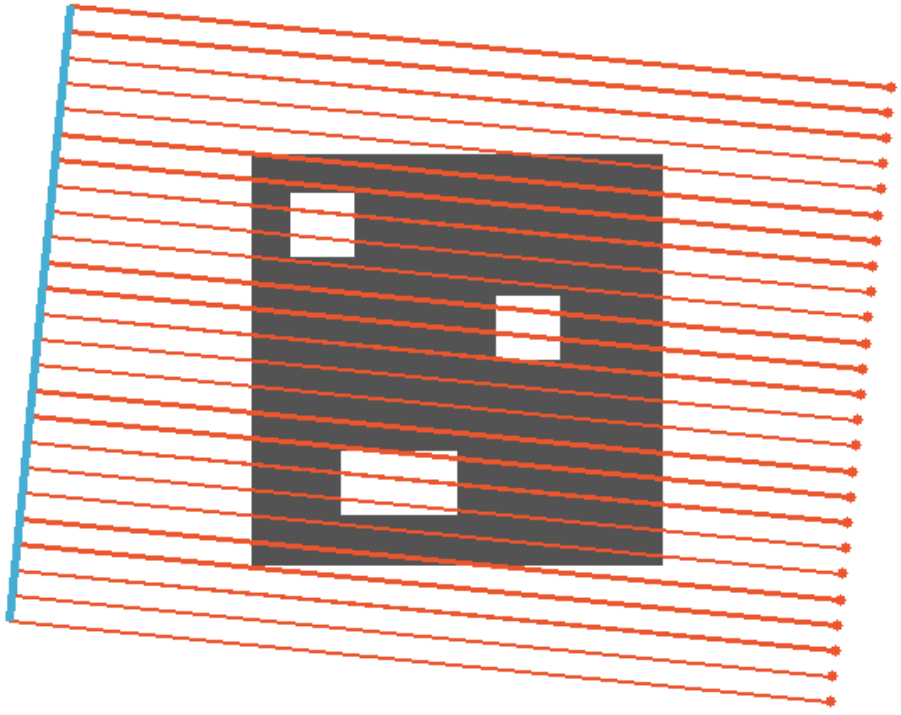

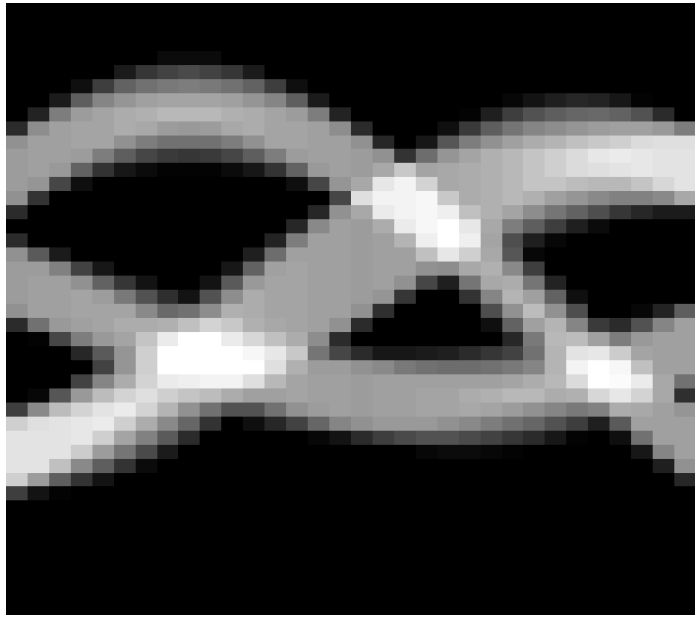

Unknown: $f \in \mathbb{R}^{32\times 32}$

Data: $Af \in \mathbb{R}^{49\times 32}$

The Singular Value Decomposition $A = UDV^T$ allows analysis of any linear inverse problem

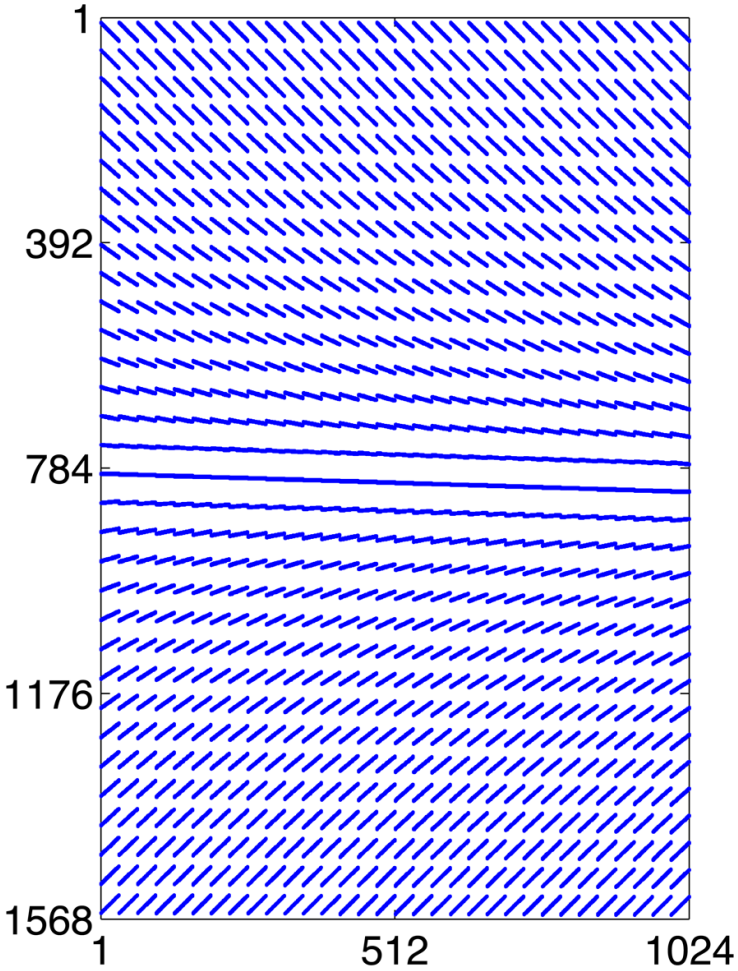

Nonzero elements of matrix A

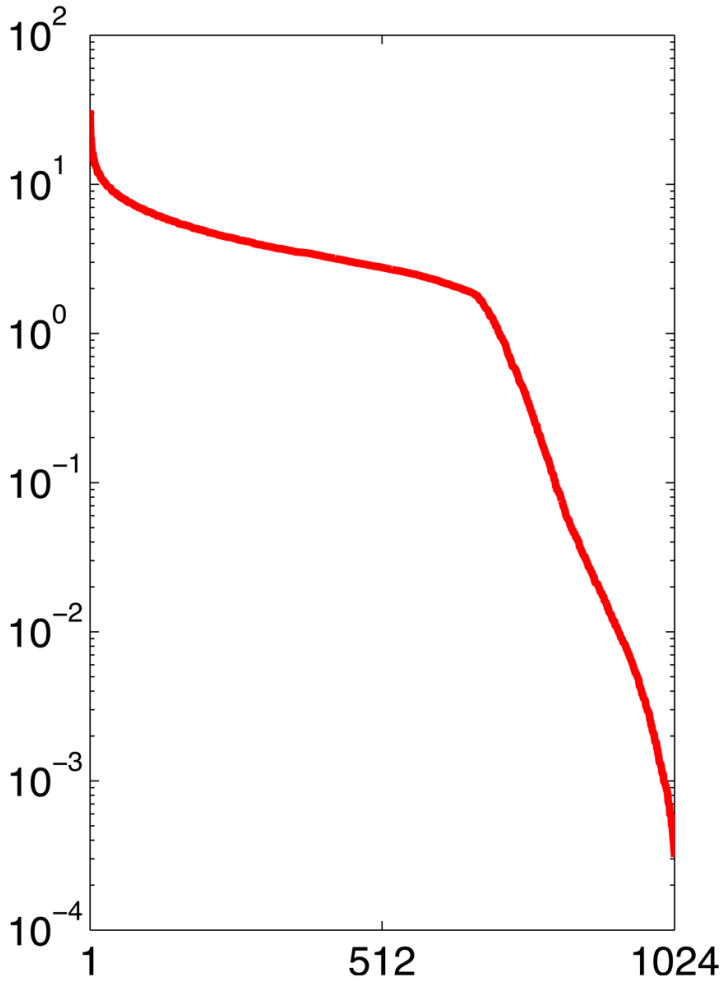

Singular values of matrix A:
diagonal of D in $A = UDV^T$

Nonuniqueness in X-ray tomography

It was noted already in [**Cormack** 1963], and later analyzed in [**Smith**, **Solmon** & **Wagner** 1977, Theorem 4.2], that a finite number of line integrals does not determine the target uniquely since the measurement operator has a nontrivial nullspace.

THEOREM 4.2. *A finite set of radiographs tells nothing at all.*

For some reason this theorem provokes merriment. It is so plainly one of those mathematical ideals untainted by any possibility of practical application.

These phantoms have almost the same sinogram

Original phantom

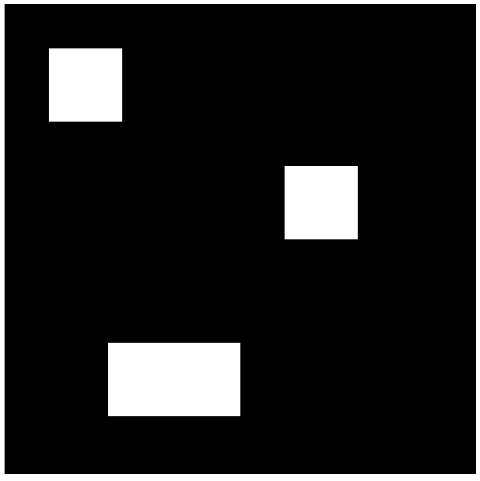

Data error 1%

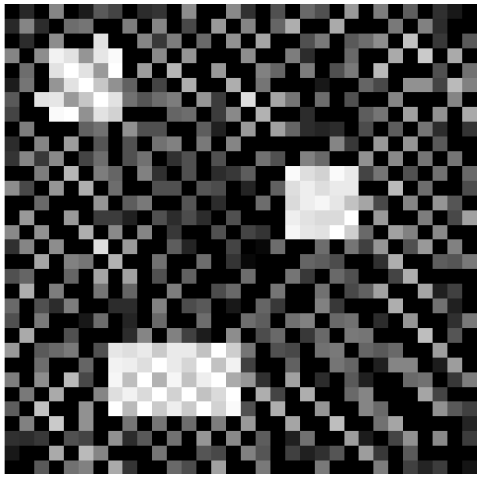

Data error 0.2%

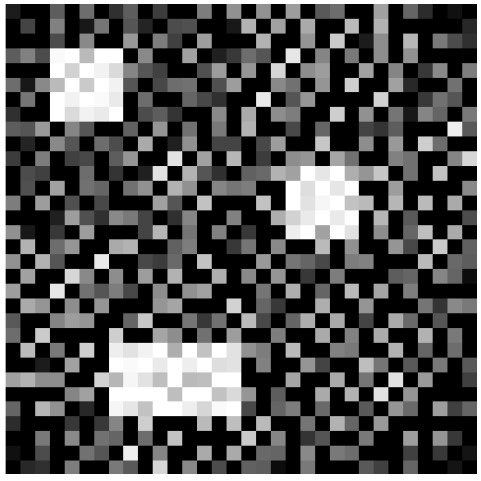

Data error 0.05%

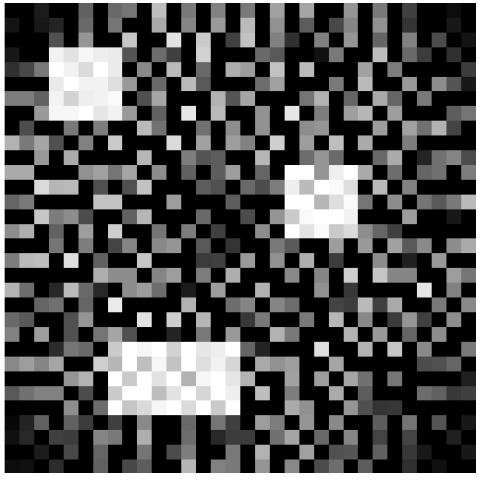

Data error 0.02%

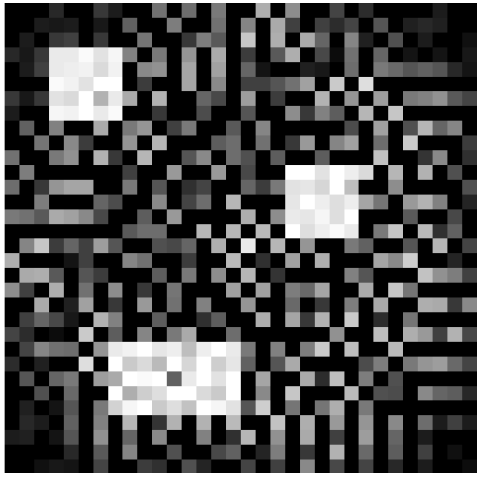

Data error 0.002%

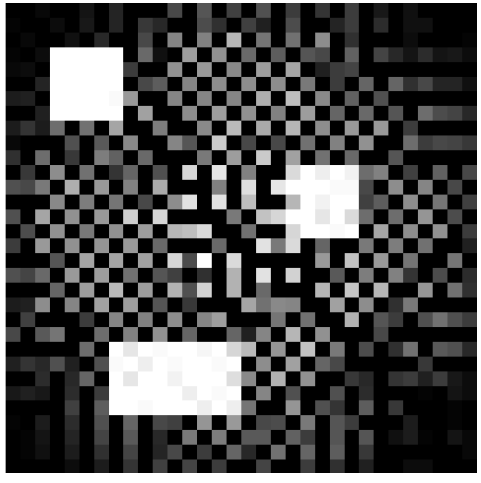

Ill-posed inverse problems are defined as opposites of well-posed direct problems

Hadamard (1903): a problem is well-posed if the following conditions hold.

1. A solution exists,
2. The solution is unique,
3. The solution depends continuously on the input.

Well-posed direct problem:
Input f, find infinite-precision data Af.

Ill-posed inverse problem:
Input noisy data $m = Af + \varepsilon$, recover f.

Hadamard's conditions in a linear inverse problem with forward map given by a matrix A

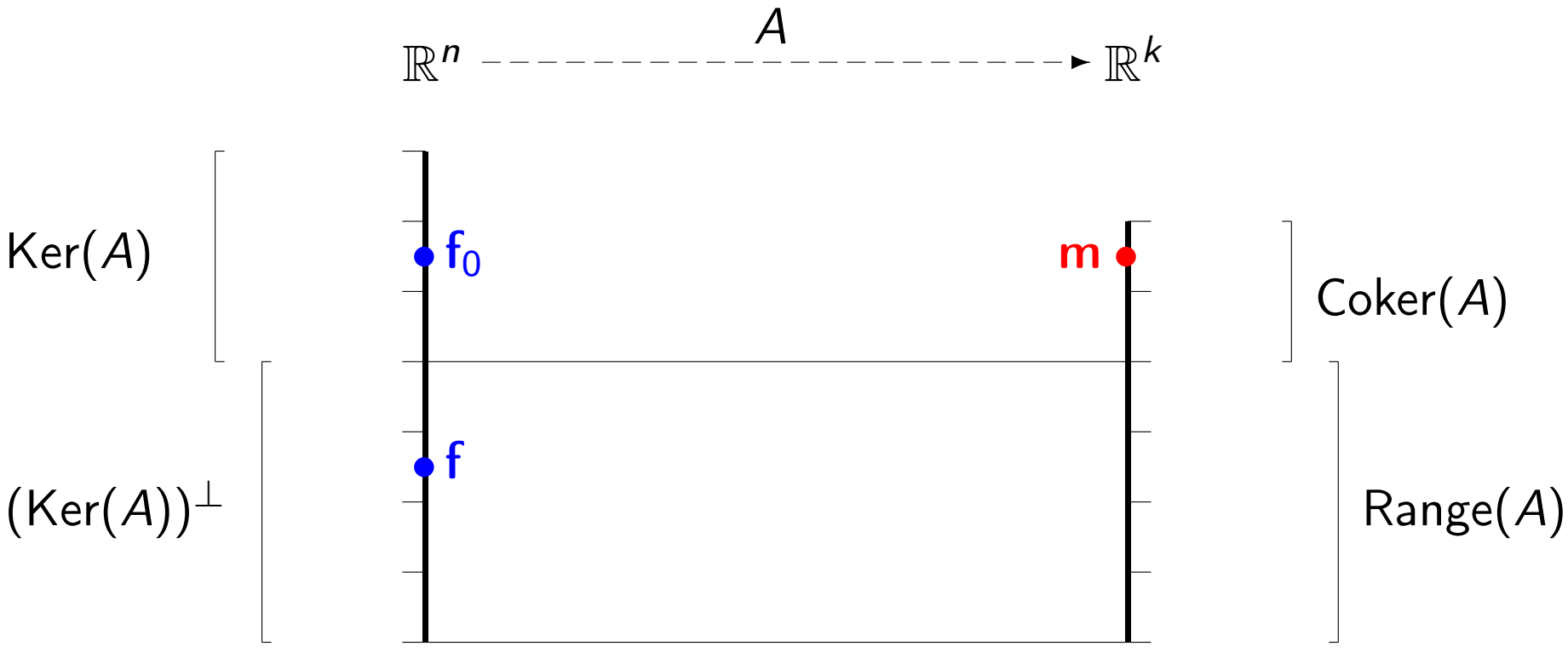

The matrix A maps bijectively between $(\text{Ker}(A))^{\perp}$ and Range(A). However, decreasing singular values may make this bijection unstable, leading to trouble with Hadamard's condition 3.

Recall the singular value decomposition (SVD) of the matrix A

$$A = UDV^T = U \begin{bmatrix} d_1 & 0 & \cdots & 0 & & \cdots & 0 \\ 0 & d_2 & & & & & \vdots \\ \vdots & & \ddots & & & & \\ & & & d_r & & & \\ & & & & 0 & & \\ & & & & & \ddots & \vdots \\ 0 & \cdots & & & & \cdots & 0 \end{bmatrix} V^T$$

Here the singular values d_j satisfy $d_1 \geq d_2 \geq \cdots \geq d_r > 0$ and $d_{r+1} = d_{r+2} = \cdots = d_{\min\{k,n\}} = 0$.

Note that in the case $r = \min\{k, n\}$ all singular values are positive. If additionally $n = k$ then A is invertible. But the *condition number* $\text{cond}(A) := d_1/d_{\min\{k,n\}}$ is large, and A^{-1} is numerically unstable.

The Moore-Penrose pseudoinverse takes care of Hadamard's conditions 1 and 2

$$A^\dagger = VD^\dagger U^T = V \begin{bmatrix} 1/d_1 & 0 & \cdots & 0 & & \cdots & 0 \\ 0 & 1/d_2 & & & & & \vdots \\ \vdots & & \ddots & & & & \\ & & & 1/d_r & & & \\ & & & & 0 & & \\ \vdots & & & & & \ddots & \vdots \\ 0 & \cdots & & & & \cdots & 0 \end{bmatrix} U^T$$

We can compute naive reconstruction as the uniquely defined *minimum norm solution* $A^\dagger m$. However, this only works for rank-deficient problems where Hadamard's condition 3 is not active.

Naive reconstruction using the Moore-Penrose pseudoinverse; data has 0.1% relative noise

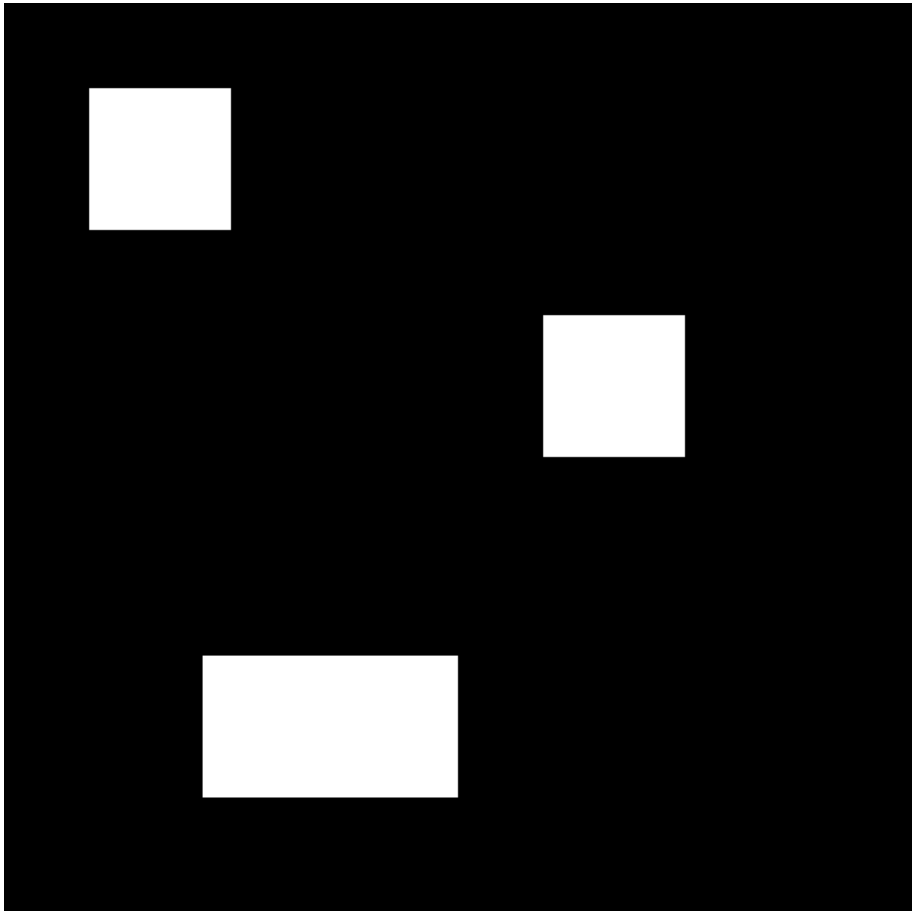

Original phantom, values between zero (black) and one (white)

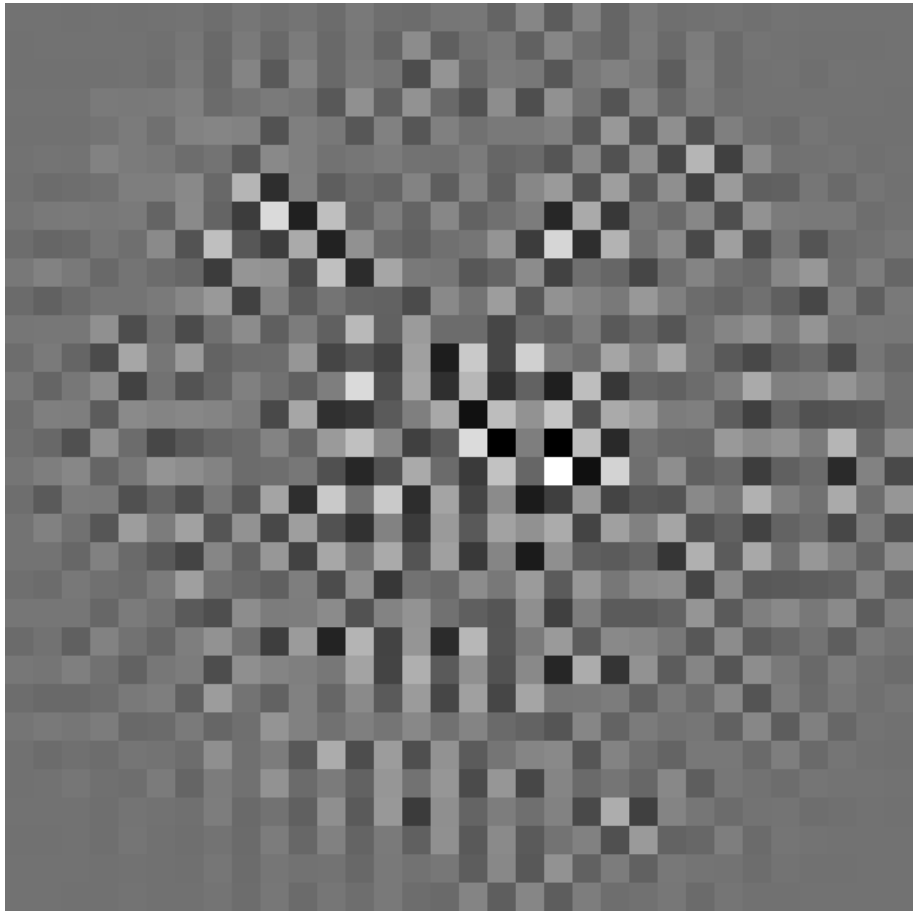

Naive reconstruction with minimum -14.9 and maximum 18.5

Outline

Inverse problem of X-ray tomography: given noisy sinogram, find a stable approximation to f

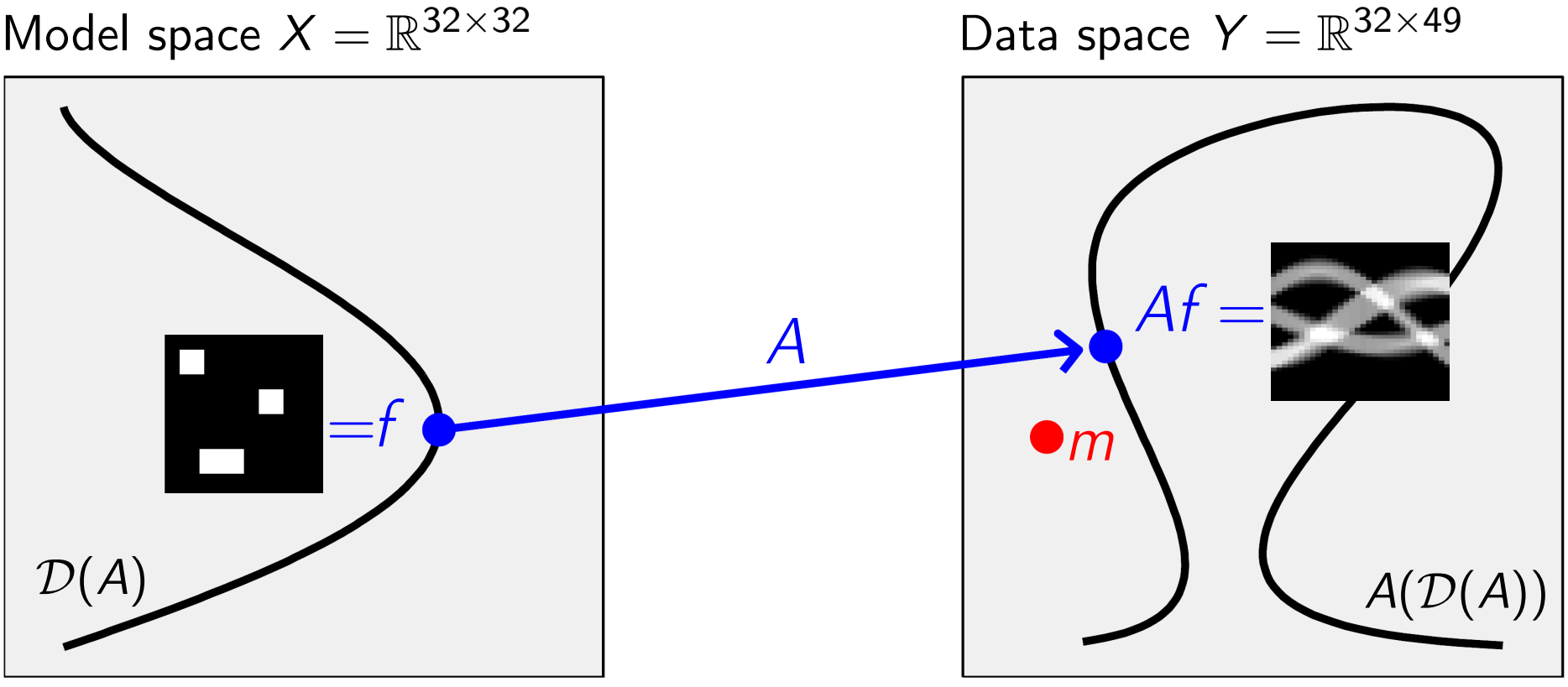

Tikhonov regularization is the classical option for noise-robust tomographic reconstruction

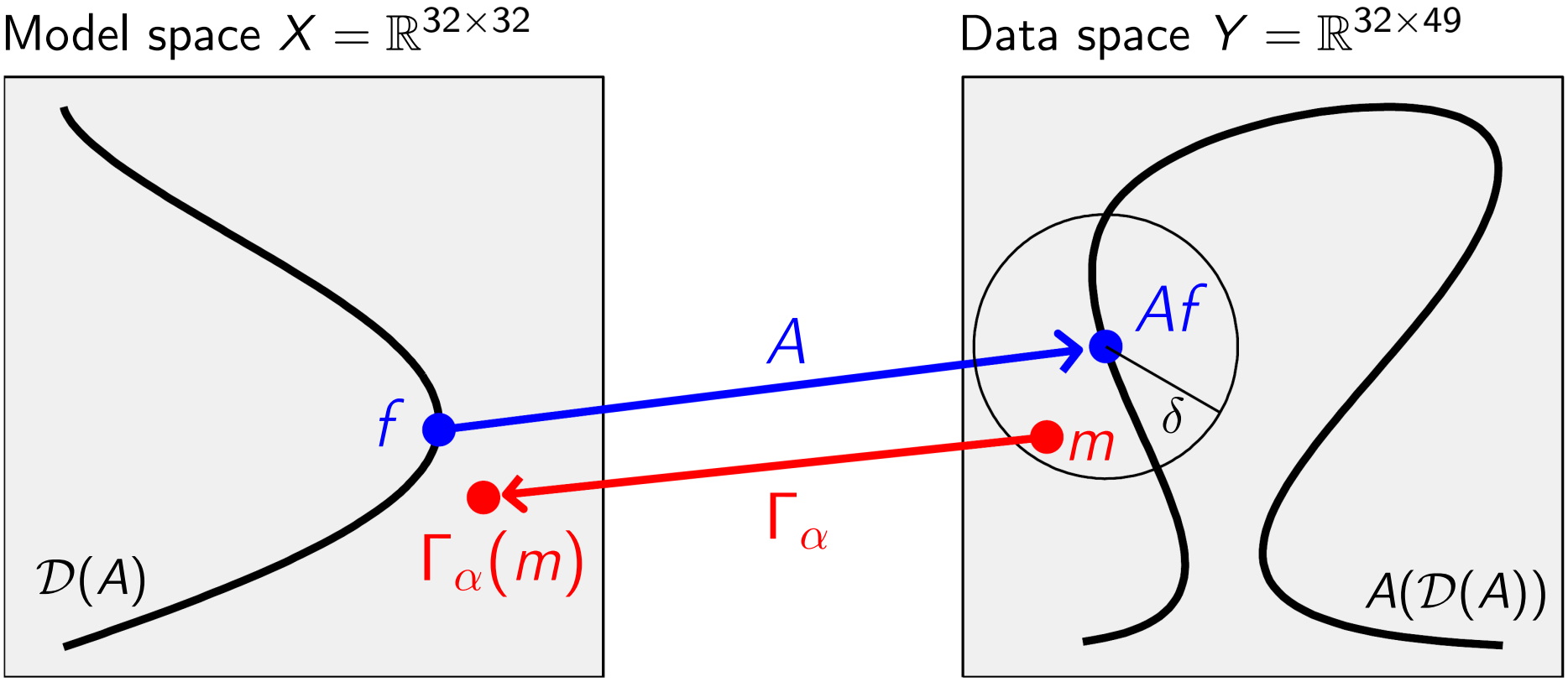

Write a penalty functional $\Phi(f) = \|Af - m\|_2^2 + \alpha\|f\|_2^2$, where $0 < \alpha < \infty$ is a regularization parameter. Define $\Gamma_\alpha(m)$ by $\Phi(\Gamma_\alpha(m)) = \min_{f\in X}\{\Phi(f)\}$.

Tikhonov regularization can be expressed as filtering the singular values of the matrix A

$$V \begin{bmatrix} \frac{d_1}{d_1^2+\alpha} & 0 & \cdots & 0 \\ 0 & \ddots & & \vdots \\ \vdots & & \ddots & 0 \\ 0 & \cdots & 0 & \frac{d_{\min\{k,n\}}}{d_{\min\{k,n\}}^2+\alpha} \end{bmatrix} U^T m$$

Constrained Tikhonov regularization

$$\underset{f \in \mathbb{R}^n_+}{\arg\min} \left\{ \|Af - m\|_2^2 + \alpha \|f\|_2^2 \right\}$$

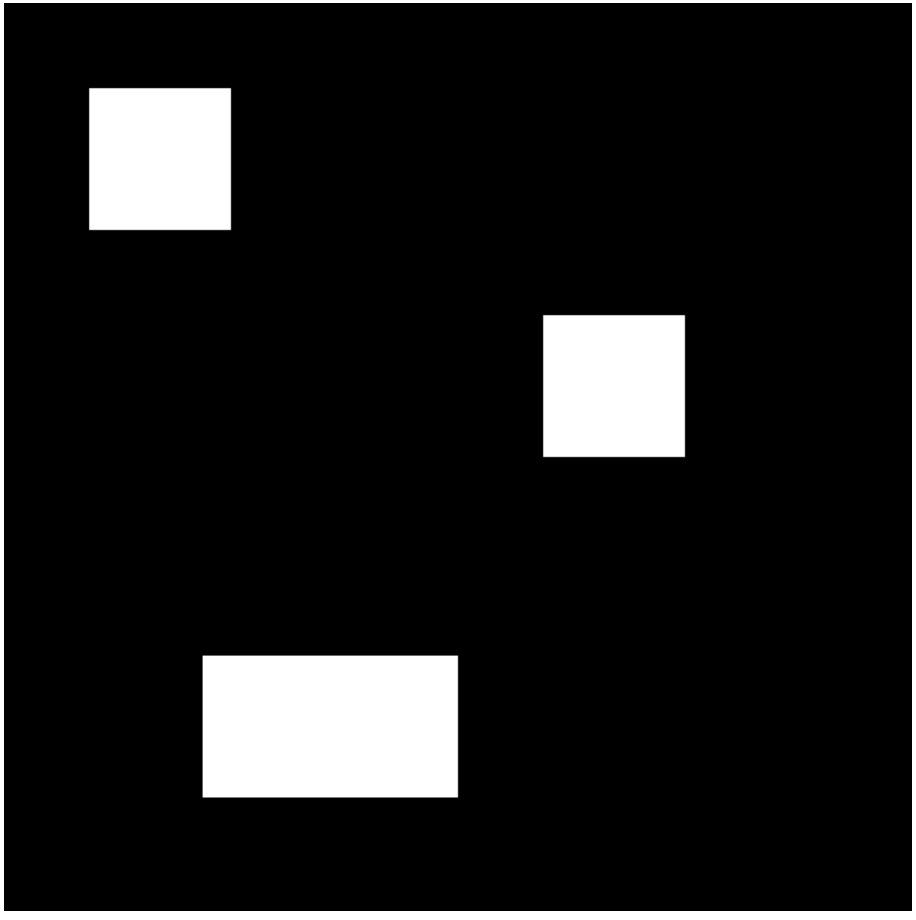

Original phantom

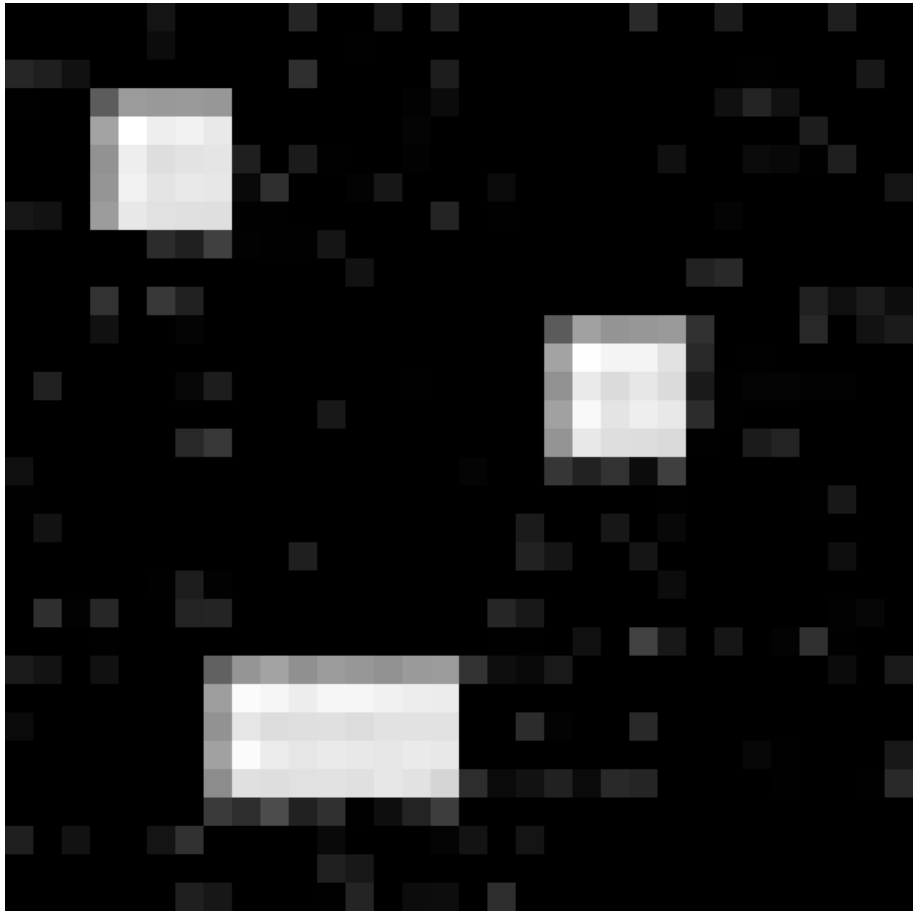

Reconstruction

Relative square norm error 35%

Rudin, Osher and Fatemi (1992): total variation regularization $\arg\min_{f \in \mathbb{R}^n_+} \left\{ \|Af - m\|_2^2 + \alpha \|\nabla f\|_1 \right\}$

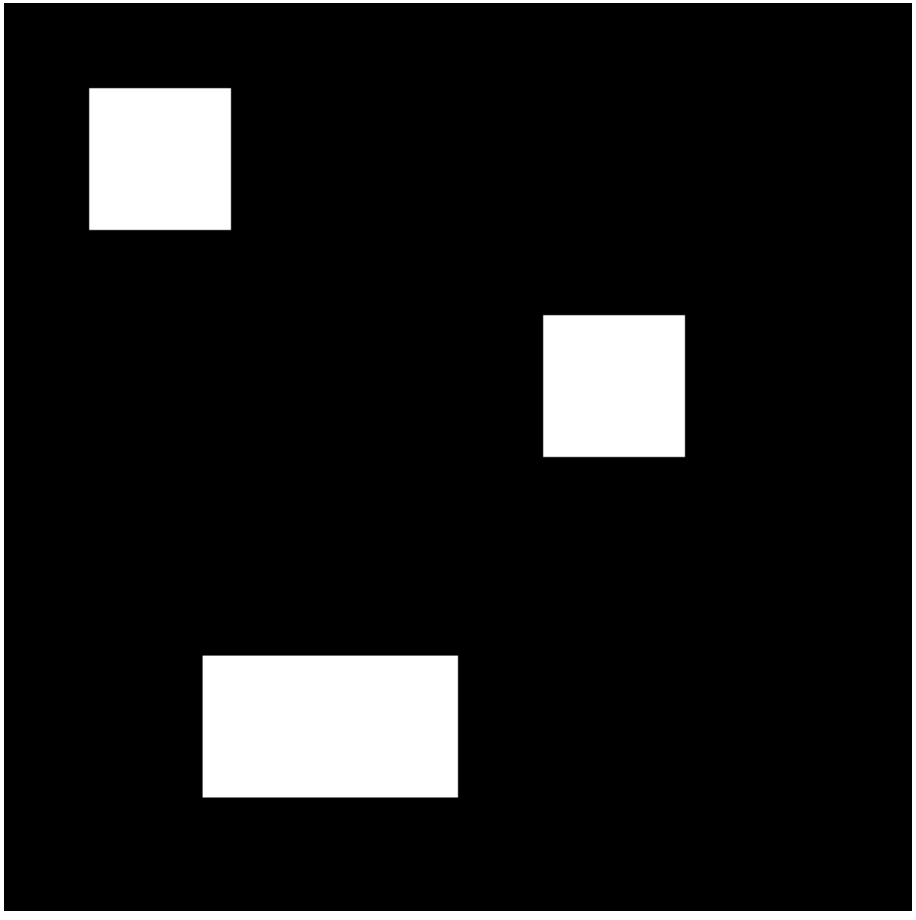

Original phantom

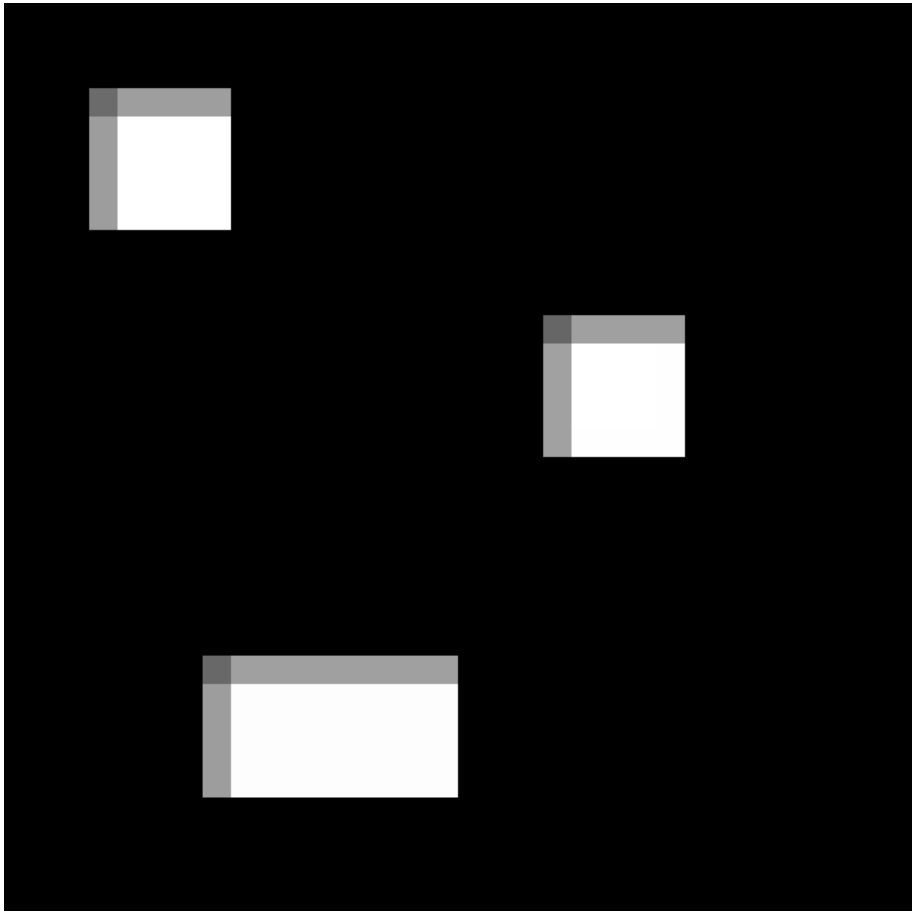

TV regularized reconstruction

Relative square norm error 32%

Naive reconstruction using the Moore-Penrose pseudoinverse

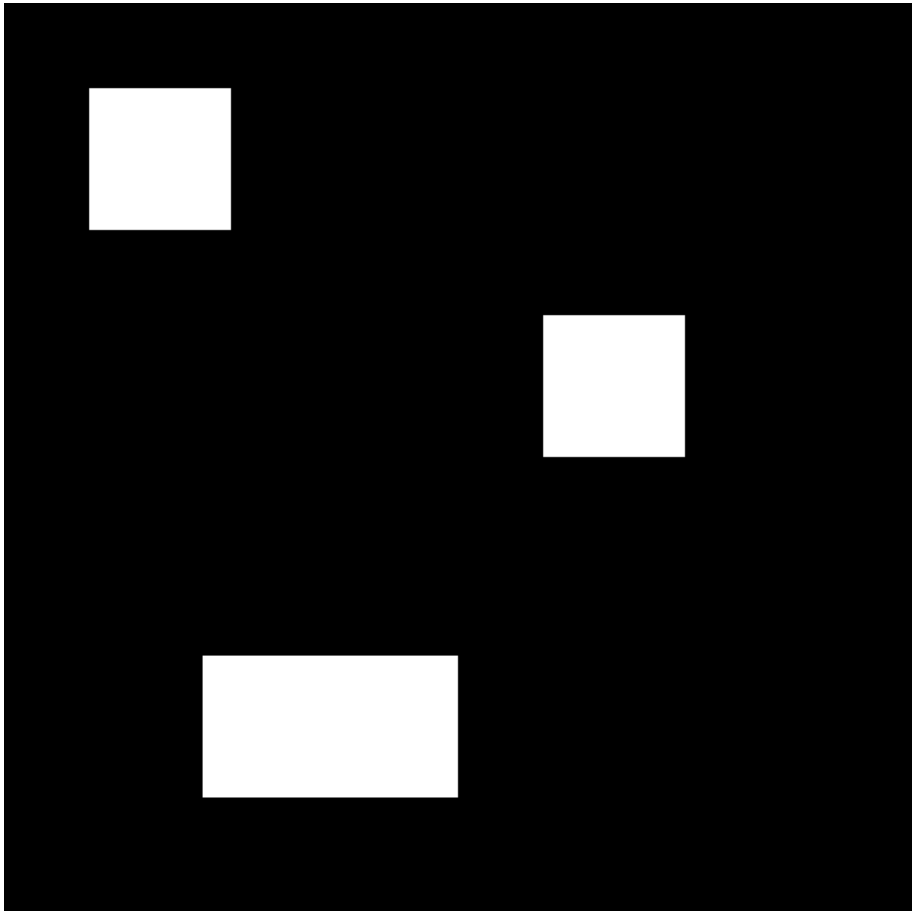

Original phantom

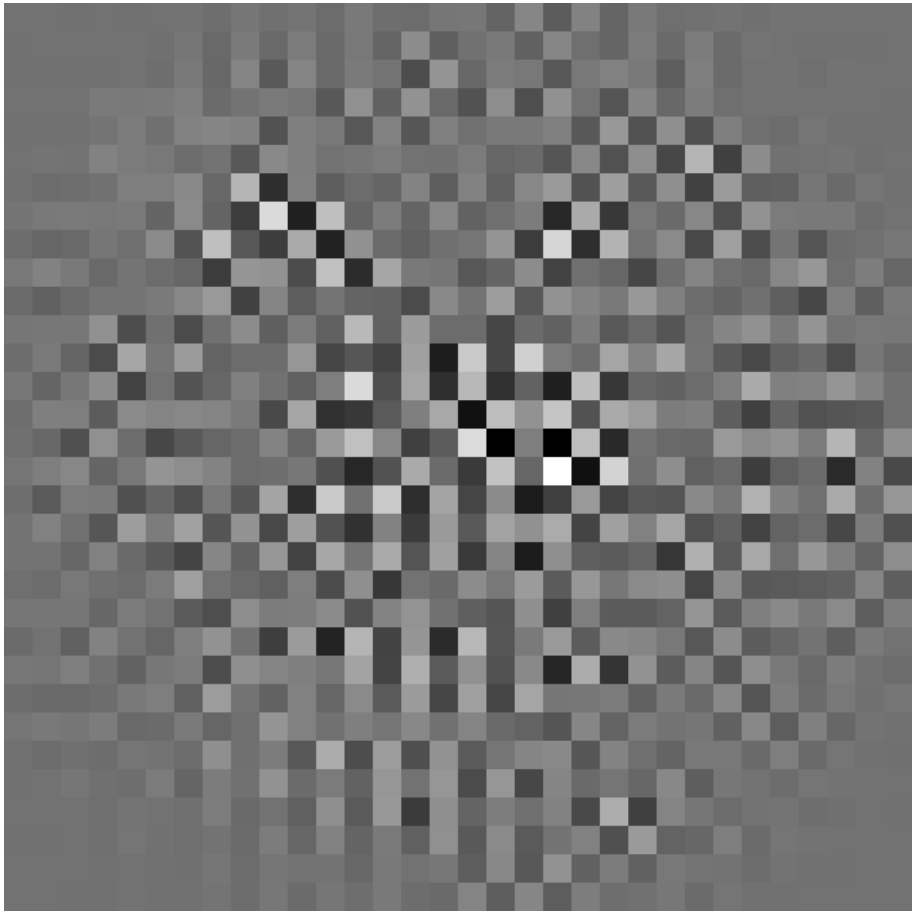

Naive reconstruction
Relative square norm error 1246%

We collected X-ray projection data of a walnut from 1200 directions

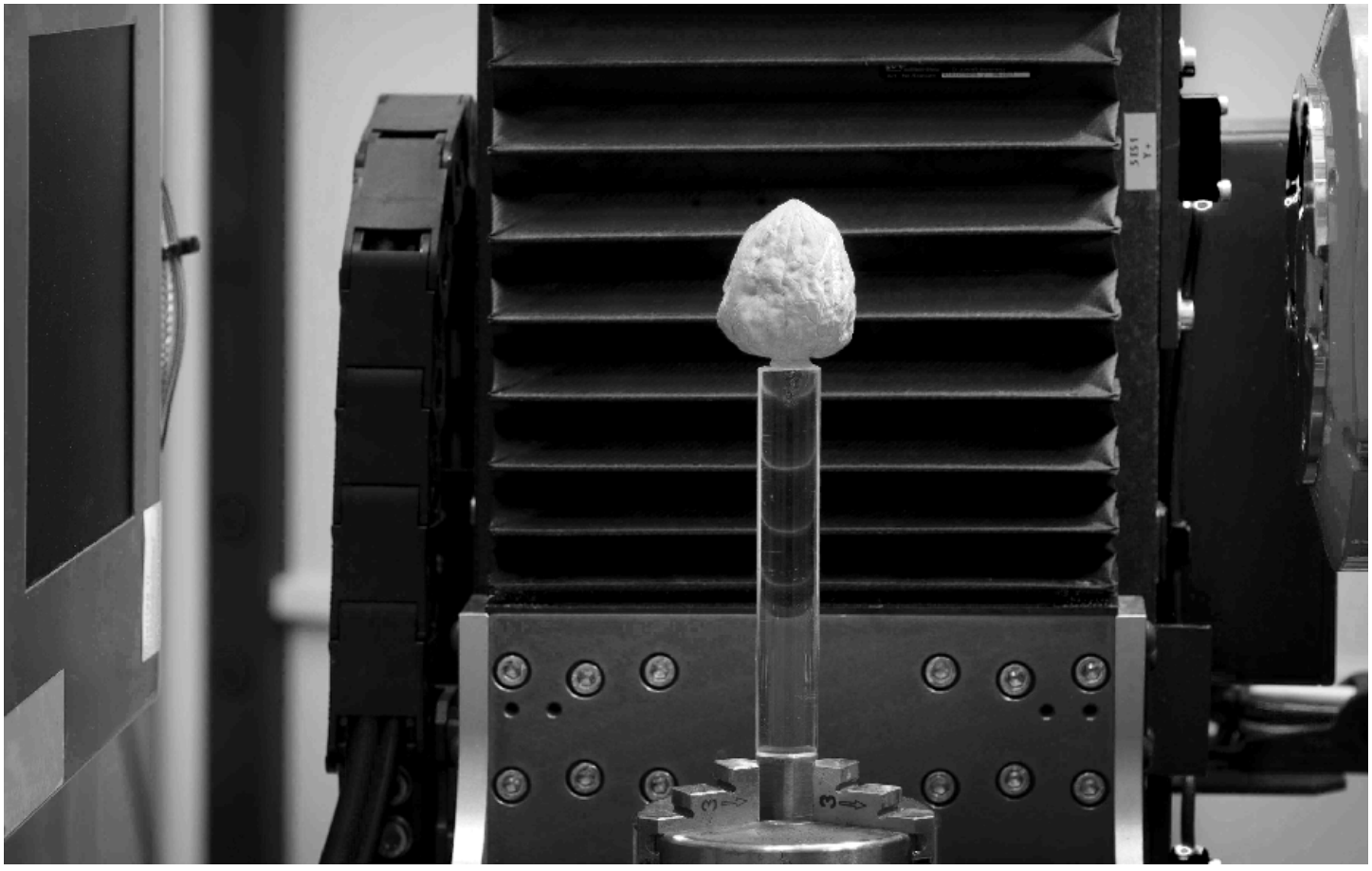

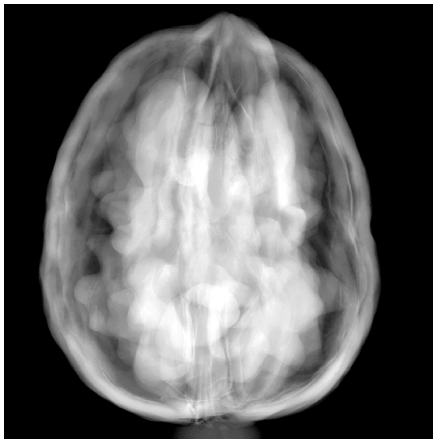

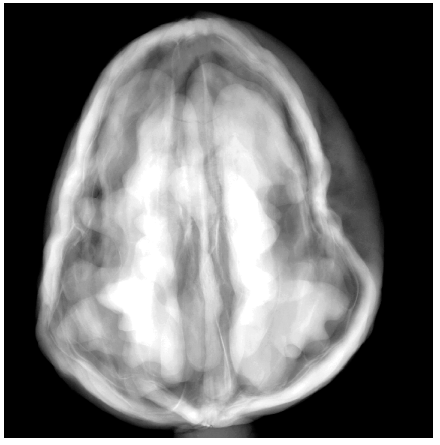

Laboratory and data collection by Keijo Hämäläinen and Aki Kallonen, University of Helsinki.

The data is openly available at http://fips.fi/dataset.php, thanks to Esa Niemi and Antti Kujanpää

Reconstructions of a 2D slice through the walnut using filtered back-projection (FBP)

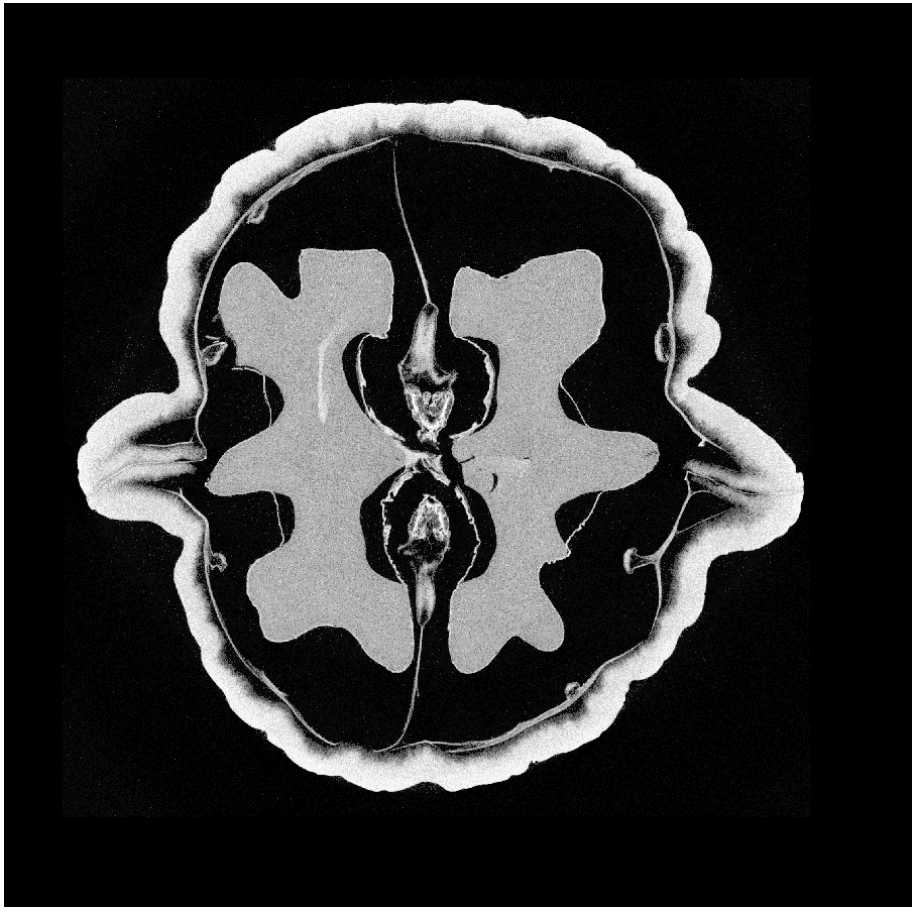

FBP with comprehensive data
(1200 projections)

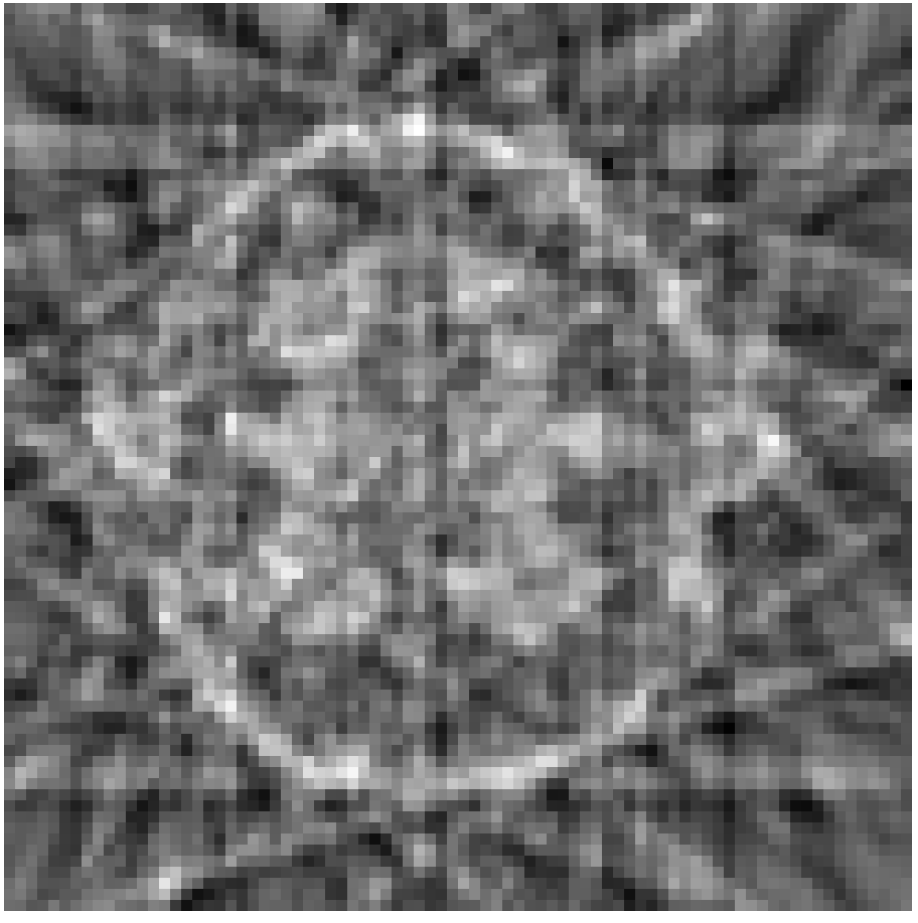

FBP with sparse data
(20 projections)

Sparse-data reconstruction of the walnut using non-negative Tikhonov regularization

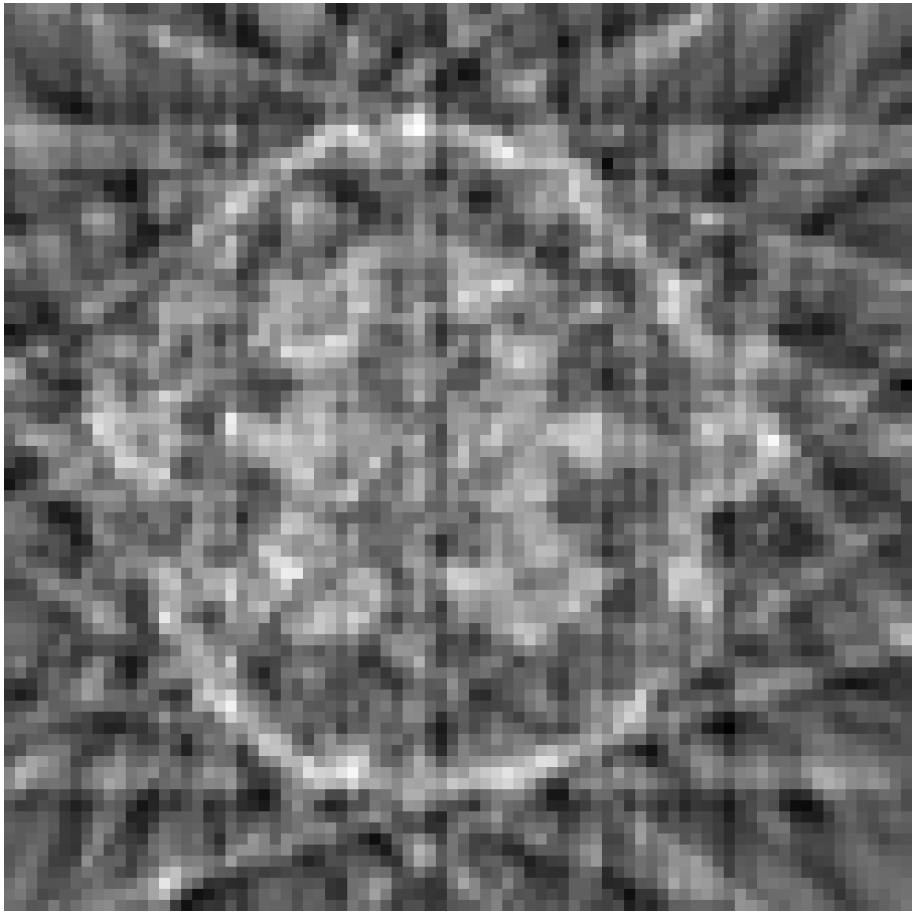

Filtered back-projection

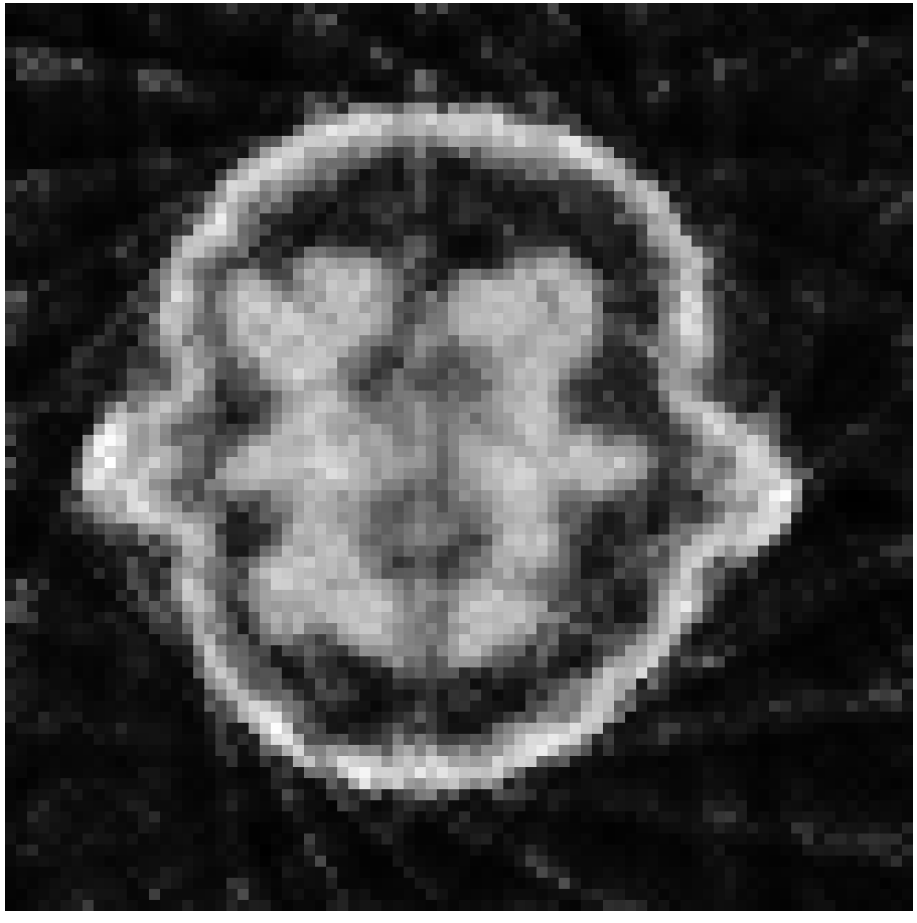

Constrained Tikhonov regularization

$$\arg\min_{f \in \mathbb{R}^n_+} \left\{ \|Af - m\|_2^2 + \alpha \|f\|_2^2 \right\}$$

Sparse-data reconstruction of the walnut using non-negative total variation regularization

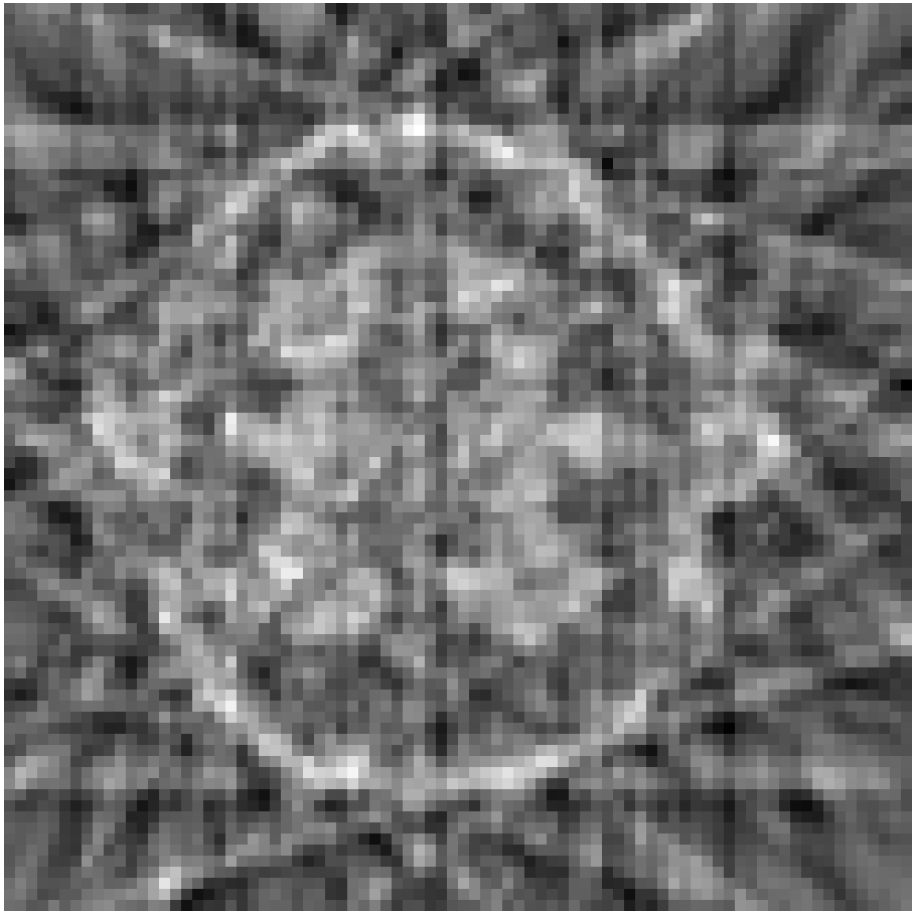

Filtered back-projection

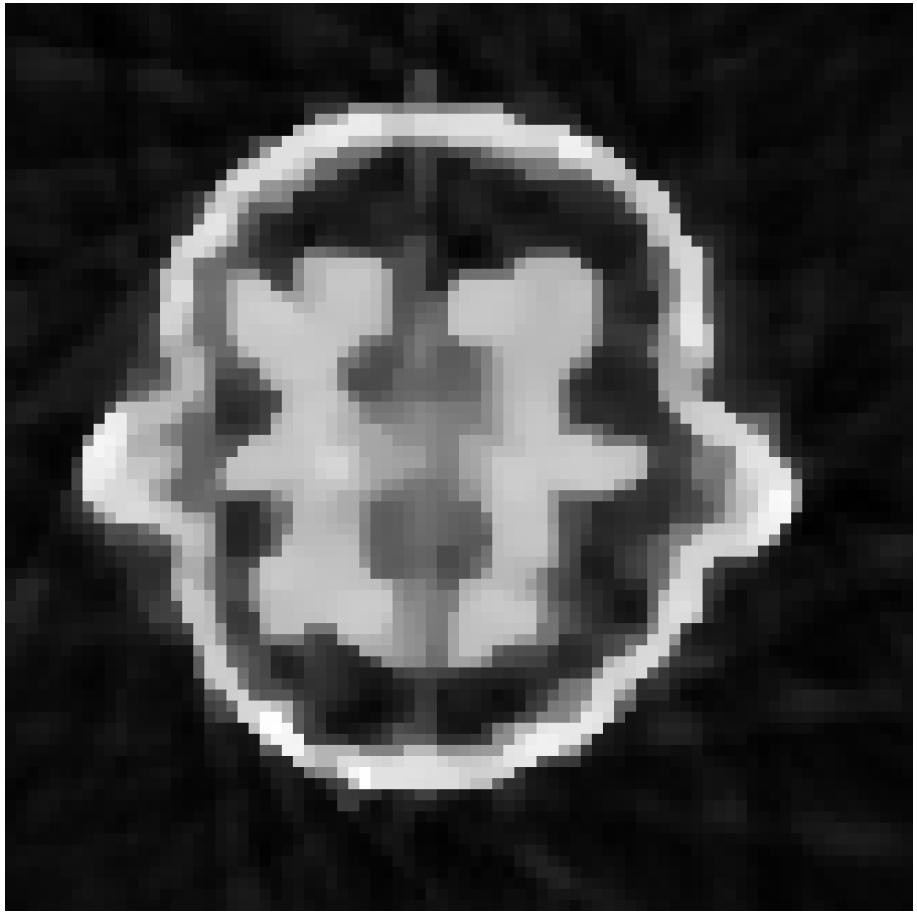

Constrained TV regularization

$$\arg\min_{f \in \mathbb{R}^n_+} \left\{ \|Af - m\|_2^2 + \alpha \|\nabla f\|_1 \right\}$$

Take-home messages from our overview of X-ray tomography

Uniqueness does not save us.
Even with an injective forward map, failure of Hadamard's condition 3 means that we need regularization for solving the inverse problem.

Non-uniqueness can be handled.
Our stable regularization strategy just needs enough *a priori* information for picking out a unique object among those with same data.

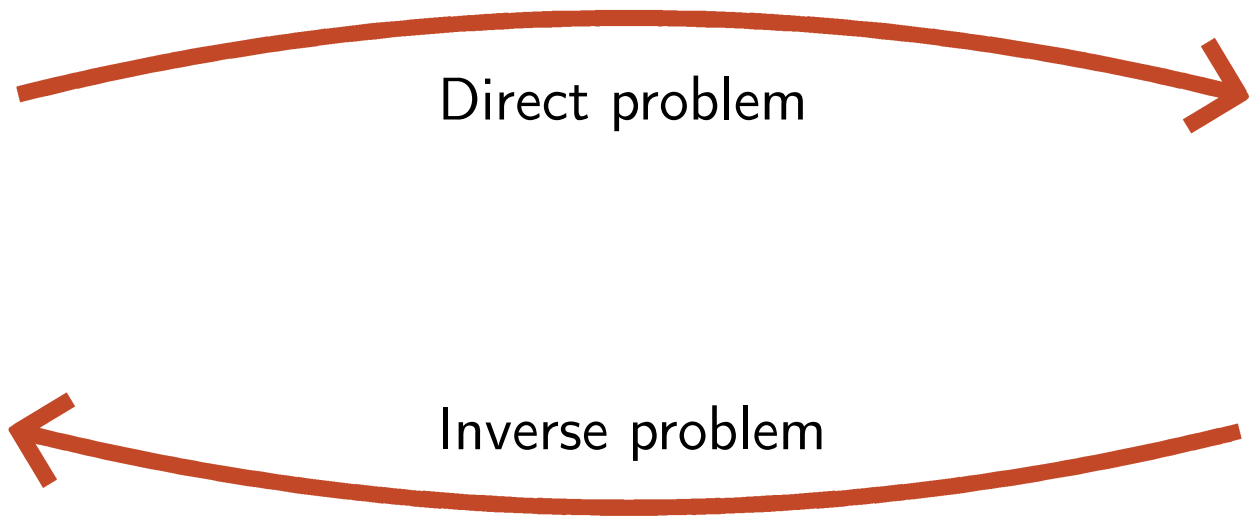

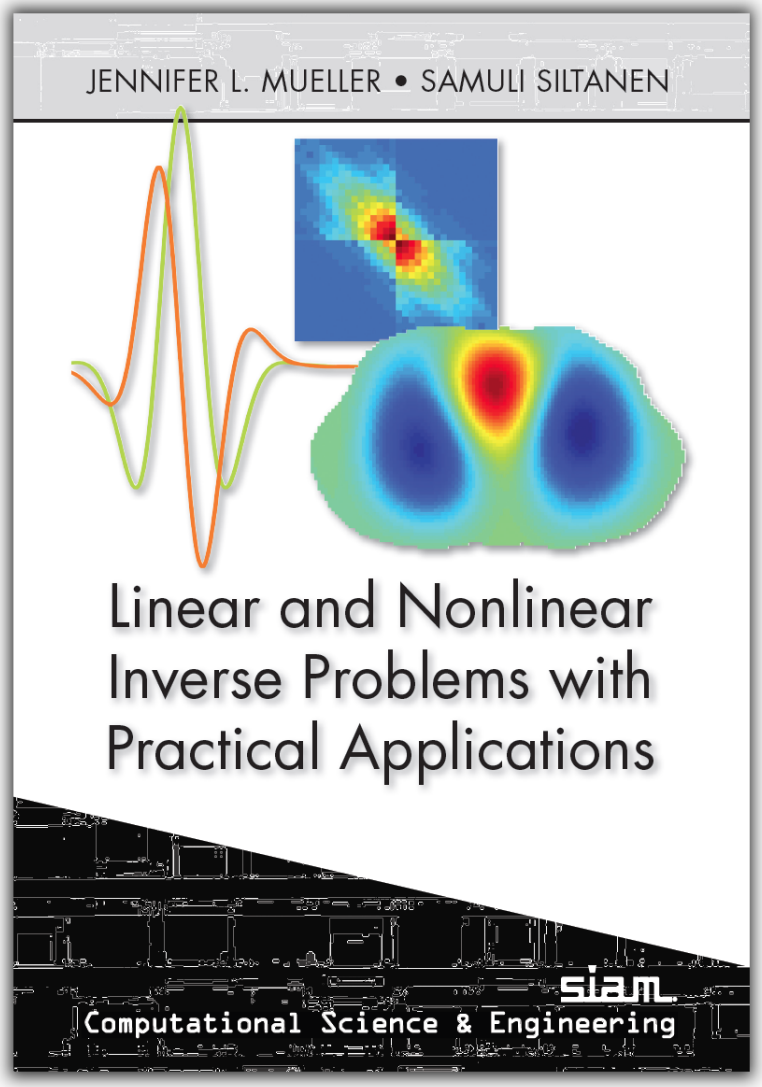

All Matlab codes freely available at this site!

Part I: Linear Inverse Problems

1 Introduction
2 Naïve reconstructions and inverse crimes
3 Ill-Posedness in Inverse Problems
4 Truncated singular value decomposition
5 Tikhonov regularization
6 Total variation regularization
7 Besov space regularization using wavelets
8 Discretization-invariance
9 Practical X-ray tomography with limited data
10 Projects

Part II: Nonlinear Inverse Problems

11 Nonlinear inversion
12 Electrical impedance tomography
13 Simulation of noisy EIT data
14 Complex geometrical optics solutions
15 A regularized D-bar method for direct EIT
16 Other direct solution methods for EIT
17 Projects

Outline

The VT device was developed in 2001–2012 by

Nuutti Hyvönen
Seppo Järvenpää
Jari Kaipio
Martti Kalke
Petri Koistinen
Ville Kolehmainen
Matti Lassas
Jan Moberg
Kati Niinimäki
Juha Pirttilä
Maaria Rantala
Eero Saksman
Henri Setälä
Erkki Somersalo
Antti Vanne
Simopekka Vänskä
Richard L. Webber

Application: dental implant planning, where a missing tooth is replaced with an implant

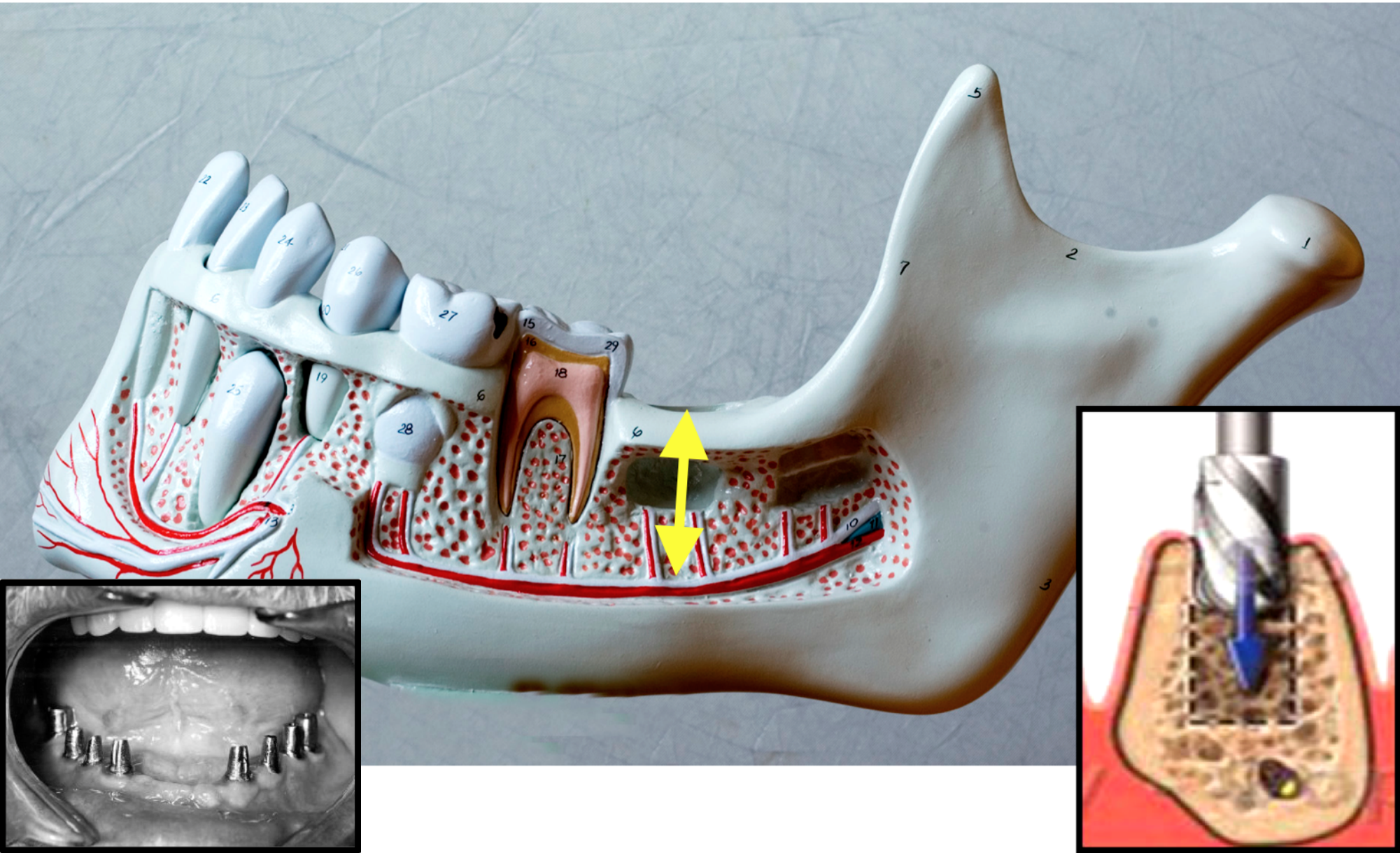

Nowadays, a digital panoramic imaging device is standard equipment at dental clinics

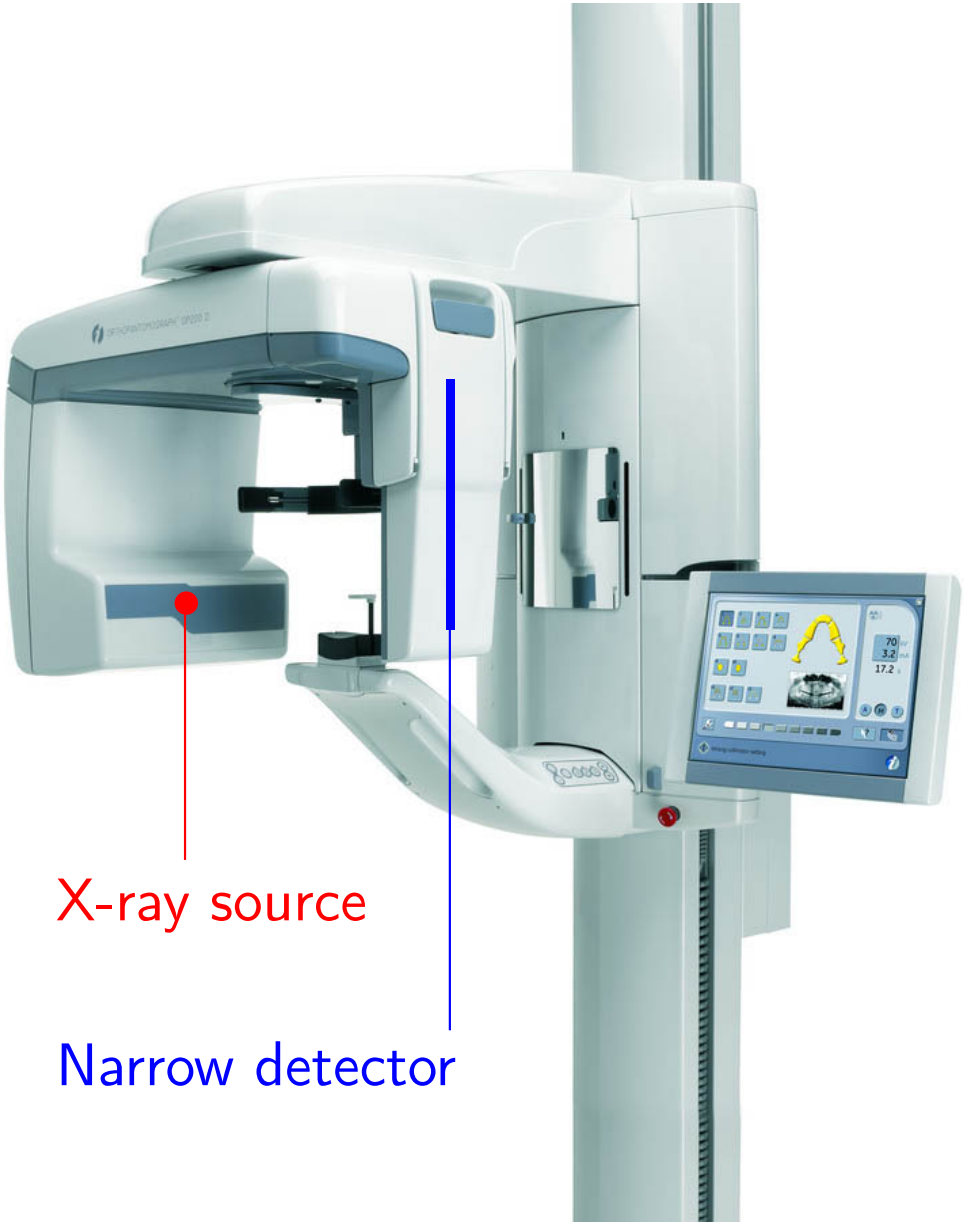

A panoramic dental image offers a general overview showing all teeth and other dento-maxillofacial structures simultaneously.

Panoramic images are not suitable for dental implant planning because of unavoidable geometric distortion.

We reprogram the panoramic X-ray device so that it collects projection data by scanning

(Loading video)

We reprogram the panoramic X-ray device so that it collects projection data by scanning

Number of projection images: **11**

Angle of view: **40 degrees**

Image size: **1000×1000 pixels**

The unknown vector f has **7 000 000** elements.

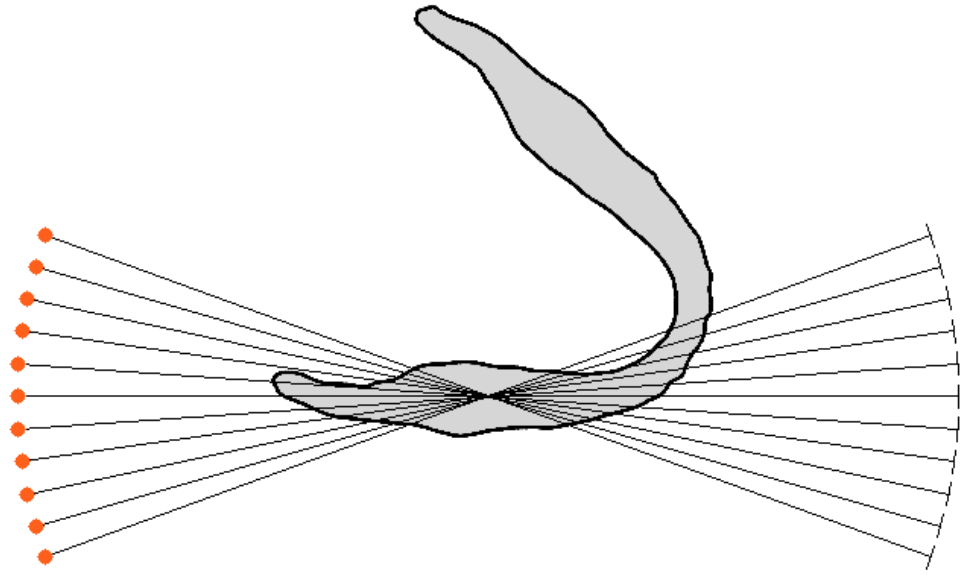



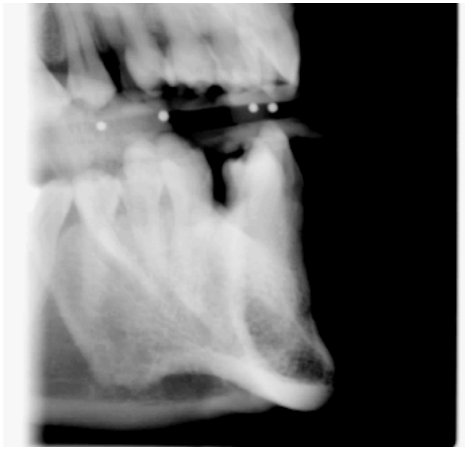
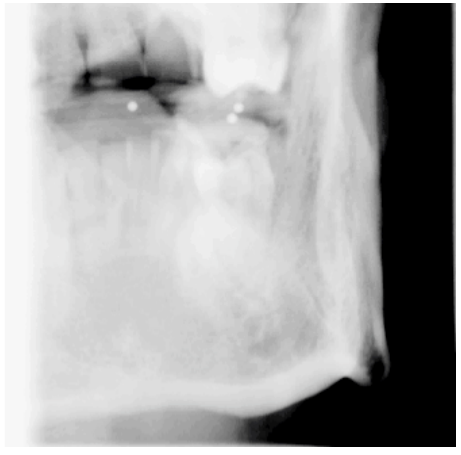

Here are example images of an actual patient: navigation image (left) and desired slice (right).

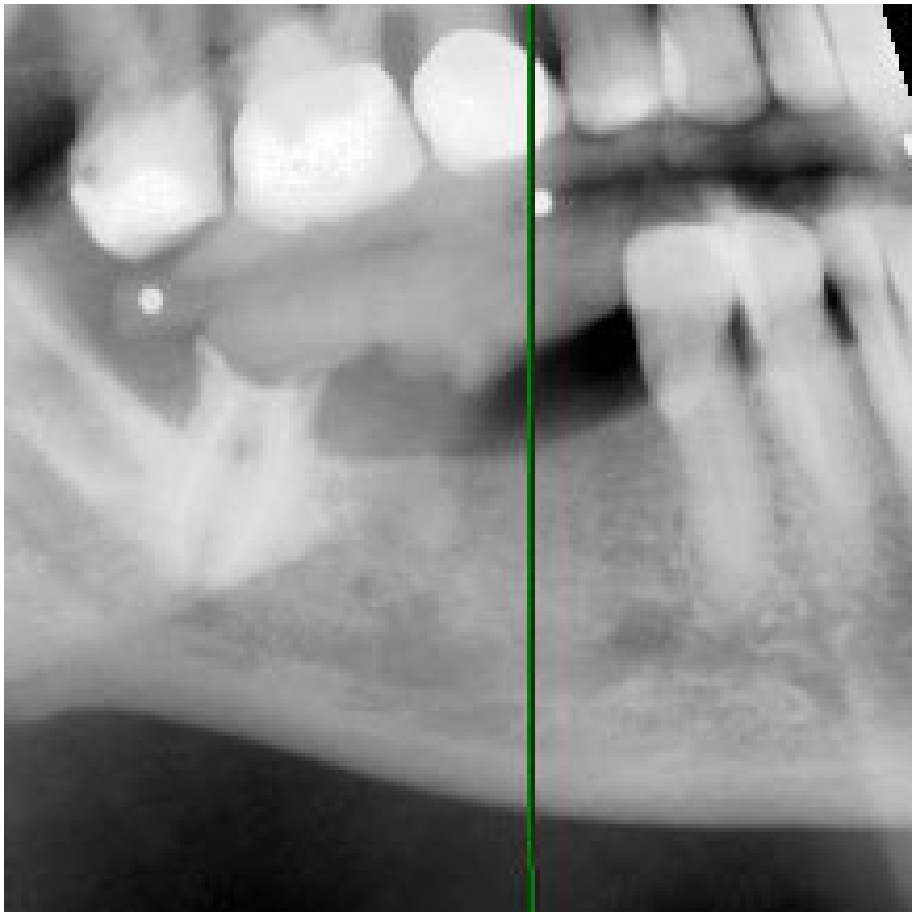

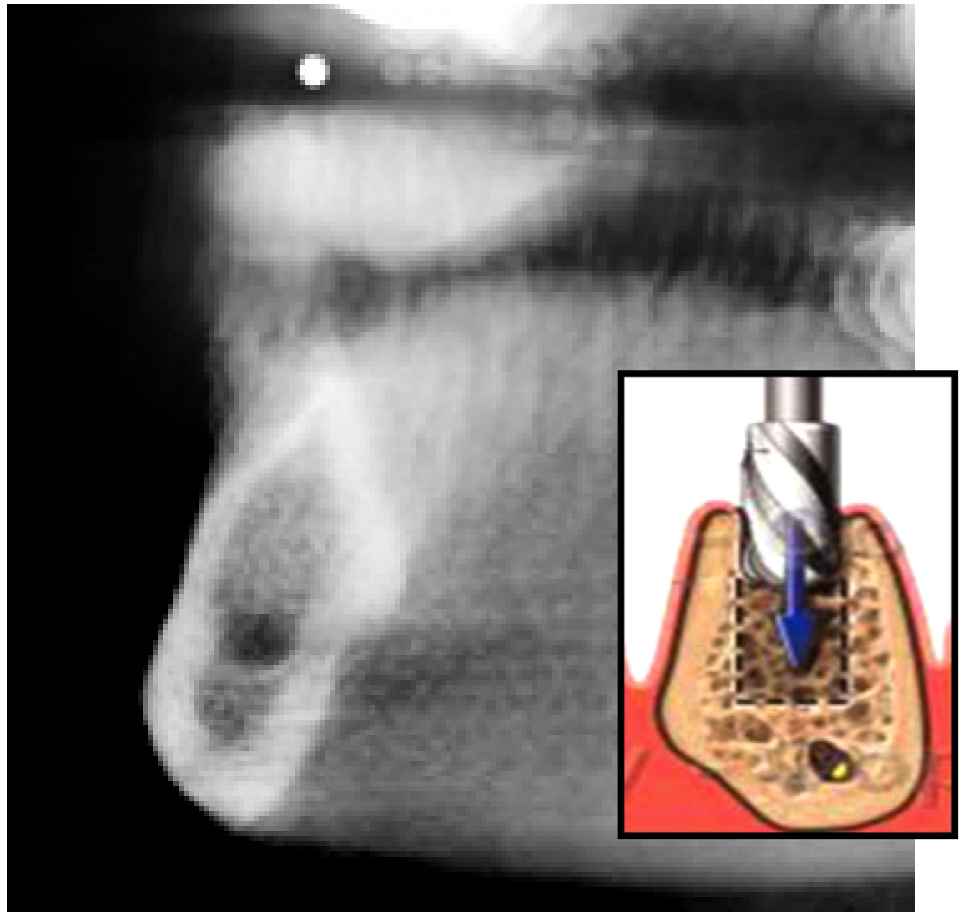

Kolehmainen, Vanne, S, Järvenpää, Kaipio, Lassas & Kalke **2006**, Kolehmainen, Lassas & S **2008**

Cederlund, Kalke & Welander **2009**, Hyvönen, Kalke, Lassas, Setälä & S **2010**, U.S. patent 7269241

The radiation dose of the VT device is lowest among 3D dental imaging modalities

Modality	μSv
Head CT	2100
CB Mercuray	558
i-Cat	193
NewTom 3G	59
VT device	**13**

[Ludlow, Davies-Ludlow, Brooks & Howerton **2006**]

The VT device has been available in the international market since 2008.

These books are recommended for learning the mathematics of practical X-ray tomography

1983 Deans: The Radon Transform and Some of Its Applications

1986 Natterer: The mathematics of computerized tomography

1988 Kak & Slaney: Principles of computerized tomographic imaging

1996 Engl, Hanke & Neubauer: Regularization of inverse problems

1998 Hansen: Rank-deficient and discrete ill-posed problems

2001 Natterer & Wübbeling: Mathematical Methods in Image Reconstruction

2008 Buzug: Computed Tomography: From Photon Statistics to Modern Cone-Beam CT

2008 Epstein: Introduction to the mathematics of medical imaging

2010 Hansen: Discrete inverse problems

2012 Mueller & S: Linear and Nonlinear Inverse Problems with Practical Applications

Another great resource is Per Christian Hansen's 3D tomography toolbox TVreg

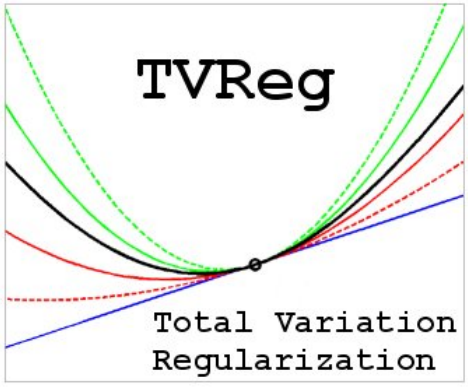

TVreg: Software for 3D Total Variation Regularization (for Matlab Version 7.5 or later), developed by Tobias Lindstrøm Jensen, Jakob Heide Jørgensen, Per Christian Hansen, and Søren Holdt Jensen.

Website: `http://www2.imm.dtu.dk/ pcha/TVReg/`

Outline

Chest imaging is the standard application example of EIT in this talk

Medical applications: monitoring cardiac activity, lung function, and pulmonary perfusion. Also, electrocardiography (ECG) can be enhanced using knowledge about conductivity distribution.

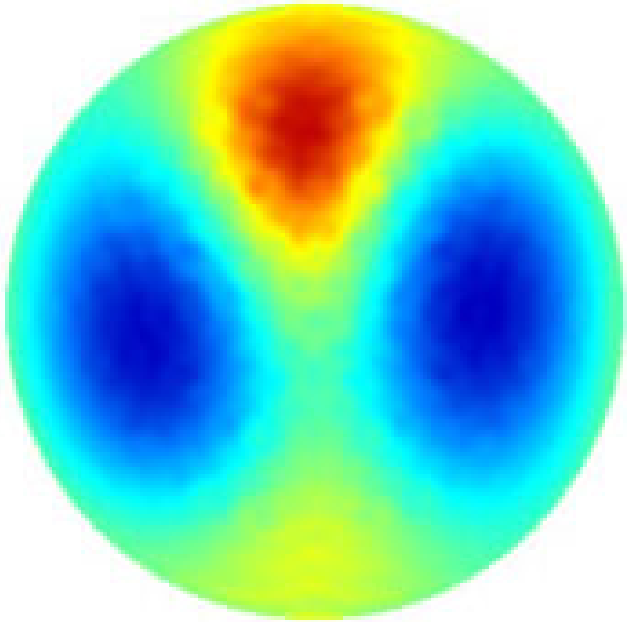

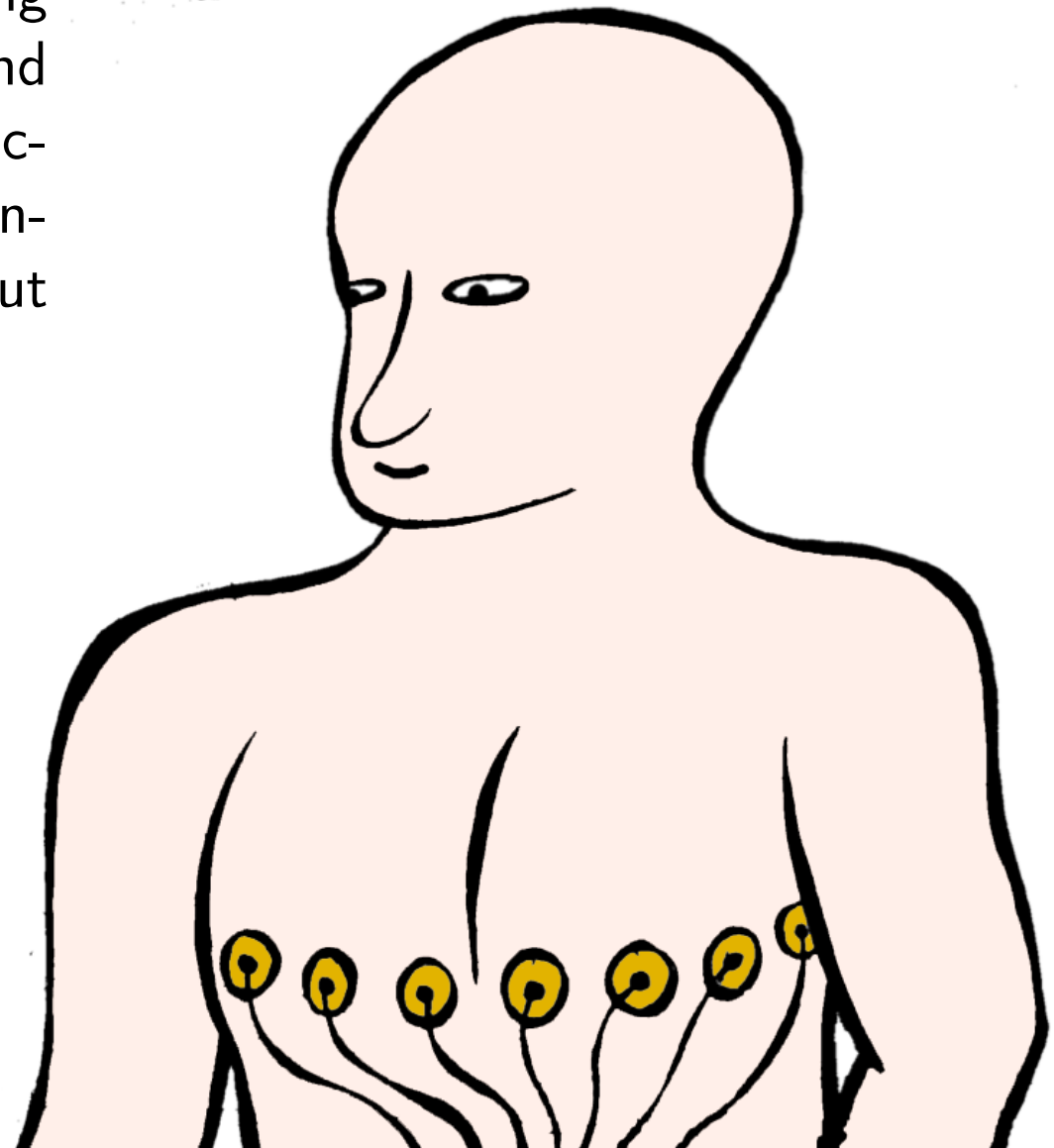

D-bar reconstruction of *in vivo* chest data

(Loading video)

[Montoya & Mueller 2012]

The most promising use of EIT is detection of breast cancer in combination with mammography

ACT4 and mammography devices

Radiolucent electrodes

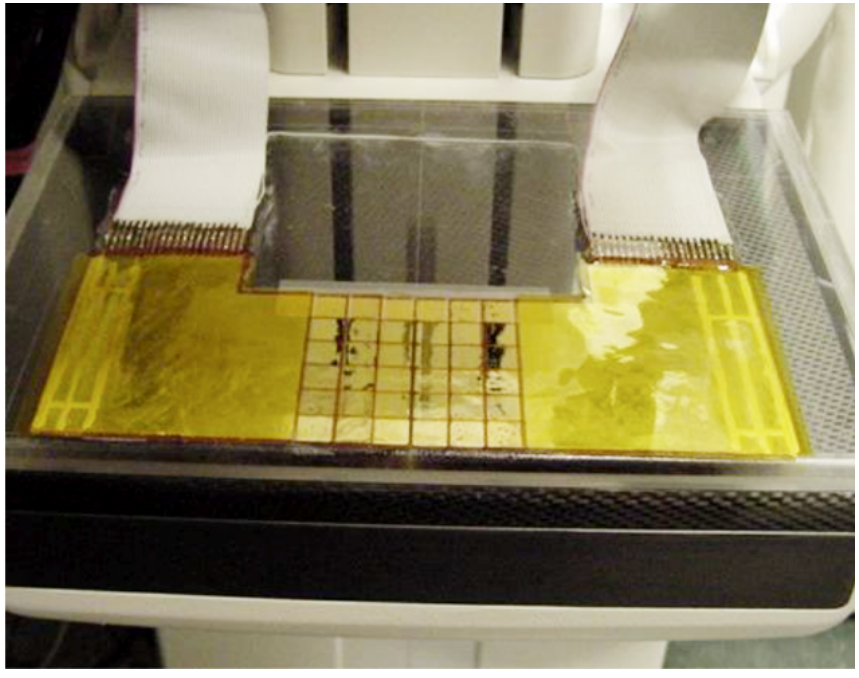

Cancerous tissue is up to four times more conductive than healthy breast tissue [Jossinet 1998]. The above experiment by **David Isaacson**'s team measures 3D X-ray mammograms and EIT data at the same time.

Which of these three breasts have cancer?

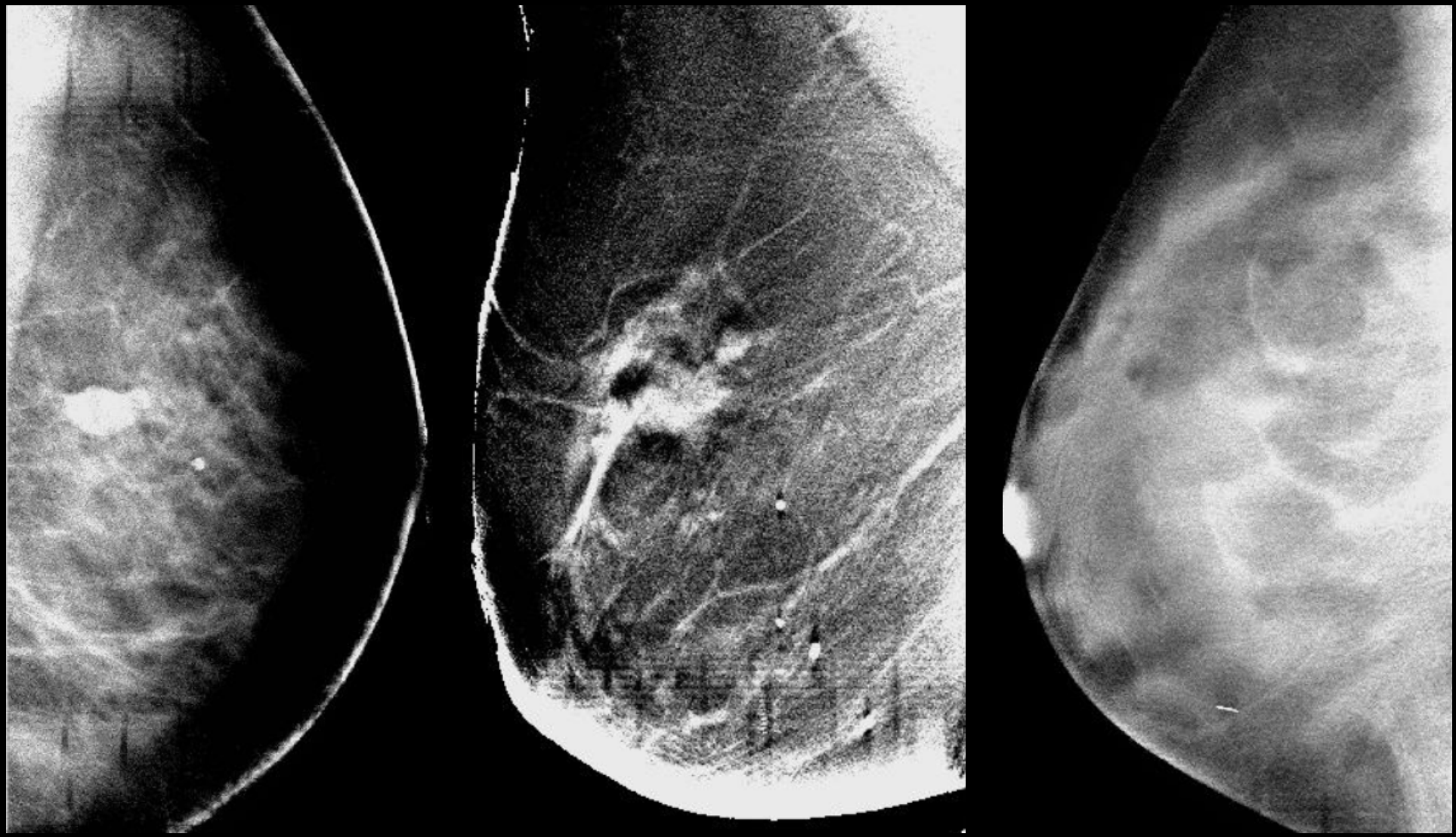

Spectral EIT can detect cancerous tissue

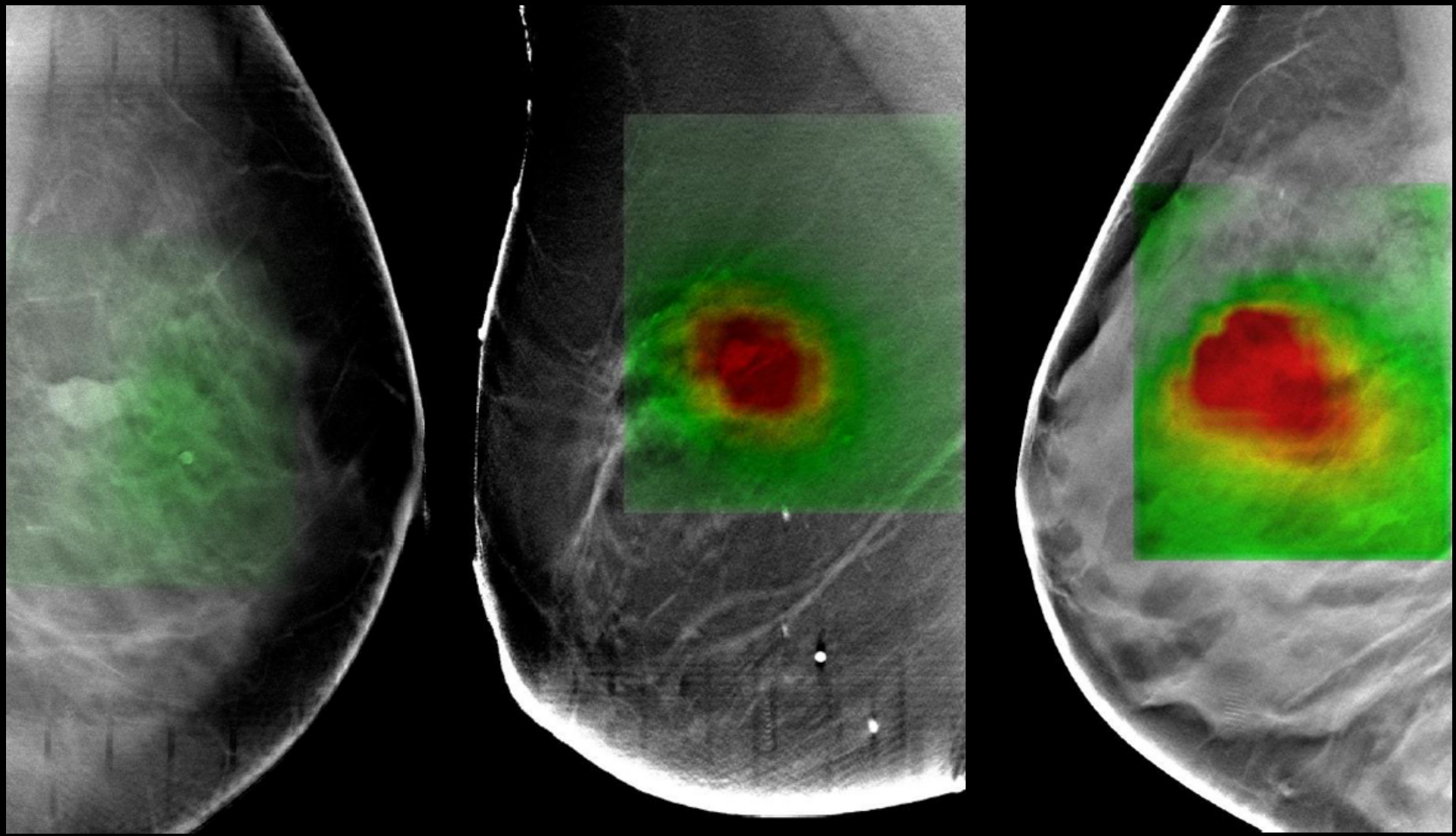

[Kim, Isaacson, Xia, Kao, Newell & Saulnier 2007]

EIT can be used for heart imaging

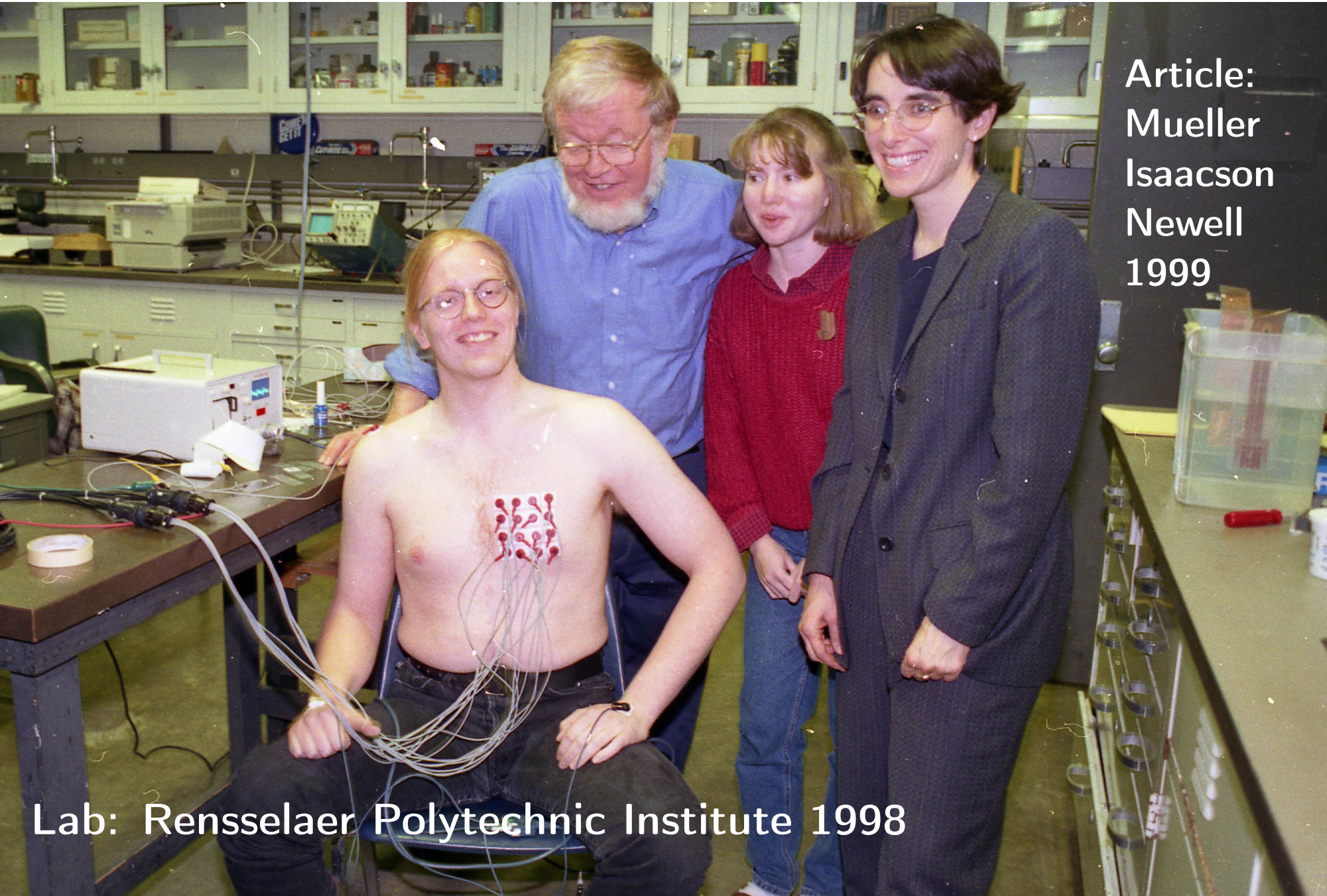

EIT can potentially be used for imaging changes in vocal folds due to excessive voice use

Laukkanen
León
Lima
Liu
Moura
Seppänen
S

EIT can perhaps be used for imaging changes in vocal folds due to dehydration

EIT can be used for nondestructive testing: here for crack detection in concrete structures

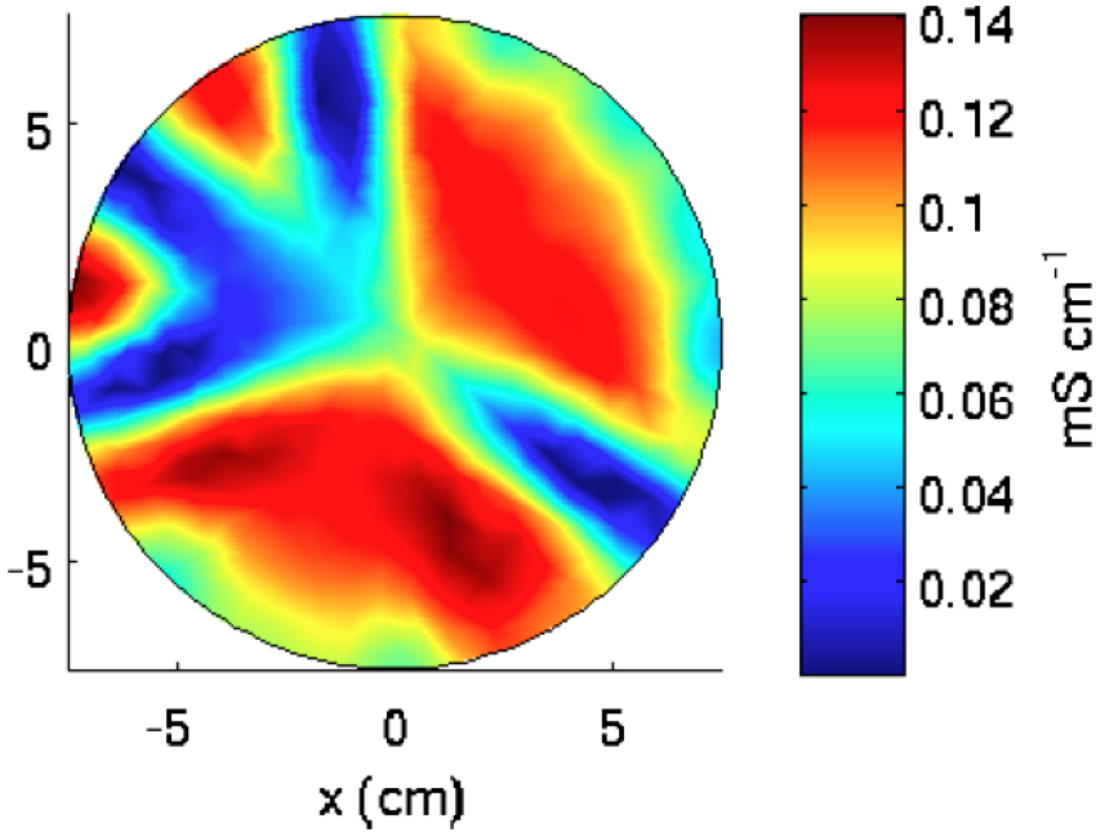

[Karhunen, Seppänen, Lehikoinen, Monteiro & Kaipio 2010]
[Karhunen, Seppänen, Lehikoinen, Monteiro, Kaipio, Blunt, Hyvönen]

EIT can be used for nondestructive testing: here for water in concrete structures

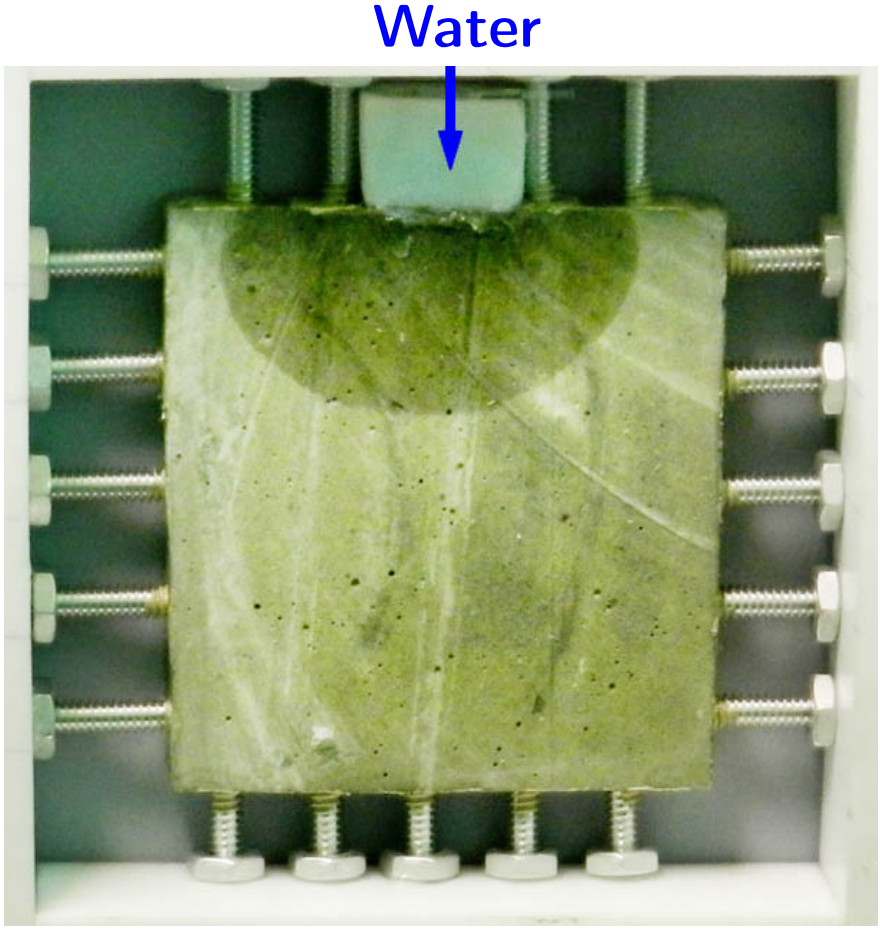

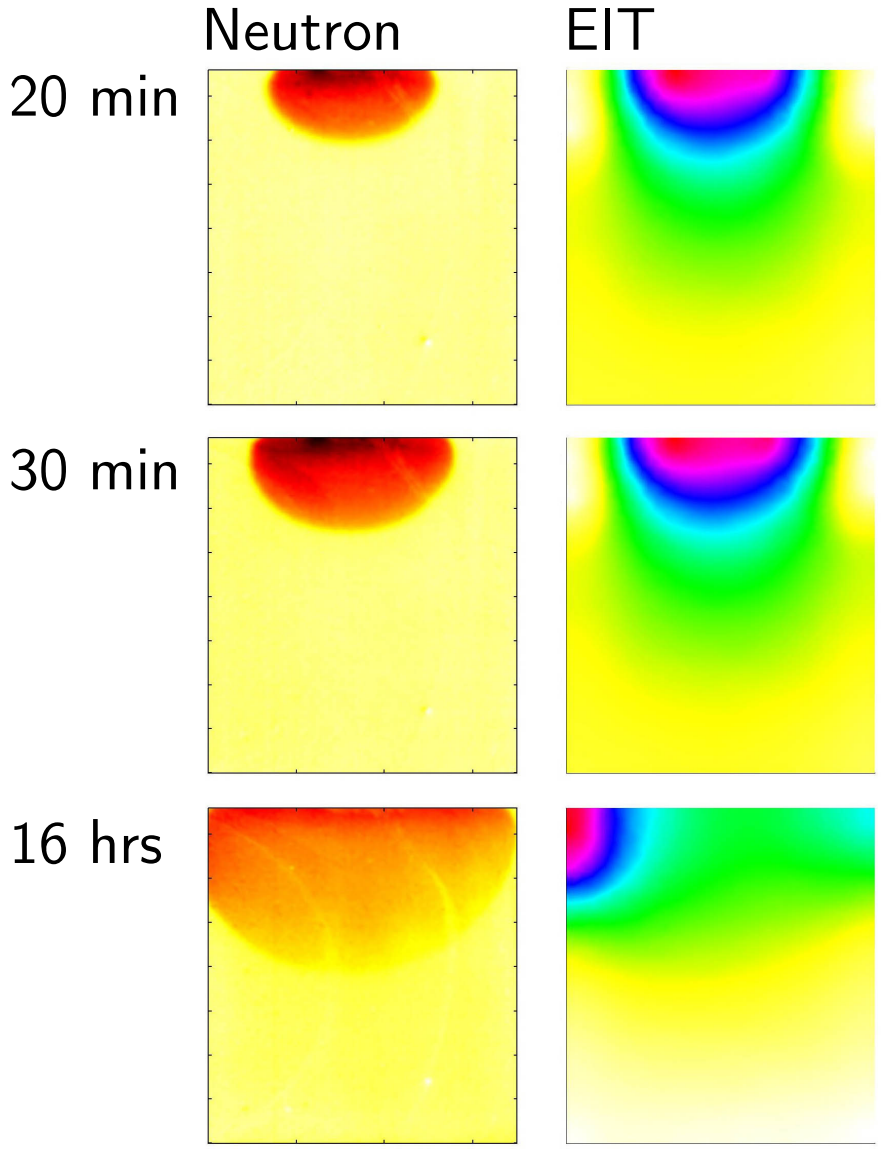

[Hallaji, Seppänen & Pour-Ghaz 2015]

Outline

Note that EIT data collection involves applying several current patterns

Saline and agar phantom

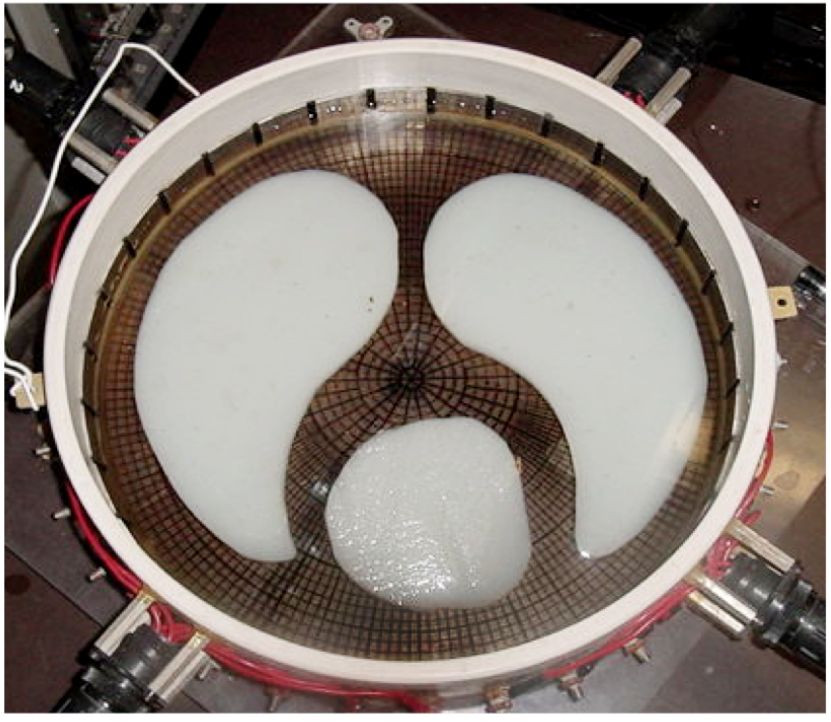

Apply current pattern $\cos\theta$

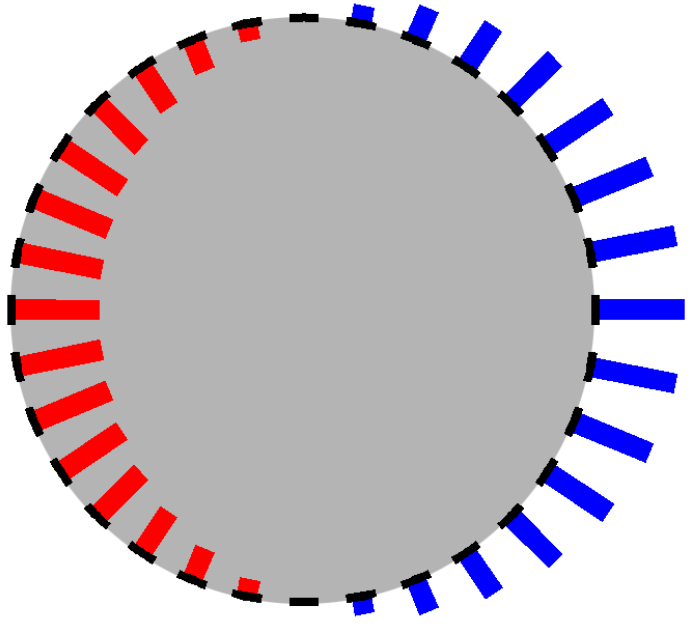

Measure the resulting voltages at the 32 electrodes

Note that EIT data collection involves applying several current patterns

Saline and agar phantom

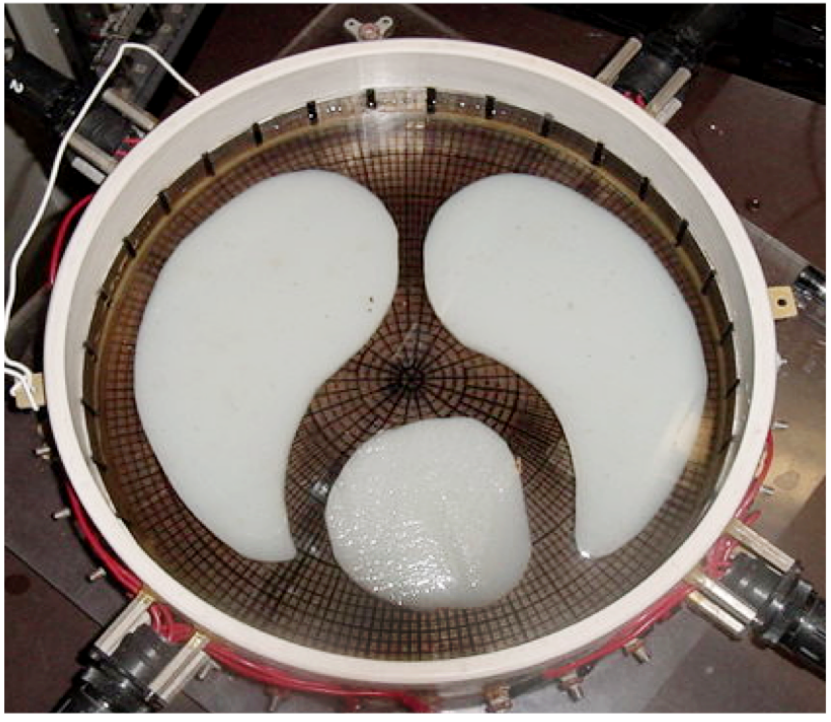

Apply current pattern $\cos 2\theta$

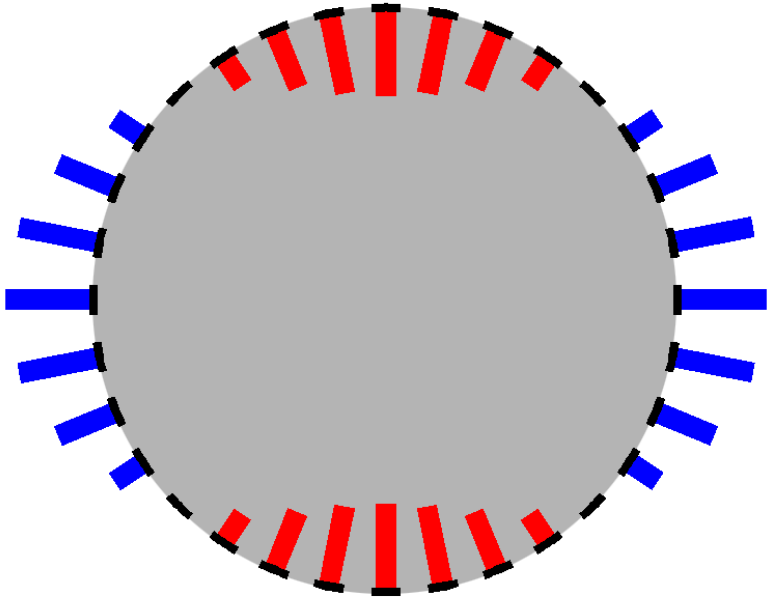

Measure the resulting voltages at the 32 electrodes

Note that EIT data collection involves applying several current patterns

Saline and agar phantom

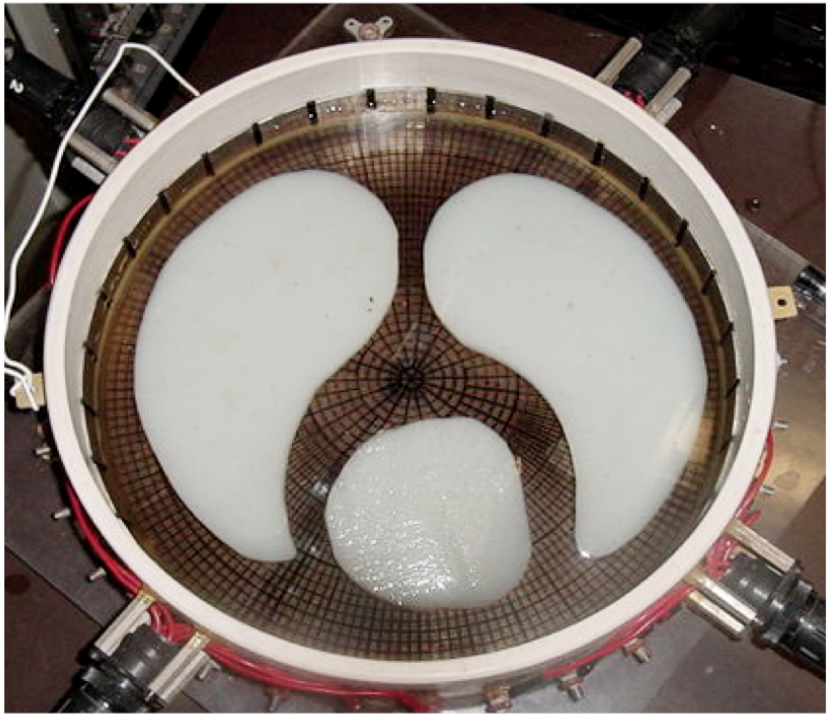

Apply current pattern $\cos 3\theta$

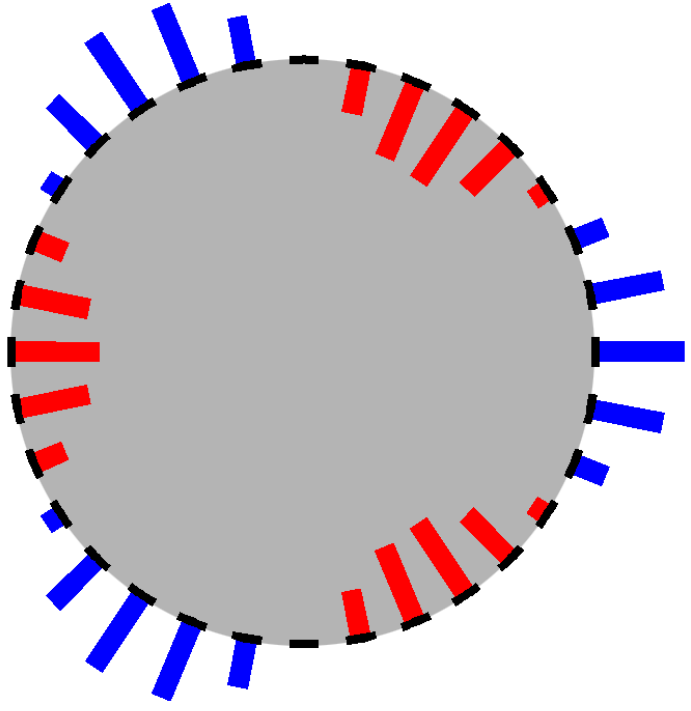

Measure the resulting voltages at the 32 electrodes

Note that EIT data collection involves applying several current patterns

Saline and agar phantom

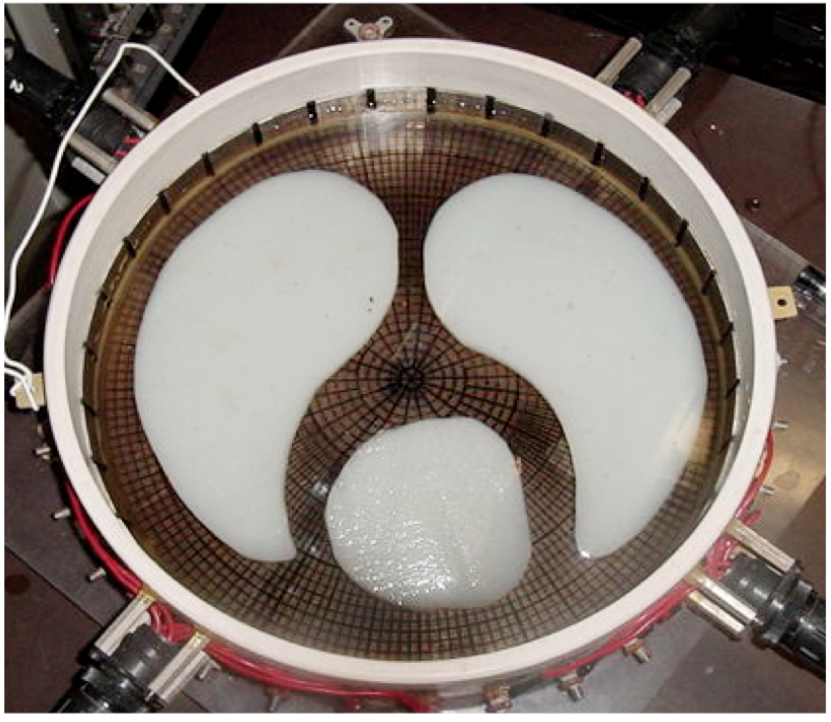

Apply current pattern $\cos 4\theta$

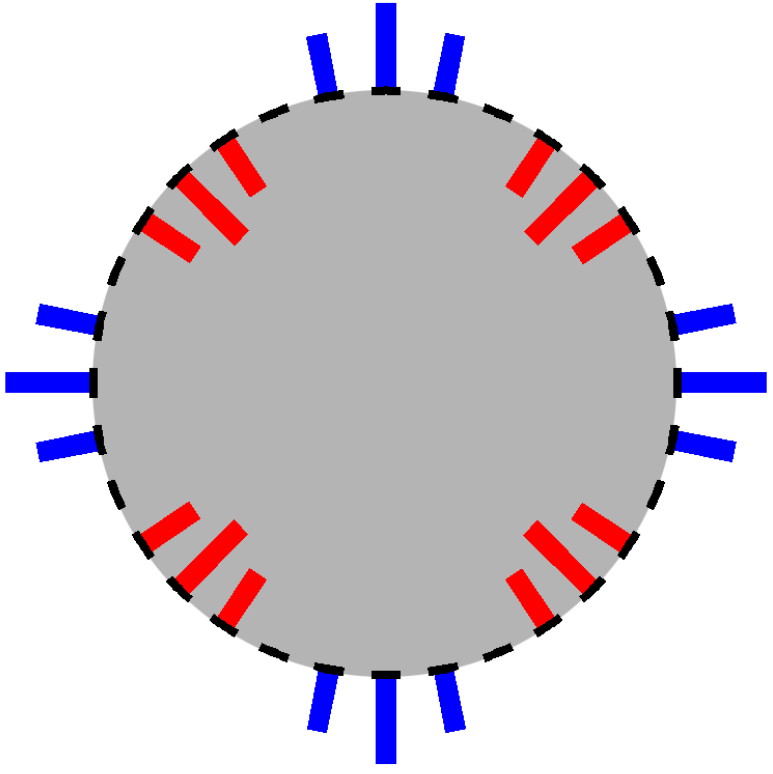

Measure the resulting voltages at the 32 electrodes

Note that EIT data collection involves applying several current patterns

Saline and agar phantom

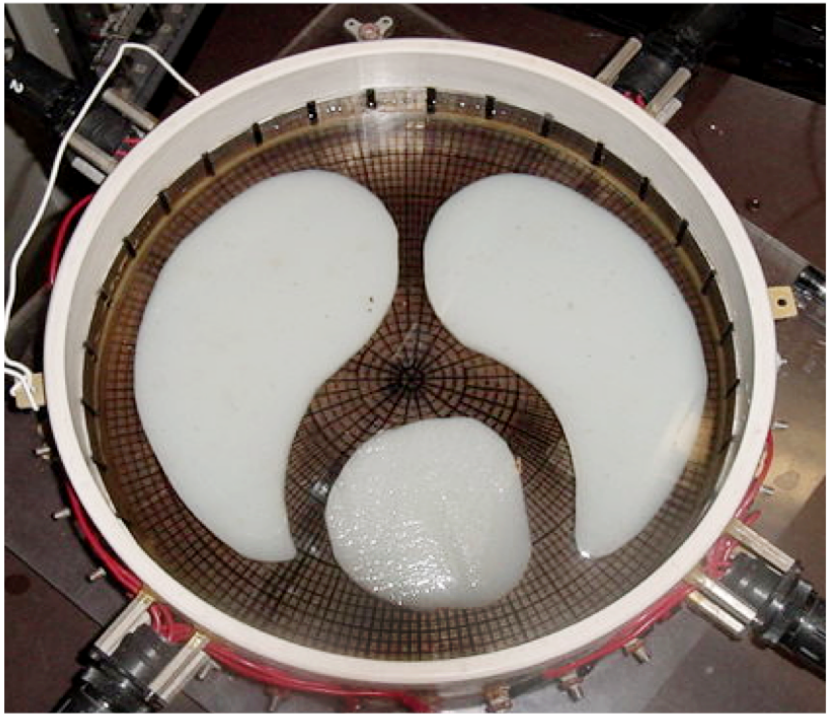

Apply current pattern $\cos 5\theta$

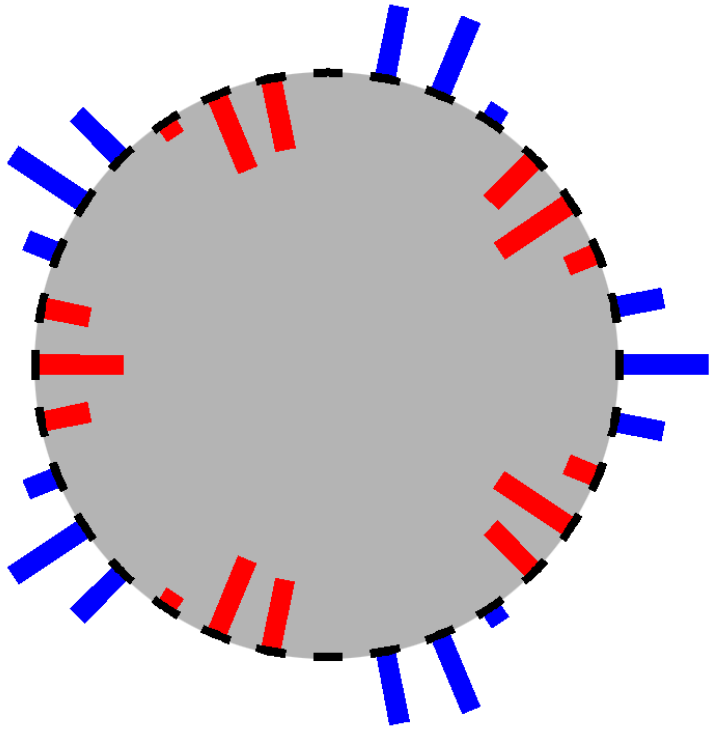

Measure the resulting voltages at the 32 electrodes

Note that EIT data collection involves applying several current patterns

Saline and agar phantom

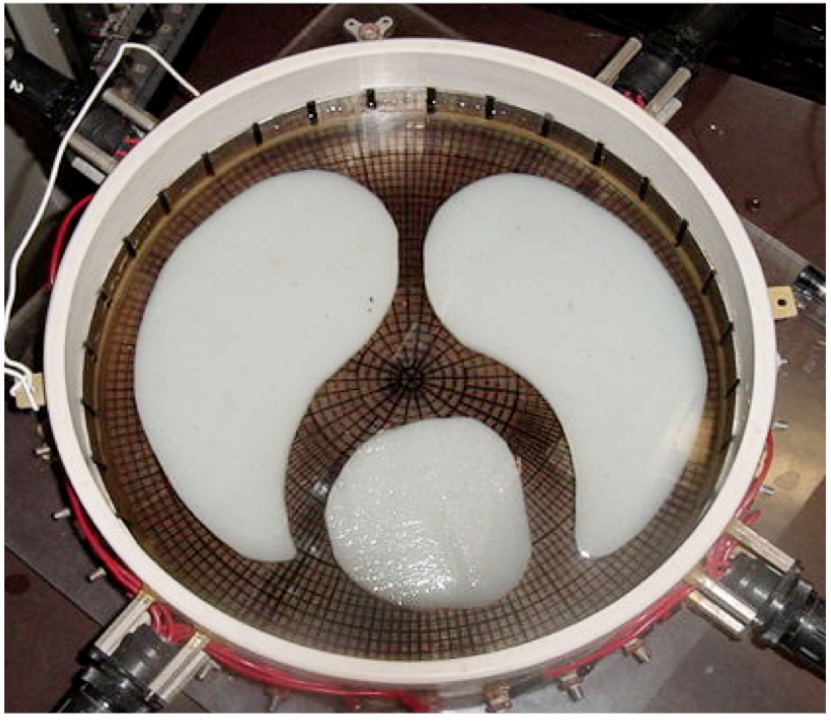

Apply current pattern $\cos 16\theta$

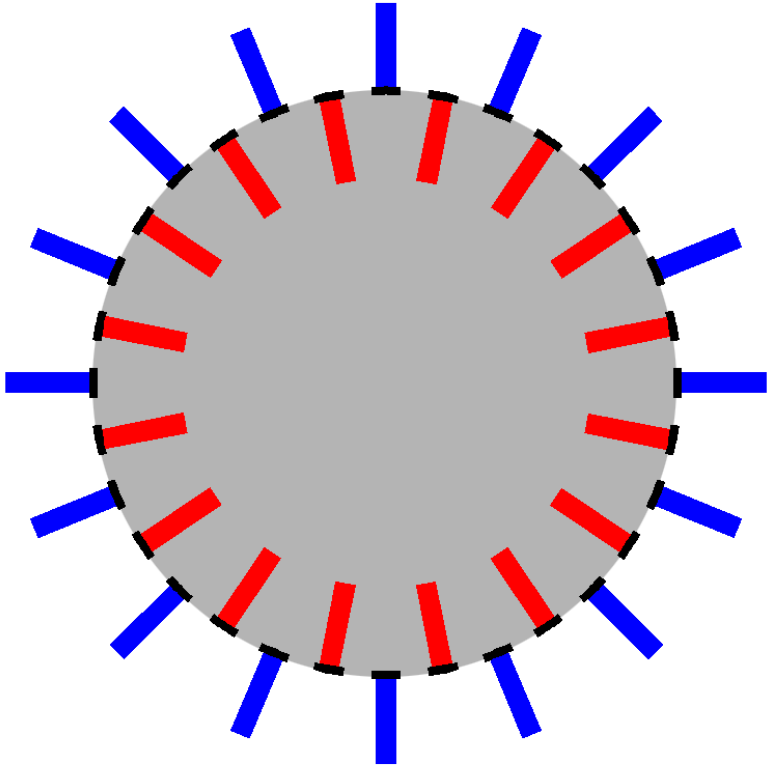

Measure the resulting voltages at the 32 electrodes

The D-bar method works for real EIT data, such as laboratory phantoms and *in vivo* human data

Saline and agar phantom

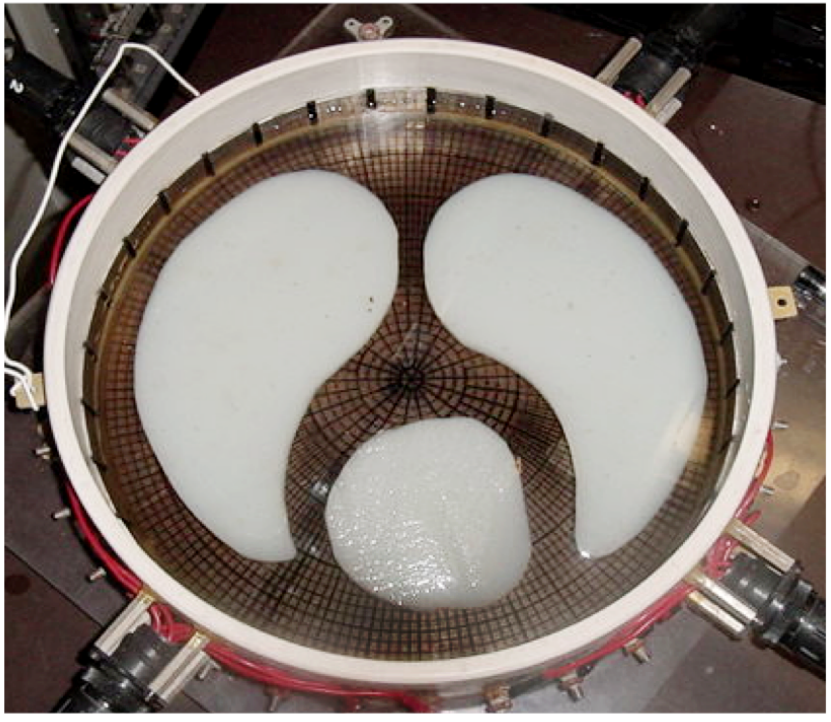

Reconstruction ($R = 4$)

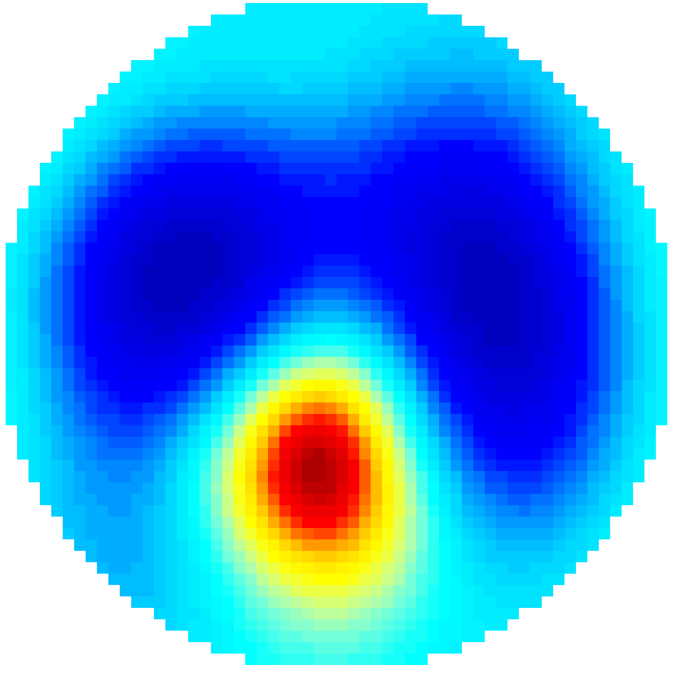

[Isaacson, Mueller, Newell & S 2004]
[Montoya 2012]

The mathematical model of EIT is the inverse conductivity problem introduced by Calderón

Let $\Omega \subset \mathbb{R}^2$ be the unit disc and let conductivity $\sigma : \Omega \to \mathbb{R}$ satisfy

$$0 < M^{-1} \leq \sigma(z) \leq M.$$

Applying voltage f at the boundary $\partial\Omega$ leads to the elliptic PDE

$$\begin{cases} \nabla \cdot \sigma \nabla u &= 0 \text{ in } \Omega, \\ u|_{\partial\Omega} &= f. \end{cases}$$

Boundary measurements are modelled by the Dirichlet-to-Neumann map

$$\Lambda_\sigma : f \mapsto \sigma \frac{\partial u}{\partial \vec{n}}|_{\partial\Omega}.$$

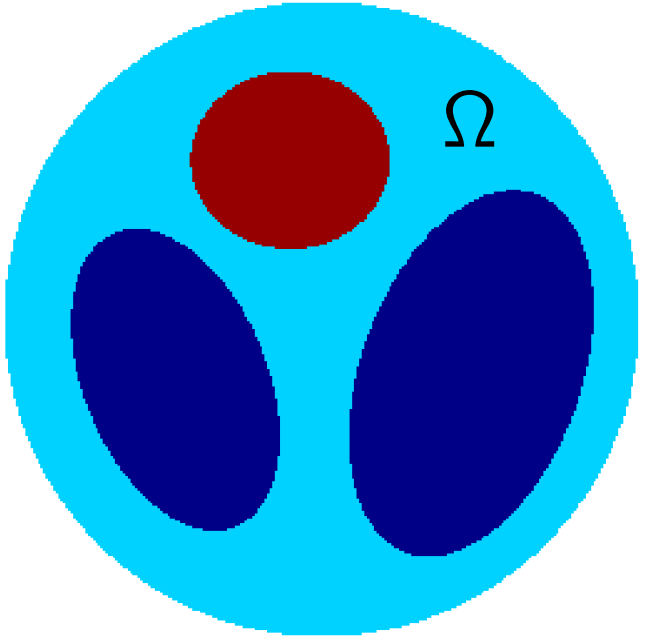

Calderón's problem is to recover σ from the knowledge of Λ_σ. It is a nonlinear and ill-posed inverse problem.

Why is the forward map $F : \sigma \mapsto \Lambda_\sigma$ nonlinear?

Define a quadratic form $\mathcal{P}_\sigma$ for functions $f : \partial\Omega \to \mathbb{R}$ by

$$\mathcal{P}_\sigma(f) = \int_\Omega \sigma |\nabla u|^2 \, dz, \tag{1}$$

where u is the solution of the Dirichlet problem

$$\begin{cases} \nabla \cdot \sigma \nabla u &= 0 \text{ in } \Omega, \\ u|_{\partial\Omega} &= f. \end{cases}$$

Now the map $\sigma \mapsto \mathcal{P}_\sigma$ is nonlinear because u depends on σ in (1). Physically, $\mathcal{P}_\sigma(f)$ is the power needed for maintaining the voltage potential f on the boundary $\partial\Omega$. Integrate by parts in (1):

$$\mathcal{P}_\sigma(f) = \int_{\partial\Omega} f \left(\sigma \frac{\partial u}{\partial \vec{n}}\right) ds = \int_{\partial\Omega} f \left(\Lambda_\sigma f\right) ds.$$

Thus the map $\sigma \mapsto \Lambda_\sigma$ cannot be linear in σ.

Outline

Ill-posed inverse problems are defined as opposites of well-posed direct problems

Hadamard (1903): a problem is well-posed if the following conditions hold.

1. A solution exists,
2. The solution is unique,
3. The solution depends continuously on the input.

Well-posed direct problem:
Input σ, find infinite-precision data Λ_σ.

Ill-posed inverse problem:
Input noisy data Λ_σ^δ, reconstruct σ.

We illustrate the ill-posedness of EIT using a simulated example

σ_1

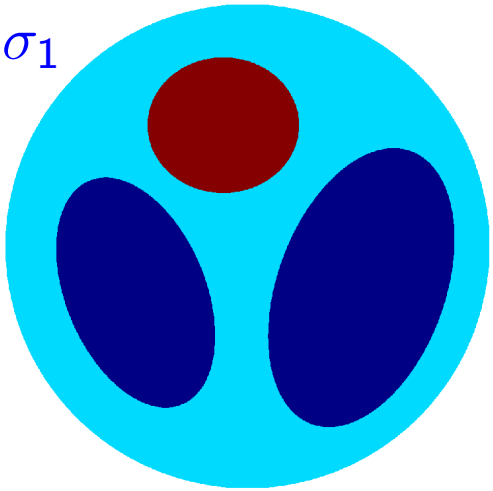

σ_2

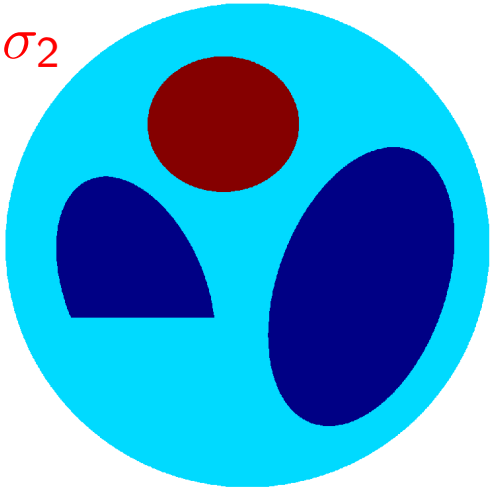

We apply the voltage distribution $f(\theta) = \cos\theta$ at the boundary of the two different phantoms

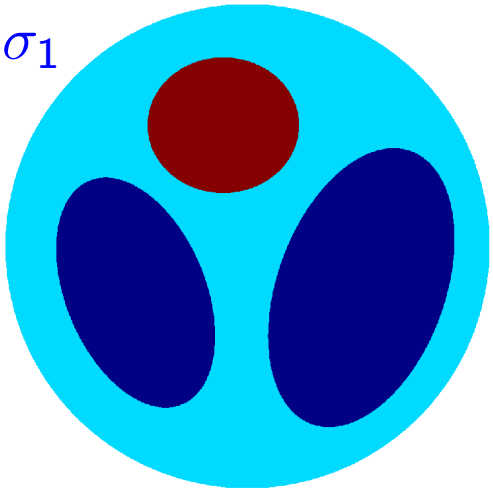

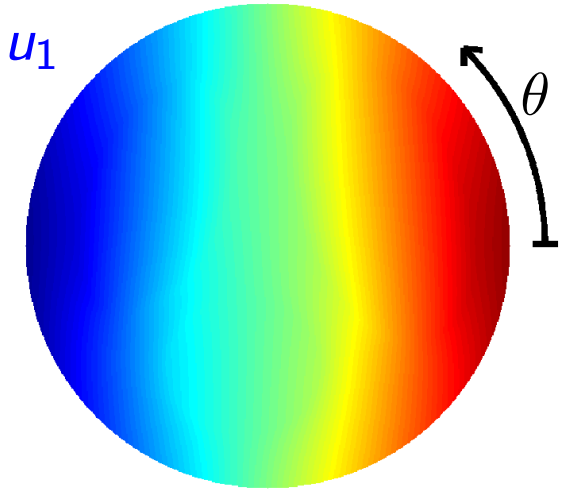

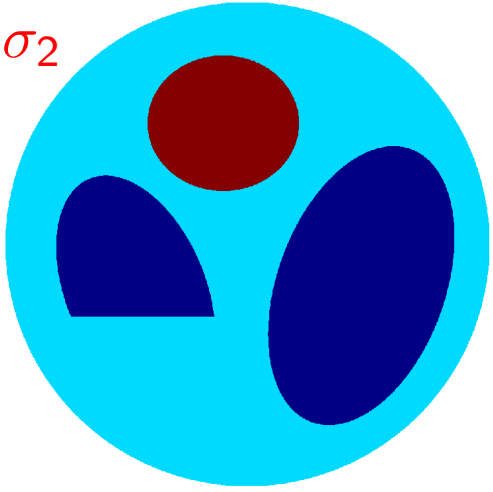

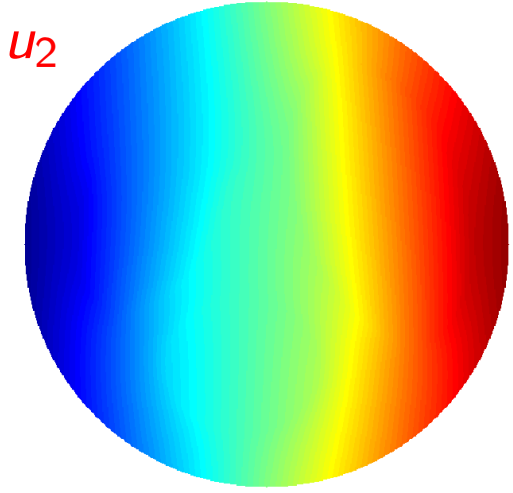

The measurement is the distribution of current through the boundary

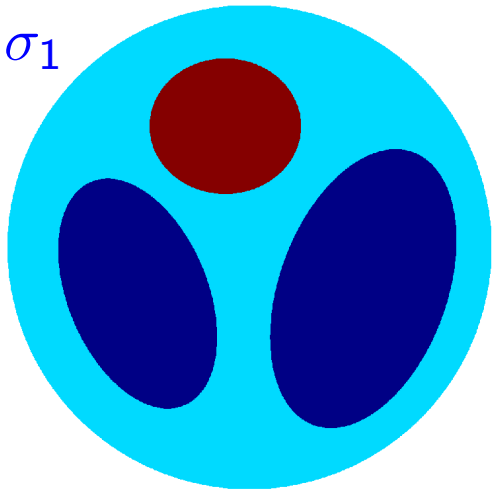

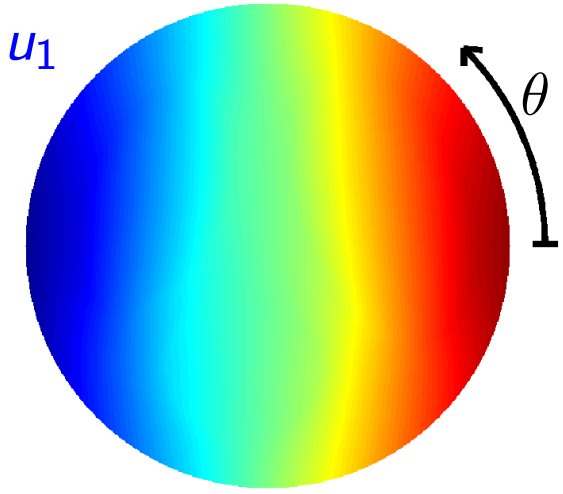

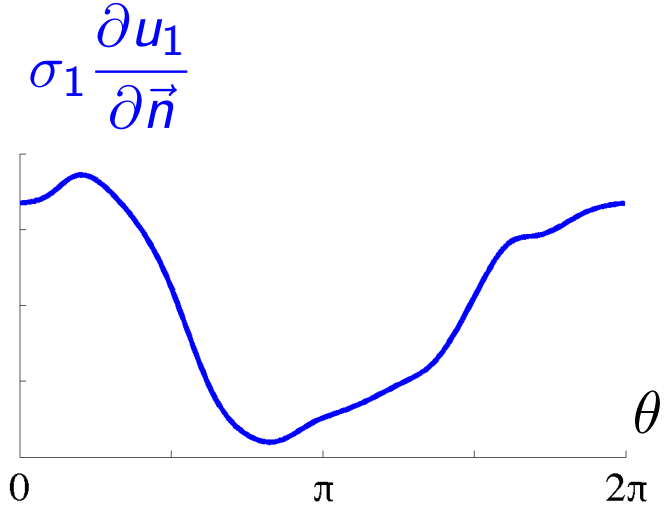

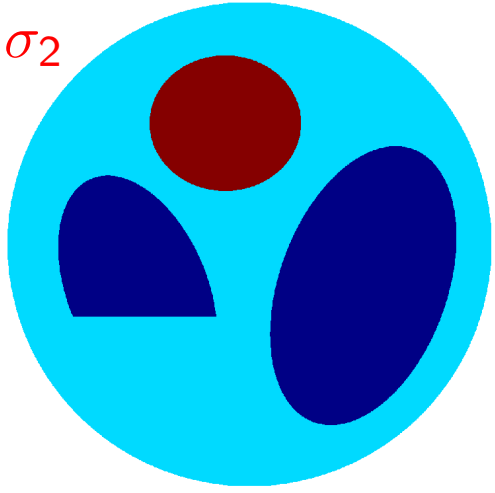

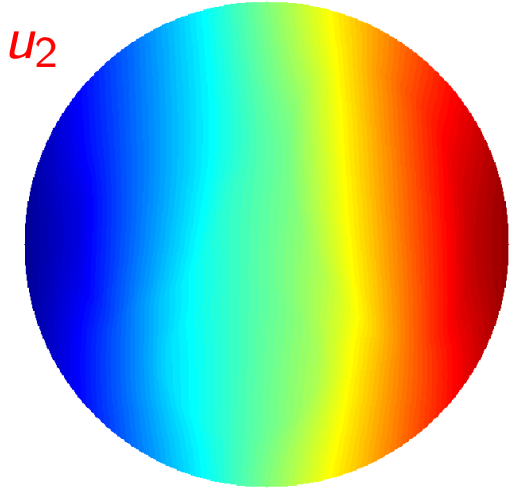

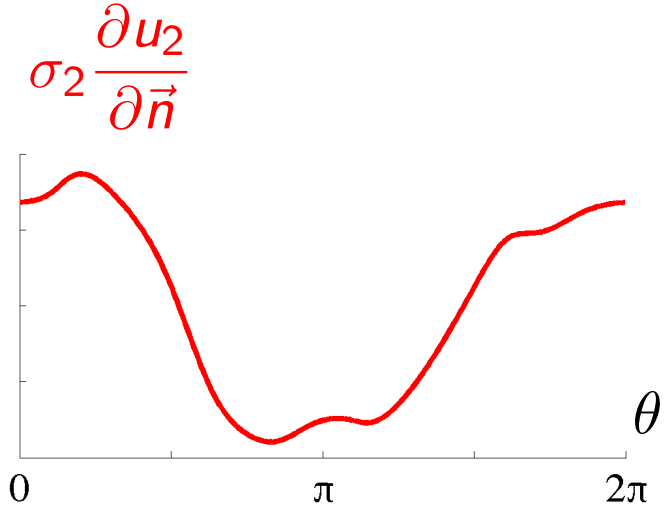

The current data are very similar, although the conductivities are quite different

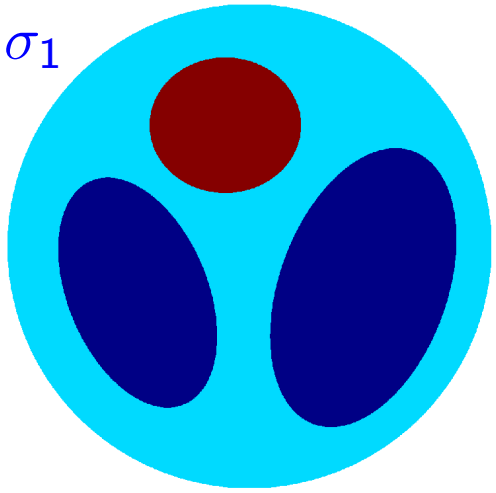

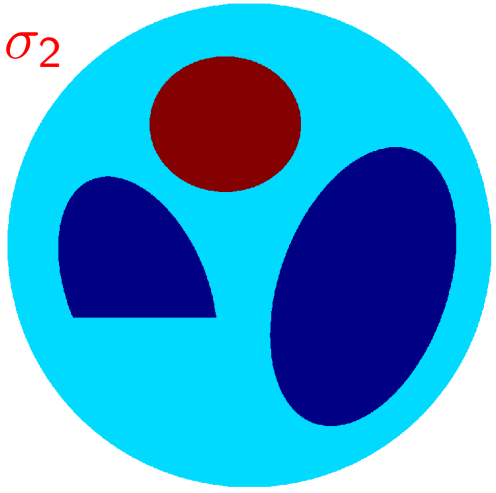

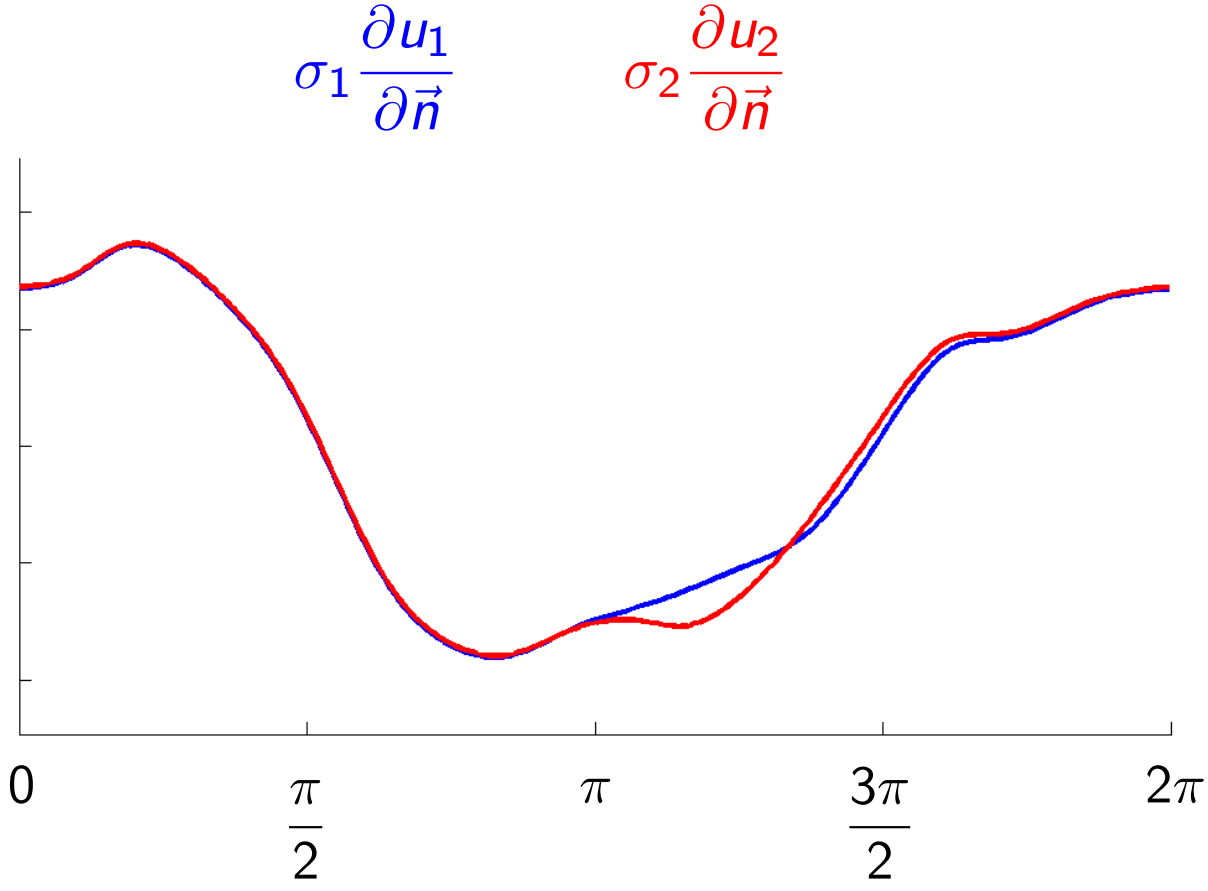

Let us apply the more oscillatory distribution $f(\theta) = \cos 2\theta$ of voltage at the boundary

σ_1

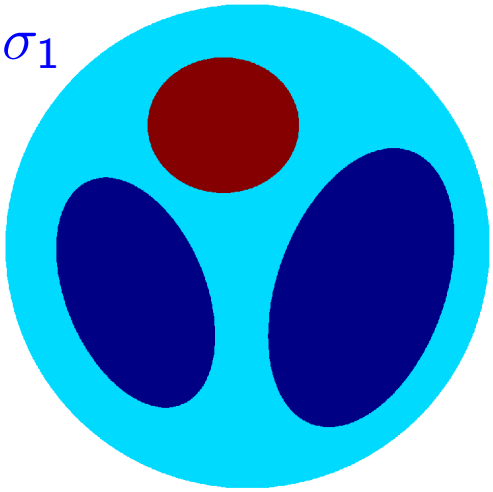

u_1

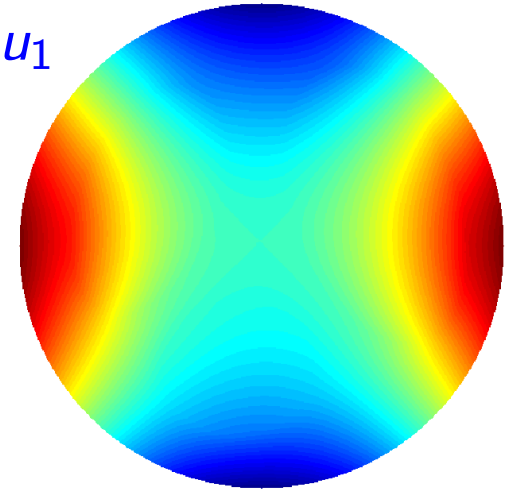

σ_2

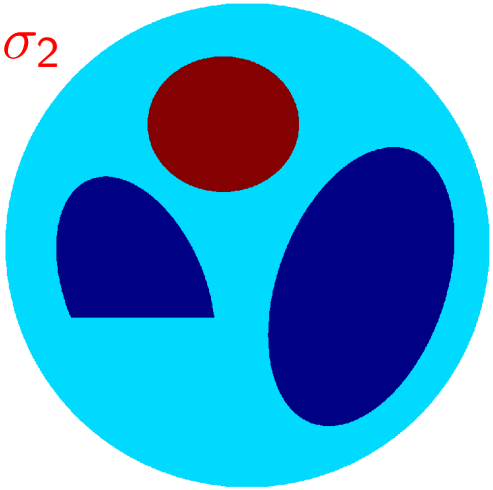

u_2

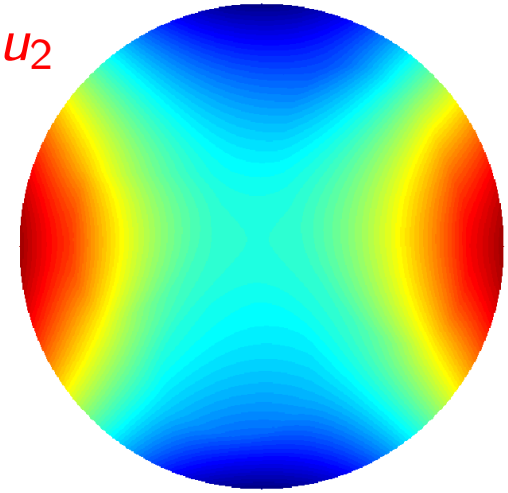

The measurement is again the distribution of current through the boundary

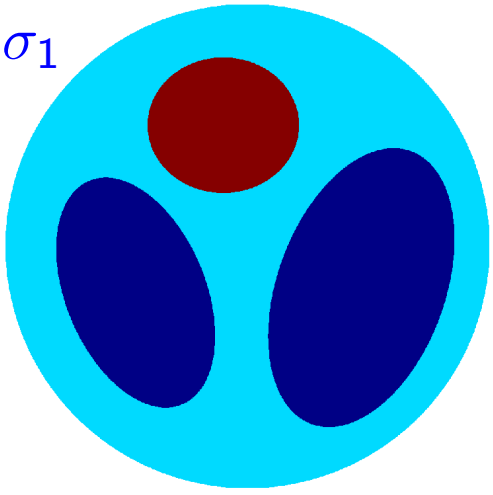

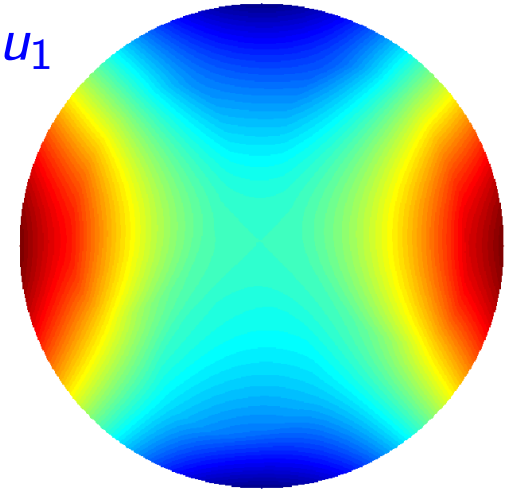

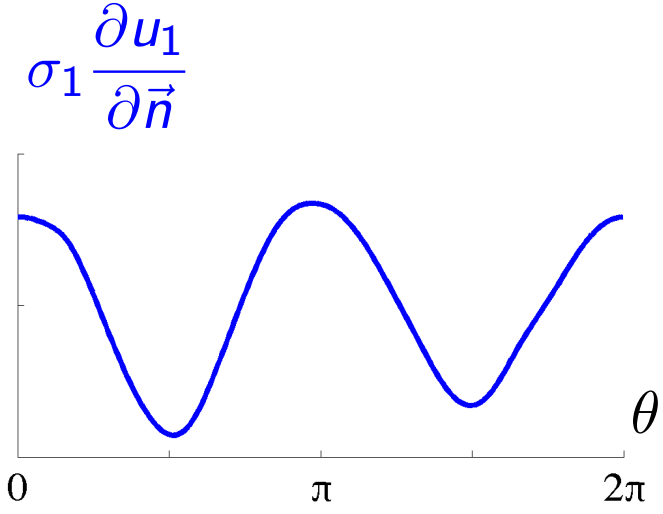

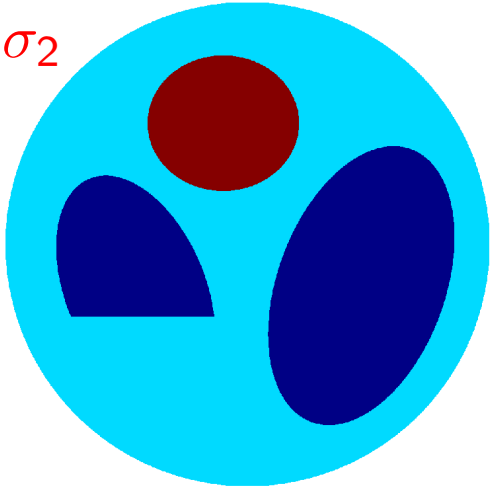

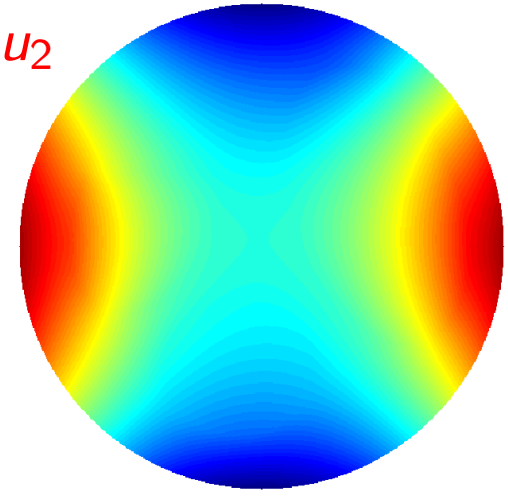

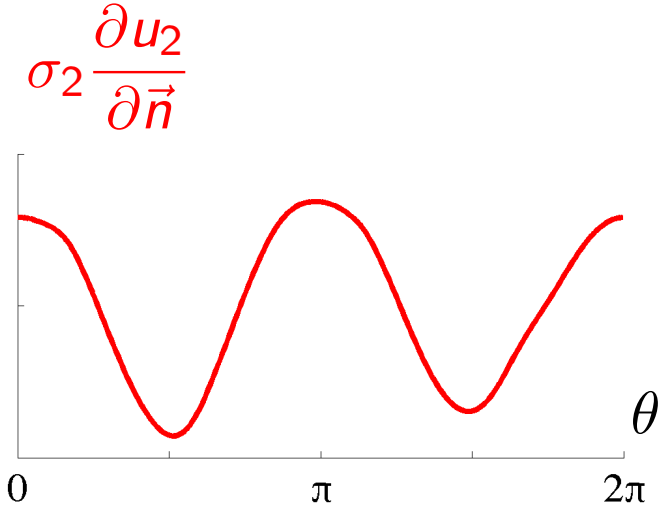

The current distribution measurements are almost the same

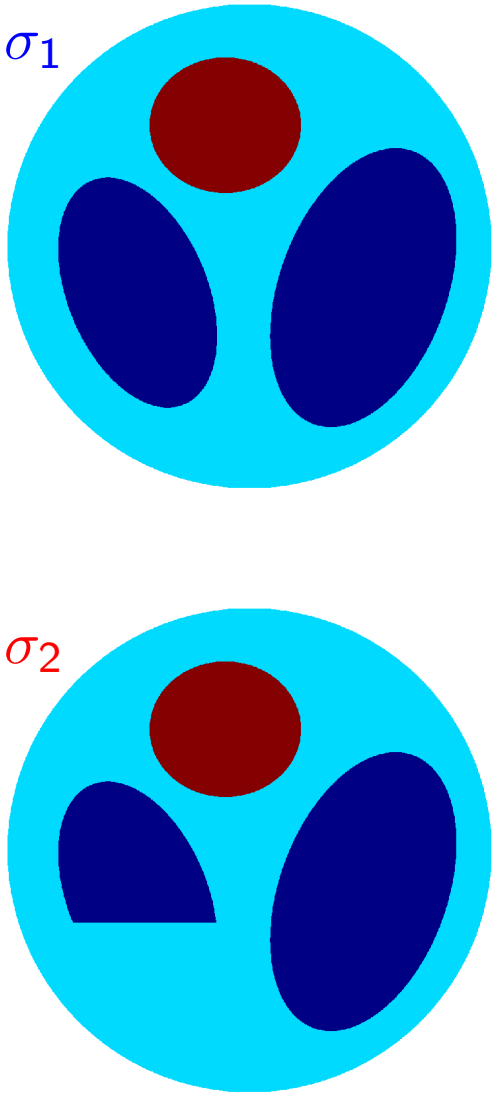

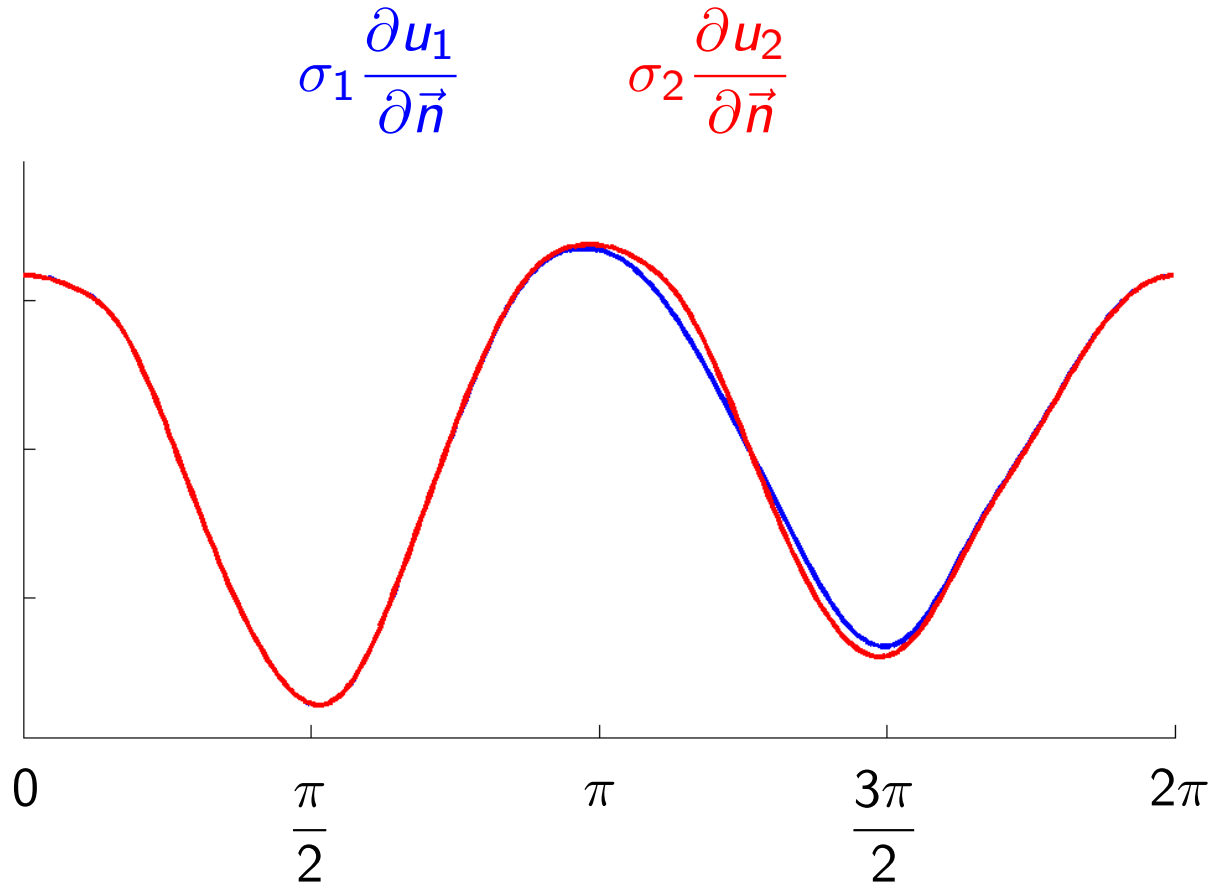

EIT is an ill-posed problem: big differences in conductivity cause only small effect in data

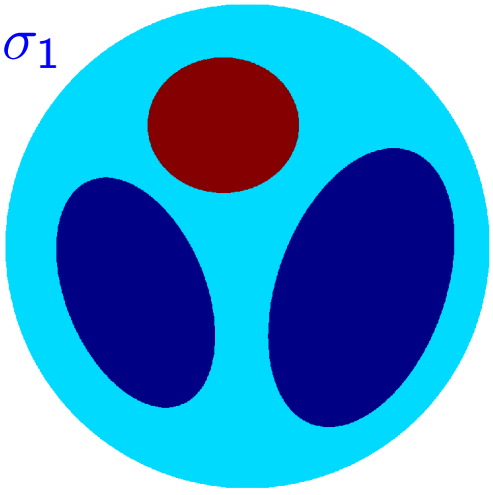

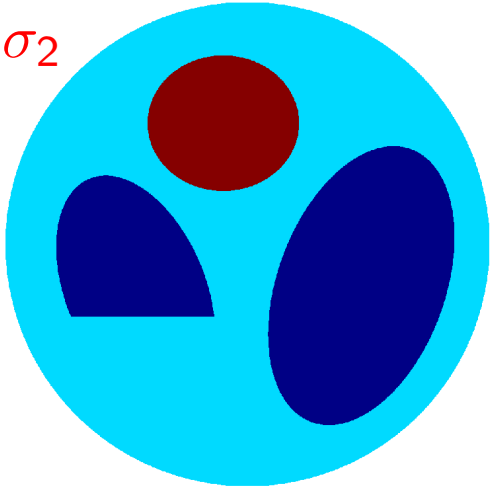

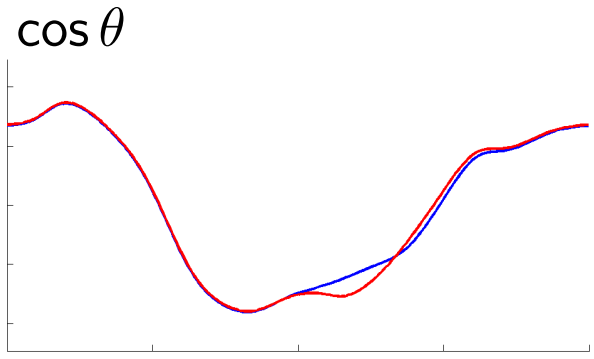

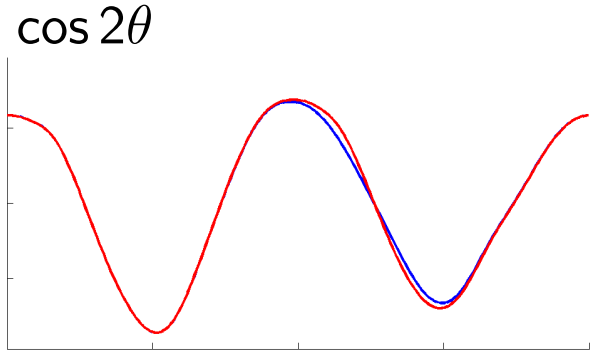

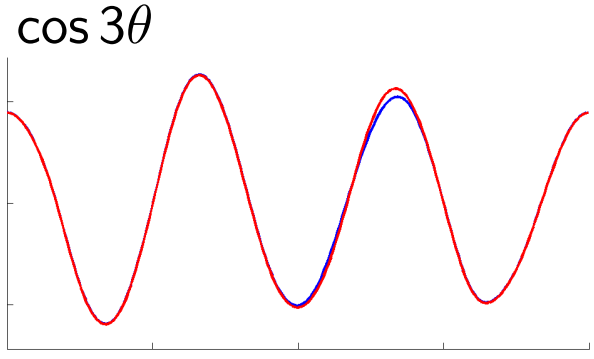

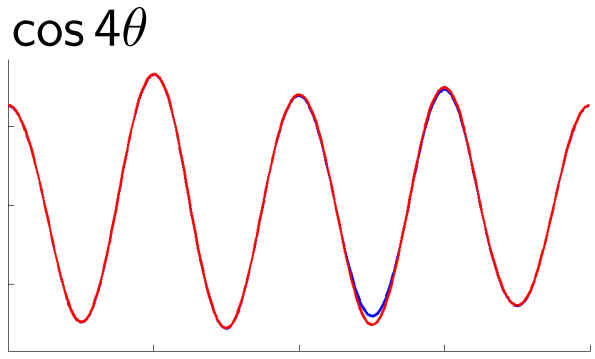

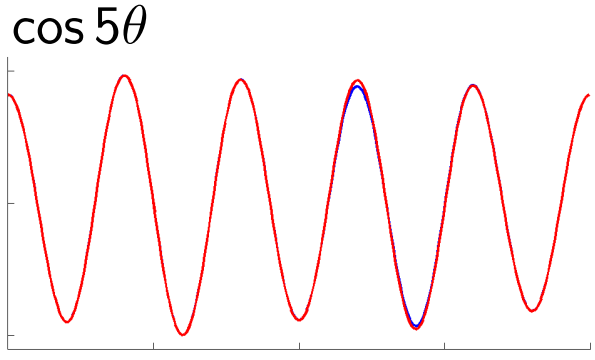

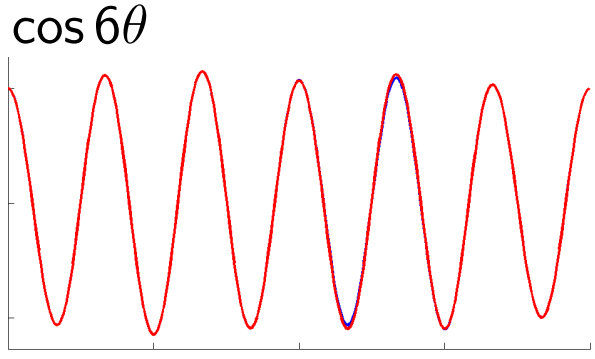

EIT is an ill-posed problem: noise in data causes serious difficulties in interpreting the data

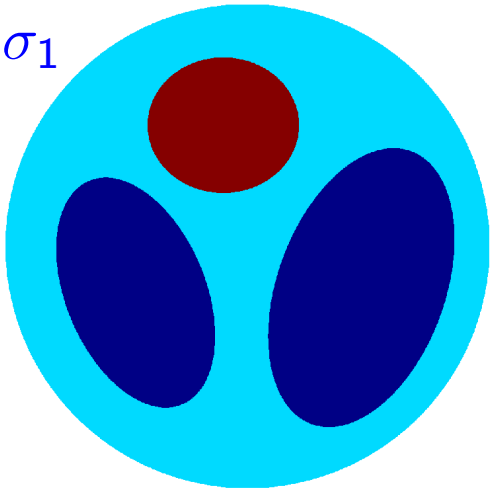

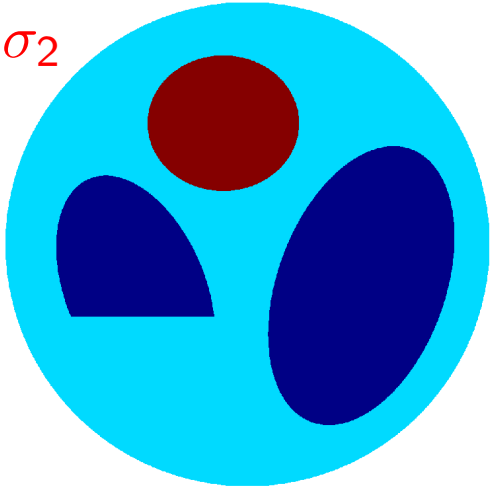

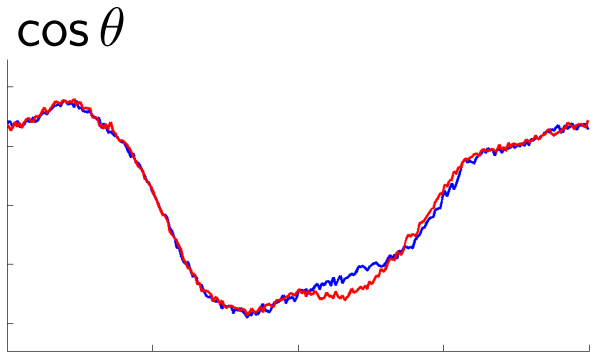

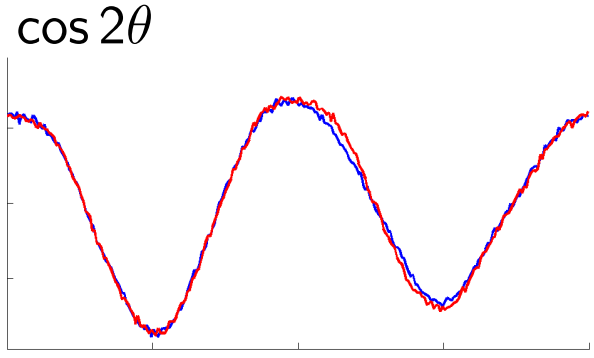

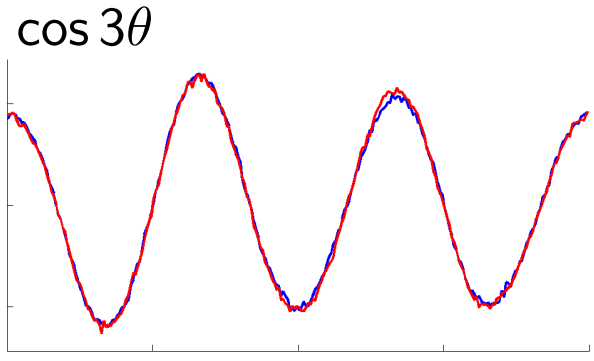

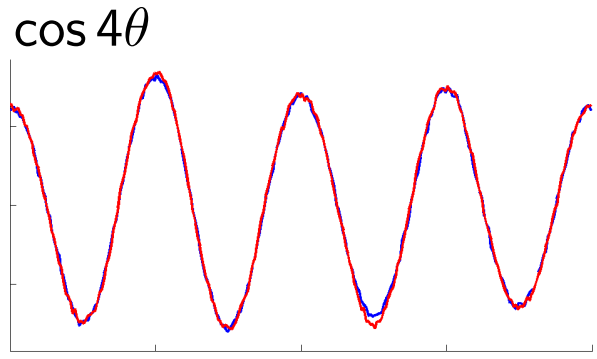

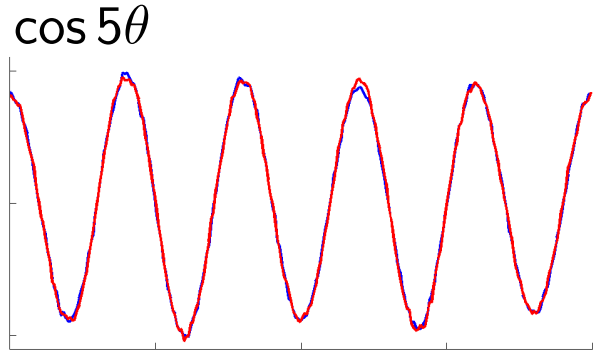

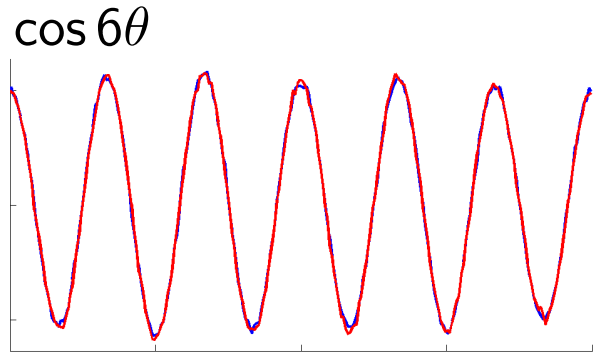

The forward map $F : X \supset \mathcal{D}(F) \to Y$ does not have a continuous inverse!

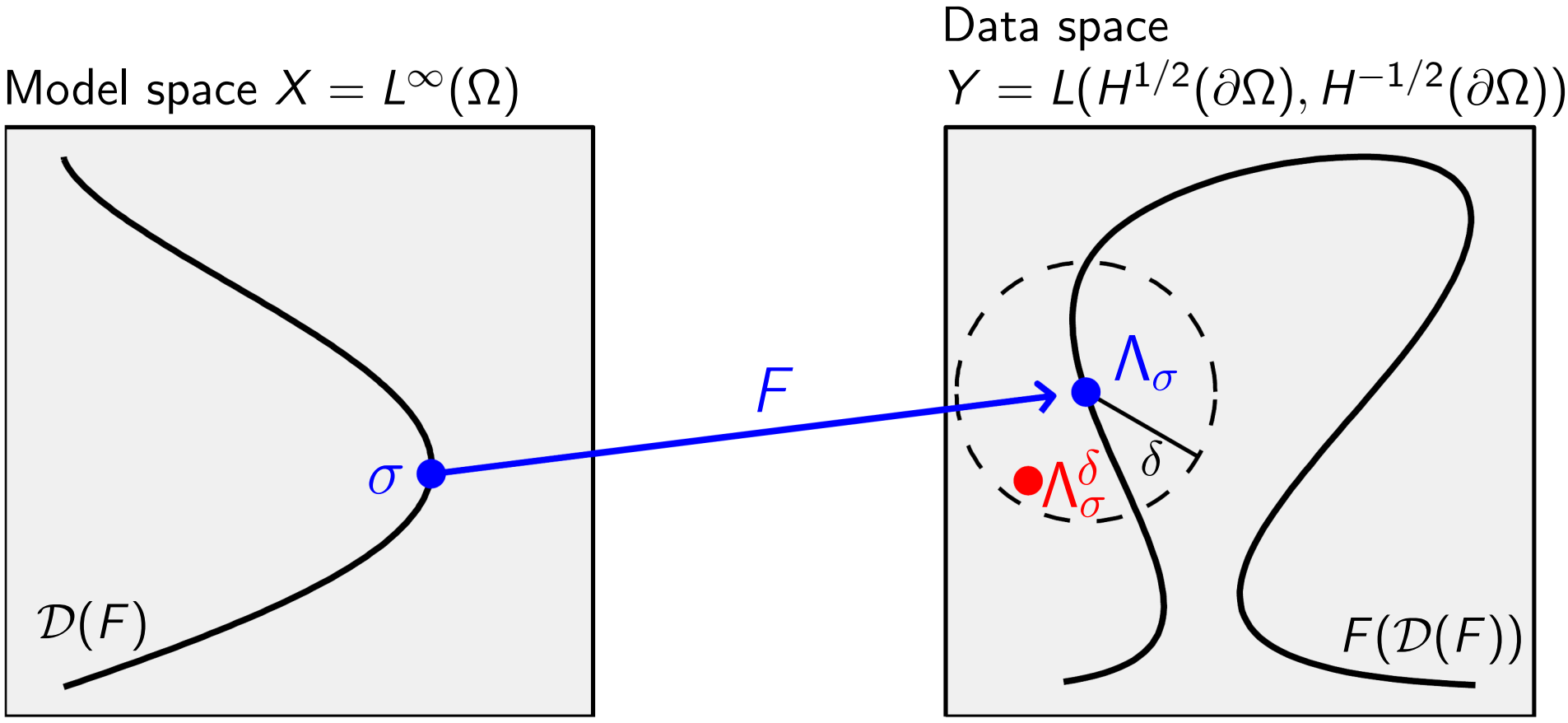

Furthermore, the noisy data Λ_σ^δ does not belong to the range $F(\mathcal{D}(F))$. So Hadamard's conditions 1 and 3 fail for EIT. How about uniqueness?

Ghosts, or invisible structures, when using point electrodes in electrical impedance tomography

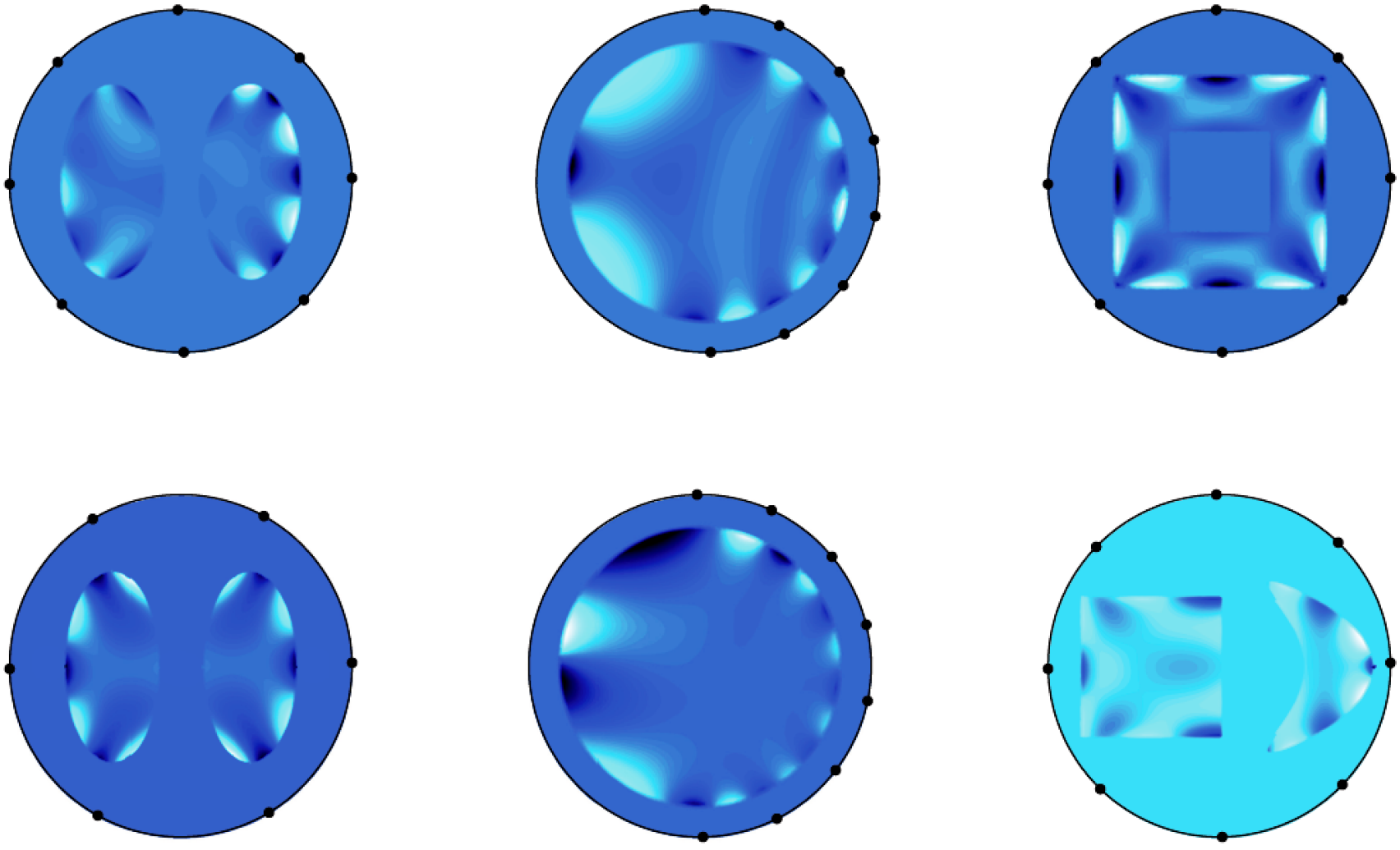

[Chesnel, Hyvönen & Staboulis 2014]

Anisotropic, or matrix-valued, conductivities σ lead to non-uniqueness in EIT

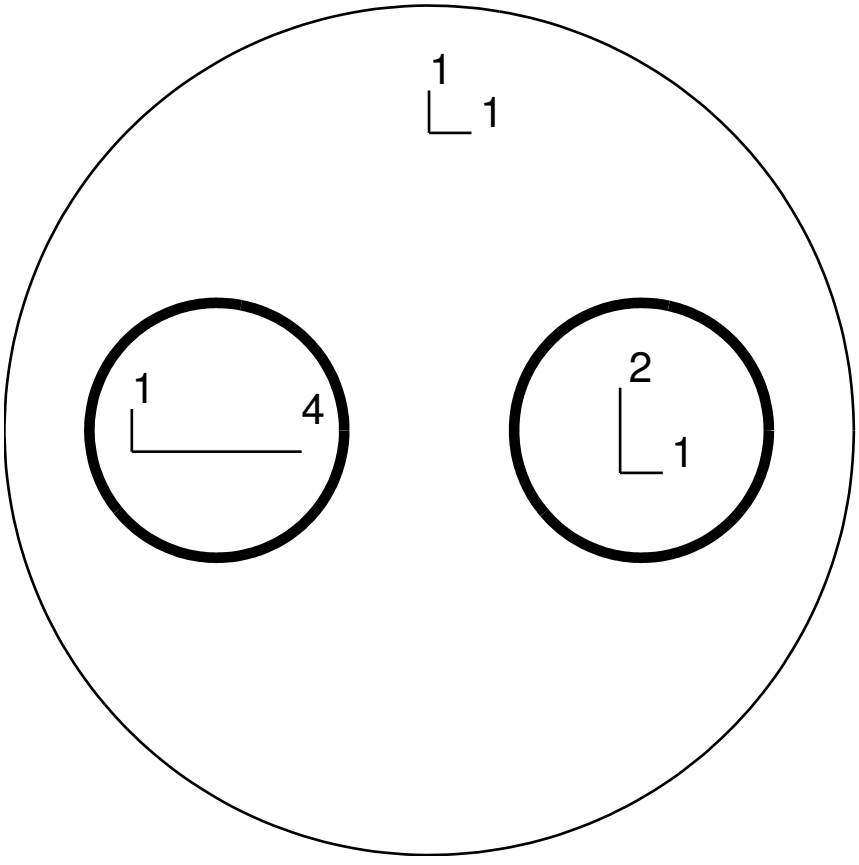

Let $\sigma(x) = [\sigma^{ij}(x)]$ be a symmetric and positive-definite 2×2 matrix. Define anisotropic DN map by

$$\Lambda_\sigma(f) = \nu \cdot \sigma \nabla u\big|_{\partial\Omega}.$$

Let $F : \Omega \to \Omega$ be a diffeomorphism with $F|_{\partial\Omega} = \text{Identity}$. Then

$$\Lambda_{F_*\sigma} = \Lambda_\sigma,$$

where F_* is the push-forward:

$$(F_*\sigma)^{ij}(y) = \frac{1}{\det\left[\frac{\partial F^i}{\partial x^j}(x)\right]} \sum_{p,q=1}^{2} \frac{\partial F^i}{\partial x^p}(x)\, \frac{\partial F^j}{\partial x^q}(x) \sigma^{pq}(x)\Big|_{x=F^{-1}(y)}$$

Outline

Regularization means constructing a continuous map $\Gamma_\alpha : Y \to X$ that inverts F approximately

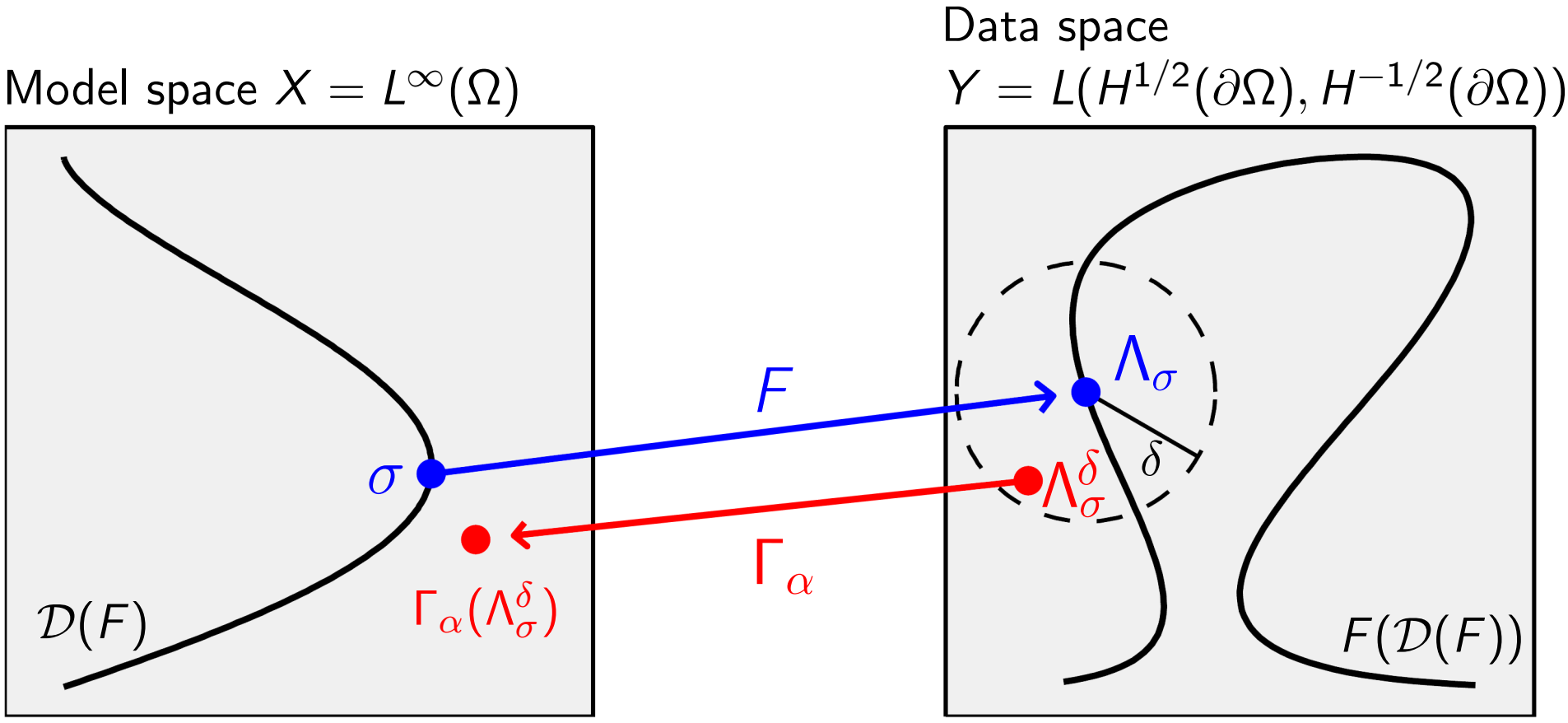

Regularization must be based on combining the incomplete measurement data with *a priori* information about the conductivity.

A *regularization strategy* needs to be constructed so that the assumptions below are satisfied

A family $\Gamma_\alpha : Y \to X$ of continuous mappings parameterized by $0 < \alpha < \infty$ is a *regularization strategy* for F if

$$\lim_{\alpha \to 0} \|\Gamma_\alpha(\Lambda_\sigma) - \sigma\|_X = 0$$

for each fixed $\sigma \in \mathcal{D}(F)$.

Further, a regularization strategy with a choice $\alpha = \alpha(\delta)$ of regularization parameter is called *admissible* if

$$\alpha(\delta) \to 0 \text{ as } \delta \to 0,$$

and for any fixed $\sigma \in \mathcal{D}(F)$ the following holds:

$$\sup_{\Lambda_\sigma^\delta} \left\{ \|\Gamma_{\alpha(\delta)}(\Lambda_\sigma^\delta) - \sigma\|_X \ : \ \|\Lambda_\sigma^\delta - \Lambda_\sigma\|_Y \leq \delta \right\} \to 0 \text{ as } \delta \to 0.$$

There are many EIT reconstruction methods:

Linearization: Barber, Bikowski, Brown, Calderón, Cheney, Isaacson, Mueller, Newell
Iterative regularization: Dobson, Gehre, Harbrecht, Hohage, Hua, Jin, Kaipio, Kindermann, Kluth, Leitão, Lechleiter, Lipponen, Maass, Neubauer, Rieder, Rondi, Santosa, Seppänen, Tompkins, Webster, Woo
Bayesian inversion: Fox, Kaipio, Kolehmainen, Nicholls, Pikkarainen, Ronkanen, Seppänen, Somersalo, Vauhkonen, Voutilainen
Resistor network methods: Borcea, Druskin, Mamonov, Vasquez
Layer stripping: Cheney, Isaacson, Isaacson, Somersalo
D-bar methods: Astala, Bikowski, Bowerman, Delbary, Hamilton, Hansen, Herrera, Isaacson, Kao, Knudsen, Lassas, Montoya, Mueller, Murphy, Nachman, Newell, Päivärinta, Perämäki, Saulnier, Santacesaria, S, Tamasan, Tamminen
Teichmüller space methods: Kolehmainen, Lassas, Ola, S
Methods for partial information: Alessandrini, Ammari, Bilotta, Brühl, Eckel, Erhard, Gebauer, Hanke, Harrach, Hyvönen, Ide, Ikehata, Isozaki, Kang, Kim, Kress, Kwon, Lechleiter, Lim, Maass, Morassi, Nakamura, Nakata, Potthast, Rossetand, Seo, Sheen, S, Staboulis, Turco, Uhlmann, Wang, ...

1. Tikhonov regularization: write a penalty functional

$$\Phi(x) = \|\Lambda_{\widetilde{\sigma}} - \Lambda_\sigma^\delta\|_Y^2 + \alpha\|\widetilde{\sigma}\|_X^2,$$

and define $\Gamma_\alpha(\Lambda_\sigma^\delta)$ by $\Phi(\Gamma_\alpha(\Lambda_\sigma^\delta)) = \min_{\widetilde{\sigma}\in X}\{\Phi(\widetilde{\sigma})\}$.

Pro: The same code applies to many problems.
Con: Repeated solution of direct problem needed.
Con: Prone to get stuck in local minima.

Current theory of iterative regularization does not cover full EIT because of high degree of nonlinearity.
[Lechleiter-Rieder 2006&2008, Harbrecht-Hohage 2009, Jin-Maass 2012].

---

2. Problem-specific regularization

Pro: Can deal efficiently with a specific nonlinearity.
Con: Each code applies to only one problem.

EIT: [Ikehata 2002, Ikehata-S 2004, Knudsen-Lassas-Mueller-S 2009]

I recommend these books for studying iterative regularization for nonlinear inverse problems

1996 Engl, Hanke & Neubauer:
Regularization of inverse problems

2008 Kaltenbacher, Neubauer & Scherzer:
Iterative regularization methods for nonlinear ill-posed problems

2012 Schuster, Kaltenbacher, Hofmann & Kazimierski:
Regularization methods in Banach spaces

This part of the talk is a joint work with

David Isaacson, Rensselaer Polytechnic Institute, USA

Kim Knudsen, Technical University of Denmark

Matti Lassas, University of Helsinki, Finland

Jon Newell, Rensselaer Polytechnic Institute, USA

Jennifer Mueller, Colorado State University, USA

There exists a nonlinear Fourier transform adapted to electrical impedance tomography

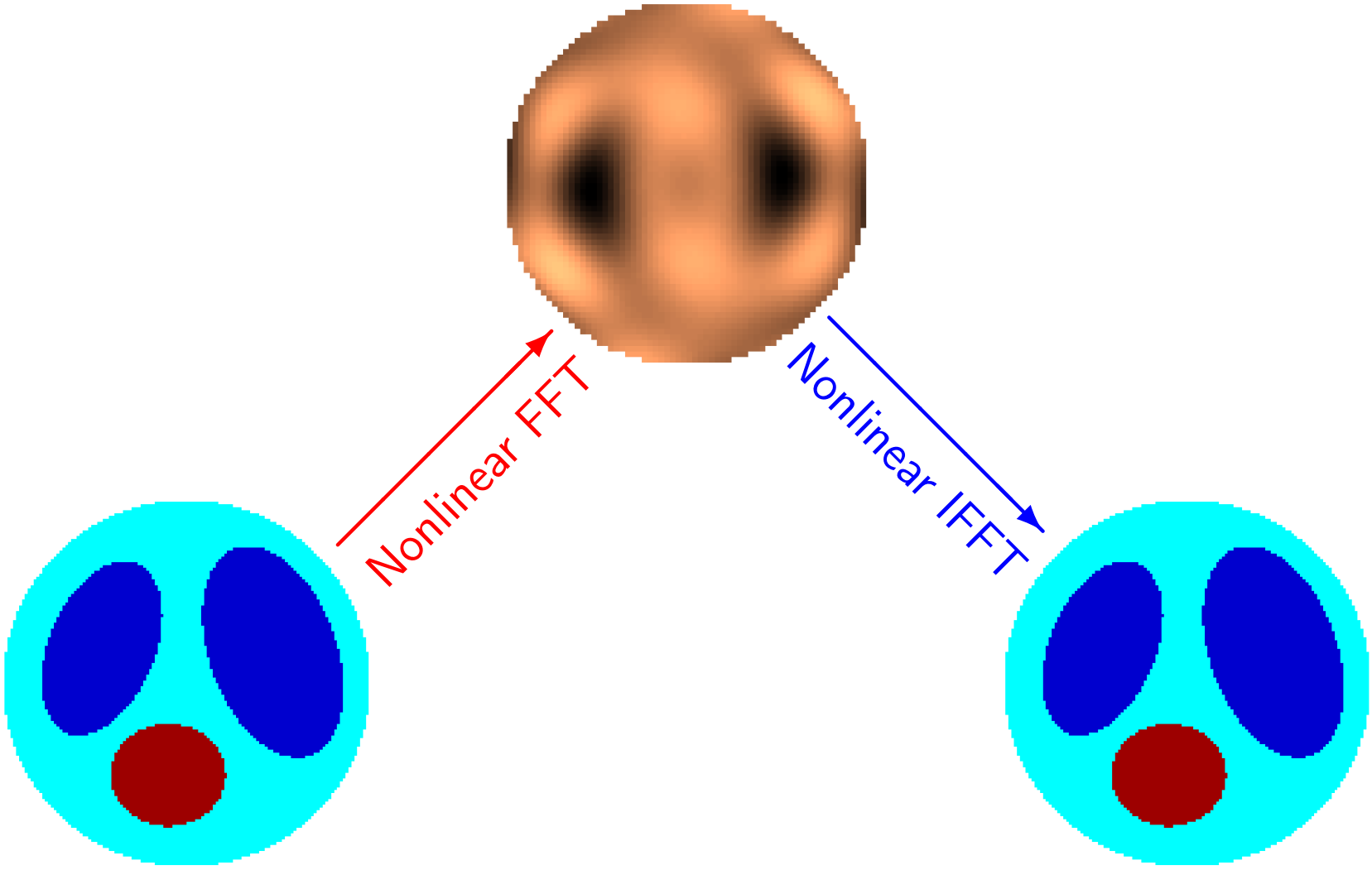

The nonlinear Fourier transform can be recovered from infinite-precision EIT measurements

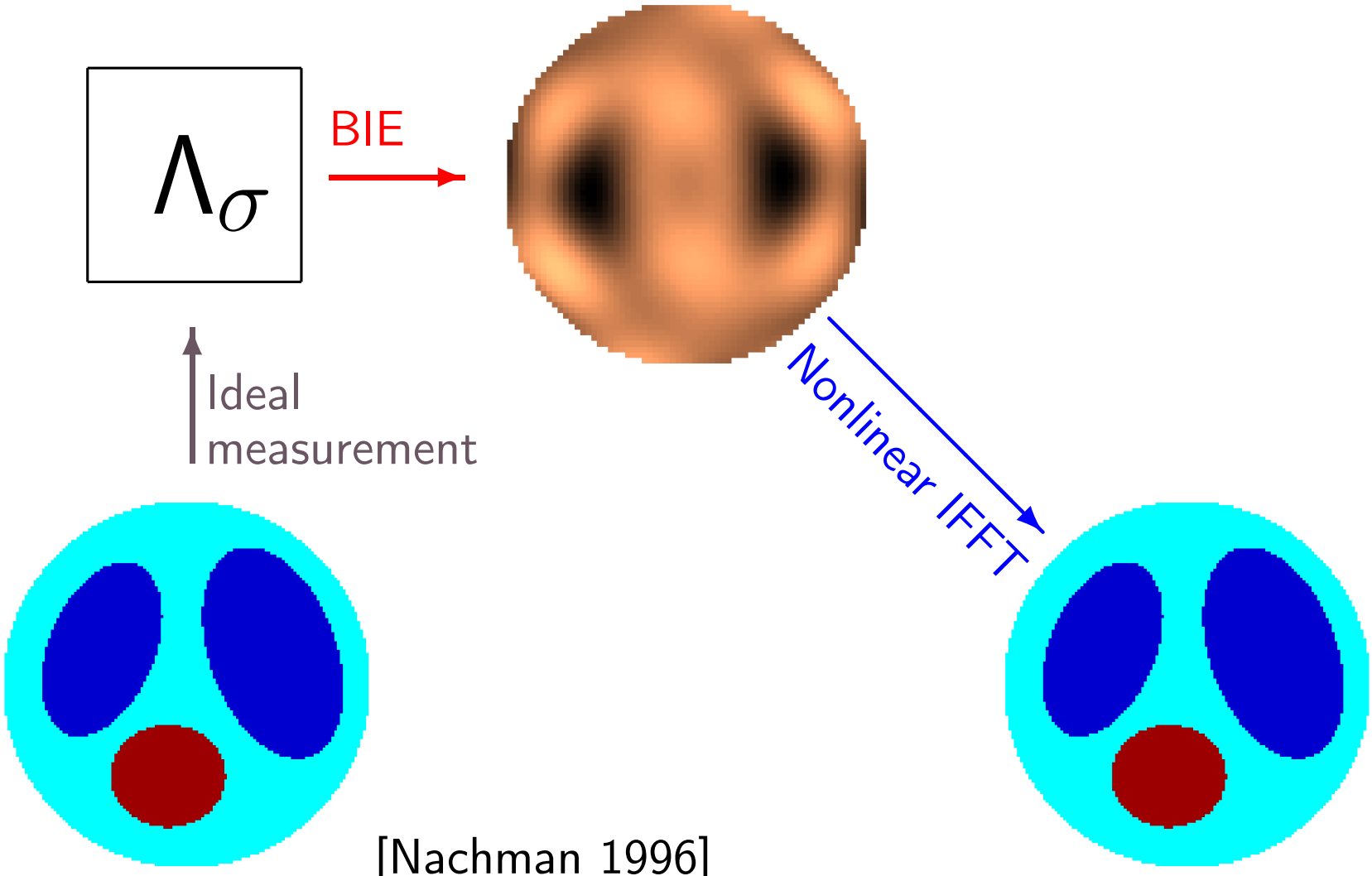

[Nachman 1996]

Measurement noise prevents the recovery of the nonlinear Fourier transform at high frequencies

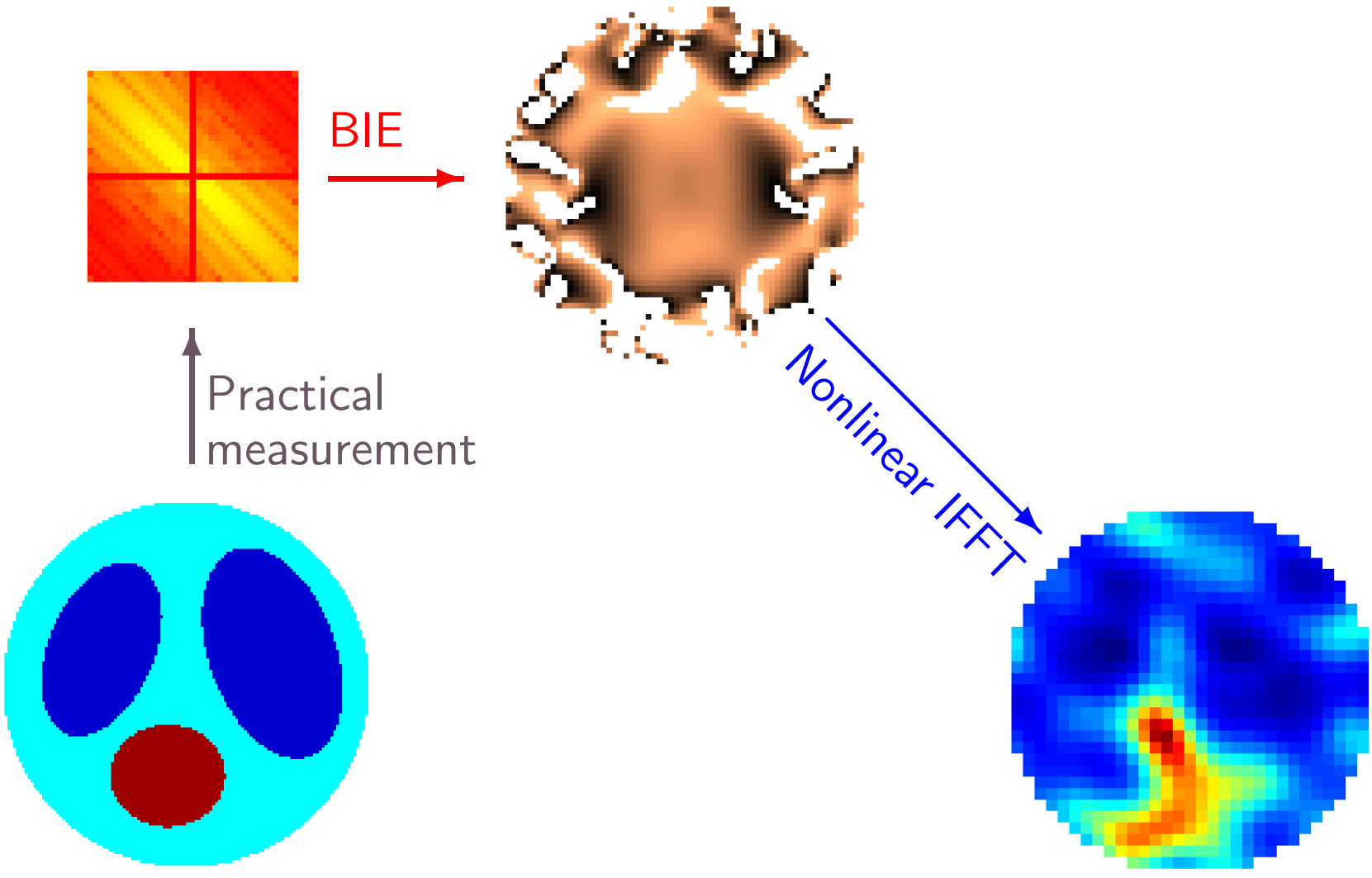

We truncate away the bad part in the transform; this is a nonlinear low-pass filter

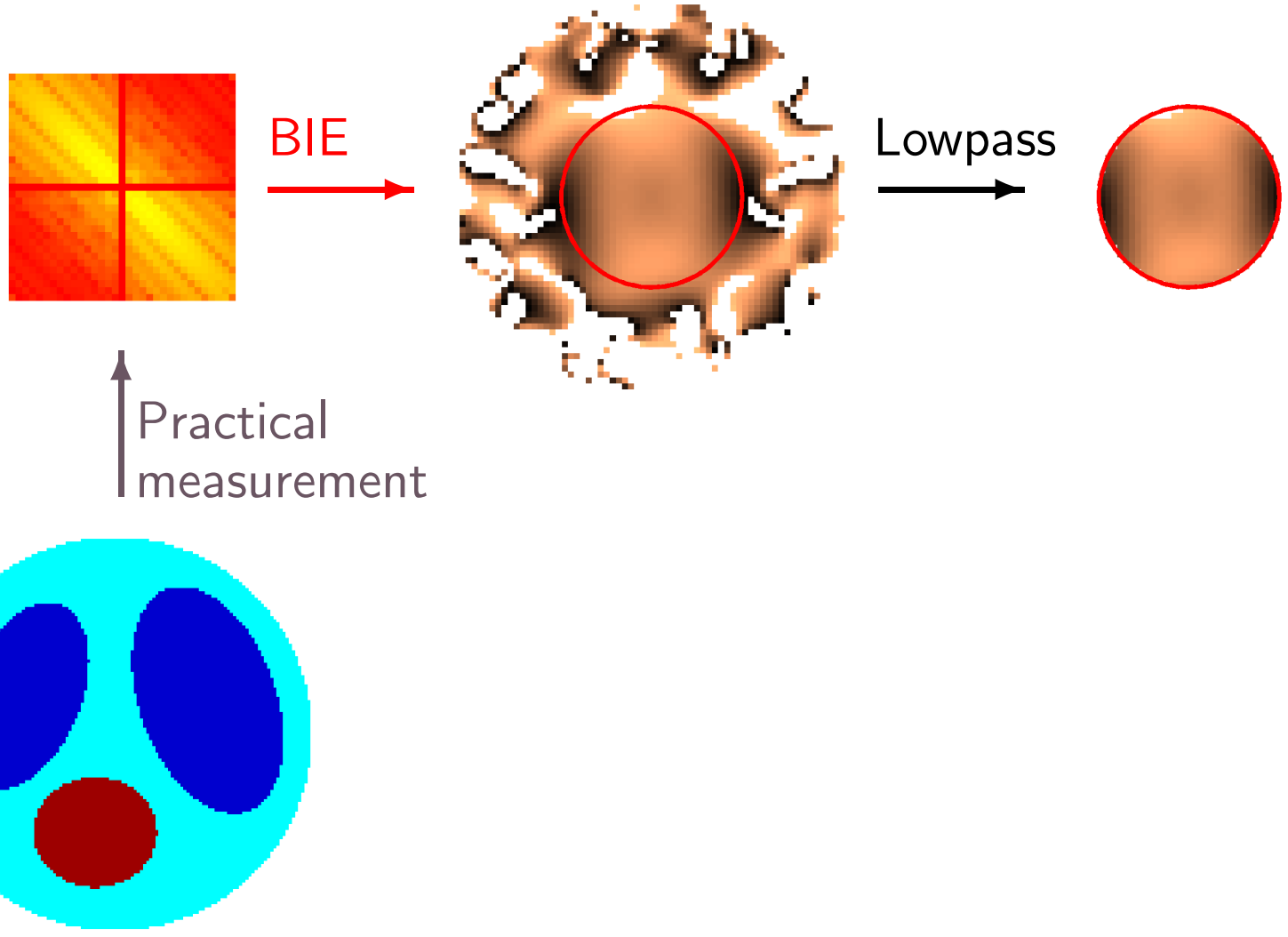

There is currently only one regularized method for reconstructing the full conductivity distribution

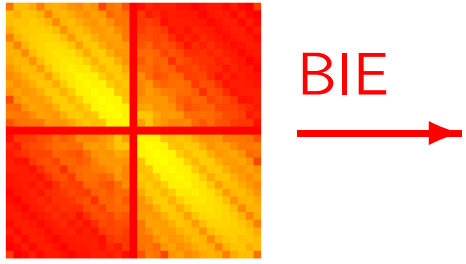

BIE

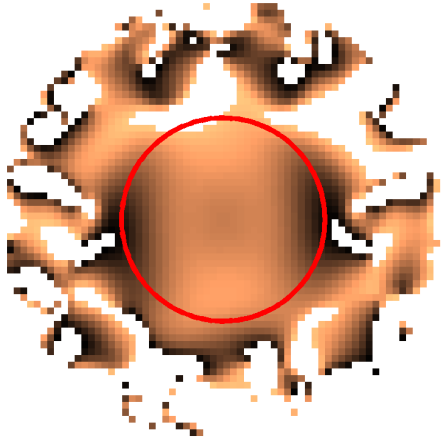

Lowpass

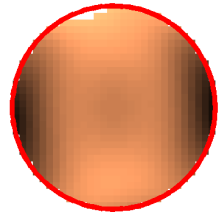

Nonlinear
IFFT

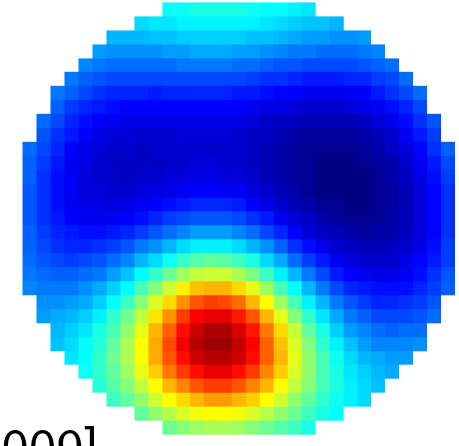

Practical
measurement

[S, Mueller & Isaacson 2000]
[Knudsen, Lassas, Mueller & S 2009]

Infinite-precision data:

Solve boundary integral equation

$$\psi(\,\cdot\,,k)|_{\partial\Omega} = e^{ikz} - \mathcal{S}_k(\Lambda_\sigma - \Lambda_1)\psi$$

for every complex number $k \in \mathbb{C} \setminus 0$.

Evaluate the scattering transform:

$$\mathbf{t}(k) = \int_{\partial\Omega} e^{i\bar{k}\bar{z}}(\Lambda_\sigma - \Lambda_1)\psi(\cdot,k)\,ds.$$

Fix $z \in \Omega$. Solve D-bar equation

$$\frac{\partial}{\partial\bar{k}}\mu(z,k) = \frac{\mathbf{t}(k)}{4\pi\bar{k}}e^{-i(kz+\bar{k}\bar{z})}\overline{\mu(z,k)}$$

with $\mu(z,\,\cdot\,) - 1 \in L^r \cap L^\infty(\mathbb{C})$.

Reconstruct: $\sigma(z) = (\mu(z,0))^2$.

Practical data:

Solve boundary integral equation

$$\psi^\delta(\,\cdot\,,k)|_{\partial\Omega} = e^{ikz} - \mathcal{S}_k(\Lambda^\delta_\sigma - \Lambda_1)\psi^\delta$$

for all $0 < |k| < R = -\frac{1}{10}\log\delta$.

For $|k| \geq R$ set $\mathbf{t}^\delta_R(k) = 0$. For $|k| < R$

$$\mathbf{t}^\delta_R(k) = \int_{\partial\Omega} e^{i\bar{k}\bar{z}}(\Lambda^\delta_\sigma - \Lambda_1)\psi^\delta(\cdot,k)\,ds.$$

Fix $z \in \Omega$. Solve D-bar equation

$$\frac{\partial}{\partial\bar{k}}\mu^\delta_R(z,k) = \frac{\mathbf{t}^\delta_R(k)}{4\pi\bar{k}}e^{-i(kz+\bar{k}\bar{z})}\overline{\mu^\delta_R(z,k)}$$

with $\mu^\delta_R(z,\,\cdot\,) - 1 \in L^r \cap L^\infty(\mathbb{C})$.

Set $\Gamma_{1/R(\delta)}(\Lambda^\delta_\sigma) := (\mu^\delta_R(z,0))^2$.

Main result: nonlinear low-pass filtering yields a regularization strategy with convergence speed

Theorem (Knudsen, Lassas, Mueller & S 2009)

There exists a constant $0 < \delta_0 < 1$, *depending only on* M *and* ρ, *with the following properties. Let* $\sigma \in \mathcal{D}(F)$ *be arbitrary and assume given noisy data* Λ_σ^δ *satisfying*

$$\|\Lambda_\sigma^\delta - \Lambda_\sigma\|_Y \leq \delta < \delta_0.$$

Then Γ_α *with the choice*

$$R(\delta) = -\frac{1}{10}\log\delta, \qquad \alpha(\delta) = \frac{1}{R(\delta)},$$

is well-defined, admissible and satisfies the estimate

$$\|\Gamma_{\alpha(\delta)}(\Lambda_\sigma^\delta) - \sigma\|_{L^\infty(\Omega)} \leq C(-\log\delta)^{-1/14}.$$

Regularized reconstructions from simulated data with noise amplitude $\delta = \|\Lambda_\sigma^\delta - \Lambda_\sigma\|_Y$

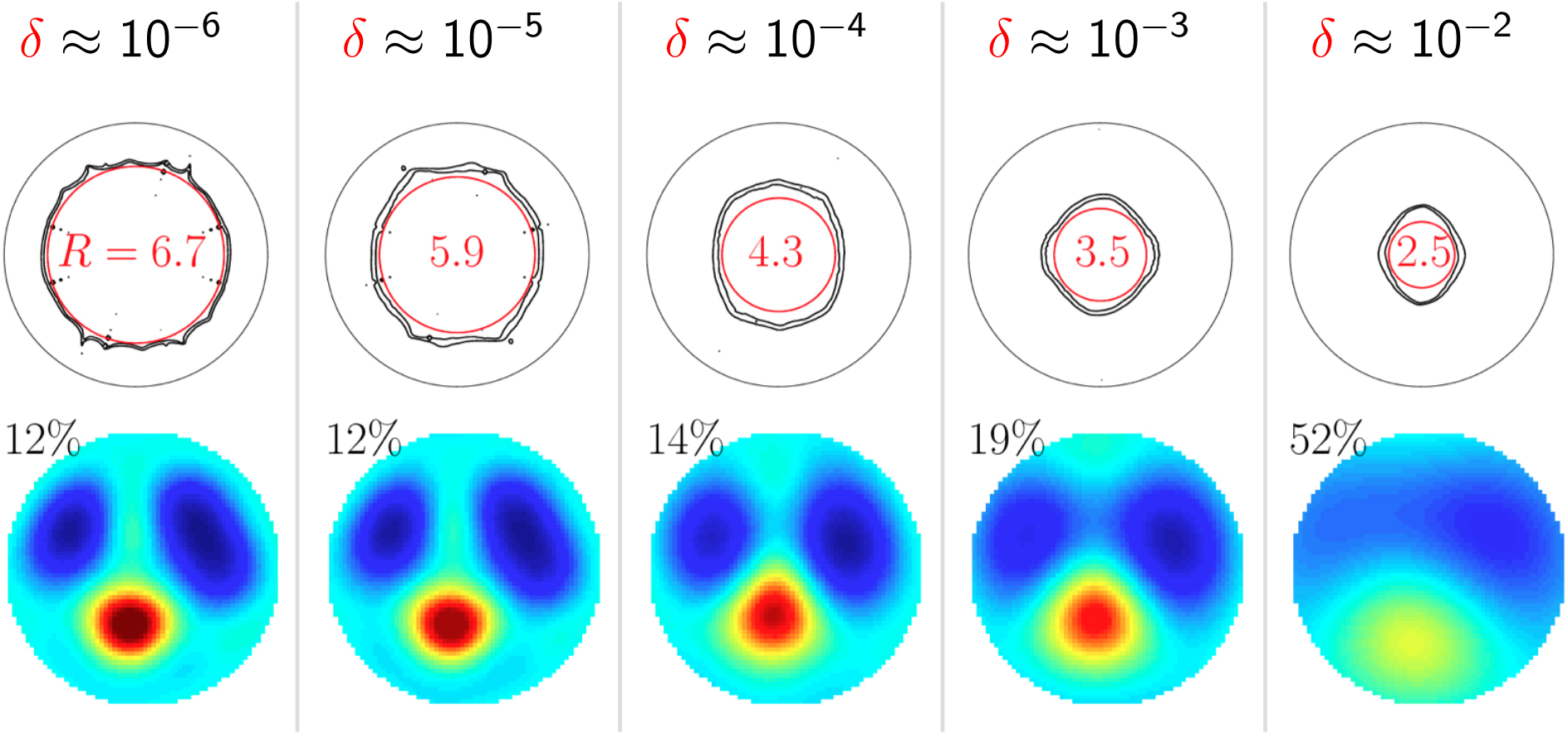

The percentages are the relative square norm errors in the reconstructions.

The observed radii are better (=larger) than those given by the theoretical formula $R(\delta) = -\frac{1}{10}\log\delta$

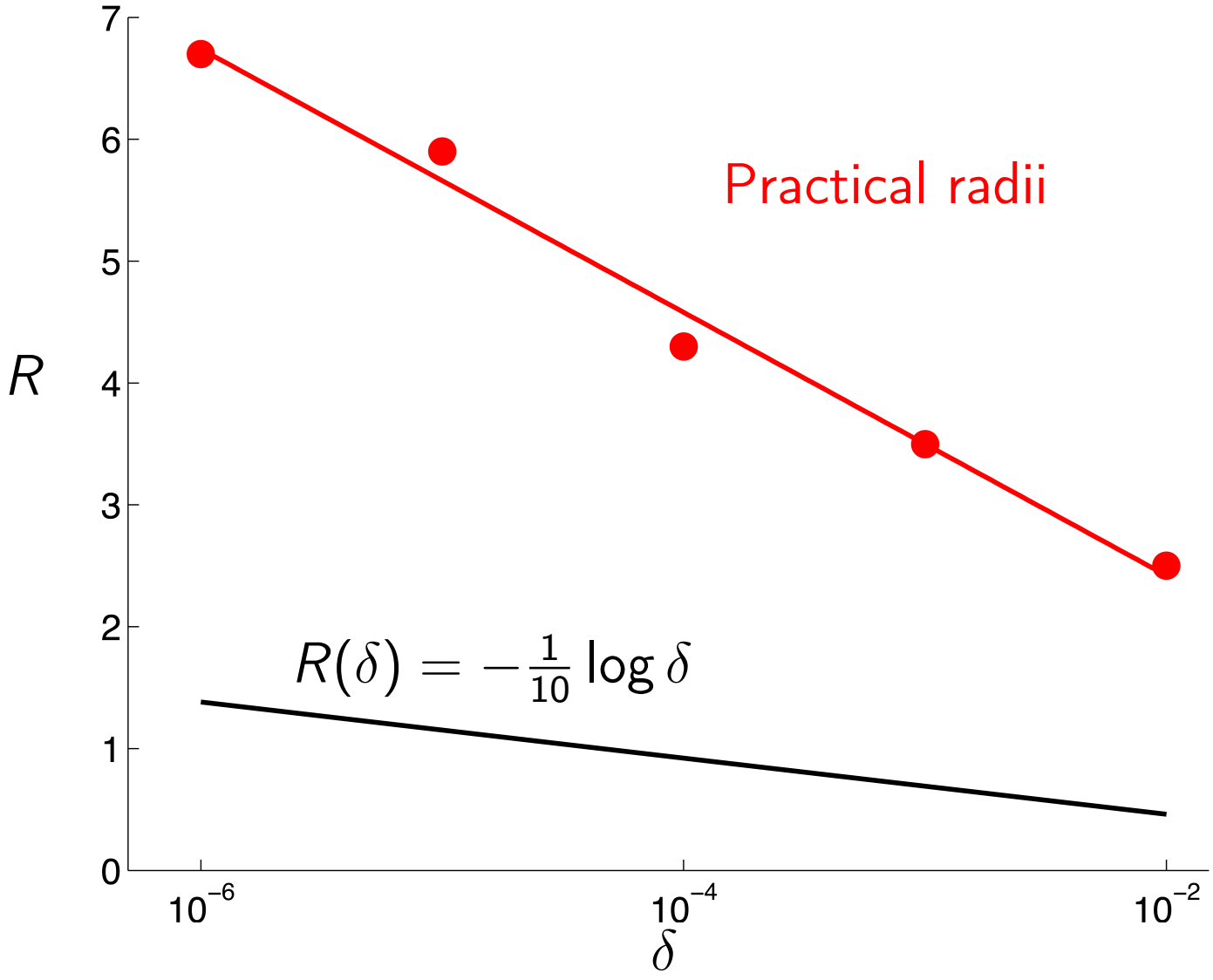

This is a brief history of the two-dimensional regularized D-bar method for EIT

1966 Faddeev: Complex geometric optics (CGO) solutions

1987 Sylvester and Uhlmann: CGO solutions for inverse boundary-value problems; uniqueness for 3D EIT with smooth conductivities and infinite-precision data

1988 R. G. Novikov: Outline of the core ideas of the D-bar method; no rigorous proof

1996 Nachman: Uniqueness and reconstruction for 2D EIT with C^2 conductivities and infinite-precision data

2000 S, Mueller and Isaacson: Numerical implementation of Nachman's proof using a Born approximation

2006 Isaacson, Mueller, Newell and S: Application of the D-bar method to EIT data measured from a human subject

2009 Knudsen, Lassas, Mueller and S: Regularization proof

The D-bar regularization strategy automatically handles non-uniqueness from anisotropy

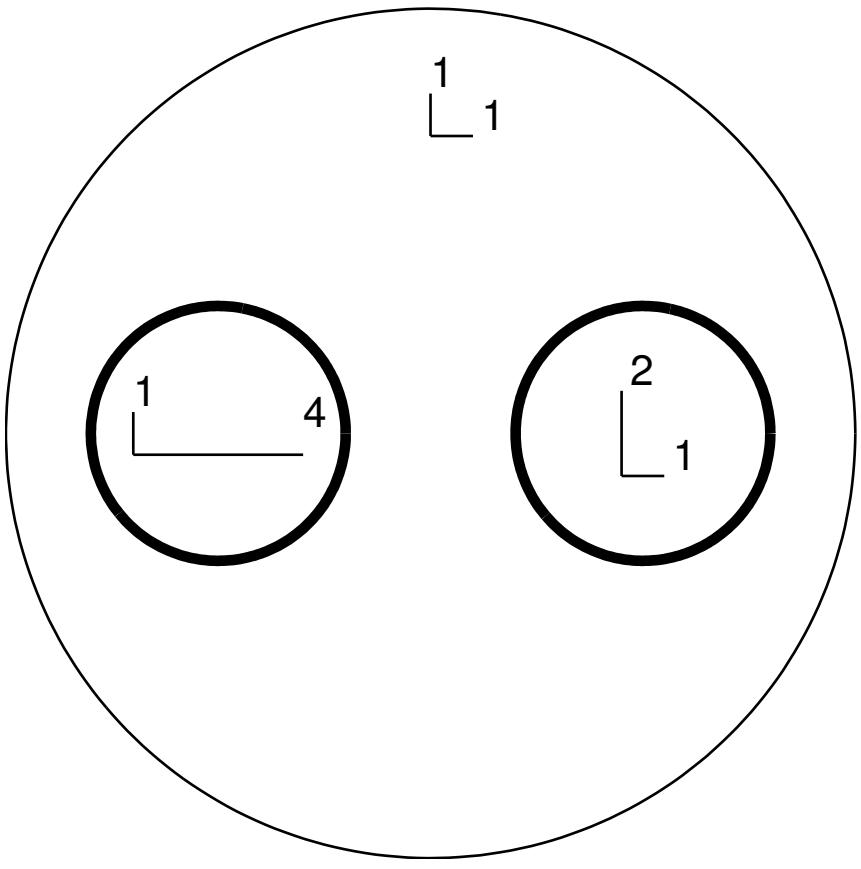

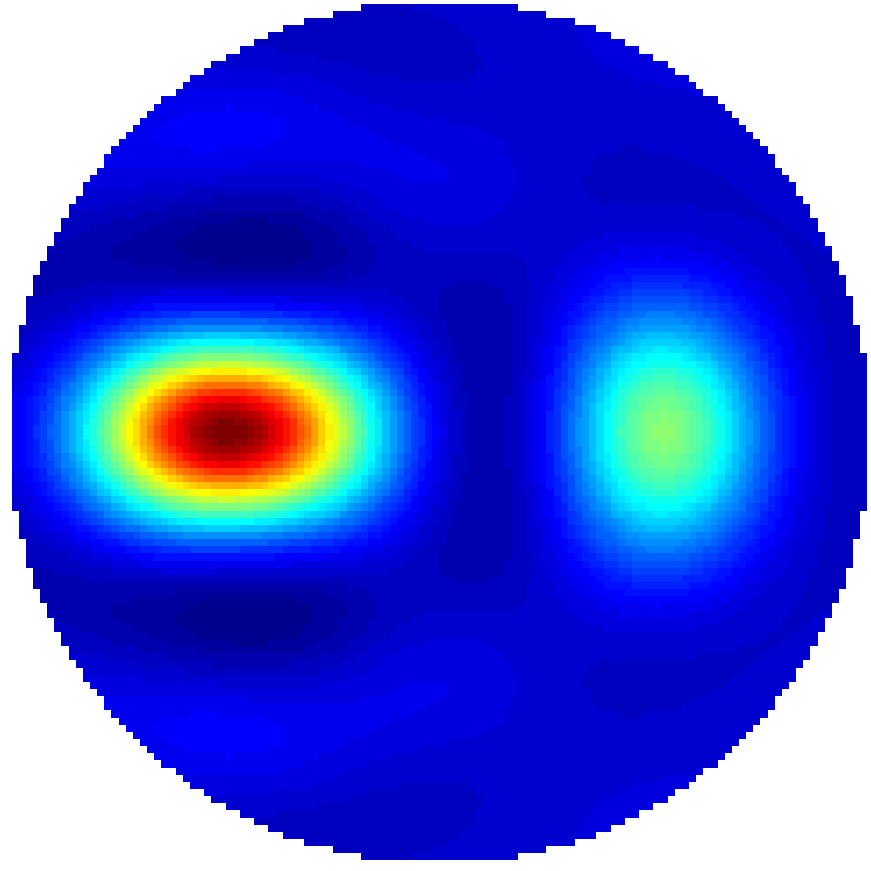

[Henkin & Santacesaria, *Inverse Problems* **26** (2010)]
[Hamilton, Lassas & S, *Inverse Problems* **30** (2014)]

Take-home messages from our overview of electrical impedance tomography

Uniqueness does not save us.
Even with an injective forward map, failure of Hadamard's condition 3 means that we need regularization for solving the inverse problem.

Non-uniqueness can be handled.
Our stable regularization strategy just needs enough *a priori* information for picking out a unique object among those with same data.

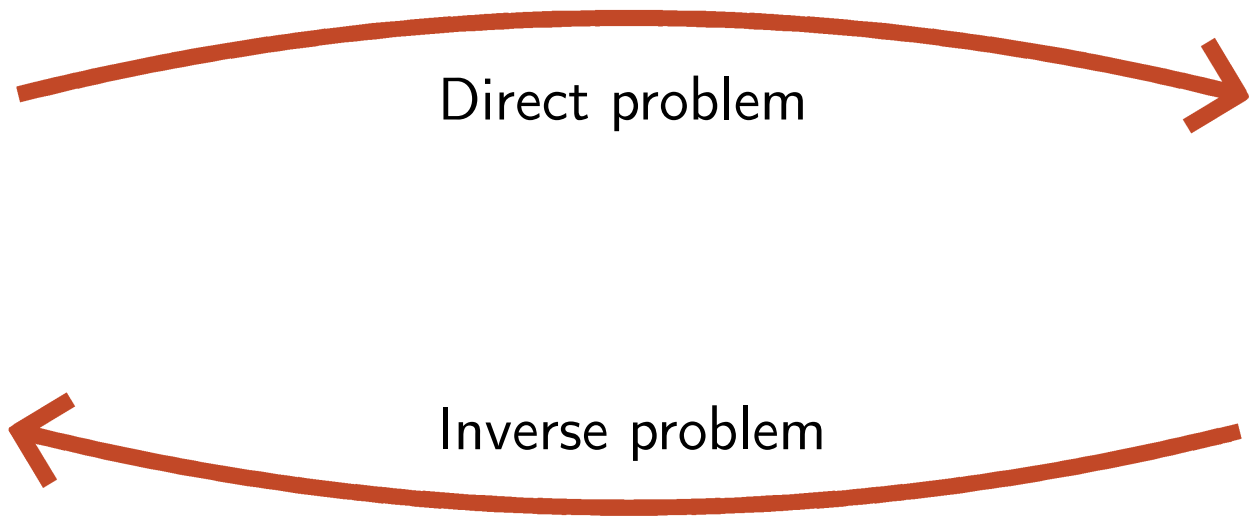

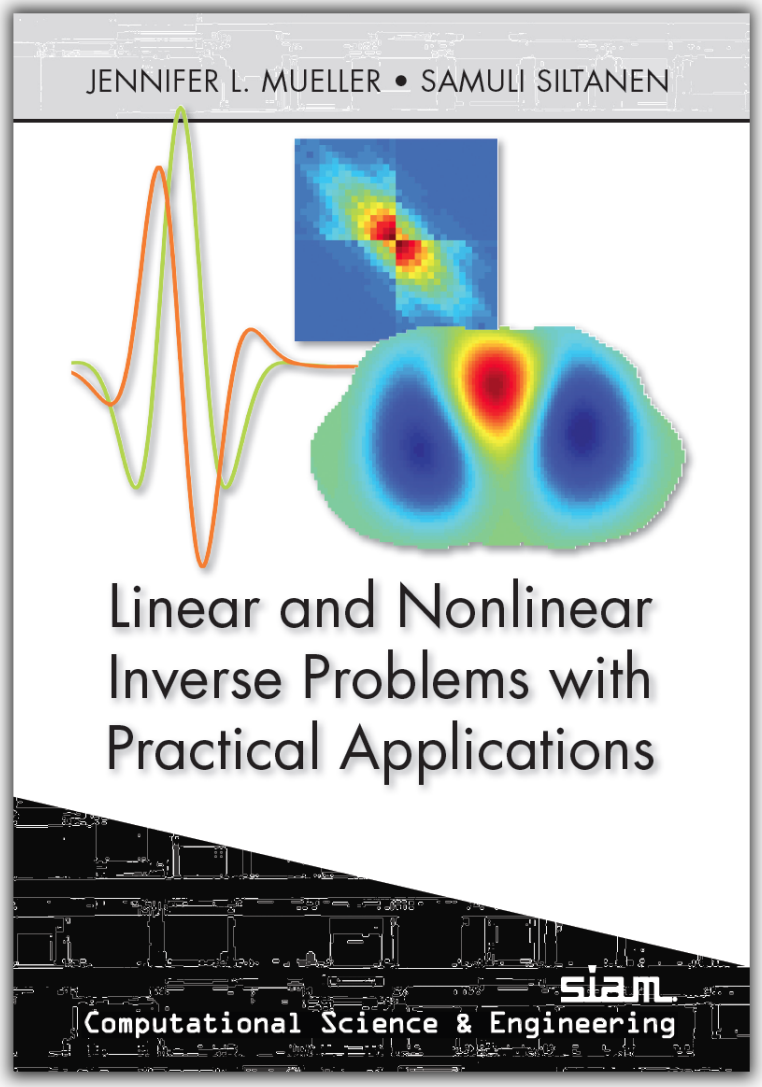

All Matlab codes freely available at this site!

Part I: Linear Inverse Problems

1 Introduction
2 Naïve reconstructions and inverse crimes
3 Ill-Posedness in Inverse Problems
4 Truncated singular value decomposition
5 Tikhonov regularization
6 Total variation regularization
7 Besov space regularization using wavelets
8 Discretization-invariance
9 Practical X-ray tomography with limited data
10 Projects

Part II: Nonlinear Inverse Problems

11 Nonlinear inversion
12 Electrical impedance tomography
13 Simulation of noisy EIT data
14 Complex geometrical optics solutions
15 A regularized D-bar method for direct EIT
16 Other direct solution methods for EIT
17 Projects

Outline

This part is a joint work with

Sarah Hamilton, University of Helsinki, Finland

Andreas Hauptmann, University of Helsinki, Finland

SalWe

CGO sinogram in the context of EIT

Solve $\psi(\,\cdot\,,k)|_{\partial\Omega} = e^{ikz} - \mathcal{S}_k(\Lambda_\sigma^\delta - \Lambda_1)\psi$ and set $\mu(z,k) = e^{-ikz}\psi(z,k)$.

Conductivity (z-plane)

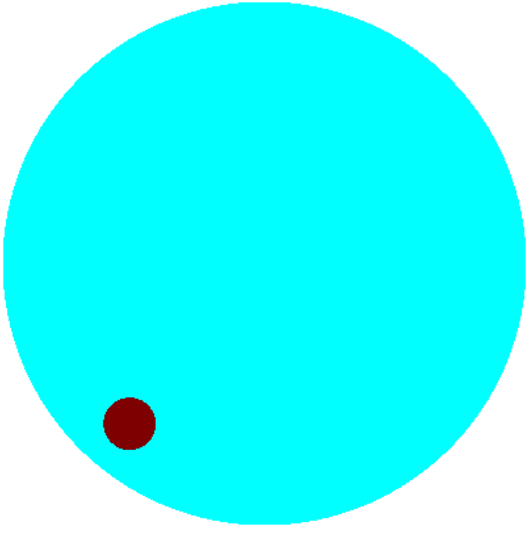

$z = e^{i\theta}$

k-plane

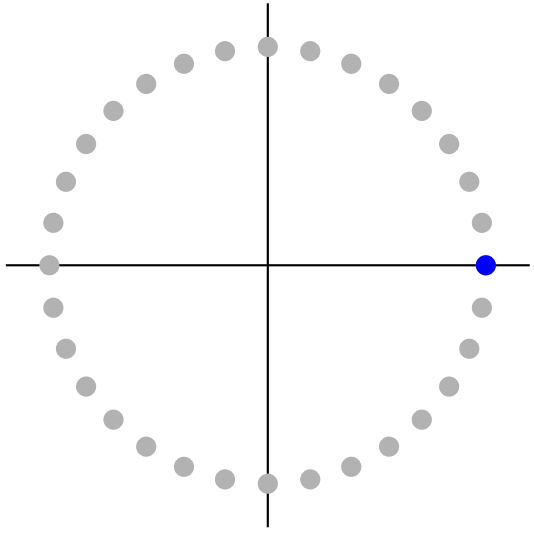

$k = Re^{i\varphi}$

CGO sinogram

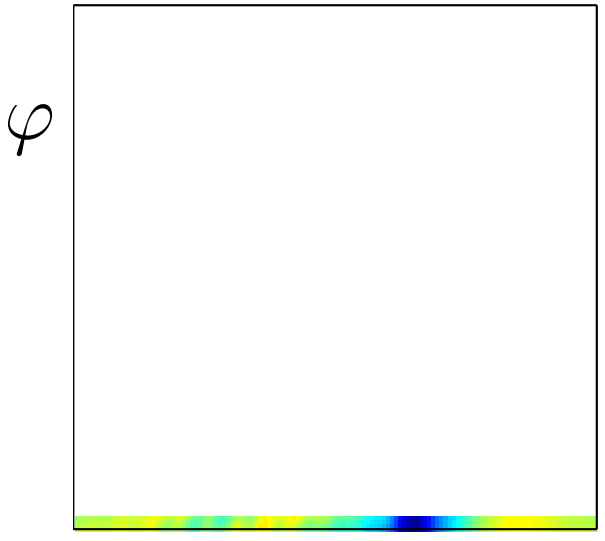

$$\mu(e^{i\theta}, Re^{i\varphi})$$

CGO sinogram in the context of EIT

Solve $\psi(\,\cdot\,,k)|_{\partial\Omega} = e^{ikz} - \mathcal{S}_k(\Lambda_\sigma^\delta - \Lambda_1)\psi$ and set $\mu(z,k) = e^{-ikz}\psi(z,k)$.

Conductivity (z-plane)

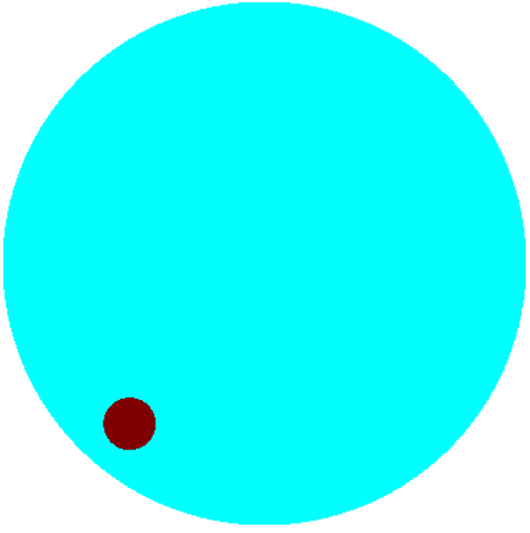

$z = e^{i\theta}$

k-plane

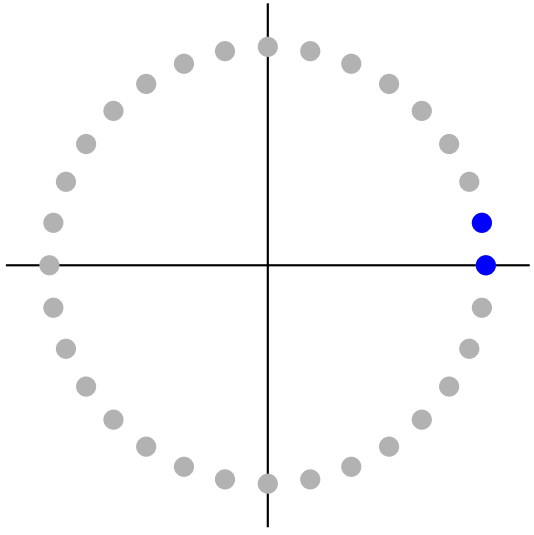

$k = Re^{i\varphi}$

CGO sinogram

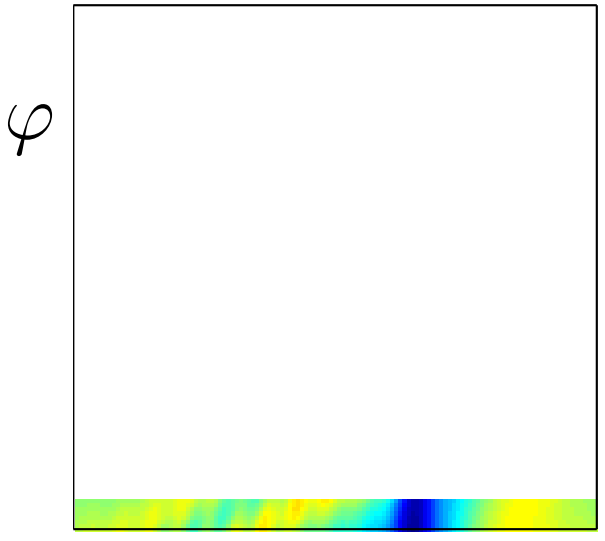

$$\mu(e^{i\theta}, Re^{i\varphi})$$

CGO sinogram in the context of EIT

Solve $\psi(\,\cdot\,,k)|_{\partial\Omega} = e^{ikz} - \mathcal{S}_k(\Lambda_\sigma^\delta - \Lambda_1)\psi$ and set $\mu(z,k) = e^{-ikz}\psi(z,k)$.

Conductivity (z-plane)

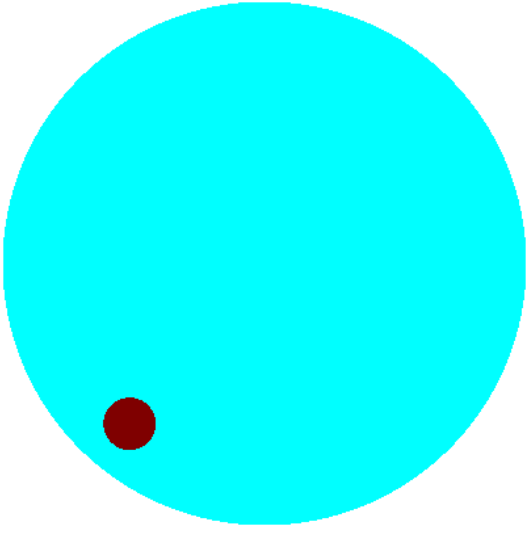

$z = e^{i\theta}$

k-plane

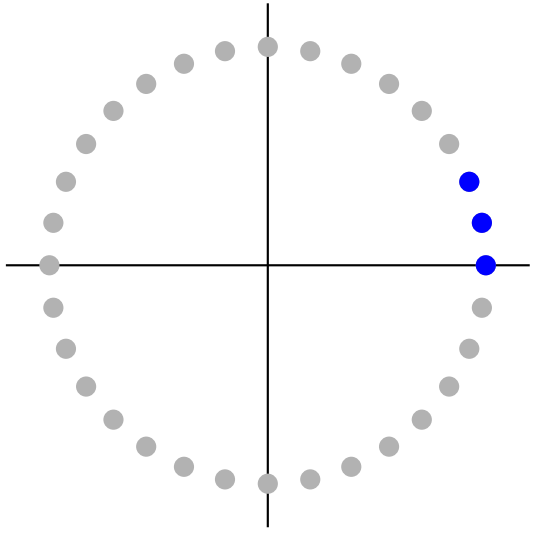

$k = Re^{i\varphi}$

CGO sinogram

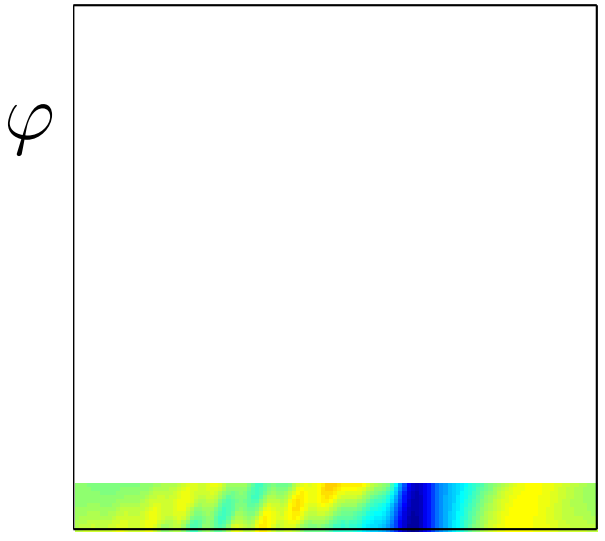

$$\mu(e^{i\theta}, Re^{i\varphi})$$

CGO sinogram in the context of EIT

Solve $\psi(\,\cdot\,,k)|_{\partial\Omega} = e^{ikz} - \mathcal{S}_k(\Lambda_\sigma^\delta - \Lambda_1)\psi$ and set $\mu(z,k) = e^{-ikz}\psi(z,k)$.

Conductivity (z-plane)

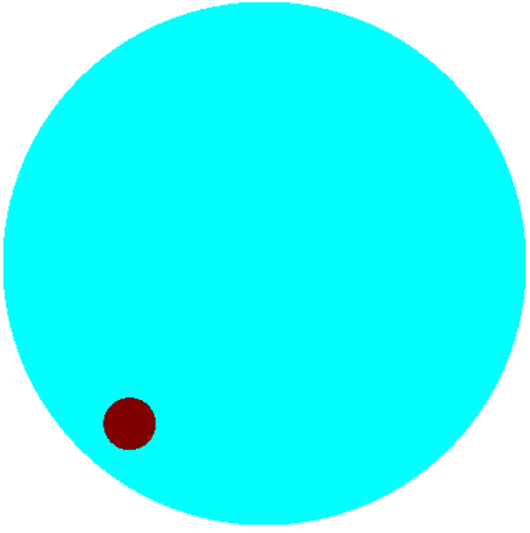

$z = e^{i\theta}$

k-plane

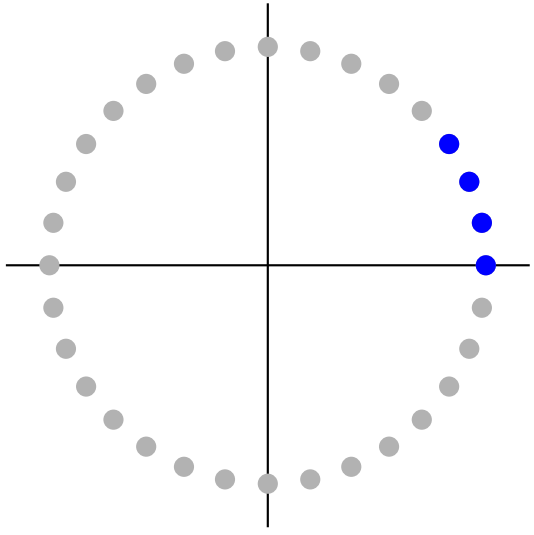

$k = Re^{i\varphi}$

CGO sinogram

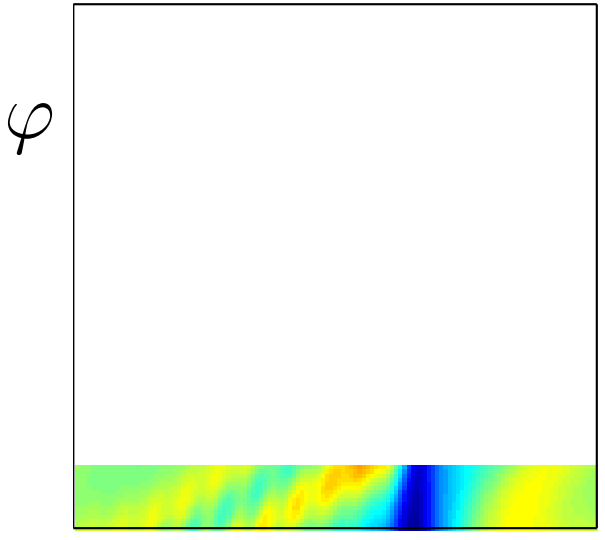

$\mu(e^{i\theta}, Re^{i\varphi})$

CGO sinogram in the context of EIT

Solve $\psi(\,\cdot\,,k)|_{\partial\Omega} = e^{ikz} - \mathcal{S}_k(\Lambda_\sigma^\delta - \Lambda_1)\psi$ and set $\mu(z,k) = e^{-ikz}\psi(z,k)$.

Conductivity (z-plane)

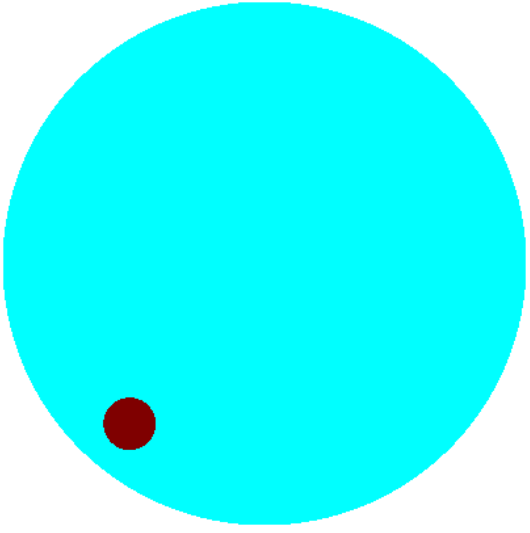

$z = e^{i\theta}$

k-plane

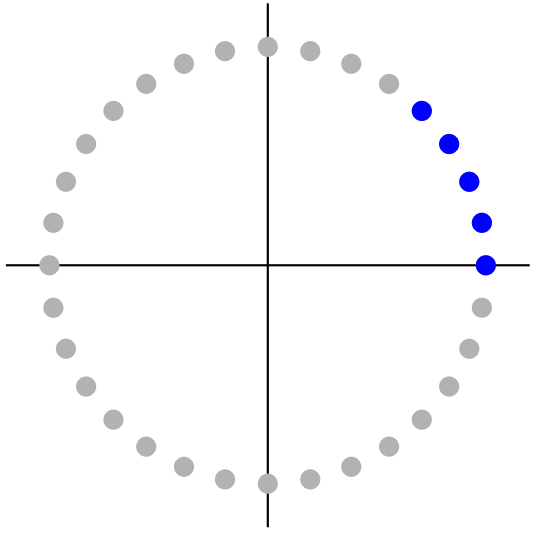

$k = Re^{i\varphi}$

CGO sinogram

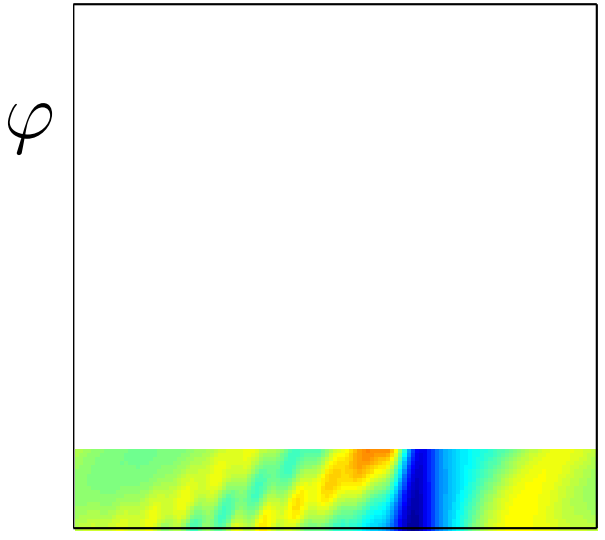

$\mu(e^{i\theta}, Re^{i\varphi})$

CGO sinogram in the context of EIT

Solve $\psi(\,\cdot\,,k)|_{\partial\Omega} = e^{ikz} - \mathcal{S}_k(\Lambda_\sigma^\delta - \Lambda_1)\psi$ and set $\mu(z,k) = e^{-ikz}\psi(z,k)$.

Conductivity (z-plane)

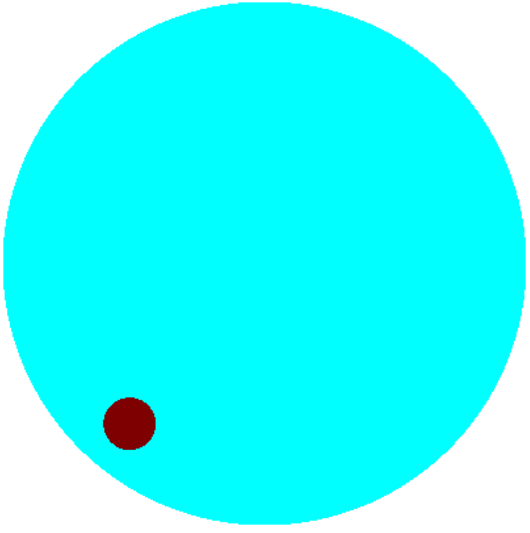

$z = e^{i\theta}$

k-plane

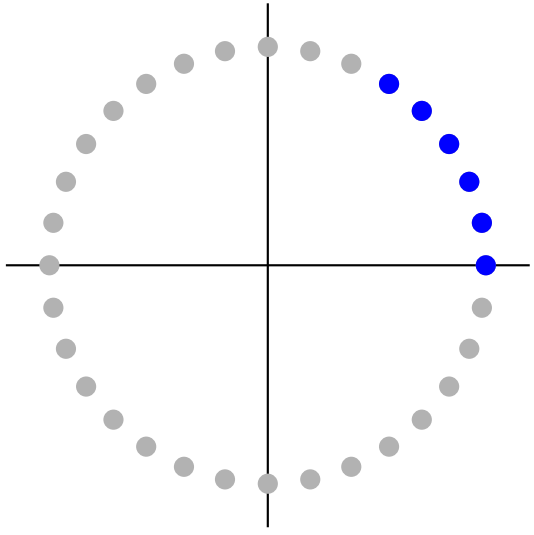

$k = Re^{i\varphi}$

CGO sinogram

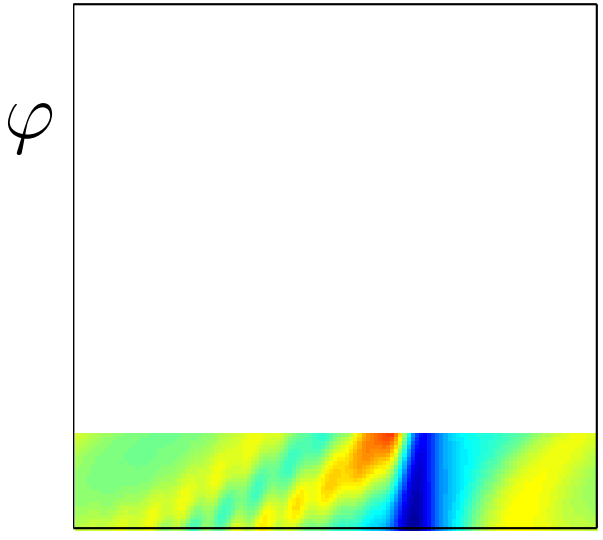

$\mu(e^{i\theta}, Re^{i\varphi})$

CGO sinogram in the context of EIT

Solve $\psi(\,\cdot\,,k)|_{\partial\Omega} = e^{ikz} - \mathcal{S}_k(\Lambda_\sigma^\delta - \Lambda_1)\psi$ and set $\mu(z,k) = e^{-ikz}\psi(z,k)$.

Conductivity (z-plane)

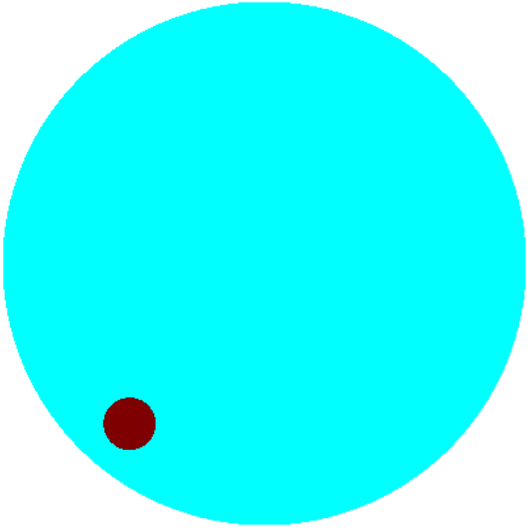

$z = e^{i\theta}$

k-plane

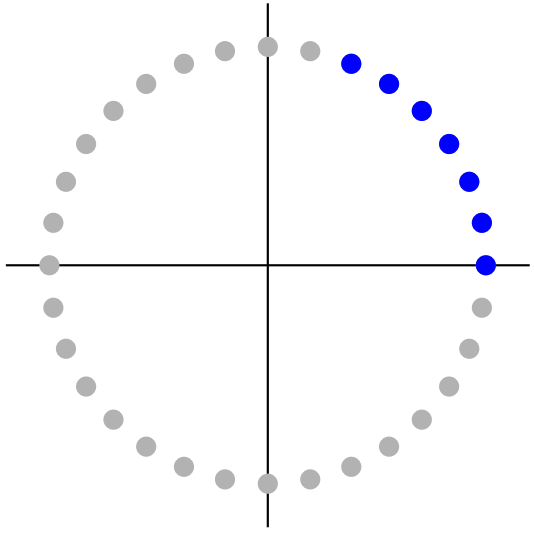

$k = Re^{i\varphi}$

CGO sinogram

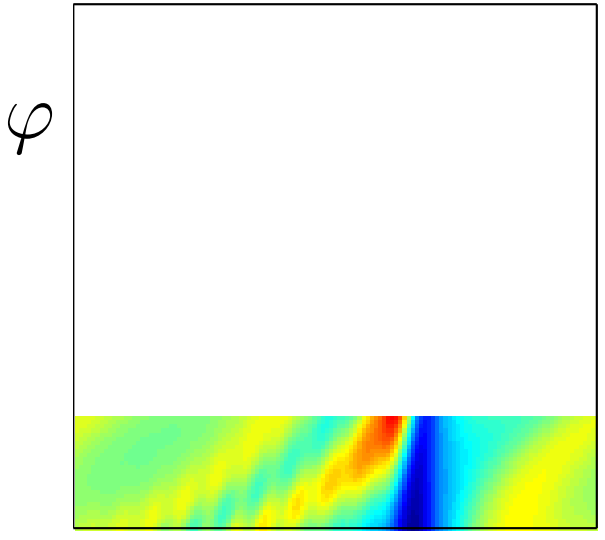

$\mu(e^{i\theta}, Re^{i\varphi})$

CGO sinogram in the context of EIT

Solve $\psi(\,\cdot\,,k)|_{\partial\Omega} = e^{ikz} - \mathcal{S}_k(\Lambda_\sigma^\delta - \Lambda_1)\psi$ and set $\mu(z,k) = e^{-ikz}\psi(z,k)$.

Conductivity (z-plane)

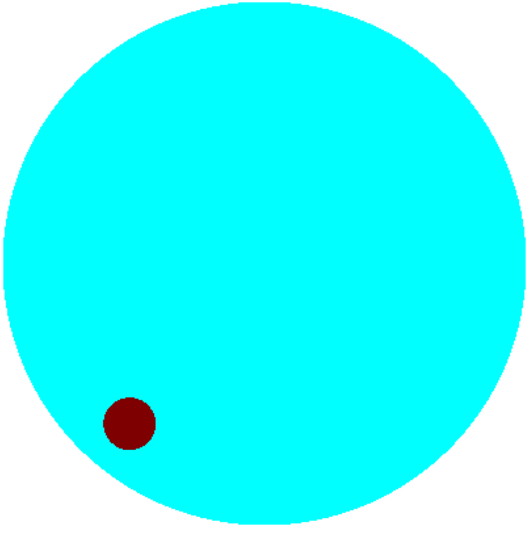

$z = e^{i\theta}$

k-plane

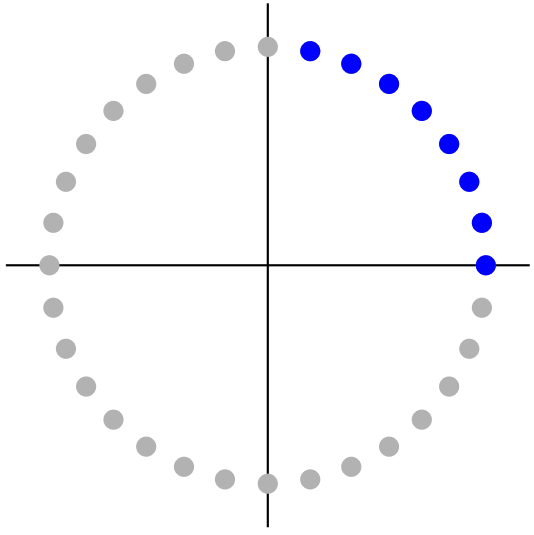

$k = Re^{i\varphi}$

CGO sinogram

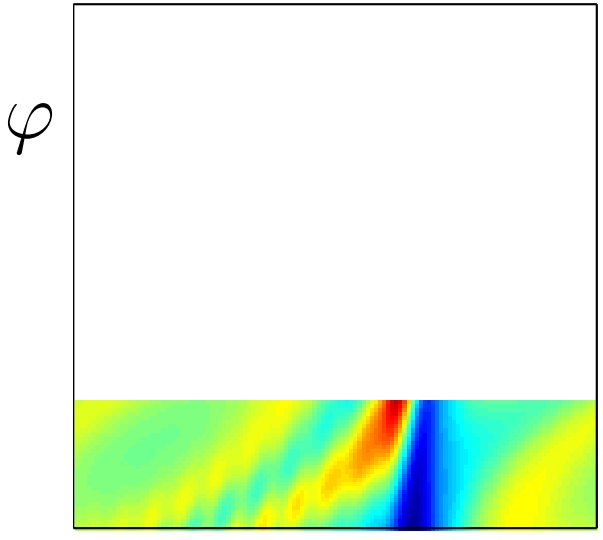

$\mu(e^{i\theta}, Re^{i\varphi})$

CGO sinogram in the context of EIT

Solve $\psi(\,\cdot\,,k)|_{\partial\Omega} = e^{ikz} - \mathcal{S}_k(\Lambda_\sigma^\delta - \Lambda_1)\psi$ and set $\mu(z,k) = e^{-ikz}\psi(z,k)$.

Conductivity (z-plane)

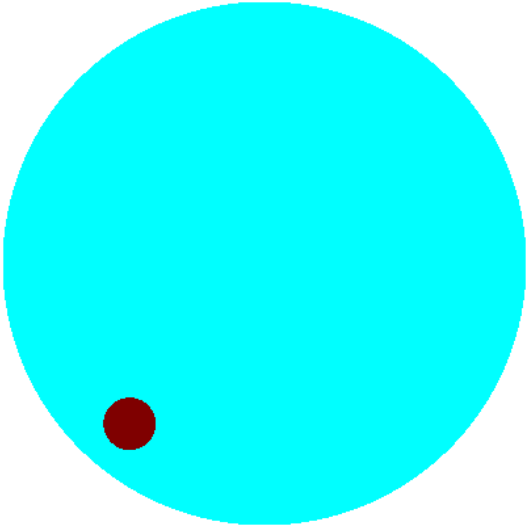

$z = e^{i\theta}$

k-plane

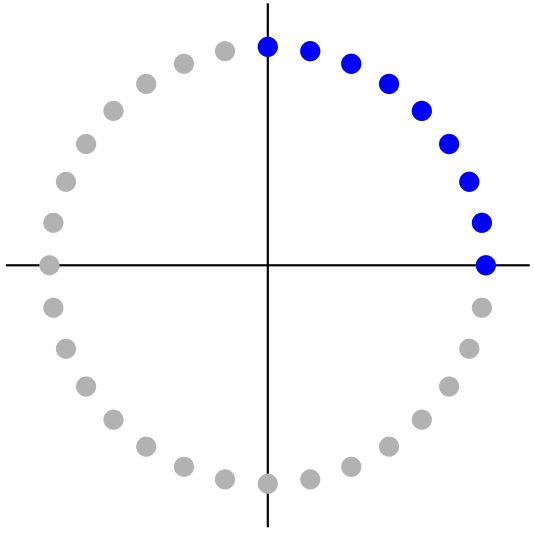

$k = Re^{i\varphi}$

CGO sinogram

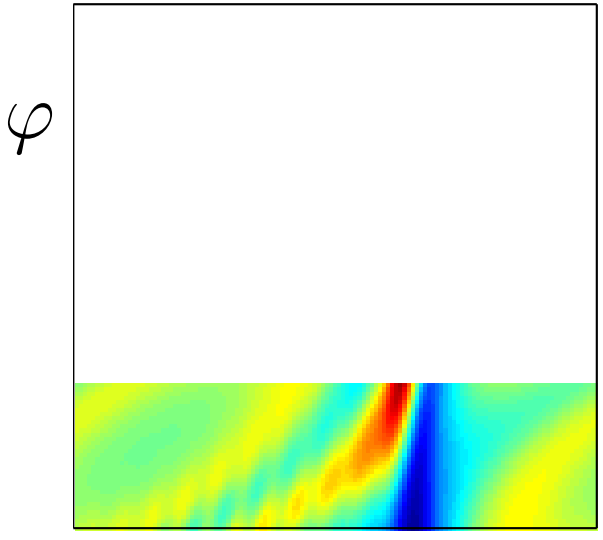

$\mu(e^{i\theta}, Re^{i\varphi})$

CGO sinogram in the context of EIT

Solve $\psi(\,\cdot\,,k)|_{\partial\Omega} = e^{ikz} - \mathcal{S}_k(\Lambda_\sigma^\delta - \Lambda_1)\psi$ and set $\mu(z,k) = e^{-ikz}\psi(z,k)$.

Conductivity (z-plane)

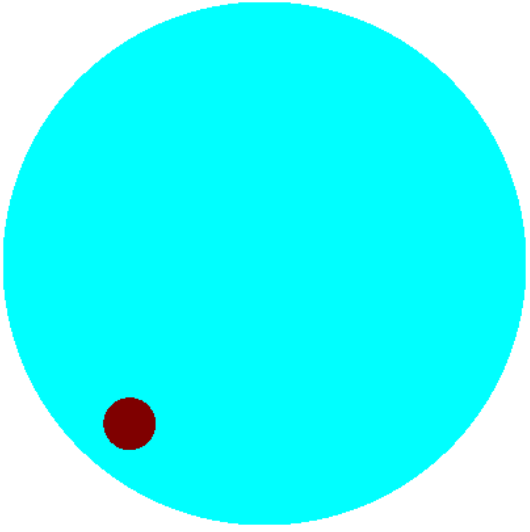

$z = e^{i\theta}$

k-plane

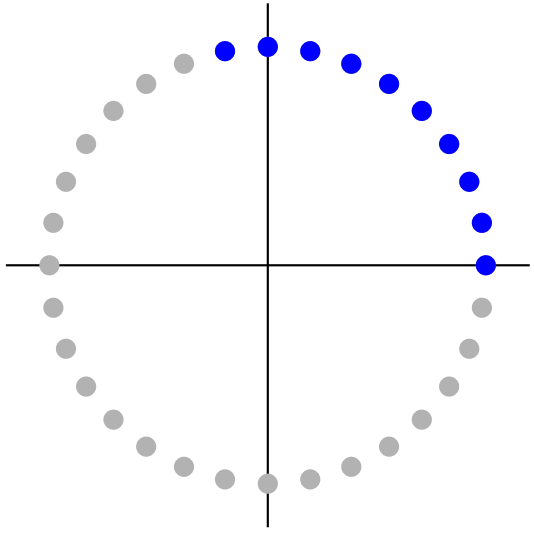

$k = Re^{i\varphi}$

CGO sinogram

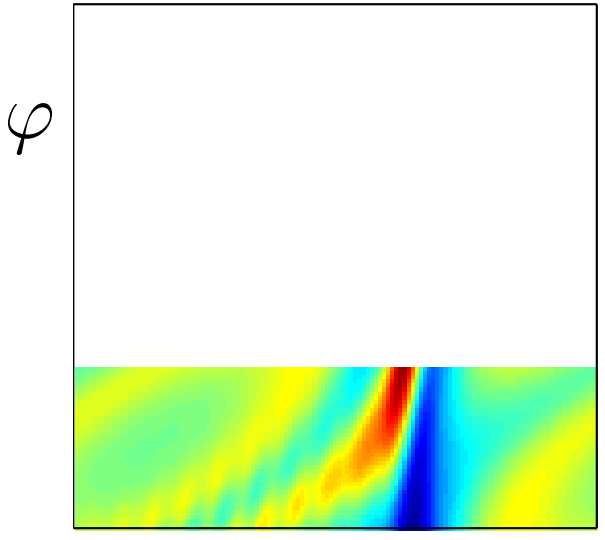

$\mu(e^{i\theta}, Re^{i\varphi})$

CGO sinogram in the context of EIT

Solve $\psi(\,\cdot\,,k)|_{\partial\Omega} = e^{ikz} - \mathcal{S}_k(\Lambda_\sigma^\delta - \Lambda_1)\psi$ and set $\mu(z,k) = e^{-ikz}\psi(z,k)$.

Conductivity (z-plane)

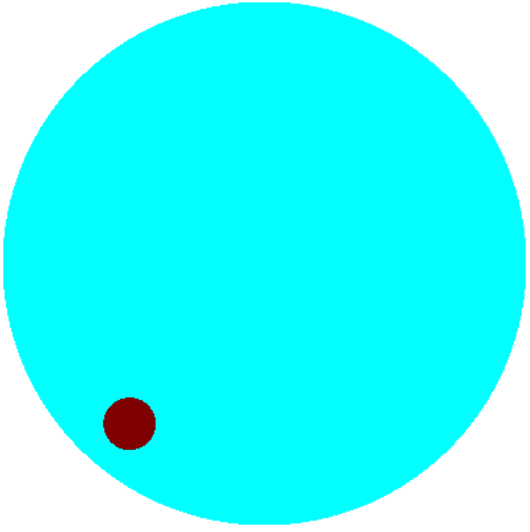

$z = e^{i\theta}$

k-plane

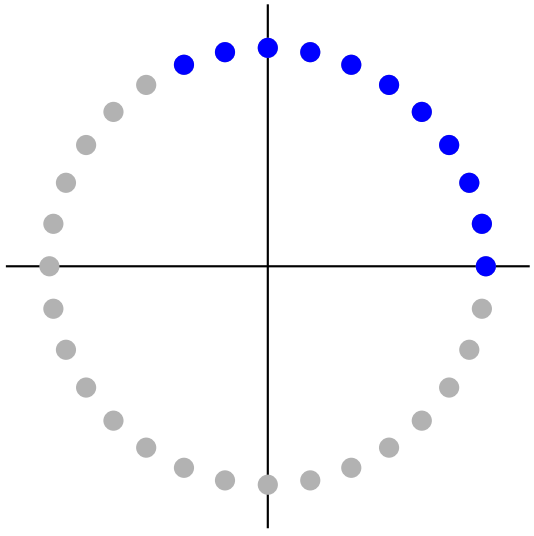

$k = Re^{i\varphi}$

CGO sinogram

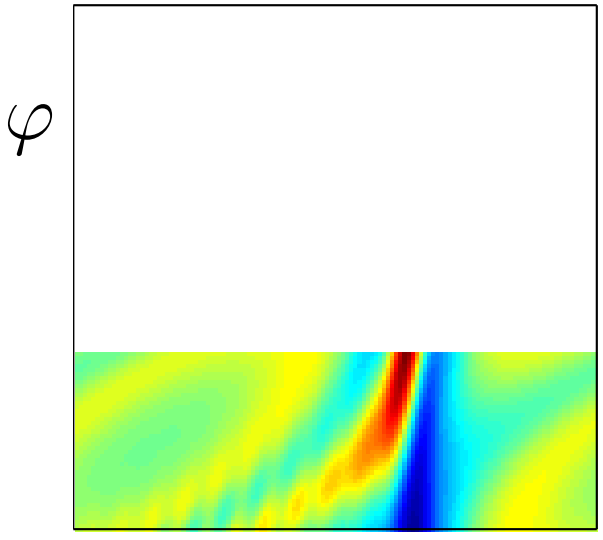

$\mu(e^{i\theta}, Re^{i\varphi})$

CGO sinogram in the context of EIT

Solve $\psi(\,\cdot\,,k)|_{\partial\Omega} = e^{ikz} - \mathcal{S}_k(\Lambda_\sigma^\delta - \Lambda_1)\psi$ and set $\mu(z,k) = e^{-ikz}\psi(z,k)$.

Conductivity (z-plane)

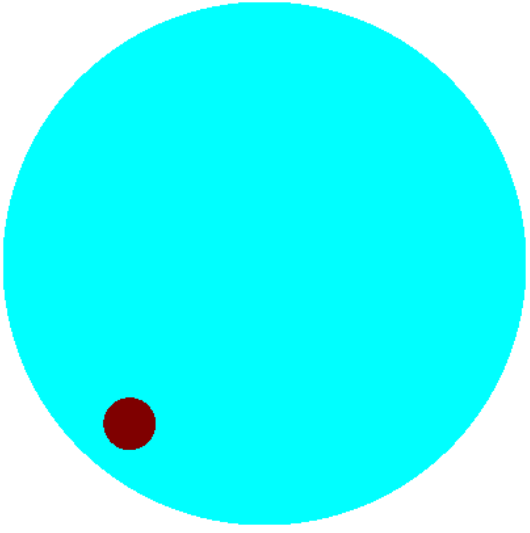

$z = e^{i\theta}$

k-plane

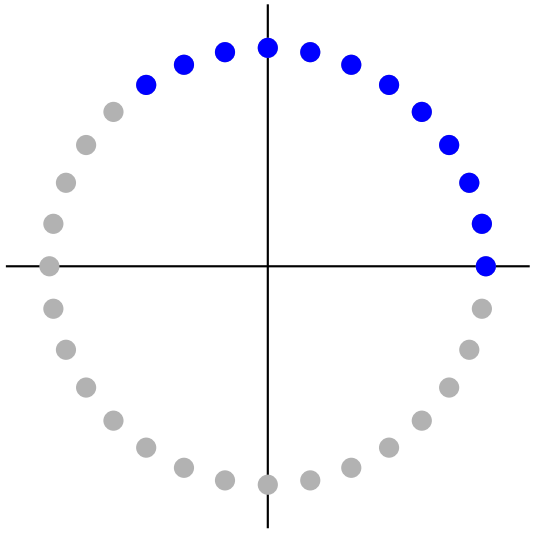

$k = Re^{i\varphi}$

CGO sinogram

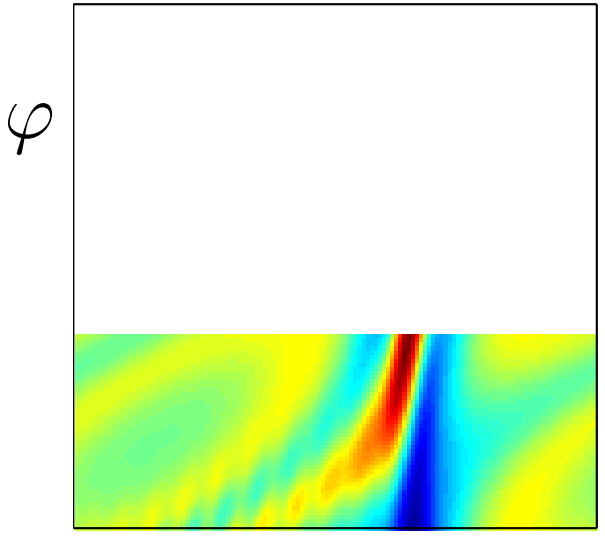

$\mu(e^{i\theta}, Re^{i\varphi})$

CGO sinogram in the context of EIT

Solve $\psi(\,\cdot\,,k)|_{\partial\Omega} = e^{ikz} - \mathcal{S}_k(\Lambda_\sigma^\delta - \Lambda_1)\psi$ and set $\mu(z,k) = e^{-ikz}\psi(z,k)$.

Conductivity (z-plane)

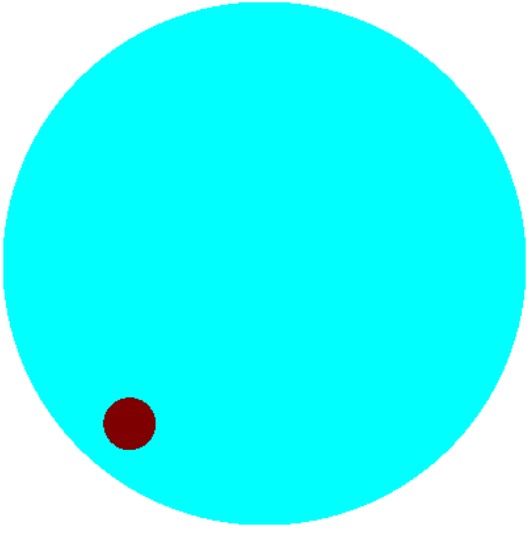

$z = e^{i\theta}$

k-plane

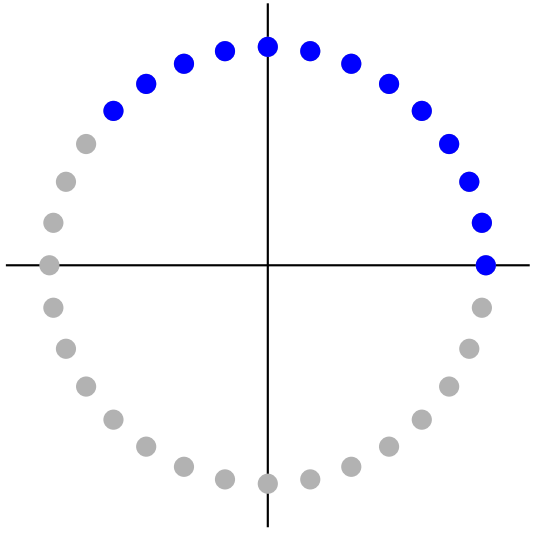

$k = Re^{i\varphi}$

CGO sinogram

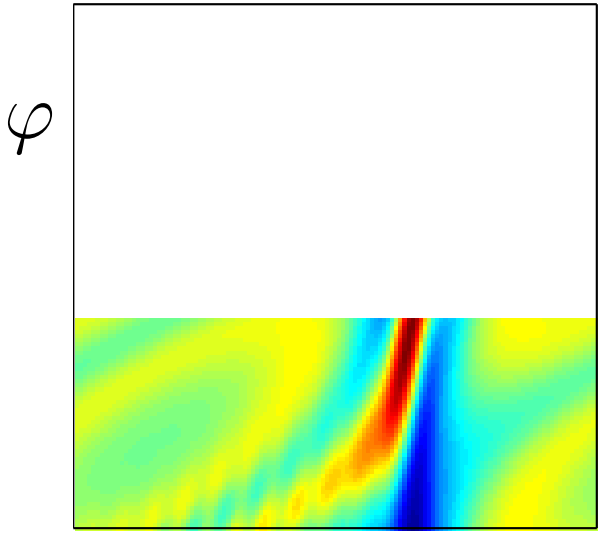

$\mu(e^{i\theta}, Re^{i\varphi})$

CGO sinogram in the context of EIT

Solve $\psi(\,\cdot\,,k)|_{\partial\Omega} = e^{ikz} - \mathcal{S}_k(\Lambda_\sigma^\delta - \Lambda_1)\psi$ and set $\mu(z,k) = e^{-ikz}\psi(z,k)$.

Conductivity (z-plane)

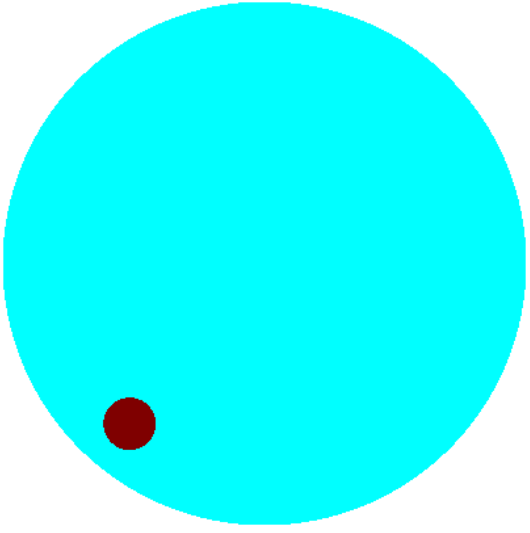

$z = e^{i\theta}$

k-plane

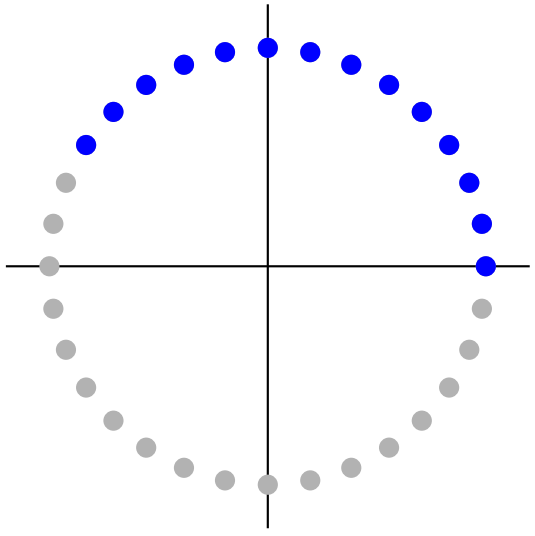

$k = Re^{i\varphi}$

CGO sinogram

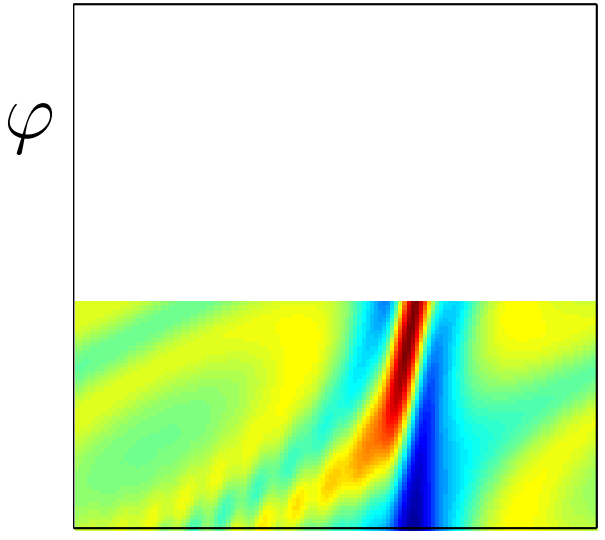

$\mu(e^{i\theta}, Re^{i\varphi})$

CGO sinogram in the context of EIT

Solve $\psi(\,\cdot\,,k)|_{\partial\Omega} = e^{ikz} - \mathcal{S}_k(\Lambda_\sigma^\delta - \Lambda_1)\psi$ and set $\mu(z,k) = e^{-ikz}\psi(z,k)$.

Conductivity (z-plane)

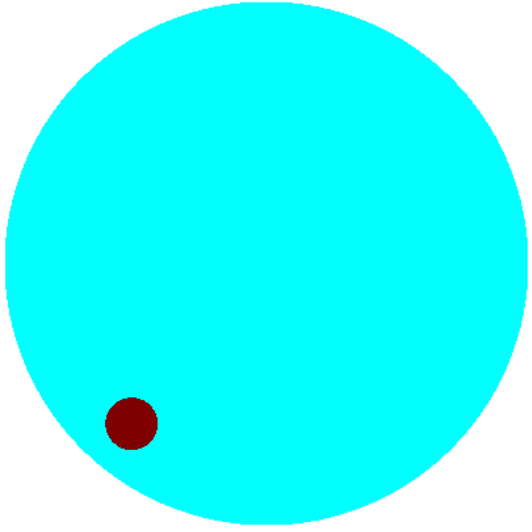

$z = e^{i\theta}$

k-plane

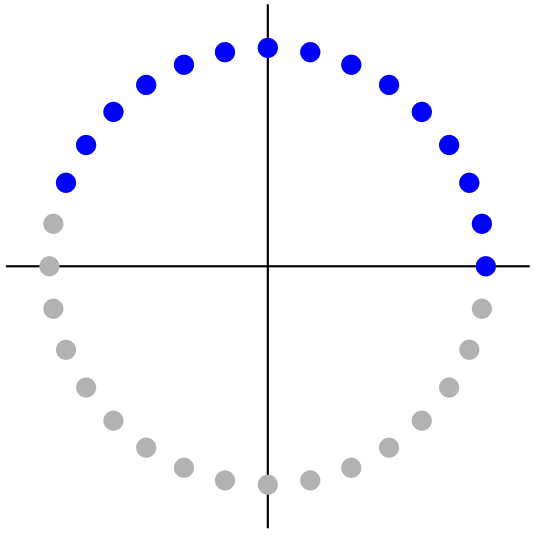

$k = Re^{i\varphi}$

CGO sinogram

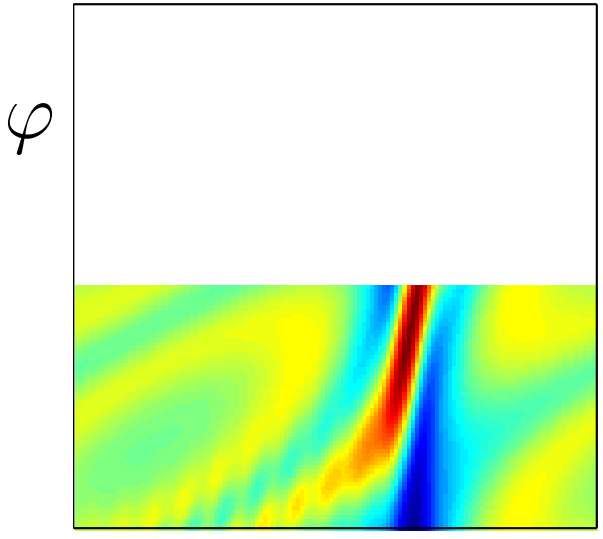

$$\mu(e^{i\theta}, Re^{i\varphi})$$

CGO sinogram in the context of EIT

Solve $\psi(\,\cdot\,,k)|_{\partial\Omega} = e^{ikz} - \mathcal{S}_k(\Lambda_\sigma^\delta - \Lambda_1)\psi$ and set $\mu(z,k) = e^{-ikz}\psi(z,k)$.

Conductivity (z-plane)

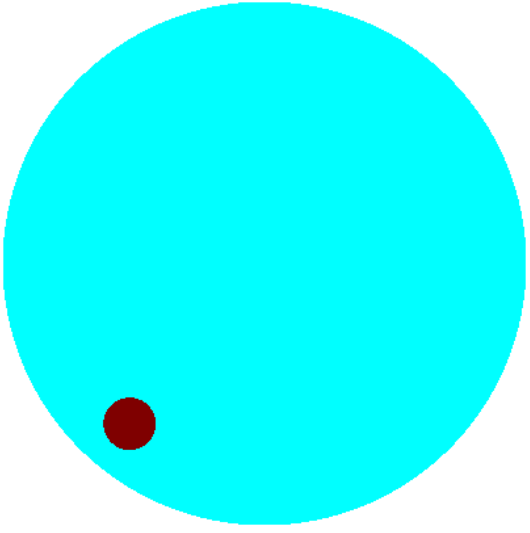

$z = e^{i\theta}$

k-plane

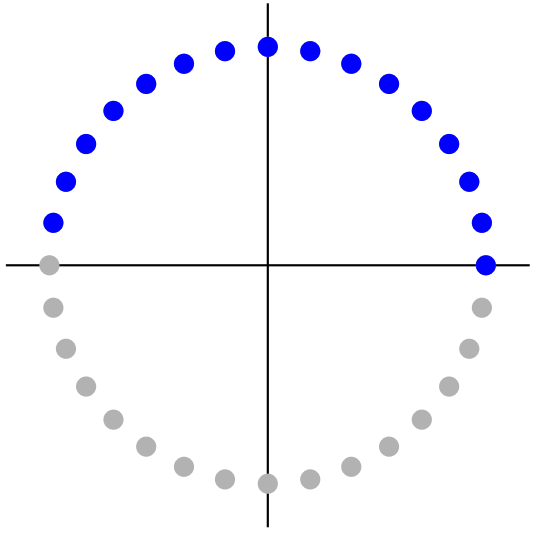

$k = Re^{i\varphi}$

CGO sinogram

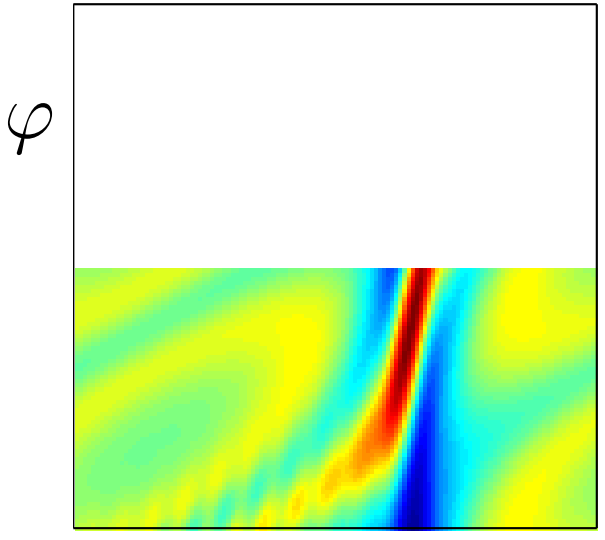

$\mu(e^{i\theta}, Re^{i\varphi})$

CGO sinogram in the context of EIT

Solve $\psi(\,\cdot\,,k)|_{\partial\Omega} = e^{ikz} - \mathcal{S}_k(\Lambda_\sigma^\delta - \Lambda_1)\psi$ and set $\mu(z,k) = e^{-ikz}\psi(z,k)$.

Conductivity (z-plane)

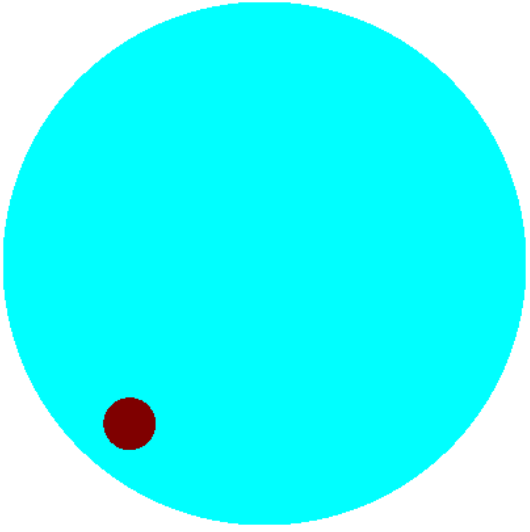

$z = e^{i\theta}$

k-plane

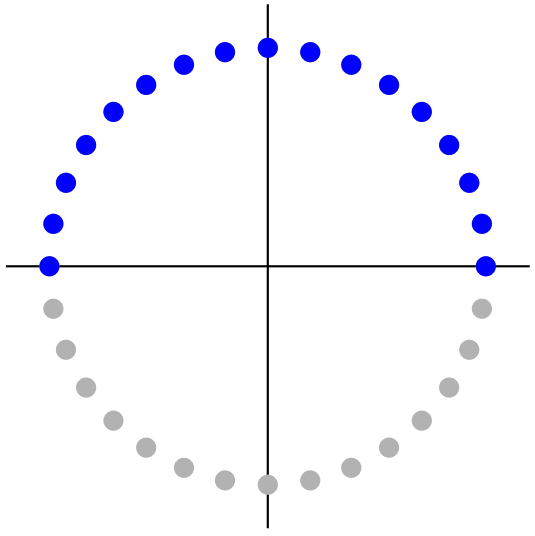

$k = Re^{i\varphi}$

CGO sinogram

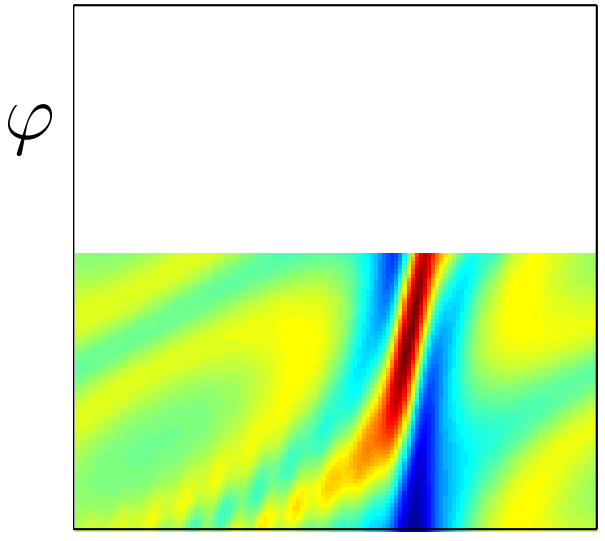

$$\mu(e^{i\theta}, Re^{i\varphi})$$

CGO sinogram in the context of EIT

Solve $\psi(\,\cdot\,,k)|_{\partial\Omega} = e^{ikz} - \mathcal{S}_k(\Lambda_\sigma^\delta - \Lambda_1)\psi$ and set $\mu(z,k) = e^{-ikz}\psi(z,k)$.

Conductivity (z-plane)

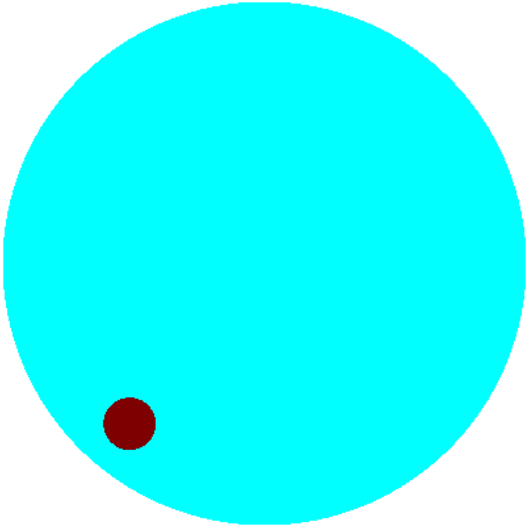

$z = e^{i\theta}$

k-plane

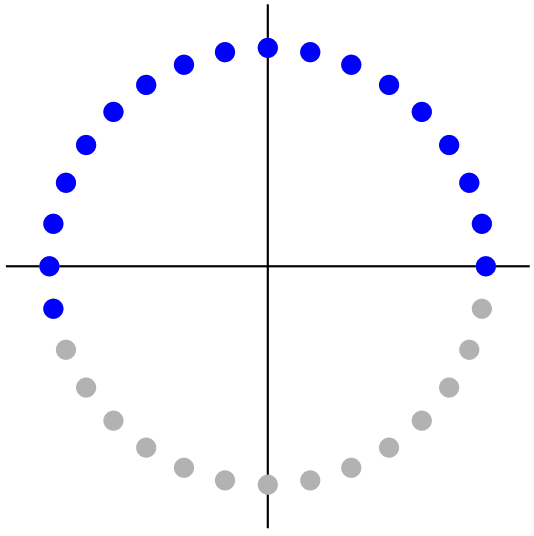

$k = Re^{i\varphi}$

CGO sinogram

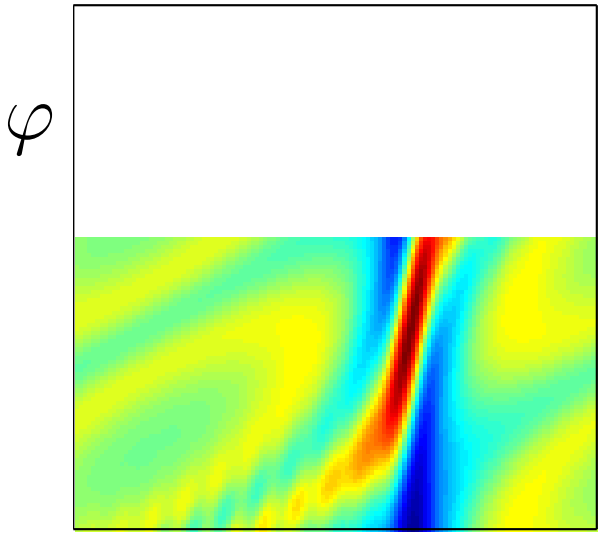

$$\mu(e^{i\theta}, Re^{i\varphi})$$

CGO sinogram in the context of EIT

Solve $\psi(\,\cdot\,,k)|_{\partial\Omega} = e^{ikz} - \mathcal{S}_k(\Lambda_\sigma^\delta - \Lambda_1)\psi$ and set $\mu(z,k) = e^{-ikz}\psi(z,k)$.

Conductivity (z-plane)

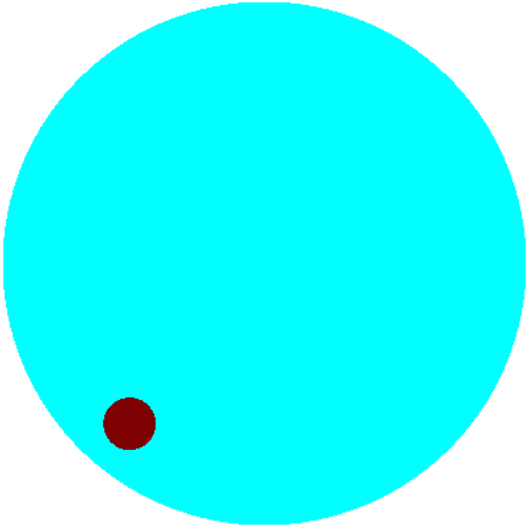

$z = e^{i\theta}$

k-plane

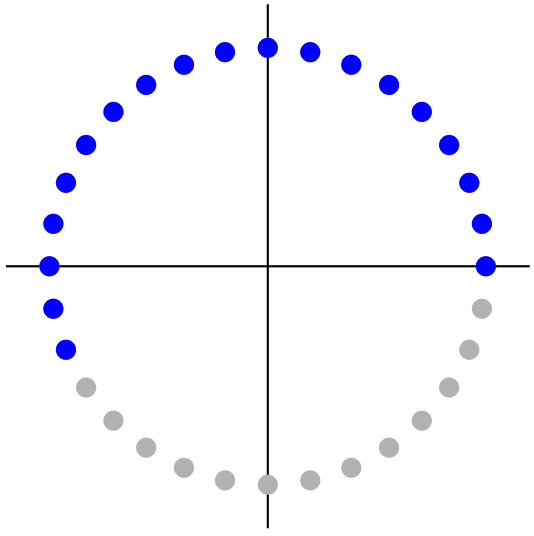

$k = Re^{i\varphi}$

CGO sinogram

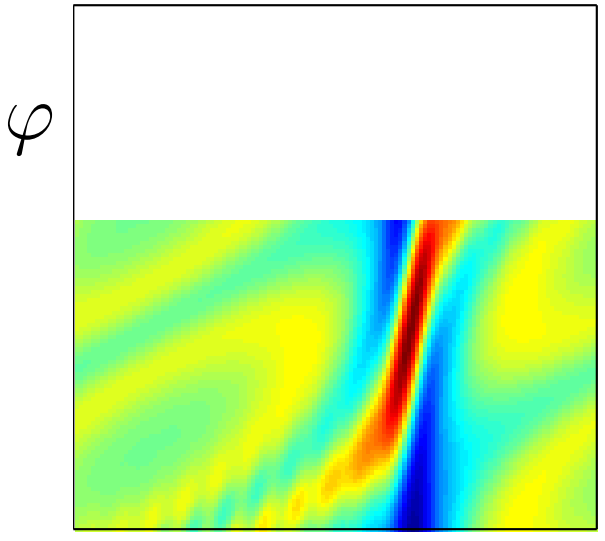

$$\mu(e^{i\theta}, Re^{i\varphi})$$

CGO sinogram in the context of EIT

Solve $\psi(\,\cdot\,,k)|_{\partial\Omega} = e^{ikz} - \mathcal{S}_k(\Lambda_\sigma^\delta - \Lambda_1)\psi$ and set $\mu(z,k) = e^{-ikz}\psi(z,k)$.

Conductivity (z-plane)

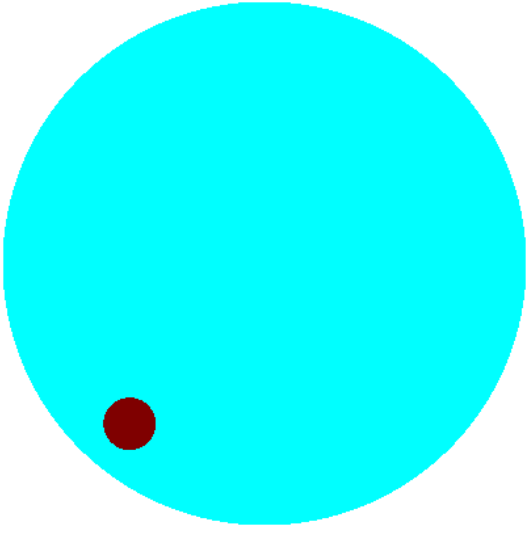

$z = e^{i\theta}$

k-plane

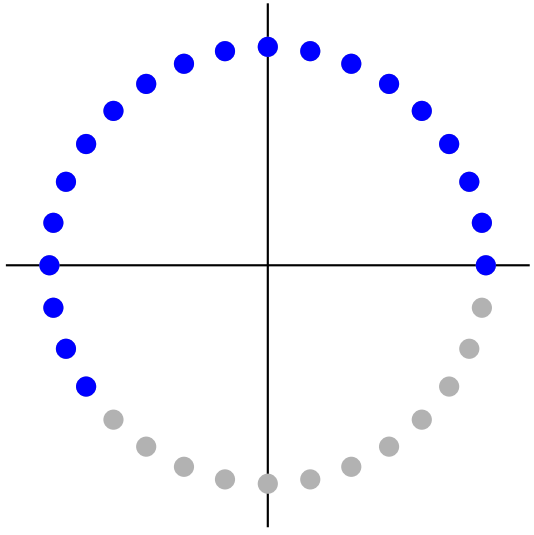

$k = Re^{i\varphi}$

CGO sinogram

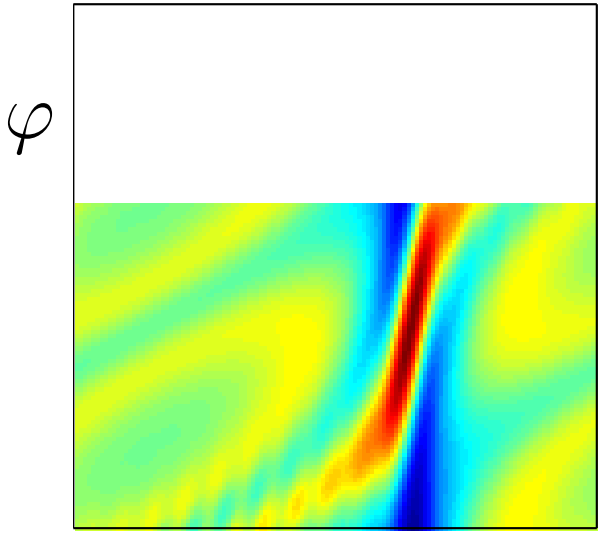

$\mu(e^{i\theta}, Re^{i\varphi})$

CGO sinogram in the context of EIT

Solve $\psi(\,\cdot\,,k)|_{\partial\Omega} = e^{ikz} - \mathcal{S}_k(\Lambda_\sigma^\delta - \Lambda_1)\psi$ and set $\mu(z,k) = e^{-ikz}\psi(z,k)$.

Conductivity (z-plane)

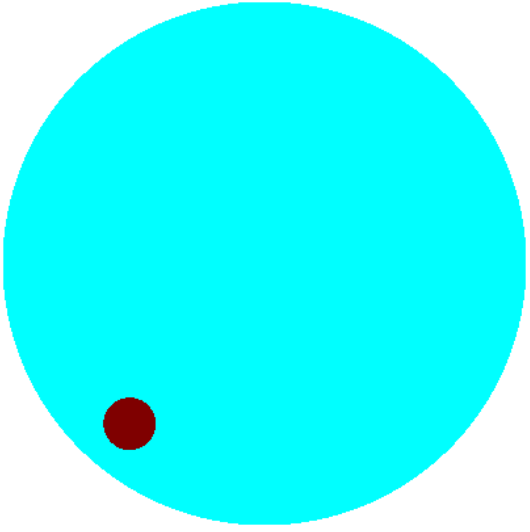

$z = e^{i\theta}$

k-plane

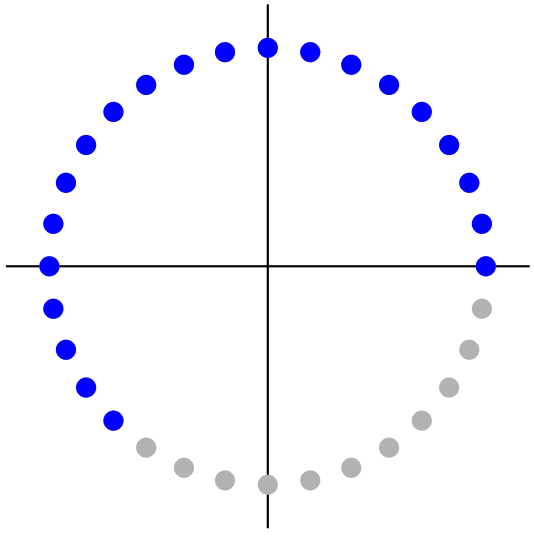

$k = Re^{i\varphi}$

CGO sinogram

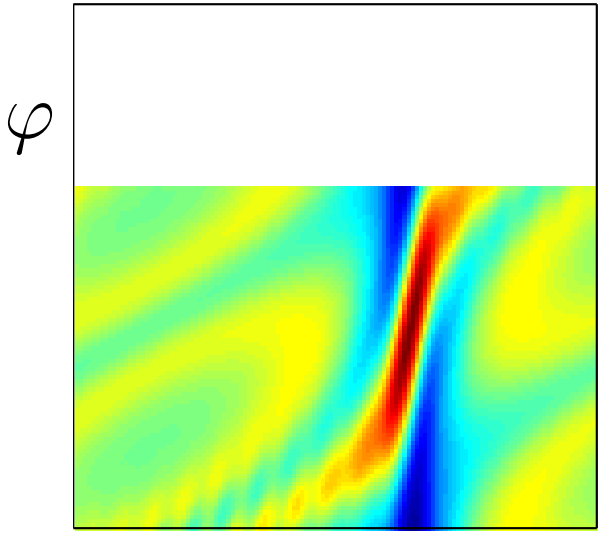

$\mu(e^{i\theta}, Re^{i\varphi})$

CGO sinogram in the context of EIT

Solve $\psi(\,\cdot\,,k)|_{\partial\Omega} = e^{ikz} - \mathcal{S}_k(\Lambda_\sigma^\delta - \Lambda_1)\psi$ and set $\mu(z,k) = e^{-ikz}\psi(z,k)$.

Conductivity (z-plane)

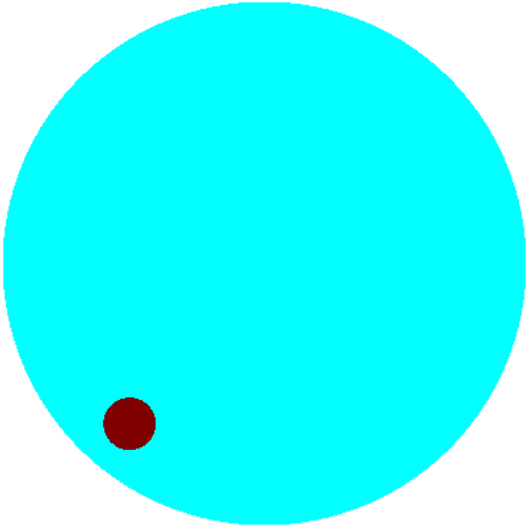

$z = e^{i\theta}$

k-plane

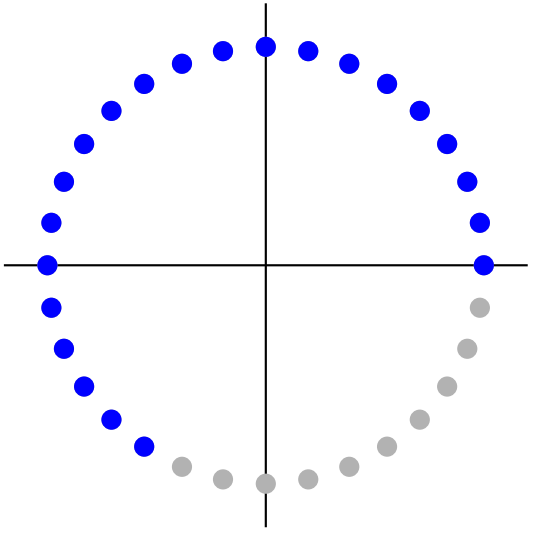

$k = Re^{i\varphi}$

CGO sinogram

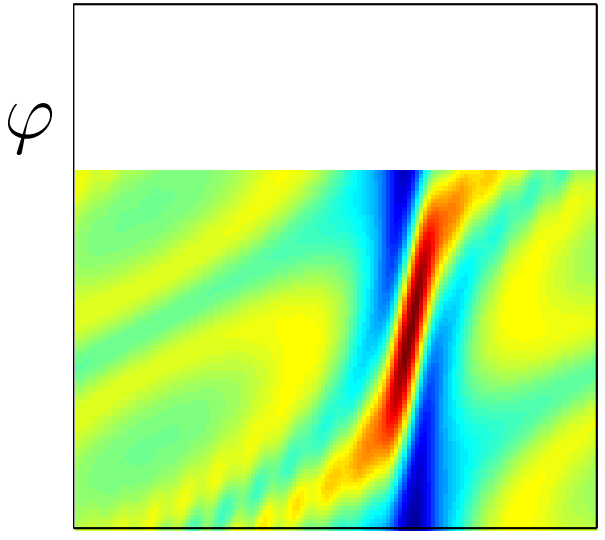

$$\mu(e^{i\theta}, Re^{i\varphi})$$

CGO sinogram in the context of EIT

Solve $\psi(\,\cdot\,,k)|_{\partial\Omega} = e^{ikz} - \mathcal{S}_k(\Lambda_\sigma^\delta - \Lambda_1)\psi$ and set $\mu(z,k) = e^{-ikz}\psi(z,k)$.

Conductivity (z-plane)

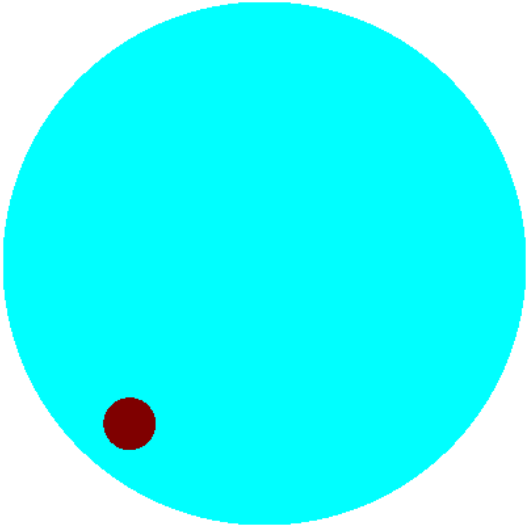

$z = e^{i\theta}$

k-plane

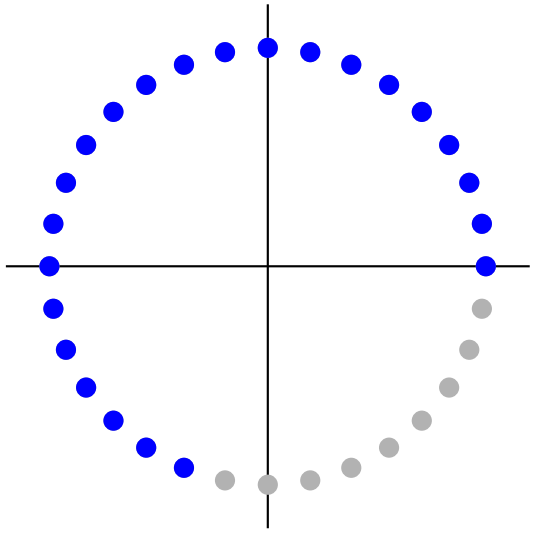

$k = Re^{i\varphi}$

CGO sinogram

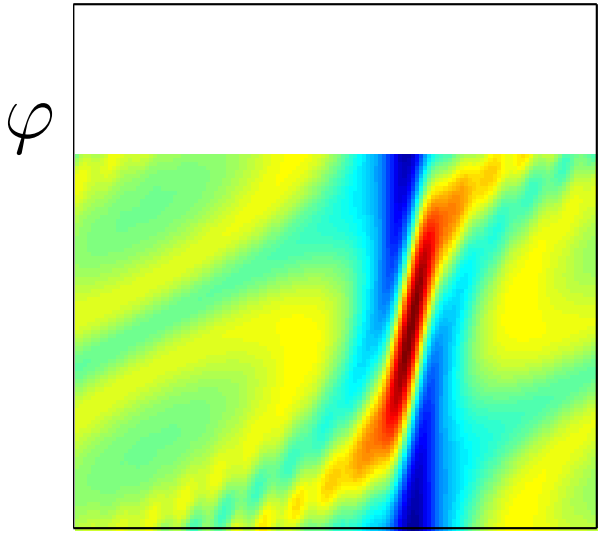

$\mu(e^{i\theta}, Re^{i\varphi})$

CGO sinogram in the context of EIT

Solve $\psi(\,\cdot\,,k)|_{\partial\Omega} = e^{ikz} - \mathcal{S}_k(\Lambda_\sigma^\delta - \Lambda_1)\psi$ and set $\mu(z,k) = e^{-ikz}\psi(z,k)$.

Conductivity (z-plane)

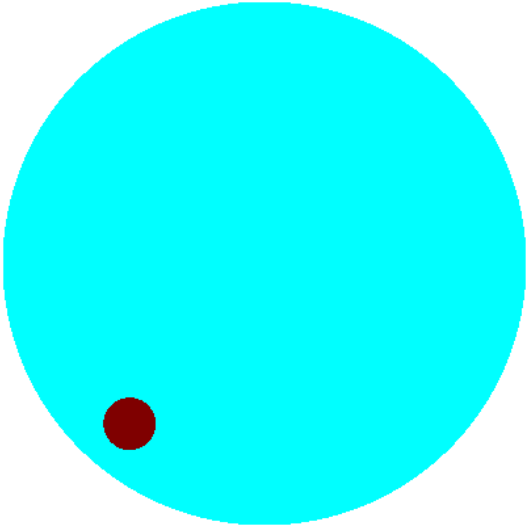

$z = e^{i\theta}$

k-plane

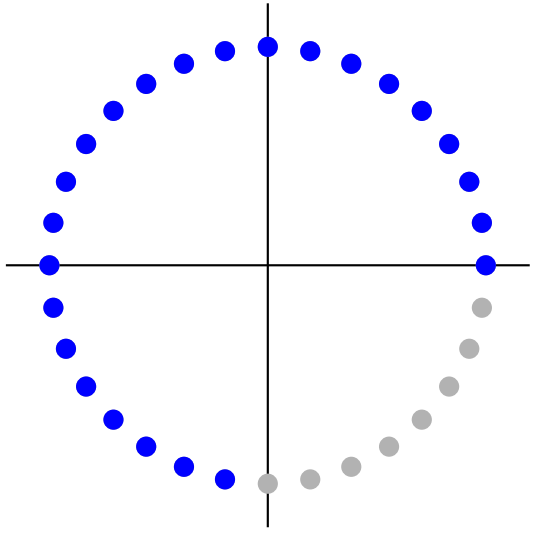

$k = Re^{i\varphi}$

CGO sinogram

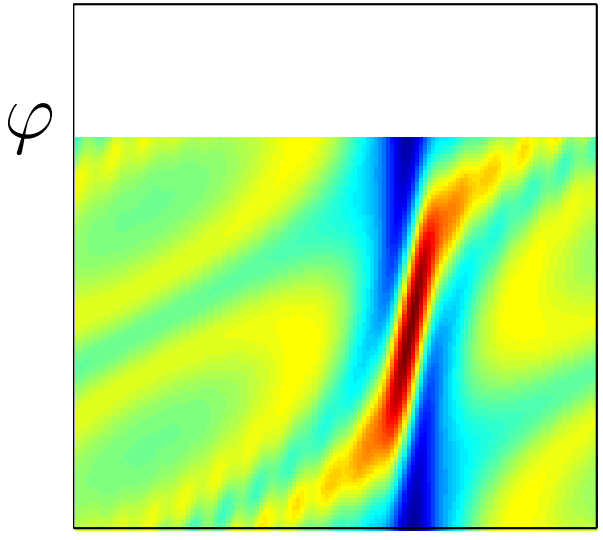

$$\mu(e^{i\theta}, Re^{i\varphi})$$

CGO sinogram in the context of EIT

Solve $\psi(\,\cdot\,,k)|_{\partial\Omega} = e^{ikz} - \mathcal{S}_k(\Lambda_\sigma^\delta - \Lambda_1)\psi$ and set $\mu(z,k) = e^{-ikz}\psi(z,k)$.

Conductivity (z-plane)

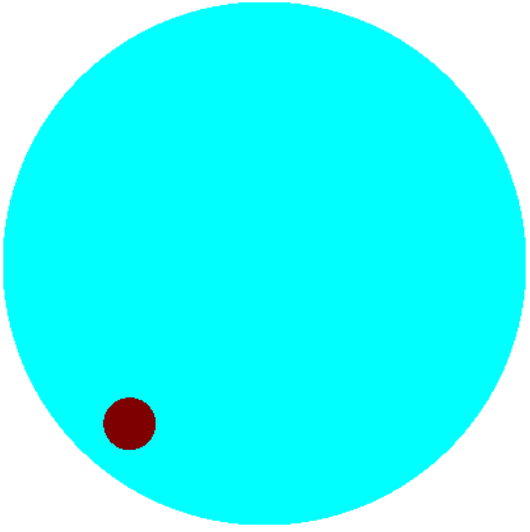

$z = e^{i\theta}$

k-plane

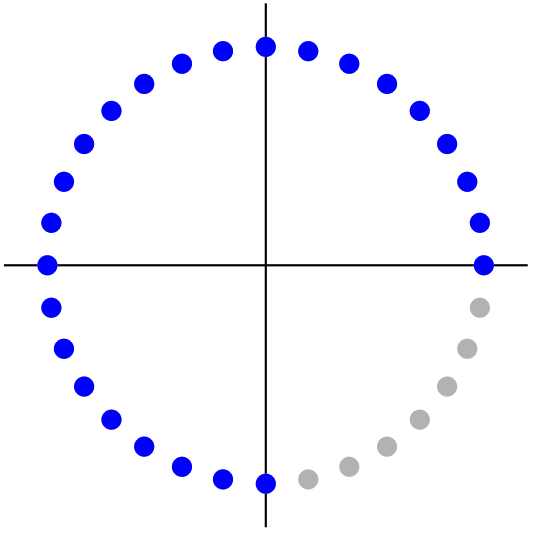

$k = Re^{i\varphi}$

CGO sinogram

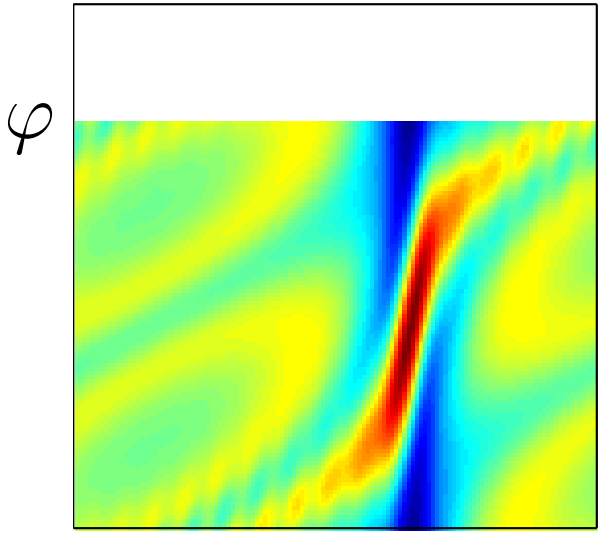

$\mu(e^{i\theta}, Re^{i\varphi})$

CGO sinogram in the context of EIT

Solve $\psi(\,\cdot\,,k)|_{\partial\Omega} = e^{ikz} - \mathcal{S}_k(\Lambda_\sigma^\delta - \Lambda_1)\psi$ and set $\mu(z,k) = e^{-ikz}\psi(z,k)$.

Conductivity (z-plane)

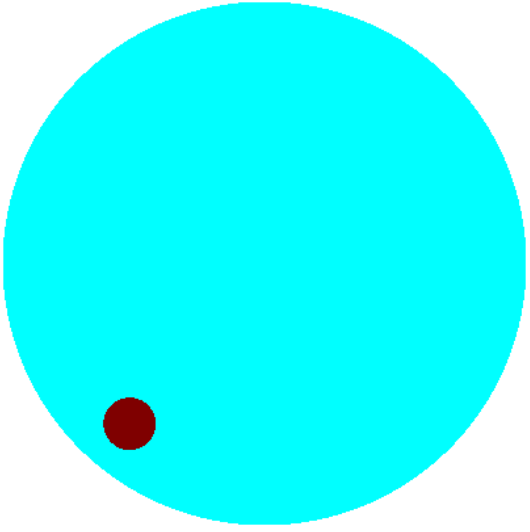

$z = e^{i\theta}$

k-plane

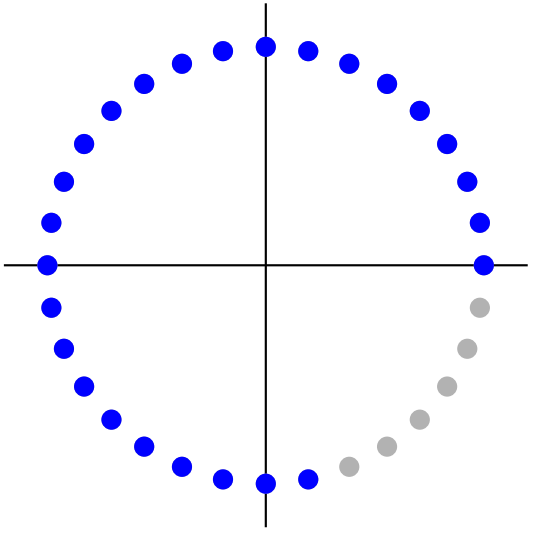

$k = Re^{i\varphi}$

CGO sinogram

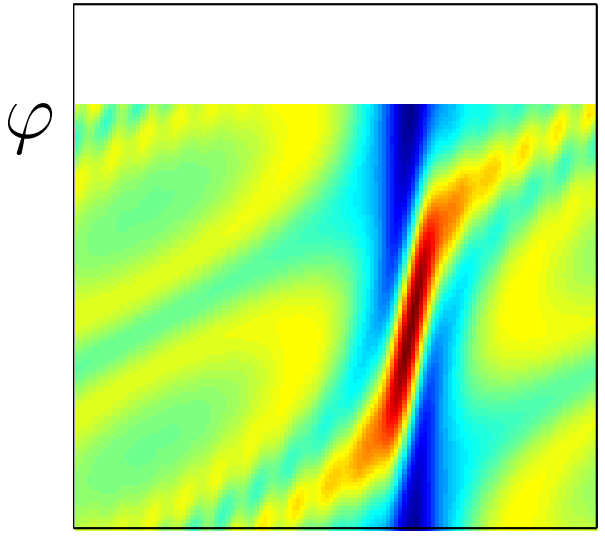

$$\mu(e^{i\theta}, Re^{i\varphi})$$

CGO sinogram in the context of EIT

Solve $\psi(\,\cdot\,,k)|_{\partial\Omega} = e^{ikz} - \mathcal{S}_k(\Lambda_\sigma^\delta - \Lambda_1)\psi$ and set $\mu(z,k) = e^{-ikz}\psi(z,k)$.

Conductivity (z-plane)

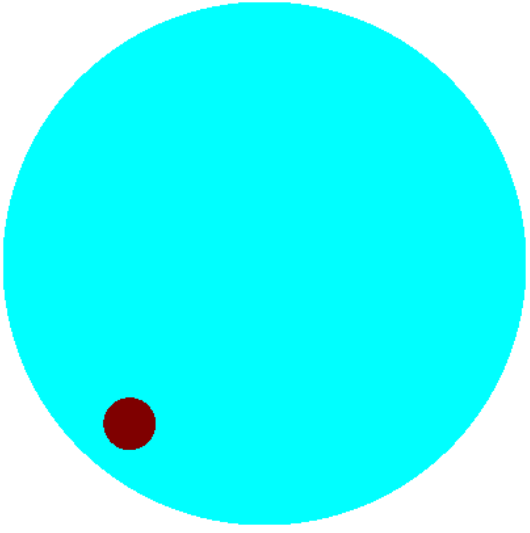

$z = e^{i\theta}$

k-plane

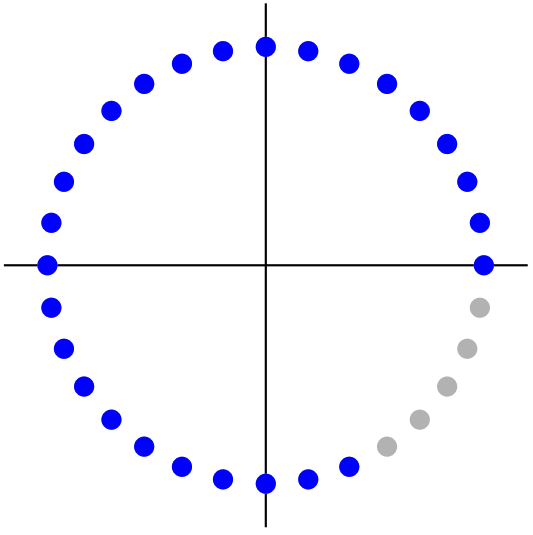

$k = Re^{i\varphi}$

CGO sinogram

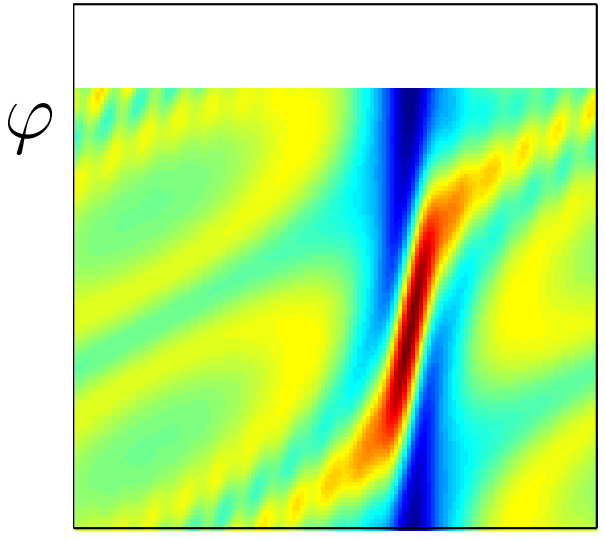

$\mu(e^{i\theta}, Re^{i\varphi})$

CGO sinogram in the context of EIT

Solve $\psi(\,\cdot\,,k)|_{\partial\Omega} = e^{ikz} - \mathcal{S}_k(\Lambda_\sigma^\delta - \Lambda_1)\psi$ and set $\mu(z,k) = e^{-ikz}\psi(z,k)$.

Conductivity (z-plane)

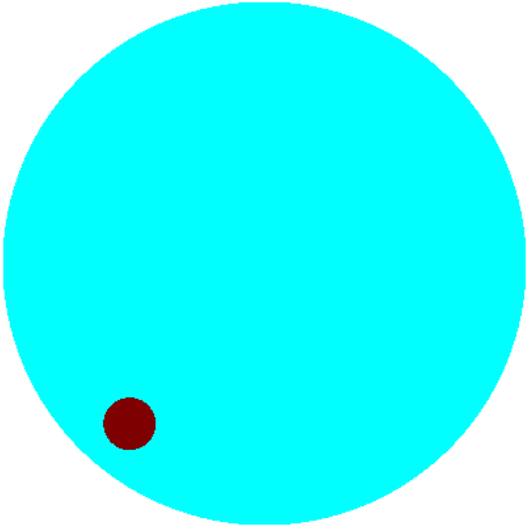

$z = e^{i\theta}$

k-plane

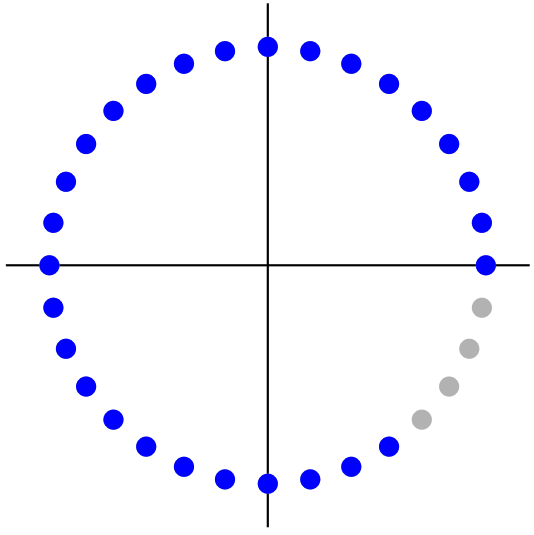

$k = Re^{i\varphi}$

CGO sinogram

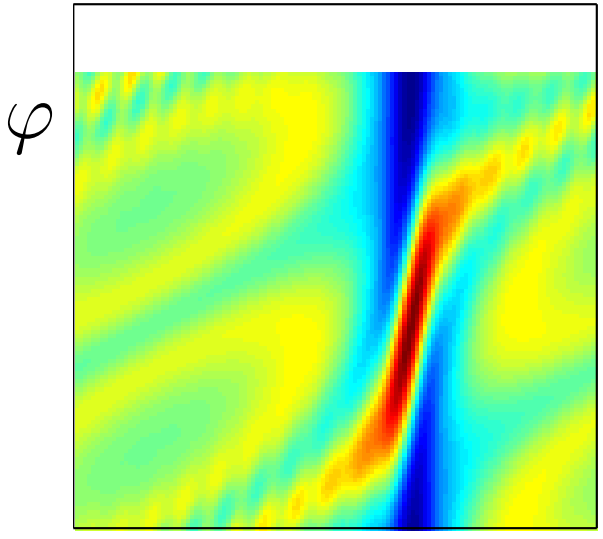

$\mu(e^{i\theta}, Re^{i\varphi})$

CGO sinogram in the context of EIT

Solve $\psi(\,\cdot\,,k)|_{\partial\Omega} = e^{ikz} - \mathcal{S}_k(\Lambda_\sigma^\delta - \Lambda_1)\psi$ and set $\mu(z,k) = e^{-ikz}\psi(z,k)$.

Conductivity (z-plane)

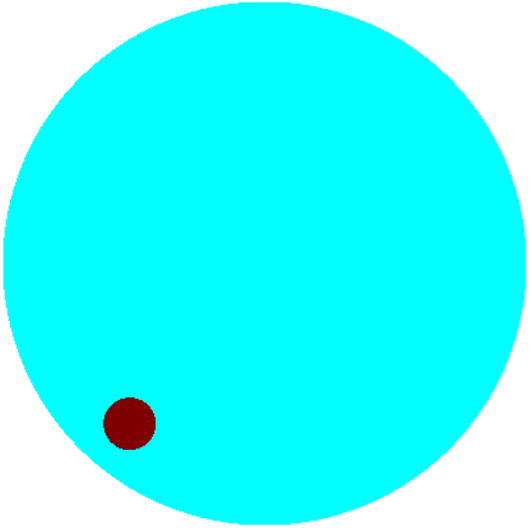

$z = e^{i\theta}$

k-plane

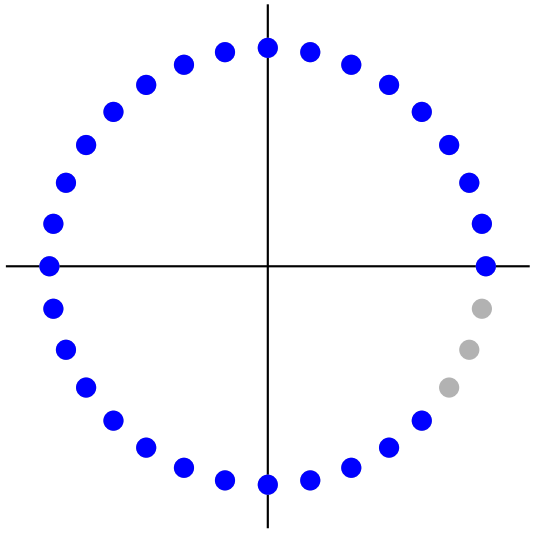

$k = Re^{i\varphi}$

CGO sinogram

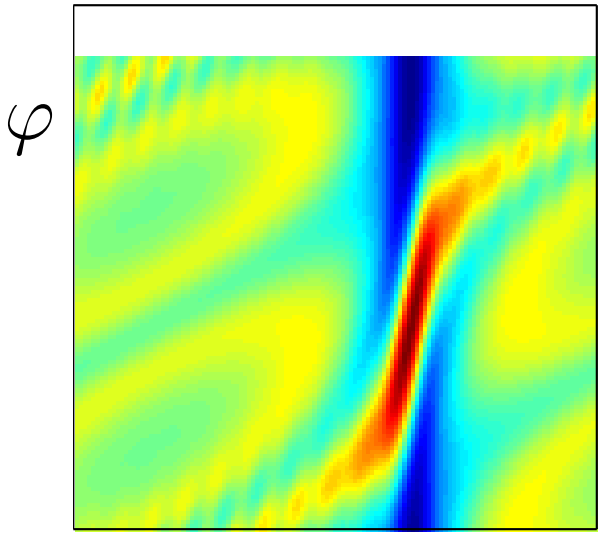

$$\mu(e^{i\theta}, Re^{i\varphi})$$

CGO sinogram in the context of EIT

Solve $\psi(\,\cdot\,,k)|_{\partial\Omega} = e^{ikz} - \mathcal{S}_k(\Lambda_\sigma^\delta - \Lambda_1)\psi$ and set $\mu(z,k) = e^{-ikz}\psi(z,k)$.

Conductivity (z-plane)

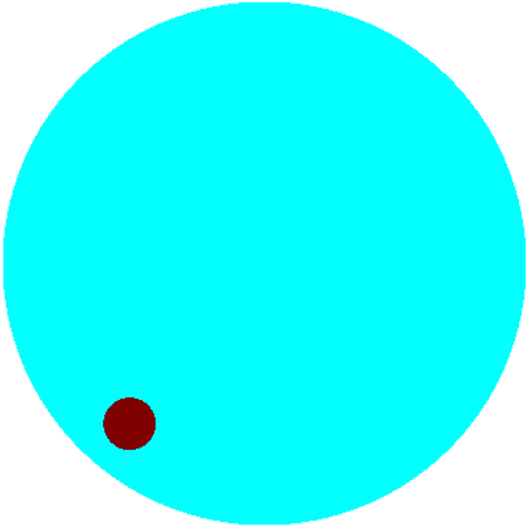

$z = e^{i\theta}$

k-plane

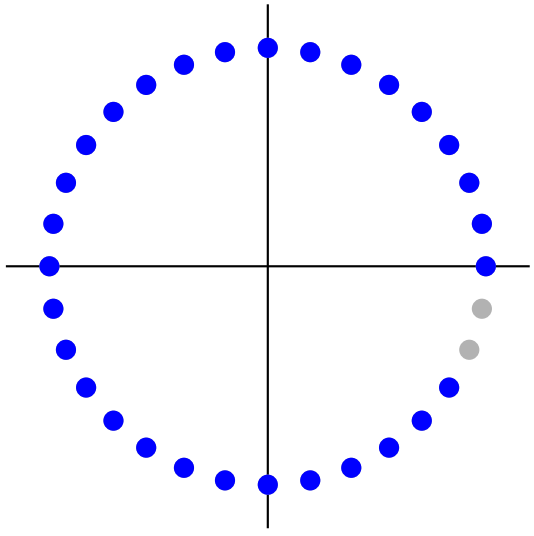

$k = Re^{i\varphi}$

CGO sinogram

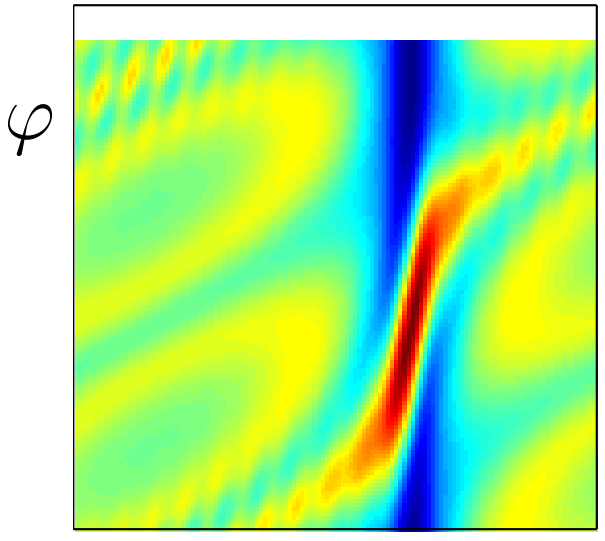

$$\mu(e^{i\theta}, Re^{i\varphi})$$

CGO sinogram in the context of EIT

Solve $\psi(\,\cdot\,,k)|_{\partial\Omega} = e^{ikz} - \mathcal{S}_k(\Lambda_\sigma^\delta - \Lambda_1)\psi$ and set $\mu(z,k) = e^{-ikz}\psi(z,k)$.

Conductivity (z-plane)

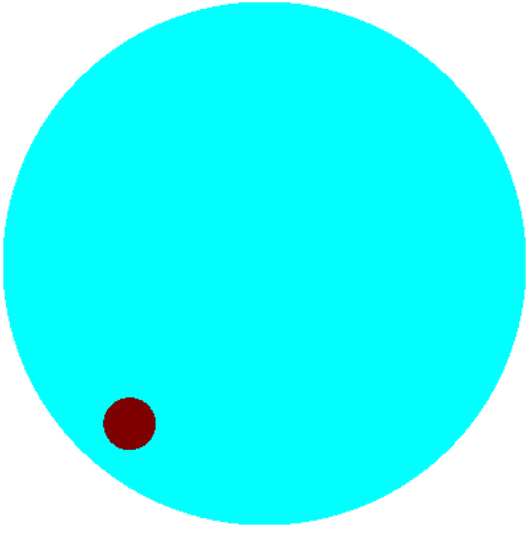

$z = e^{i\theta}$

k-plane

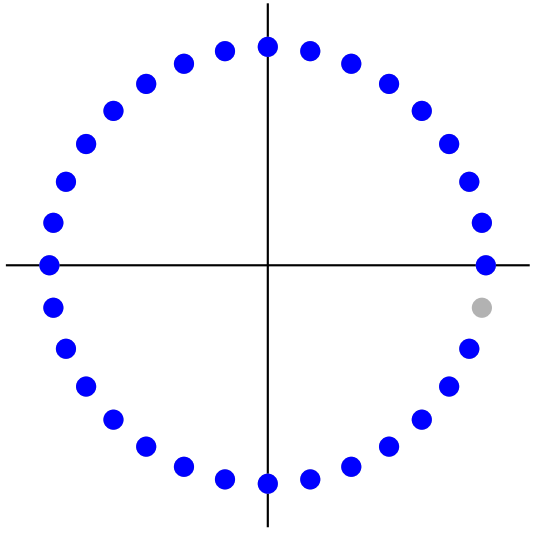

$k = Re^{i\varphi}$

CGO sinogram

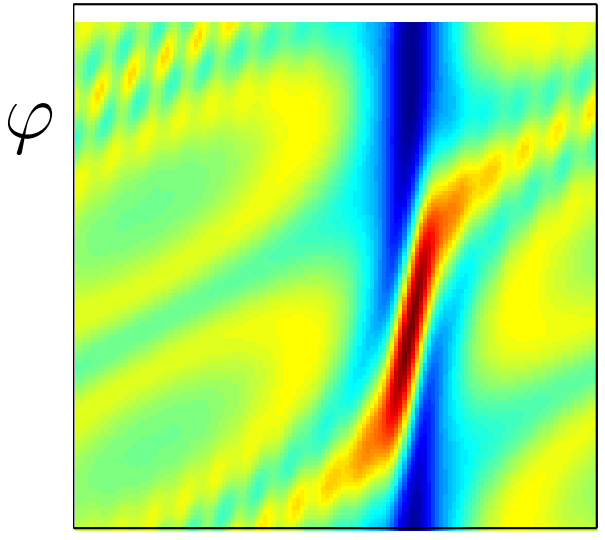

$\mu(e^{i\theta}, Re^{i\varphi})$

CGO sinogram in the context of EIT

Solve $\psi(\,\cdot\,,k)|_{\partial\Omega} = e^{ikz} - \mathcal{S}_k(\Lambda_\sigma^\delta - \Lambda_1)\psi$ and set $\mu(z,k) = e^{-ikz}\psi(z,k)$.

Conductivity (z-plane)

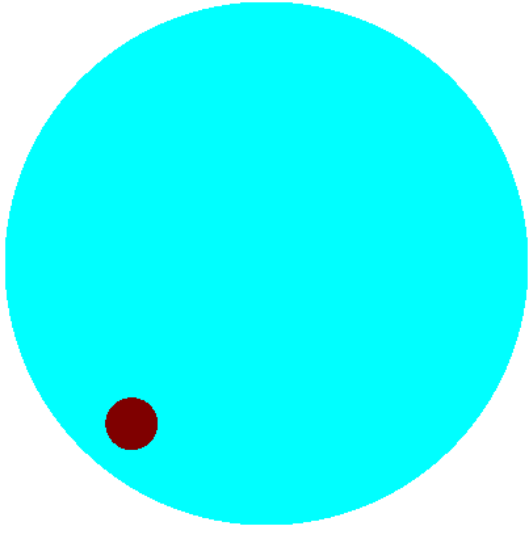

$z = e^{i\theta}$

k-plane

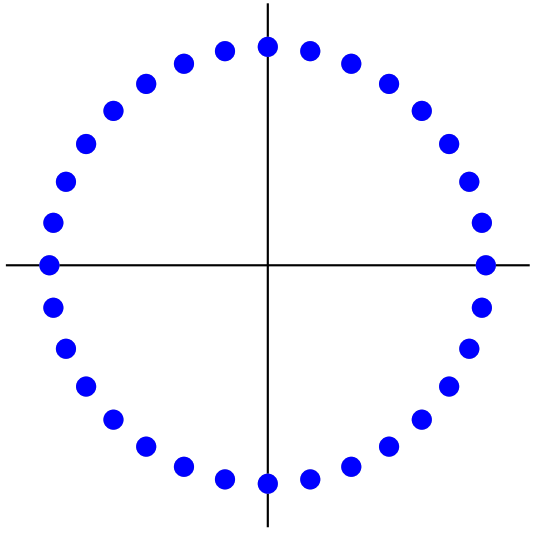

$k = Re^{i\varphi}$

CGO sinogram

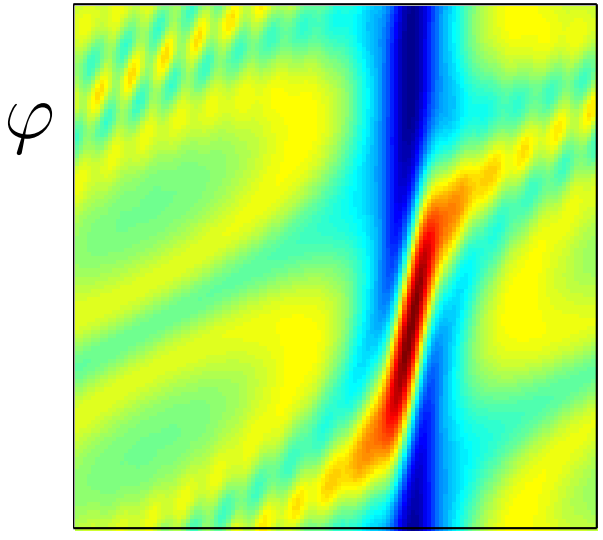

$\mu(e^{i\theta}, Re^{i\varphi})$

The CGO sinogram is more intuitive geometrically than the DN matrix: here a simple example

(Loading video)

Conductivity DN matrix CGO sinogram

Let us use the CGO sinogram for correcting the contrast in a D-bar reconstruction

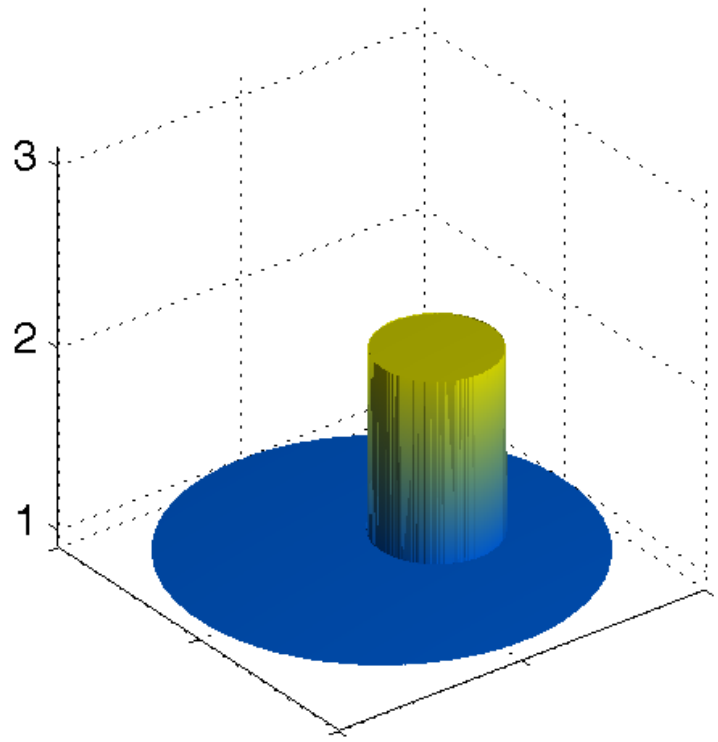

Conductivity

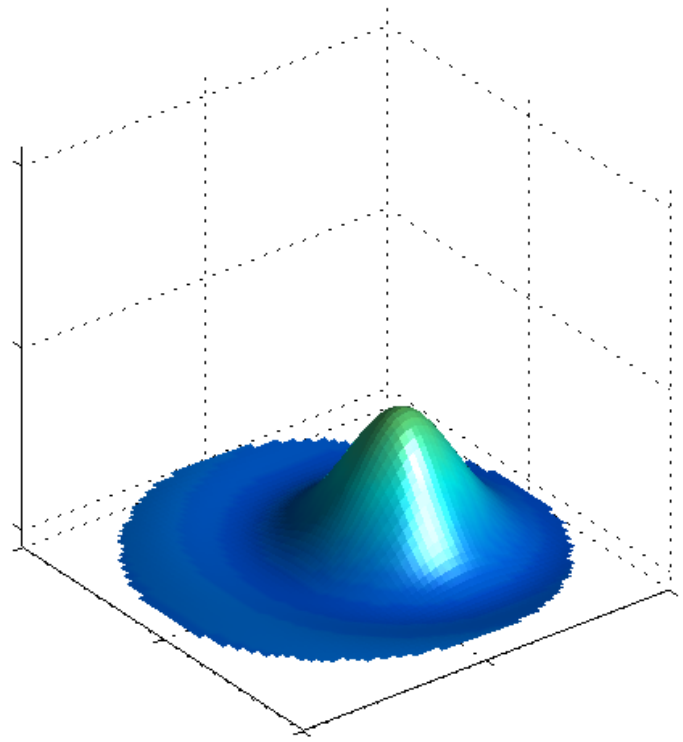

Reconstruction

We modify the contrast in the reconstruction using a parameter $0 \leq s \leq 1$

(Loading video)

(Loading video)

(Loading video)

We choose the best (contrast-enhanced) image from the Ambrosio-Tortorelli segmentation flow

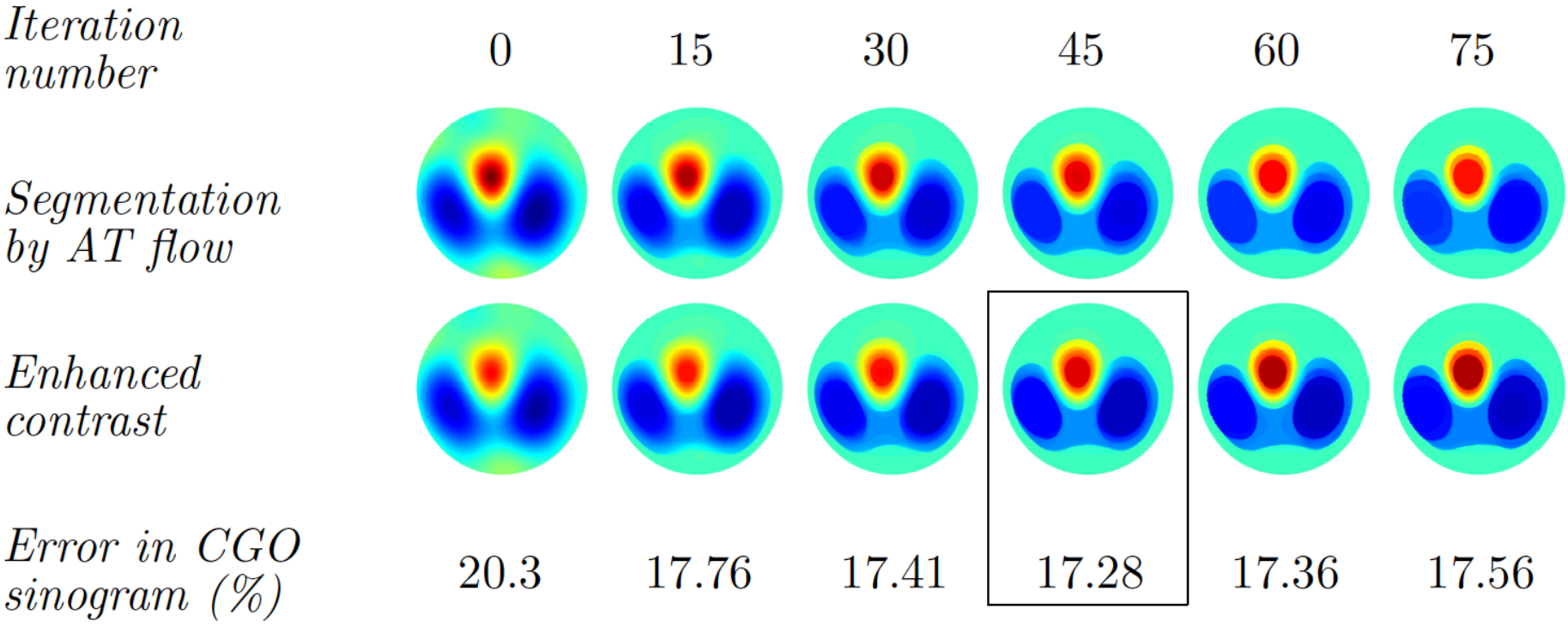

This provides a link between imaging methods and PDE-based inversion.

The CGO-controlled Ambrosio-Tortorelli flow gives a nonlinear, edge-preserving EIT method

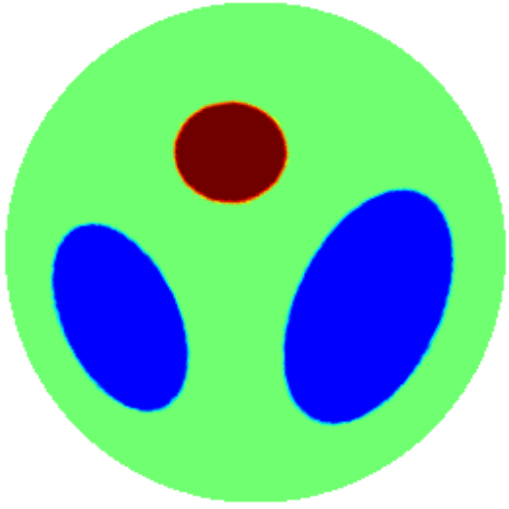

Conductivity

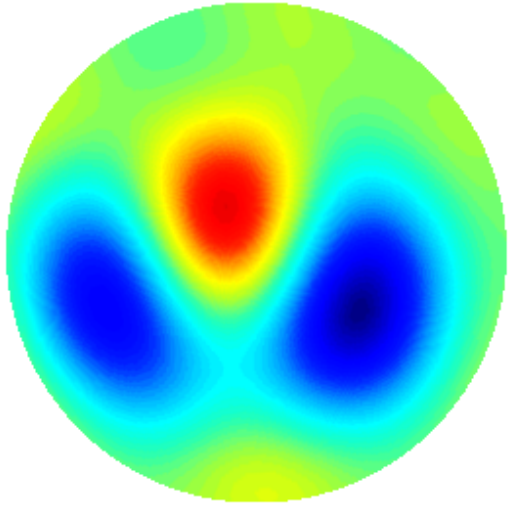

D-bar reconstruction

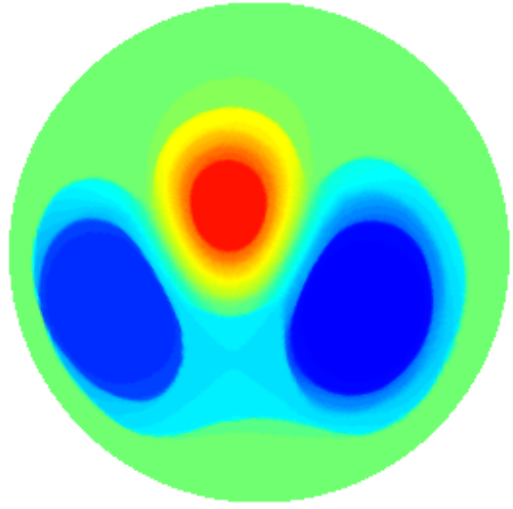

AT and D-bar

[Hamilton, Hauptmann & S 2014]

Outline

Uniqueness: can two different objects produce the same infinite-precision data?

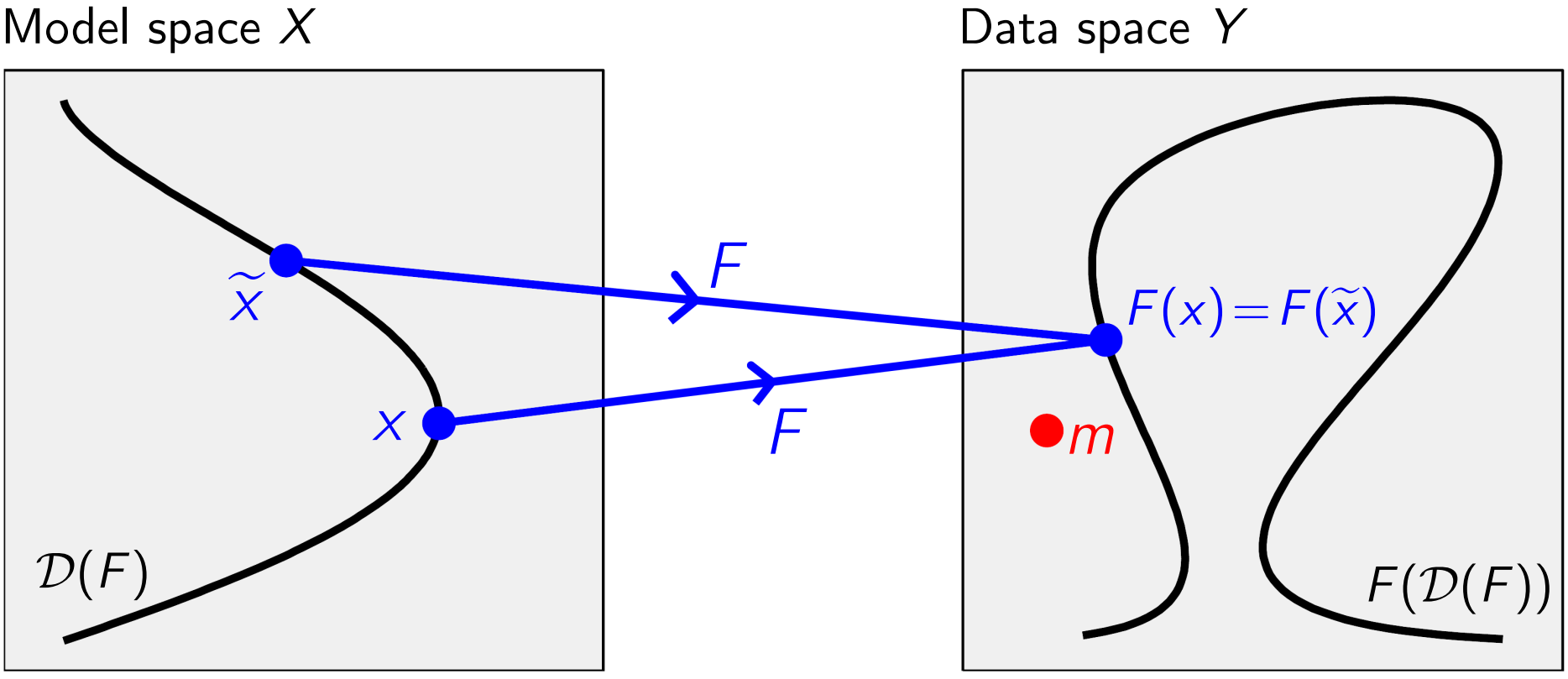

Conditional stability research studies the difference between images and preimages

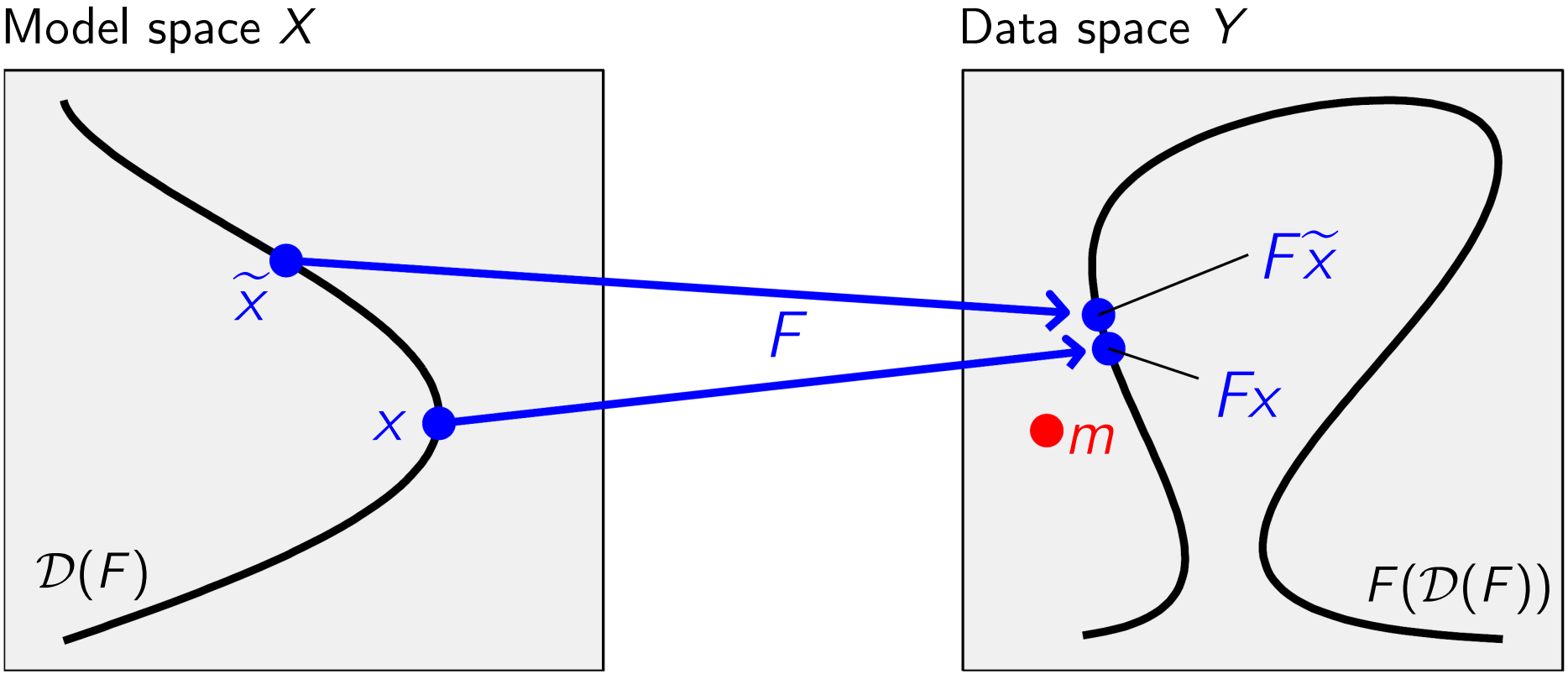

Conditional stability results have the form $\|x - \widetilde{x}\|_X \leq f(\|Fx - F\widetilde{x}\|_Y)$, where $f : \mathbb{R}^+ \to \mathbb{R}^+$ is a continuous function satisfying $f(0) = 0$.

However, in general the data is not in the range: $m \notin F(\mathcal{D}(F))$.

The D-bar method based on the Schrödinger equation ($\sigma \in C^2(\Omega)$) is currently most developed

Theoretical studies

Uniqueness, no-noise reconstruction

1996 Nachman

Conditional stability

1997 Liu

Regularization strategy

2009 Knudsen, Lassas, Mueller, S

Computational methods

Feasibility study

2000 S, Mueller, Isaacson
2003 Mueller, S
2004 Knudsen, Mueller, S

Reconstruction from measured data

2004 Isaacson, Mueller, Newell, S
2006 Isaacson, Mueller, Newell, S
2007 Murphy, Mueller, Newell
2010 deAngelo, Mueller

Real-time algorithm

2014 Dodd, Mueller

The D-bar method based on a 2×2 system ($\sigma \in C^1(\Omega)$) extends to complex impedances

Theoretical studies

Uniqueness, no-noise reconstruction

1997 Brown, Uhlmann

2000 Francini

Conditional stability

2001 Barceló, Barceló, Ruiz

2010 Beretta, Francini

Regularization strategy

TO DO!

Computational methods

Feasibility study

2001 Knudsen, Tamasan

2003 Knudsen

2012 Hamilton, Herrera, Mueller, von Herrmann

2013 Hamilton, Mueller

Reconstruction from measured data

2015 Herrera, Vallejo, Mueller, Lima

The D-bar method based on Beltrami equation can deal with discontinuities ($\sigma \in L^\infty(\Omega)$)

Theoretical studies

Uniqueness, no-noise reconstruction

2003 Astala, Päivärinta

2005 Astala, Lassas, Päivärinta

Conditional stability

2007 Barceló, Faraco, Ruiz

2008 Clop, Faraco, Ruiz

Regularization strategy

TO DO!

Computational methods

Feasibility study

2010 Astala, Mueller, Päivärinta, S

2011 Astala, Mueller, Päivärinta, Perämäki, S

2014 Astala, Päivärinta, Reyes, S

Reconstruction from measured data

TO DO!

The D-bar method based on Beltrami equation seems to have the appropriate convergence

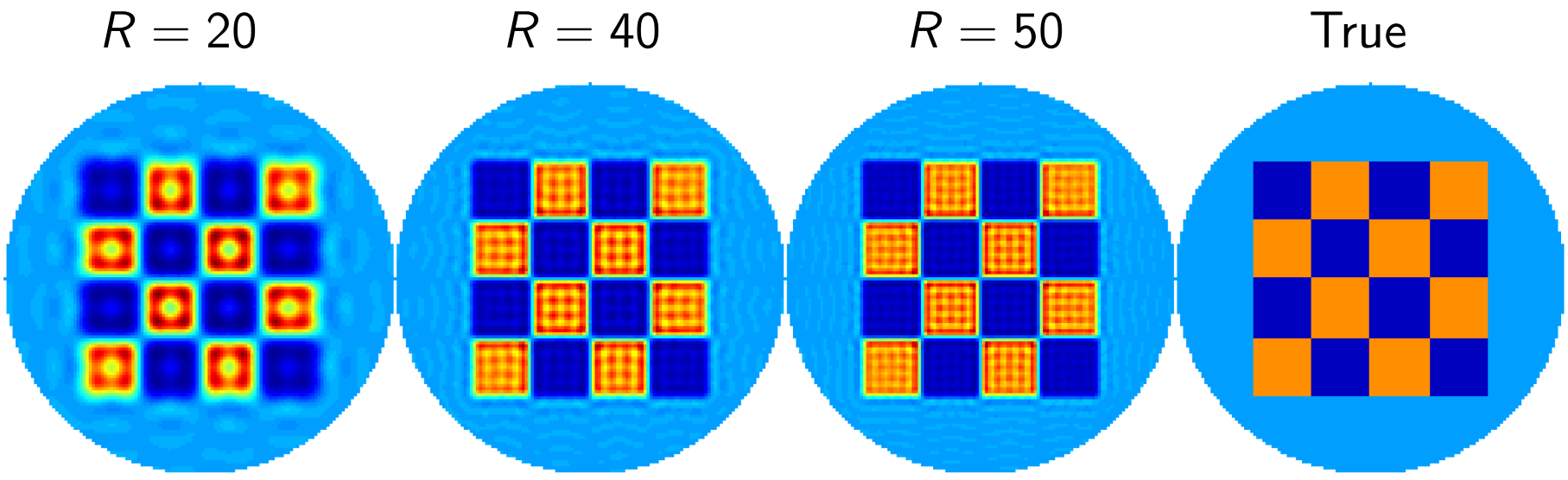

[Astala, Päivärinta, Reyes & S 2014]

Tailor-made regularization is needed for many nonlinear inverse problems, not only EIT

A nonlinear Fourier transform approach is available for seismic tomography (positive-energy CGO) and near-infrared optical tomography (negative-energy CGO).
Regularization strategies for them would lead to

- effective subsurface imaging and geophysical prospection, and
- monitoring for hemorrhages in neonatal brains.

Currently there are no regularization results available for nonlinear inverse boundary-value problems for parabolic or hyperbolic PDE's.
Such regularization strategies and their computational implementations would be a paradigm shift in inverse problems and imaging science.

Applied Inverse Problems

Conference in
Helsinki, Finland
May 25-29, 2015

http://aip2015.fips.fi

Thank you for your attention!